UNIVERSITÉ DE STRASBOURG

ÉCOLE DOCTORALE DES SCIENCES CHIMIQUES

LBP – UMR 7021

THÈSE

Antoine COMBES

soutenue le : **13 mars 2023**

pour obtenir le grade de : **Docteur de l'université de Strasbourg**

Discipline/ Spécialité : Chimie-Polymères

Influence de la structure des polymères sur la formation de nanoparticules fonctionnelles par nanoprécipitation

THÈSE dirigée par :

Dr. Andreas REISCH — Maître de conférences, Université de Strasbourg

RAPPORTEURS :

Dr. Olivier SANDRE — Directeur de recherches, Université de Bordeaux

Dr. Catherine LADAVIERE — Directrice de recherches, Université Lyon 1

EXAMINATEURS :

Dr. Fouzia BOULMEDAIS — Directrice de recherches, Université de Strasbourg

Dr. Muriel LANSALOT — Directrice de recherches, Université Lyon 1

Pr. Rachel MEALLET-RENAULT — Professeure, Université Paris – Sacley

À mes parents

Acknowledgement

L'accomplissement de ce projet de thèse est le fruit d'un long travail durant lequel j'ai interagit avec de nombreuses personnes, que ce soit lors de collaborations scientifiques ou sur un plan plus personnel. Chacune de ces personnes m'a permis d'avancer, tenir bon, décompresser, m'ont guidé ou réconforté, et sont à l'origine de souvenirs inestimables. Ainsi, je tiens à remercier celles et ceux qui m'ont permis d'en arriver là, que vous étiez à mes côtés durant ces trois dernières années ou bien avant cela.

Dans un premier temps, je tiens remercier les membres de mon jury de thèse, le Dr Olivier Sandre, la Dr Catherine Ladavière, la Dr Fouzia Boulmedais, la Dr Muriel Lansalot et la Pr Rachel Méallet-Renault, d'avoir accepté et pris le temps d'examiner mes travaux.

Je remercie également toutes les personnes qui ont contribué à ce projet de près, notamment Valérie Mazan pour les expériences de stopped-flow, Corinne Crucifix pour les images TEM, Mélanie Legros pour les analyses SEC et Estefania Oliva, Delphine Garnier et Chen Deng pour leur aide précieuse en RMN. Beaucoup d'autres personnes m'ont apporté aide ou conseils sur divers sujets, toujours avec une grande bienveillance. Merci à Pascal Didier, Frédéric Przybilla, Romain Vauchelles, Nicolas Humbert, Marlyse Wernert, Ingrid Barthel, Tania Steffan et Philippe Chabert. Un grand merci également à Mayeul Collot, car bien qu'extérieur à mon projet, je pouvais souvent venir te trouver pour discuter de chimie ou te demander un avis sur quoi que ce soit. Enfin merci beaucoup à Andrey Klymchenko pour toutes les interactions que l'on a pu avoir, que cela soit au sujet de la vie du laboratoire, lors des group-meetings ou autres discussions scientifiques mais également en dehors du travail. Rien de tel qu'un bowling, un barbecue ou une virée au marché de noël pour resserrer les liens au sein de l'équipe ! Je suis vraiment heureux d'avoir pu effectuer ma thèse dans ton équipe et j'espère rencontrer d'autres personnes aussi inspirantes que toi dans le futur.

Je tiens ensuite à remercier profondément mon directeur de thèse, Andreas Reisch. Tout d'abord, merci de m'avoir confié ce projet, et de m'avoir guidé tout au long de sa réalisation. Tu as su progressivement me faire évoluer, me poussant à me perfectionner en accompagnant tes exigences d'une grande bienveillance. Grâce à toi j'ai vécu ce projet comme une grande aventure personnelle dans laquelle tu marchais à mes côtés. Tu as su

m'éclairer au long de ce chemin difficile que tu m'as permis d'arpenter plus loin que ce que j'aurais pu imaginer. Merci de m'avoir autant impliqué dans ce projet, merci pour toutes les discussions parfois très pointues que l'on a pu avoir, merci pour ton approche toujours positive sur mes résultats, merci de m'avoir fait découvrir tant de choses. Je suis sincèrement reconnaissant des opportunités que j'ai eues, de découvrir la culture cellulaire, le monde de la microscopie, et d'avoir pu participer à autant de congrès passionnants qui m'ont laissé des souvenirs incroyables. Merci enfin pour ton soutien lors de la rédaction de ce manuscrit. La fin de ma thèse est une page importante qui se tourne dans ma vie et je suis heureux que tu aies fait partie des personnages nécessaires à son écriture. Je te souhaite le meilleur dans ton avenir professionnel et personnel.

J'ai également eu la chance d'avoir des super collègues stagiaires, doctorants et post-doctorants. Lucie, avec qui j'ai partagé plein de choses et de bons moments, en particulier parce qu'on se comprenait très bien. Parmi les plus beaux souvenirs de ma thèse sans aucun doute, notre périple en Guadeloupe restera gravé à vie dans ma mémoire. Rémi avec qui j'ai partagé le labo pendant la majorité de ma thèse, j'ai rarement rencontré quelqu'un d'aussi passionné et investi dans la science que toi ! Nathan qui est une source d'histoires rocambolesques incroyable, Carla avec qui je compte bien continuer de grimper ou skier, Valentine qui apporte une énergie nouvelle dans la team et Sonia que je connais depuis un bout de temps maintenant. Qui aurait cru qu'un week-end à Thonon aurait de telles conséquences ! Merci à Elisabete pour ta bonne humeur au quotidien et ton enthousiasme survolté, tu es une des pépites de ce laboratoire. Merci Sophie pour ta capacité d'écoute et le soutient dont tu faisais preuve dans les moments plus difficiles. Un grand merci à Corentin, qui a activement contribué à cette thèse durant son stage, je te souhaite le meilleur dans la thèse que tu as commencée. Je n'oublie pas Ilya qui était le Jésus du laboratoire, capable de miracles et d'apporter une réponse à chaque problème. Merci d'avoir partagé tes connaissances et ton expertise avec moi. Merci enfin à toutes les autres personnes avec qui j'ai partagé des moments en commun et qui ont égayé ces moments passés à la fac de pharma, Anne, Bohdan, Dmytro, Emre, Fei, Gianluca, JB,Khanh-Nam, Kyong, Mario, Maxence, Nina, Nour, Ophélie, Paraskevi, Raphaël, Sophie, Stefano, Sylvie, Tanushree, Tesla et Yann.

Je remercie chaleureusement le Dr Antoine Mirloup ainsi que la Dr Albane Neckebroeck pour toutes les discussions que l'on a pu avoir, notamment lors des pauses

café qui étaient, de fait, des excellents moments que j'ai passé en votre compagnie. Merci d'avoir partagé vos expériences personnelles avec nous. Tous ces échanges ont été, je pense, plus enrichissants pour moi que ce que vous ne pensez.

Le parcours m'ayant amené jusqu'à cette thèse a été fortement influencé par des professeurs géniaux qui m'ont donné goût à la science et donné envie de toujours poursuivre mes études. Ces personnes qui m'ont marqué sont Mr Lefebvre, Mr Thérond, Mr Richard, Mr Tisserand, Mr Etienne, Mme Urvoaz, Mme Stackler, Mr Stempfle, Mme Margathe, Mme Schmitt, Mme Loew, Mr Roussey, EZ, Mr Brandel et Mr Müller.

De nombreux amis m'ont tenu compagnie sur les bancs de l'école et j'ai une pensée pour Cyril, Matthieu, Colin, Maxime C., Romuald, Auriane, Ben, ainsi que toutes les personnes avec qui j'ai vécu des moments inoubliables au théâtre : Cédric, Emilien, Alexis, Anthony, Kevin, Amandine, Camille, Nolwenn, Madeline, Chloé, Mathieu, Florine, Marie et Pauline. J'ai également des histoires mémorables avec mes amis de BTS : Tiffany, Florian, Guillaume, Mélissa, Luc, Johan, Thomas, Julien, Thibaud, Maxime, Philippe, Aurélien et Emma. J'ai une pensée émue pour tous mes amis de prépa et pour tout ce qu'on a vécu ensemble. Cette époque était vraiment particulière et je suis heureux de vous avoir eu dans ma vie à ce moment-là. Merci William, Raphaël, Adeline, Valentin, Quentin, Maxime, Jérémie, Anthony et Julie, la meilleure binôme de kholles au monde.

Vient le tour des amis de l'école d'ingénieur et la liste est longue. Ces années ont été parmi les plus intenses que j'ai vécues, et ce grâce aux personnes formidables qui les ont partagées avec moi. Je remercie les personnes qui m'ont intégré à l'école et m'y ont fait me sentir comme à la maison : Hugo, Cécou, Joachim, Paul, Damien, Justine, Rodolphe, Sam, Jérémi, Romane, Simon, Nicolas, Flo, Alexis et Caroline. Un immense merci à mes camarades de promo, Clem, Maude et Milane de la team cancers, mon frérot Alex et toutes ses théories (avec une préférence pour celle des piliers même si celle des gens moyen-beaux est pas mal), Arthur cet homme particulièrement habile avec ses blagues, Quentin (Vive le sport !), Ziyed qui sait mettre l'ambiance en TP, Marek qui a le don de glisser des pépites dans les conversations, Clément mon jungler pref, Chloë l'inventrice des trans-afternoon ainsi que Raph avec qui on faisait trop de bruit en strock. Je fais plein de bécots à celles et ceux que j'ai eu le plaisir de voir arriver à l'école, Jules, Sibyline, Vivi, Francis,

Valentin, Arthur, Lorenzo, Marc, Nathan, Emile, Lisa, sans oublier ma famille Doriane, Loann, Chloé, Mathis et Apolline, vous êtes incroyables.

Certaines des personnes que j'ai rencontrées pendant ces années ont décidé de rester à Strasbourg pour jouer les prolongations. Merci les amis pour tous ces moments si importants passés en parallèle de la thèse. Camille la légendaire 2ème dauphine, Barbara toujours respom dans mon cœur, Quentin ce rider de l'extrême, Charlotte qui a des nouvelles histoires à chaque fois qu'on se voit, Korantin qui décidément tarde à ouvrir une brasserie, Alexis le diable et Clara qui n'est pas en reste, Justine que j'entends taper du pied depuis Bordeaux et Nina, toujours dans les bails celle-là.

Une mention spéciale pour les colocs que j'ai eus pendant la thèse, Hadrien, Thomas, Hugo et Etienne, avec qui je pouvais enfin parler d'autre choses que de sciences ! Dans cette lignée je remercie Sam et Jason, je n'aurais jamais cru rencontrer des Aussies aussi cool au-dessus de chez moi. Un énorme merci à la team escalade, constituée de personnes exceptionnelles qui m'ont apporté un grand soutien pendant la thèse : Lauri, Macha, Paula et Julia.

Durant ces dernières années il y a des personnes avec qui j'ai passé énormément de temps. Et puis il y a Maxime. Même si on n'arrive pas à se voir, le temps qui passe n'entame pas notre amitié. Je sais qu'il suffit d'un regard en coin pour qu'on parte en fou rire. Merci pour toutes les histoires qu'on a vécues et pour avoir gardé un lien aussi fort. Il a pour moi une valeur inestimable.

J'ai eu la chance de pouvoir compter sur de nombreuses personnes pendant ma thèse, qui m'ont fourni des appuis indispensables pour aller de l'avant. Les personnes qui suivent ont été pour moi des piliers monumentaux. Des colosses capables de me porter à bout de bras et qu'aucune tempête ne saurait faire vaciller. Merci Kitirina, car avec toi je peux me laisser aller, tout te confier car on a tant de choses en commun dans notre personnalité. Merci de m'avoir emmené en vadrouille en Italie, merci pour les moments de jeux de rôles, de peinture et d'échanges linguistiques. I'm so glad we are friends. Un immense merci à Kim, ta compagnie est toujours si apaisante. C'était tellement précieux pour moi d'avoir quelqu'un qui me comprenait sans avoir besoin d'expliquer quoi que ce soit. J'admire ta résilience et ta détermination, et je te souhaite le meilleur dans ta reconversion professionnelle et dans ton épanouissement personnel. Je remercie

profondément Lazare de sa présence à mes côtés depuis si longtemps. Nos nombreux sujets de discussion, de réflexion voire de débat ont largement contribués à me faire évoluer sur le plan personnel. Je n'arrive pas à imaginer ce qu'aurait été la thèse si nous n'avions pas été dans le même labo, tellement nous étions impliqués ensemble dans cette aventure. Pouvoir partager nos résultats, découvertes, doutes, joies et tracas tout au long de nos thèses a été d'une importance primordiale pour moi. Merci d'avoir été là. Je te souhaite une brillante carrière de chercheur et le meilleur dans la vie.

Alan, Hippolyte et Justin. Vous comptez tellement pour moi que je ne peux pas l'exprimer avec des mots. Dans les faits, vous le savez, je serai toujours là pour vous, comme vous l'avez été pour moi. Merci, merci tellement pour toutes les dingueries que l'on a vécues et pour celles à venir. Merci pour ce lien unique qui nous relie, j'ai hâte de vivre de nouvelles aventures avec vous.

Enfin je remercie chaleureusement ma famille qui m'a apporté tellement d'amour. Le côté paternel, mamie Suzanne, papi Daniel, tonton Philippe, Sabine et Alex mon cousin. Malheureusement la distance a fait que je n'ai pas pu profiter de vous autant que je l'aurais voulu. Pour autant je me sens très poche de vous et j'espère bien rattraper une partie du temps perdu. Et bien sûr Papa, merci pour toutes les choses que tu m'as apprises et pour avoir toujours cru en moi. Le côté maternel, avec mamie Colette et papi Louis, merci pour tous les moments passés ensemble, pour les vacances merveilleuses à Contrexard et pour m'avoir partagé votre passion pour la montagne et la randonnée. Je n'ai que des bons souvenirs des moments passés à vos côtés. Merci à toutes mes tantes, Dominique, Agnès et Catherine ainsi que mes cousins-cousines. Je suis toujours ravi de vous revoir ainsi que de voir grandir mes petits cousins et petites cousines. Merci énormément à Nicolas, Johanna, Lison et Eugène avec qui j'ai construit des liens plus forts que ceux du sang. Merci Angèle, ma sœur d'amour, je suis extrêmement fier de tes choix et de la personne que tu es. Enfin merci Maman pour l'amour inconditionnel que tu nous portes et pour avoir toujours souhaité le bonheur de tes enfants. Merci d'être là pour nous, de tout mon cœur.

General introduction

Loaded polymeric nanoparticles are a versatile class of nanomaterials used notably in biomedical applications. A very attractive method for their synthesis is nanoprecipitation: this process is easy to operate and allows a large-scale production of nanoparticles. Nanoprecipitation is a kinetically controlled process, where many parameters are involved and may influence the final properties of particles. Some of them have been studied in details experimentally or with computational models such as mixing, polymer concentration, solvents or the use of additives. It has also been observed that polymer chemistry plays an important role in this process. However, systematic studies of the influence of polymer chemistry on particle formation remain scarce and the influence of the other parameters makes comparisons between different studies hazardous. In this context, we decided to study the influence of polymer chemistry on the formation of dye-loaded nanoparticles obtained by nanoprecipitation of polymers with different chemical and structural compositions.

In the first chapter, the principles of nanoprecipitation are reviewed as well as the role of polymer chemistry in the formation of polymeric NPs, followed by an overview of the major techniques used in this study. In chapter II, we investigated the influence of polymer chemistry on the kinetics of nanoprecipitation using different polymers and mixing methods. We were notably interested to observe in which case the mixing or the polymer chemistry has a predominant effect on nanoprecipitation. We further studied the nanoprecipitation of polymers with different levels of hydrophobicity thanks to a stopped-flow device in order to determine characteristic times to achieve polymer assembly.

The presence of charged or hydrophilic groups in polymers has a strong influence on the formation of nanoparticles. In chapter III, we studied in more details the influence of their distribution along polymer chains. This study was notably performed with charged groups, an aspect rarely studied in the literature. Statistical or block co-polymers containing hydrophilic groups were also investigated. Finally, in the last chapter, we attempted to make use of the kinetic control offered by nanoprecipitation to formulate a new type of nanoparticles that combine a small size and high stability in biological media. Inspired by proteins we wanted to create particles combining positive and negative

charges on their surfaces. We hypothesized that the kinetically controlled nature of nanoprecipitation could allow the assembly of oppositely charged polymers while avoiding charge paring.

Table of contents

Acronyms and abbreviations

ACN	Acetonitrile
ACQ	Aggregation caused quenching
AIBN	Azobisisobutyronitrile
CCD	Charge-coupled device
CFD	Continuous flow dynamics
cmc	Critical micelle concentration
CTA	Chain-transfer agent
CY5	Cyanine 5
DCM	Dichloromethane
DLS	Dynamic light scattering
DLVO	Derjaguin Landau Verwey Overbeek
DMEM	Dulbecco's Modified Eagle Medium
DMF	Dimethylformamide
DMSO	Dimethylsulfoxide
e.g.	Exempli gratia
EMA	Ethyl methacrylate
Et al	Et alia
EtOH	Ethanol
F12-TPB	Tetrakis[3,5-bis(trifluoromethyl)phenyl]borate
F5-TPB	Tetrakis(pentafluorophenyl)borate
FBS	Fetal bovine serum
FRET	Förster resonance energy transfer
FRP	Free radical polymerization
SEC	Gel permeation chromatography
HEMA	Hydroxyethyl methacrylate
i.e.	Id est
LALS	Low-angle light scattering
MAA	Methacrylic acid
MeOH	Methanol

mPEG	Methoxy polyethylene glycol
mPEG-SH	Methoxy polyethylene glycol thiol
M_n	Number average molecular weight
M_w	Weight average molecular weigh
MWCO	Molecular weight cut-off
NDF	Number density for aggregates
NMR	Nuclear magnetic resonance
NPs	Nanoparticles
PAAm	Polyacrylamide
PCL	Polycaprolactone
PDI	Polydispersity index
PEG	Polyethylene glycol
PEMA	Poly(ethyl methacrylate)
PF5	Pentafluorophenyl methacrylate
PGMA	Poly(glycidyl methacrylate)
pH	Potential of hydrogen
PHAs	Polyhydroxyalkanoates
PHEMA	Poly(hydroxyethyl methacrylate)
PISA	Polymerization-Induced Self-Assembly
PLA	Poly(lactic acid)
PLGA	Poly(lactic-co-glycolic acid)
PMAA	Poly(methacrylic acid)
PMMA	Poly(methyl methacrylate)
ppm	Parts per million
PS	Polystyrene
PSD	Particle size distribution
PVA	Poly(vinyl alcohol)
PVP	Polyvinylpyrrolidone
QY	Quantum yield
R18	Rhodamine 18
RAFT	Reversible addition−fragmentation chain transfer

RALS	Reverse-angle light scattering
SANS	Small-angle neutron scattering
SAXS	Small-angle X-ray scattering
TEA	Triethylamine
TEM	Transmission electron microscopy
THF	Tetrahydrofuran
w/w	Weight/weight

Chapter I: Introduction

1 Loaded polymeric nanoparticles: features and applications

Many recent advances in medicine arise from nanomaterials and their unique properties[1–3], notably related to their size, defined to range from one to one hundred of nanometers[4]. Polymeric nanoparticles (NPs) are part of this wide family. A great feature of polymeric NPs is that they may be loaded with various compounds such as drugs or contrast agents[5–7]. Their main purpose in biomedical applications is to act as a vehicle to protect, carry and in some cases release their load in a controlled manner. Their size, shape and surface properties have a tremendous impact on how this role can be fulfilled[8–11]. Another important characteristic of NPs is their ability to encapsulate the compound of interest. In many cases, a high loading capacity (high ratio between load and polymer mass) is preferred as well as good control of its release (or its absence). Indeed, in the case of fluorescent particles, leakage can lead to non-specific labelling while in drug delivery system it may engender systemic toxicity. A wide range of techniques is available for the preparation of loaded polymeric NPs as well as for the choice of the nature and architecture of polymers used for their constitution[12–15]. In fact, NPs can be prepared from pre-formed polymers assembled into nanostructures or from monomers directly polymerized into nanoparticles. Both techniques have advantages and limitations, and the choice of the appropriate method depend on the load to encapsulate and the size and surface properties sought for the NPs. In all cases, it is crucial to master their synthesis, that is understand chemical and physical forces driving their formation to have a good control on their final properties.

Drug delivery is one of the principal application domains of polymeric NPs because they have a high potential for medicine, notably in the fight against cancer, thanks to their encapsulation and targeting properties. In fact, even though great progresses have been made in the development of new anticancer drugs, they may suffer from limitations such as off target toxicity[16], systemic toxicity[17,18], poor water solubility and a lack in bio-availability[19,20]. The use of polymeric NPs as nanocarriers helps to overcome these issues[21,22]. Encapsulating drugs in NPs protect them from degradation in biological environment. Careful design of the particle surface allows to grant these NPs with long circulation life-time by preventing opsonization and phagocytosis. Indeed, NPs may be

designed to have stealth properties, by using blood compatible polymers such as PEG, mPEG, PVA or polysorbate. The surface of NPs may be functionalized with ligands (e.g., peptides, proteins, antibodies, aptamers…) in order to bind to specific receptors of cancer cells (Figure 1). This allows active targeting and accumulation of drug in the tumor region.

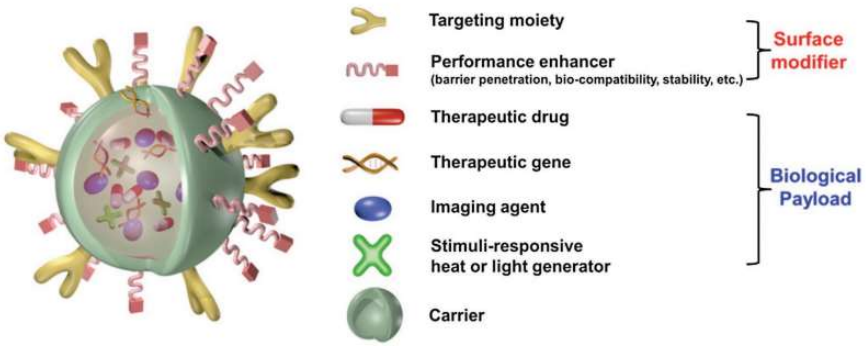

Figure 1: Schematic representation of a nanoparticle loaded with various compounds. The surface of the nanoparticle is functionalized to ensure its stability and grant targeting properties. Reproduced from reference[23].

Polymeric nanoparticles may reach a high loading capacity (> 50% w/w) with efficient encapsulation of many hydrophobic drugs[24]. In order to deliver the drugs, the hydrophobic polymer composing the core of NPs may be biodegradable. Several polymers are degraded into harmless molecules such as PLGA, PHAs, PCL and PLA. Polymers can be degraded passively, typically by hydrolysis, or be designed to degrade in conditions specific to the targeted medium such as pH or the presence of specific enzymes[25,26]. The degradation rate may also be controlled through polymer design[27]. Finally, it is possible to trigger particle degradation using an external source like in photo thermal therapy coupled with drug delivery[28].

Bioimaging is another application field where NPs may shine. Bioimaging is defined as the set of all techniques which has for goal to image living organisms in order to deliver a diagnostic, prepare a chirurgical intervention or for scientific research purposes[29,30]. They are based on different physical phenomena and allow the observation of various body parts. For example, X-ray are used in radiography, NMR in magnetic resonance imaging, ultra sounds in echography, and light in optic microscopy. These techniques are used in tumor imaging[31,32], observation of cellular processes[33–35] and early diagnostic of diseases[36,37]. However, some staining agents can be cytotoxic[38–40] or have their emission reduced due to environmental conditions (pH, aqueous medium)[41,42]. One way to solve this issue is to encapsulate the imaging compound in polymeric NPs (Figure 2).

Further surface functionalization of these particles allows specific targeting, resulting in their accumulation in the area of interest. Combined with the high loading capacity of NPs, this results in a powerful signal and a better contrast of the subject imaged[43,44]. Thanks to the encapsulation properties of NPs, contrast and therapeutics agents can be mixed within the same particle to create theranostic agents. The latter are used to monitor biodistribution and drug release, and allow to evaluate therapeutic efficacy using a single nanocarrier[7].

Imaging of fluorescent NPs also allows to study their own behavior in biological media. Indeed, the same NPs may be used in drug delivery (only the load is changing), so NPs loaded with contrast agents provide crucial information on their fate in in vivo conditions. Circulation life time[45,46], NPs internalization in cells[47,48], specific targeting of NPs[49,50], load delivery[51] and single particle tracking[52,53] may be observed via fluorescence imaging.

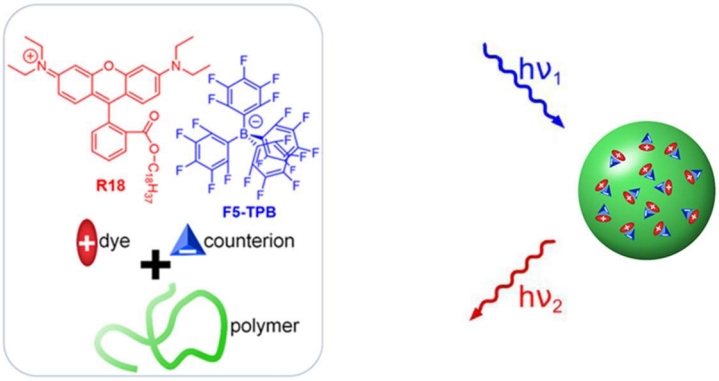

Figure 2: Schematic representation of a dye loaded fluorescent nanoparticle.

2 Fabrication processes

Different techniques are used to form loaded polymeric NPs leading to various sizes, size distributions, encapsulation efficiencies or surface properties. The choice of a particular technique depends on the applications considered for the particles. There are two notable approaches for their synthesis: the polymerization of monomers from an emulsion or the use of pre-formed polymers assembled into particles.

2.1 Fabrication from monomers

One approach to synthetize polymeric NPs is to start from monomers and polymerize them directly into particles. Most techniques involve an emulsion of monomers in water. The dispersed phase containing the monomers is stabilized by a surfactant, forming very small droplets, which act as tiny reactors. The polymerization reaction inside the droplets leads to the formation of the particles. Differences between polymerization reactions taking place in emulsions are mainly due to the quantity of surfactant used and the way of emulsification. Three techniques are distinguished (Figure 3):

- Conventional emulsion polymerization[54] is widely used to obtain latex dispersion of polymers with a low water solubility. An emulsion is formed with a hydrophobic monomer in presence of a surfactant in water. Excess of surfactant forms micelles where monomers will diffuse. Initiators used are water-soluble and the polymerization starts when a radical (or an ion) meets a monomer molecule dissolved in water. The chain will start its growth and rapidly enter a micelle, reacting with the monomers inside. In this mechanism monomer droplets act as reservoirs from which monomers will diffuse to form new micelles or feed micelles with a growing chain. In the end the system is composed of polymer particles of few hundreds of nm in suspension in water.

- Mini-emulsion polymerization[55] differs from the previous method for the reason that the quantity of surfactant used is typically below the critical micelle concentration (cmc). In order to obtain small monomer droplets, a hydrophobic stabilizer and high shear forces are used. Polymerization takes place directly in the droplets, leading to nanoparticles and encapsulating any compound initially present in the dispersed phase. Size of the NPs are typically in the 30 to 200 nm range.

- Micro-emulsion polymerization[56] is the emulsion technique with the smallest monomer droplets and therefore it allows to form very small NPs from 5 to 50 nm. This is due to the very high amount of surfactant used to stabilize the droplets, spontaneously forming a thermodynamically stable emulsion. Initiation occurs either in water phase or in the droplets.

These techniques allow to obtain nanoparticle dispersions with high solid content (usually ranging from 40 to 55 vol %[57]). However, one limitation is that in most cases,

remaining surfactant needs to be removed, so surfactant-free emulsion polymerization techniques have been developed[58].

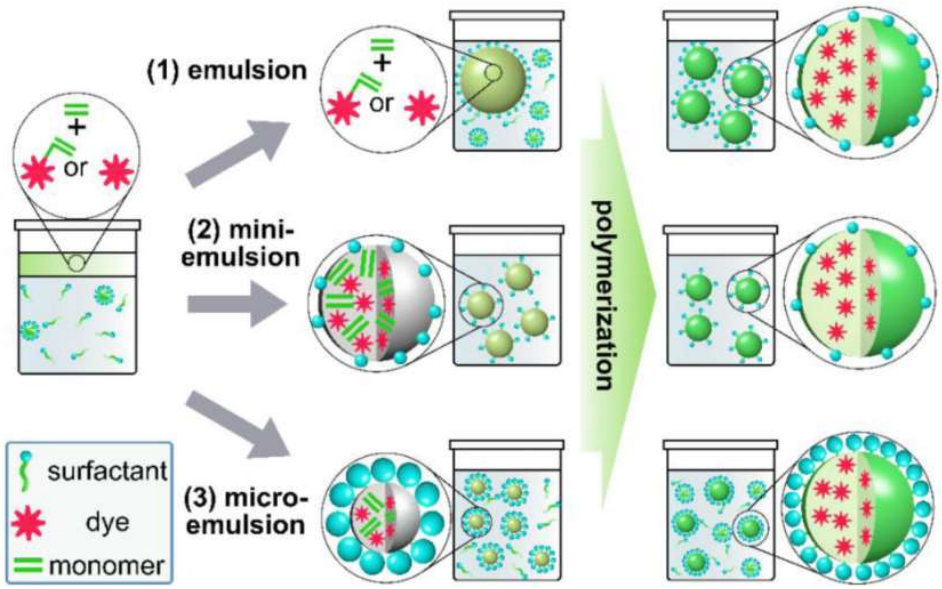

Figure 3: Preparation of dye-loaded polymeric NPs through conventional emulsion, mini-emulsion, or micro-emulsion polymerization. The type of emulsion formed depends on the concentration of the surfactant (typically > cmc in emulsion, < cmc in mini-emulsion, >> cmc in micro-emulsion) and the method of homogenization (shear in emulsion, high shear, ultrasound in mini-emulsion, low shear in micro-emulsion)[6].

Another approach to form NPs during polymerization is polymerization-induced self-assembly (PISA). In this process, a water-soluble polymer chain in solution is extended with a monomer forming an insoluble block. The formation of this block is the driving force for the self-assembly of nanoparticles. Many nanostructures can be obtained depending on the relative size of the blocks, such as micelles, worms and vesicles[59]. Therefore, PISA is a powerful tool to synthetize nanomaterials of various morphology via a one-pot reaction (Figure 4).

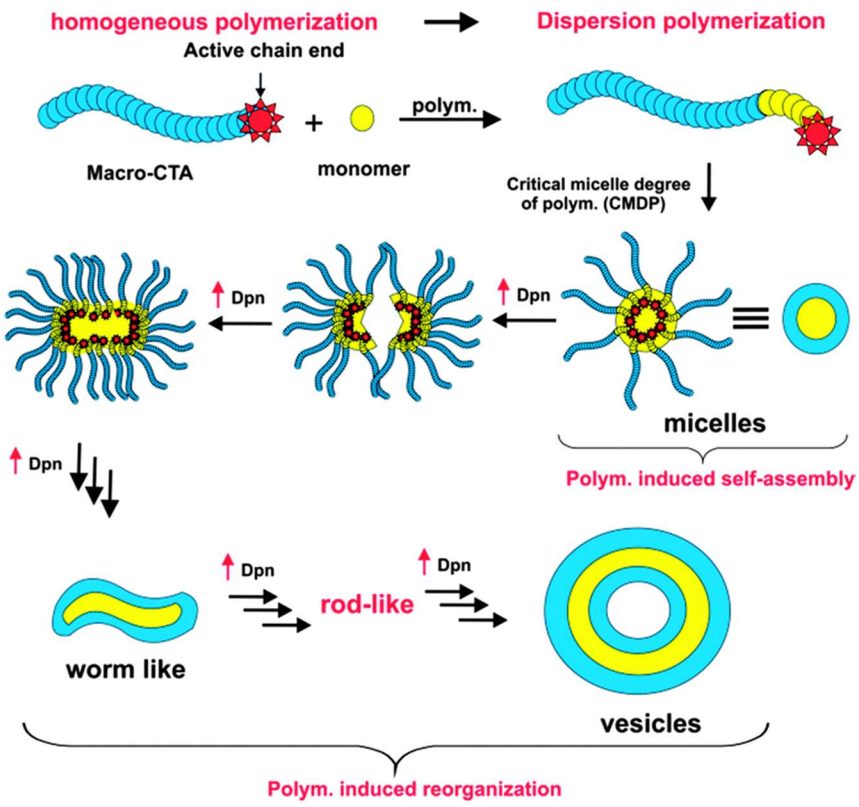

Figure 4: Evolution of the self-assembly process during PISA as polymerization of the hydrophobic block progresses[60].

2.2 Fabrication from polymers

The other fundamentally different approach to form polymeric NPs is to use pre-formed polymers and assemble them into NPs. Different methods exist and rely on the insolubility of the polymers (or a part of the polymer chain) in the dispersed phase to achieve particle formation. One of the key differences between existing techniques is the speed at which the particles are formed. Rather slow processes allow polymer chains to self-organize in a thermodynamically favorable configuration whereas rapid formation of particles leads to kinetically frozen structures.

The self-assembly of amphiphilic polymers is a thermodynamically controlled phenomenon that can lead to the formation of nanoparticles, cylindrical micelles (worms) or vesicles. When formed by self-assembly, these objects have a core-shell structure with an insoluble core and a solvent swollen shell responsible of their stability. Various conditions can be used to form NPs by self-assembly but they are all based on the same principle. In initial conditions, the polymer is in solution until a change in its environment

induce the aggregation of one of its block, forming the core of the particle. The solubility decrease of the core-block may be triggered by lowering the temperature of the solution, changing its pH, increasing the concentration of polymer above the cmc[61], or by a slow addition of a non-solvent miscible with the continuous phase[62] (Figure 5). The size of the particles is mainly affected by the length of the two blocks and usually range from 10 to 100 nm. Because NPs stabilization is ensured by the polymer itself, no surfactants are needed. Various polymers may be used as hydrophilic block (PEG, PVA, PGMA, PMAA) and as hydrophobic block (PMMA, PCL, PLA, PLGA, PS).

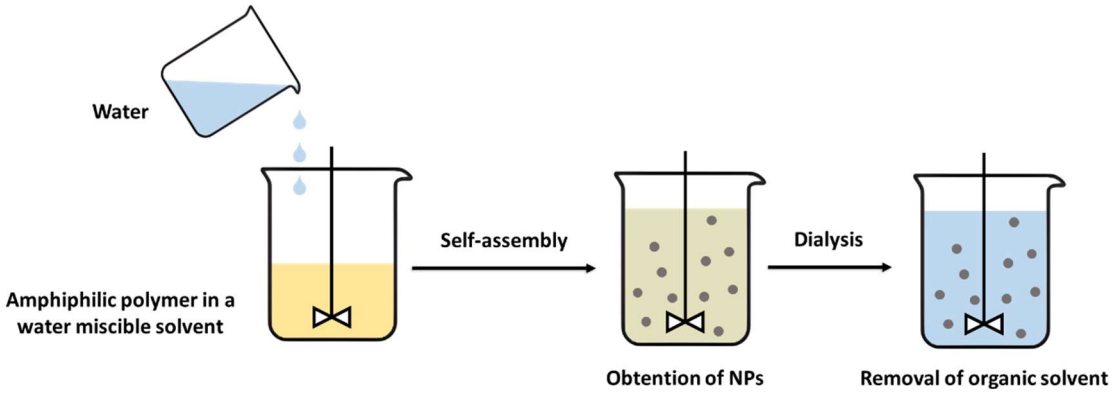

Figure 5: Schematic representation of the self-assembly process by addition of a non-solvent to a polymer solution.

Contrary to polymer self-assembly, nanoprecipitation is a kinetically controlled process used to obtain polymeric NPs. Hydrophobic polymers are dissolved in a water miscible organic solvent such as acetone, acetonitrile or THF. Upon mixing with a large excess of water, the polymer become insoluble and precipitate in the form of nanoparticles. Mixing can be performed manually or with the use of a microfluidic device. These mixers allow to scale up the production of NPs but also grant a faster mixing of the two phases (Figure 6). The stability of the NPs is ensured by the presence of hydrophilic groups on their surfaces. They may be introduced directly in the polymer chain as hydrophilic or charged monomers. Surfactants, most of the time amphiphilic polymers, can also be added in the formulation to stabilize the NPs by adsorption on their surface. Loaded NPs are readily formed be dissolving a hydrophobic compound to encapsulate in the organic phase prior precipitation. Upon mixing with water, the latter becomes insoluble and co-precipitate with the polymer, resulting in a load physically entrapped inside the polymer matrix of the particles. This way, high amount of materials can be encapsulated inside the NPs. Many parameters can influence the formation of particles

obtained by nanoprecipitation such as polymer chemistry, the solvents used, and the mixing process. This will be discussed in details in the following section.

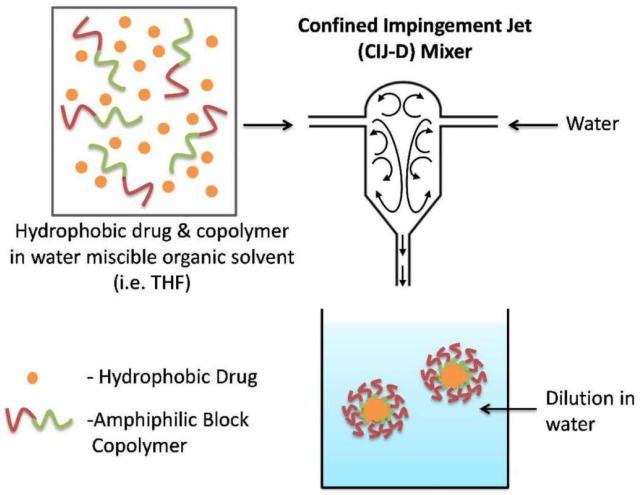

Figure 6: Schematic representation of loaded polymeric nanoparticles formed through nanoprecipitation with a micro fluidic device[63].

3 NPS obtained by nanoprecipitation

3.1 Principle and kinetics

Nanoprecipitation is commonly used for the preparation of nanoparticles from polymers or small molecules.[64–66] This process is easy to set up and allows to form loaded NPs down to 10 nm of diameter. Hydrophobic, or at least partially water insoluble, materials (contrast agent or drug and polymer) are generally dissolved in a water miscible organic solvent. Upon mixing with water, they become insoluble and phase separation occurs, which can under certain conditions lead to the formation of NPs. For this reason, nanoprecipitation is sometime called solvent displacement method. The composition of the system solute-solvent-non solvent may be represented as a ternary diagram (Figure 7). It shows the different thermodynamic states possible for the system depending on its composition.

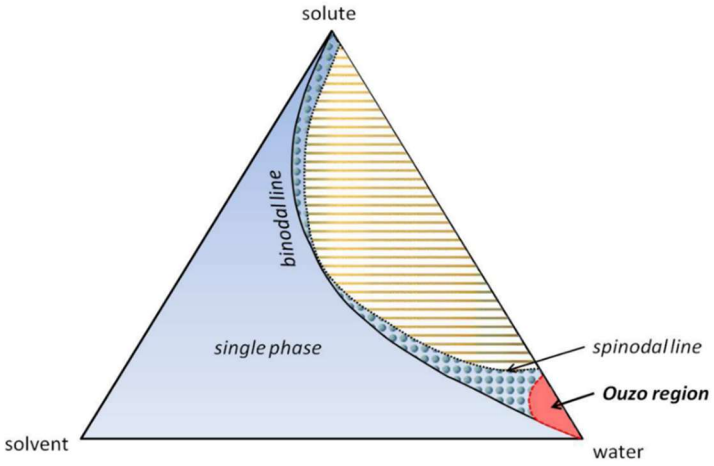

Figure 7: Phase diagram for a solute-solvent-water ternary mixture when the solute is not soluble in water[67].

In the case of nanoprecipitation,[65,68] the system is originally a mixture of a hydrophobic solute (polymer and load) and solvent. Above the binodal line (blue part of the diagram), the system only has one phase. When the water (non-solvent) content is increased, the global solvent quality decreases and the system crosses the binodal line, corresponding to the solubility limit. This system is called supersaturated (Equation 1), where the supersaturation value S is defined as:

$$S = \frac{[polymer]}{[polymer\ solubility]} \qquad \text{(Equation 1)}$$

with [polymer] the polymer (and/or load) concentration and [polymer solubility] its equilibrium solubility limit. Supersaturation is the driving force for phase separation. The formation of nanoparticles only occurs in a small region in-between the binodal (solubility limit) and the spinodal (stability limit) curve, the so-called "Ouzo-region", in which spontaneous emulsification is observed, leading to formation of kinetically stable particles.[69,70] The "Ouzo-region" is characterized by low polymer concentration and high water to solvent ratio. The absence of entanglements of the polymer chains in this region was noted,[69] even though at relatively low polymer concentrations entanglement effects seem to be of minor importance.[71] Beyond the spinodal curve the instability typically leads to rapid aggregation and macroscopic phase separation. The system undergoes spinodal decomposition and becomes heterogeneous. In the case of small organic molecules, reaching the "ouzo region" spontaneously leads to the formation of an emulsion as it is the case with anethol, water and ethanol, present in the Ouzo beverage. The amount of polymer, solvent and water employed have to be carefully chosen in order

to have a final system in this domain of the ternary diagram. For this reason, relatively low amounts of polymer are dissolved in the organic phase (generally between 1 to 10 $g.L^{-1}$). One must remember that the phase diagram in Figure 11 describes a system where the solute is a hydrophobic molecule. Polymers are a more complex system since polymer chains may adopt various configurations and physically interact with each other.

Ternary diagrams allow to understand the driving force of nanoprecipitation with a thermodynamic approach of the phenomenon, explaining phase separation and formation of NPs as well as to visualize the localization of the Ouzo region. A related view, showing the global procedure of nanoprecipitation is presented in Figure 8[72]: The system starts with the load and polymer dissolved in the organic phase at their initial concentration $C_{o,0}$ $C_{p,0}$. Upon mixing with the aqueous phase the water fraction ξ increases. Here, first the load reaches its solubility limit at ξ_o, then the polymer at ξ_p, and finally a 1 to 1 mixture of organic and aqueous phase is obtained corresponding to a final composition of $\xi_{mix} = 0.5$.

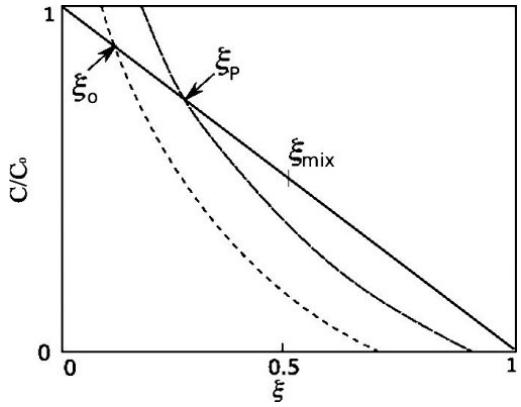

Figure 8: Representation of nanoprecipitation in terms of the water fraction ξ. The dashed and closed curves give the solubility limit of the load and polymer, respectively. The straight line represents a typical nanoprecipitation process: C and C_0 correspond to the current and initial concentration of load and/or polymer. ξ_o and ξ_p are the solubility limits of the load and polymer, respectively, ξ_{mix} is the final composition after mixing.

We have treated the system up to now from a thermodynamic point of view. However, it is well known that nanoprecipitation is a kinetically controlled process.[64,68,73] This comes from the circumstances that in the Ouzo region the system is metastable and that the obtained "final" state is only kinetically stable. In consequence, it depends on how the formation of the colloids, the nanoprecipitation, occurs, and, for example, the mixing speed has a large influence on particle formation.[73] Moreover, it has been shown that NPs formed by nanoprecipitation don't exchange unimer contrary to polymeric micelles[74]. This means that they are not in dynamic equilibrium or, said differently, that

they are kinetically frozen. Therefore, different approaches have been developed to understand the mechanism of nanoprecipitation and explain the relations between the size of the particles obtained by nanoprecipitation and the process parameters (mixing rates, concentration of polymers, solvent involved…).

A first approach is to describe the formation of NPs as a nucleation and growth process, as for example by Johnson and Prud'homme,[75] based on classical nucleation and growth theory, which has originally been developed for crystallization processes.[76–79] In this model, once supersaturation is achieved, spontaneous, homogeneous nucleation occurs through local concentration fluctuations or diffusion controlled encounter of the precipitating molecules. Association of molecules creating a new phase leads on the one hand to an increase in free energy due to surface energy and on the other hand to a decrease in free energy due to hydrophobic or attractive interactions between the molecules. Once a critical radius r_c is reached, a stable nucleus forms (Equation 2).

$$r_c = \frac{2\gamma\tilde{v}}{k_B \mathrm{T} \ln(1+S)} \qquad \text{(Equation 2)}$$

With γ the surface energy, ν the molecular volume and k_B Boltzmann constant. A nucleation rate, corresponding to number of newly formed nuclei with time, can be determined according to equation 3:[80]

$$N = \frac{2D}{d^5} \exp\left(-\frac{16\pi\gamma^3\tilde{v}^2}{3k_B^3 \mathrm{T}^3 [\ln(S)]^2}\right) \qquad \text{(Equation 3)}$$

Where D is the diffusion coefficient of the polymer and d its molecular diameter. Particle growth is then considered to occur with a rate depending on diffusional processes and the probability of integration into the particle. Aggregation between particles is considered to be a separate process. In this model, the final particle size and size distribution strongly depends on the relative rates of nucleation, growth, and aggregation. Fast nucleation, with respect to growth, leads to the formation of a large number of growing nuclei and thus results in smaller particles. The width of the size distribution depends on the overlap of nucleation and growth. In the case where nucleation is very rapid compared to growth, the nucleation phase is terminated before appreciable growth. Then all particles grow in parallel, which should lead to a very narrow size distribution, similar to what is achieved in living polymerization processes. In principle, growth in this

model stops once all the free polymers are consumed (or more precisely, when supersaturation has vanished). From this point on, increase in particle size only occurs through combination of existing particles, that is through aggregation. The rate of aggregation strongly depends on the stabilization of particles. Typically, a ζ-potential of +/- 30 mV is considered sufficient to slow down aggregation.

A second approach is to consider particle formation in nanoprecipitation as diffusion limited aggregation using a population balance equation. [72,81,82] Kinetics of such a system are based originally on Smoluchowski, who described it as occurring from binary collisions (reactions) of hard spheres, which stick together when they come into contact. The frequency of their encounter is based on Brownian diffusion. The associated rate constant is in this case practically independent of particle size (independent for similar sizes and only slight dependence for very unsimilar ones) and only depends on temperature and viscosity. This model was extended later on by Fuchs, to take into account an interaction potential between approaching particles, that modify the encounter frequency and efficiency. In particular, attractive van-der-Waals interactions and repulsive electrostatic interactions, based on DLVO theory, are taken into account, but other types of interactions as steric repulsion can also be considered. Population balance equation modeling then allows evaluating the kinetics of aggregation of such systems. An example of its application to nanoprecipitation of polymer and load was proposed by Cheng et al.,[72] based on a previous model for formation of block copolymer micelles.[83] In such an approach, the polymer chains (and the load molecules) are considered as unimer particles using an aggregation kernel that takes into account attractive and repulsive forces between particles. Stabilization of growing particles comes from steric stabilization through hydrophilic polymer chains (blocks). Interestingly, they evidenced that the number of free chains (unimers) during precipitation decreases very rapidly, suggesting that growth of particles relies mainly on the fusion of polymer aggregates (Figure 9). Accordingly to previous models, they found that the energy barrier to aggregates fusion has a crucial role in growth limitation of the particles and so in the final size distribution.

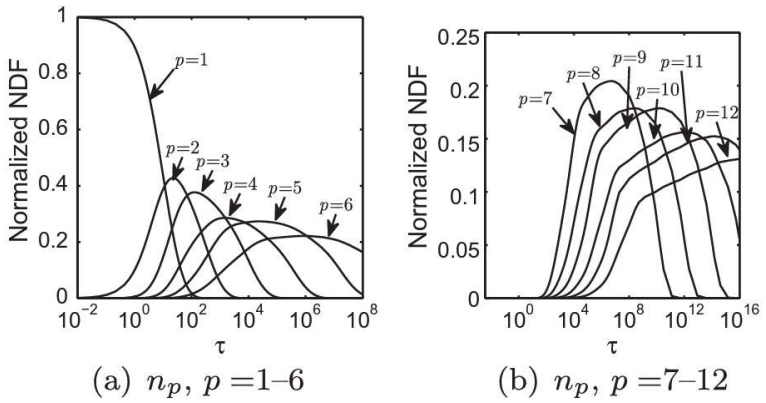

Figure 9: Normalized number density for aggregates (NDF) of p polymer chains versus time modelled for nanoprecipitation[72].

In this model, the presence of organic molecules does not perturb the particle size distribution (PSD), whereas precipitated alone, the organic compound lead to a broad PSD. This was explained by the presence of the copolymer, in particular the tendency of organic molecules to attach to the hydrophobic block in the early stage of precipitation.

A third approach to understand particle formation is taken by molecular dynamics simulations, which has the particular advantage that system parameters can be selectively studied.[84,85] However, due to the complexity of such systems only few polymer chains and short times can typically be simulated. Nikoubashman et al. simulated formation of NPs from polymers in the absence of stabilizing agents.[84] On the level of a single polymer chain, a decrease in solvent quality (corresponding to mixing with the aqueous phase) led to a rapid collapse of the chain. For instantaneous mixing, this happens on a time scale of the order of 2 ns, but this time increases with increasing mixing time. Multiple polymer chains then aggregated in the further course of the simulation. In the absence of charges, aggregates grew to an infinite size, but in the presence of charges, particles with a finite size were obtained. The characteristic time scale for aggregation was governed by diffusion, with the contact time of the order of 0.1 to 0.6 µs, depending on polymer concentration. The final NP size increased with increasing concentration and less negative ζ-potential. It is supposed that the speed of mixing influences the particle size when the collapse time becomes much larger than the contact time. To reach longer time scales molecular dynamics simulation, yielding microscopic details, were then combined with kinetic Monte Carlo simulations to access the particle growth process.[85] The results evidenced a fast growth regime while the surface charge is still low, followed by a slow growth regime when sufficient surface charge has built up.

Interestingly, neither diffusion limited aggregation models nor simulations evidenced a specific nucleation phase or even the formation of nuclei in the case of nanoprecipitation of polymers. In both approaches the stabilization mechanism is key in explaining the final particle size, whether this is brought about by electrostatic or steric repulsion. In general, increasing concentration leads to increasing particle sizes as it increases the speed (or frequency) of encounters due to diffusion and in this way the growth speed. The influence of mixing becomes apparently significant when it leads to an overlap of single chain reorganization and aggregation of several chains.

Despite all the insights provided by these models, there is still a lot of work to precisely characterize polymer nanoprecipitation. For example, the chain collapse process that occurs in the early stage of nanoprecipitation is rarely mentioned in dedicated reviews. Moreover, most of the studies focus on the precipitation of block copolymers leading to a lack of knowledge concerning statistical copolymers. Because nanoprecipitation of polymers is widely used, these models have been confronted to experimental results numerous times. Effects of process parameters such as mixing rates, polymer concentration or solvents used are usually in good agreement with models. However, systematic studies on the effects of polymer chemistry on nanoprecipitation kinetics are rarer. Unfortunately, the important effects of the other parameters make the comparison of the results from different studies hazardous. The following section briefly covers the stabilization processes involved during NPs formation then the effect of polymer chemistry on the final state of the system are discussed.

3.2 Influences on particle properties in nanoprecipitation

Among the most important properties that define the suitability of loaded polymer NPs for biomedical applications are notably their size and size distribution, their surface properties, as well as their loading capacity and the speed of release. Size and size distribution have important implications for the distribution of particles in biological systems, ranging from their access to different parts of the body to the way of their excretion,[86] but also their interaction and internalization in cells.[87] The NP surface not only defines the stability of the particles over time and in different media, but also how they interact with biological systems, notably as it influences the formation of the so called protein corona.[88] Encapsulation and release of active compounds are of prime

importance for the pharmaco-kinetics following uptake of NPs, but also for example for their performance as contrast agents, [89] as in the case of fluorescent dye-loaded polymer NPs.[6] In the following, the influence of several major parameters of nanoprecipitation on these properties will be discussed.[64,66,78,80]

3.2.1 Concentrations and compositions:

A first parameter having a clear influence on the particle size is the polymer concentration in the organic phase. The higher the concentration the bigger the resulting NPs.[66,80,84,90,91] This is typically explained by increasing supersaturation and reduced diffusion lengths, which increase the driving force and the encounter frequency, respectively. At high concentrations the limit is imposed by the limit of the Ouzo region, where macroscopic aggregation starts. At low concentrations, this also leads to low concentrations of NPs, which can be a severe drawback for certain applications. Besides the concentration, the fraction of organic phase also can play a significant role, with bigger particles obtained for higher organic phase fractions.[91] Furthermore, the presence (or absence) of stabilizers and their concentration can have an important influence on NP formation in nanoprecipitation.

3.2.2 Solvent:

The organic water miscible solvent used to dissolve the polymer and the load also has a significant influence on the obtained NPs. Different solvent parameters have been found that could influence the final NP size. For example, particle size increased with the solvent water interaction parameter χ, that is the smallest NPs were formed for the best water solvent interactions (in this case ethanol).[92] Bovone *et al.* [93] notably established for various solvents a critical water fraction of growth arrest (Φ_c) corresponding to a solvent composition at which the assembly of polymer chains is stopped. In the model they developed, the size of the NPs depends on the time taken to kinetically freeze the nanostructures, i.e. prevent any growth by unimer addition or particle aggregation. This point was defined as "the critical water fraction of growth arrest, Φ_c" and was measured by turbidimetry of polymer solutions undergoing successive additions of water. Acetone, ACN, THF, DMF and DMSO were tested and particle size was found to increase proportionally to Φ_c (Figure 10). The size of the NPs also increased with the concentration of the polymer in the organic solution.

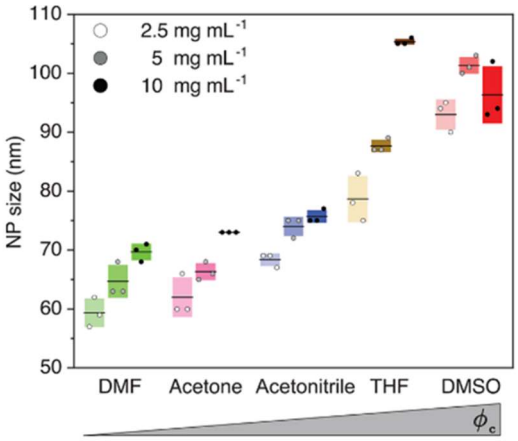

Figure 10: NPs size of PEG-b-PLA precipitated in solvents ranked by increasing critical water fraction of growth arrest Φ_c [93].

3.2.3 Mixing:

The kinetic control of nanoprecipitation has the consequence that the way and speed of mixing of the organic and aqueous phase have a strong influence on particle formation.[64,73,94] Typically, it has been observed that improved mixing leads in general to smaller NPs with narrower size distributions.[64,94] In consequence, mixing parameters were strongly improved, from dropwise addition to the use of specifically designed mixers using collision of flows or herringbone mixers. [73,95–97] Nanoprecipitation using fast mixing was termed flash nanoprecipitation. Fast mixing means that the change in solvent quality is very rapid and, in consequence, that the system rapidly reaches a high supersaturation. In terms of Figure 8, this means that the system rapidly evolves to high water fraction ξ_{mix}. Mixing speed has been increased experimentally by increasing the flow rate in impact jet mixers. The results showed a decrease in particle size up to a certain limit, from where on further increase in mixing speed did not lead to smaller NPs.[75] This was interpreted as the mixing time becoming of the same magnitude as the aggregation time. Not only the particle size, but also encapsulation depends on the mixing speed, as evidenced by increasing fluorescence quantum yields (QY) with increasing flow rates.[98]

Whereas the choice of the solvent might be restricted due to the polymer and load solubility, flash nanoprecipitation appears as the most effective technique to obtain small NPs. Repeating the experiment presented in Figure 10 with a coaxial jet mixer decreased the size of the NPs of roughly 20%, conserving the same trend depending on Φ_c. The

explanation relies in the mixing time of the two phases which is greatly reduced with the use of microfluidic mixers. This leads to a decrease in the time required to reach Φ_c, thus stopping the growth of the nanoparticles earlier.

3.2.4 Polymer chemistry:

A further parameter that has an important influence on the properties of the obtained NPs is the chemical nature of the polymer. This point has rarely been studied systematically, however, several results from the literature allow to interfere some major influences. As we have seen above, the growth and/or aggregation of particles is stopped once these reach a sufficient kinetic stability. During nanoprecipitation, NP stability is ensured either by charge or steric repulsion. Species responsible for stabilization can be incorporated in the polymer chain or, in some cases, surfactants are used as additive in the nanoparticle formulation. Because the presence of surfactant hides the influence of polymer chemistry, only surfactant-free systems will be discussed here. In the following we will, therefore, first explain electrostatic and steric repulsion before discussing the influence of various aspects of polymer chemistry.

Steric stabilization:

Steric stabilization relies on the use of a solvated segment of polymer linked to the nanoparticle in order to stabilize it thanks to steric hindrance. For this purpose, diblock or triblock polymers are the most used architectures. Commonly used blocks to stabilize NPs in water are PEG, poly(vinyl alcohol) (PVA), poly(hydroxyethyl methacrylate) (PHEMA), polyacrylamide (PAAm), dextran and polyvinylpyrrolidone (PVP). Steric stabilization is especially useful in environments with high ionic strength or in organic solvents because electrostatic stabilization is not effective in these conditions. It is also efficient independently of the NP concentration, allows reversible flocculation and is more efficient after a freeze thaw procedure[99].

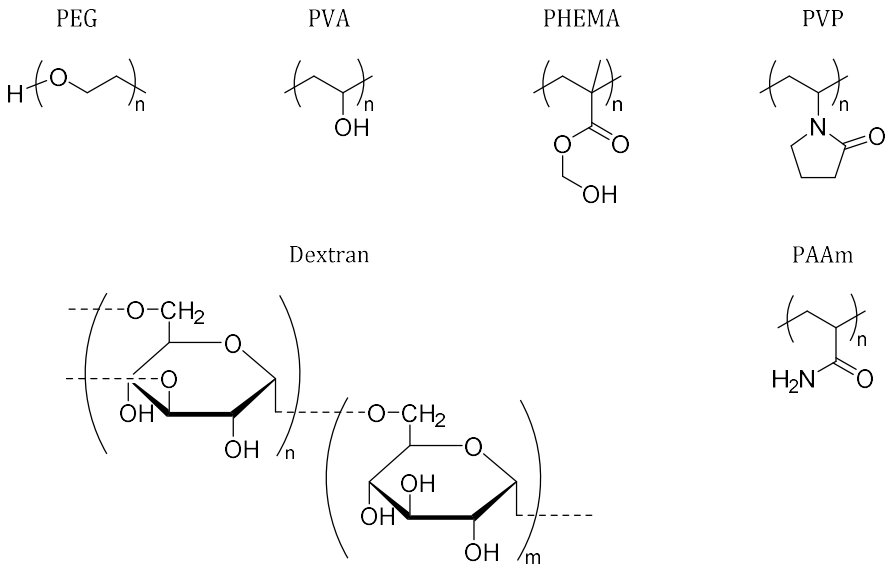

Figure 11: Commonly used polymers for steric stabilization of NPs.

Steric stabilization is "short distance" stabilization. The thickness of the steric layer L is equal to the radius of gyration of the polymer chain for low grafting densities and approaches the contour length (L) for high grafting densities. If the distance d between two particle cores is > 2L there is no steric interaction between the particles. If L < d < 2L, polymer chain may undergo segmental interpenetration, which reduces the number of conformation they can adopt. This decrease the entropy of the system therefore this state is not thermodynamically favorable and particles will move away from each other to reduce this effect. Finally, if d<L, both compression and interpenetration may occur[100] (Figure 12).

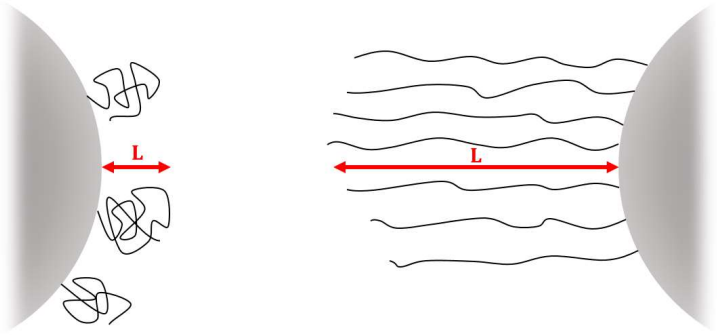

Figure 12: Schematic view of the possible conformations of hydrophilic polymer chains on the surface of a NP depending on the grafting density adapted from ref[101].

Electrostatic stabilization:

Electrostatic stabilization of NPs relies on repulsive Coulomb forces between charged groups on their surface. These charges usually come from a small amount of monomers added in the hydrophobic polymer chain during polymerization. They may be located at the end of polymer chains, statistically distributed or segregated in the case of block copolymers. Methacrylic / acrylic acid, primary amine bearing monomers, ammonium and sulfonate salts are commonly used for this purpose[90,102,103] (Figure 13).

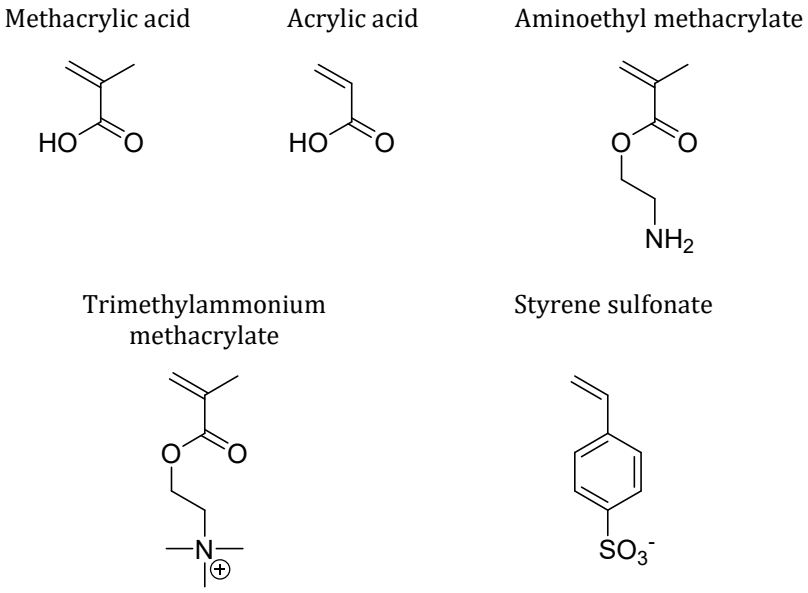

Figure 13: Commonly used monomers for electrostatic stabilization.

Unlike sterically stabilized NPs, repulsion occurs before particles enter in contact due to electrostatic repulsion. Stability conditions are given by the Derjaguin-Landau-Verwey-Overbeek (DLVO) theory[104]. The repulsive electrostatic forces are in competition with van der Waals attractive forces. Both forces are notably dependent on the distance between particles and the potential energy of two identical particles may be expressed in respect to this parameter (Figure 14). When the interaction energy is positive, repulsive forces are predominant ensuring colloidal stability of the system. However, if this energy barrier is crossed into the primary minimum, irreversible agglomeration of the particles occurs.

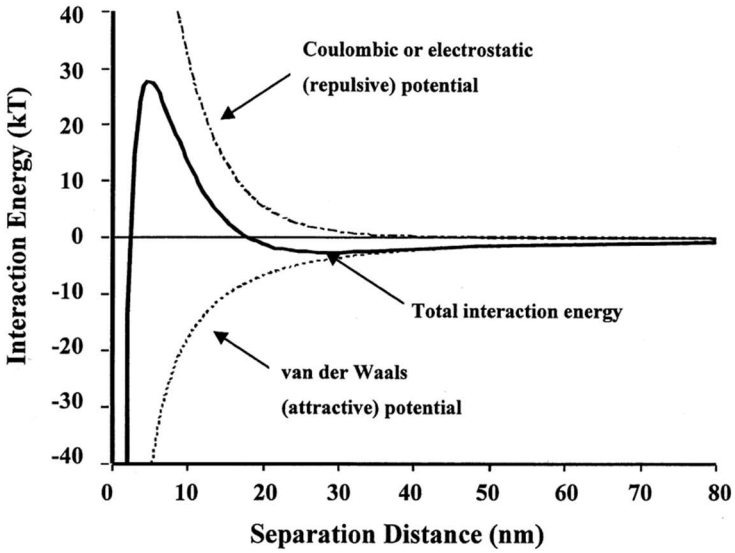

Figure 14: Schematic interaction energy versus distance profiles of DLVO interaction[104].

A way to determine the strength of electrostatic forces is to measure the ζ-potential of the particles (see method section). High ζ-potential (greater than 40 mV) ensures a long time stability of the particles[105]. Otherwise, the repulsive force between particles may be too weak to prevent aggregation. This is likely what is happening in the early stage of nanoprecipitation. Collapsed chains aggregates until the resulting particles have a ζ-potential too high to allow further aggregation or unimer insertion. The ζ-potential of particles may be pH dependent if charged groups come from acidic or basic functions. In this case the stability of the dispersion will be pH sensitive as protonation (or deprotonation) of such group will remove its charge.

Electrostatic stabilization is highly impacted by the concentration of electrolytes in solution. The presence of ions has a screening effect on the charge, reducing the range of the electrostatic potential[106] (Figure 15). Multivalent ions may have a strong impact on the stability of dispersion resulting in rapid aggregation even at low concentrations[107].

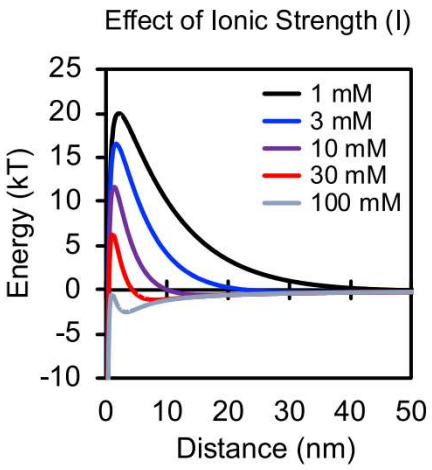

Figure 15: Computed DLVO interaction potentials of two spherical particles in water with variation of ionic strengths.

Molecular weight

The overall molecular weight of the polymers does not seem to have a major influence on particle size within the studied range[108,109]. Typically, somewhat smaller NPs are obtained for lower molecular weight,[80,90] but this might actually be linked to other parameters like number of end groups or changes in diffusion behavior. In the case of biodegradable polymers, it should be noted that a lower molecular weight might increase the degradation rate of the particles, leading to a faster release of their load[110]. However, this parameter can be controlled otherwise[111]. Overall, the molecular weight of the polymers used in nanoprecipitation does not appear as a key parameter.

Hydrophobicity

The influence of the overall hydrophobicity of the polymers has been rarely studied in detail. In one study from our group this point has been addressed by varying systematically the composition of statistical copolymers. [13] Typically, HEMA was used as hydrophilic monomer and combined with different hydrophobic methacrylates in varying proportions, while including a small amount of charged monomers (Figure 16). Increasing the overall hydrophobicity either by increasing the fraction of the hydrophobic monomer or by increasing its hydrophobicity led to an increase in the size of the obtained NPs. At the same time, hydrophobicity also influenced encapsulation, as evidenced by increasing fluorescence quantum yield with increasing polymer hydrophobicity.

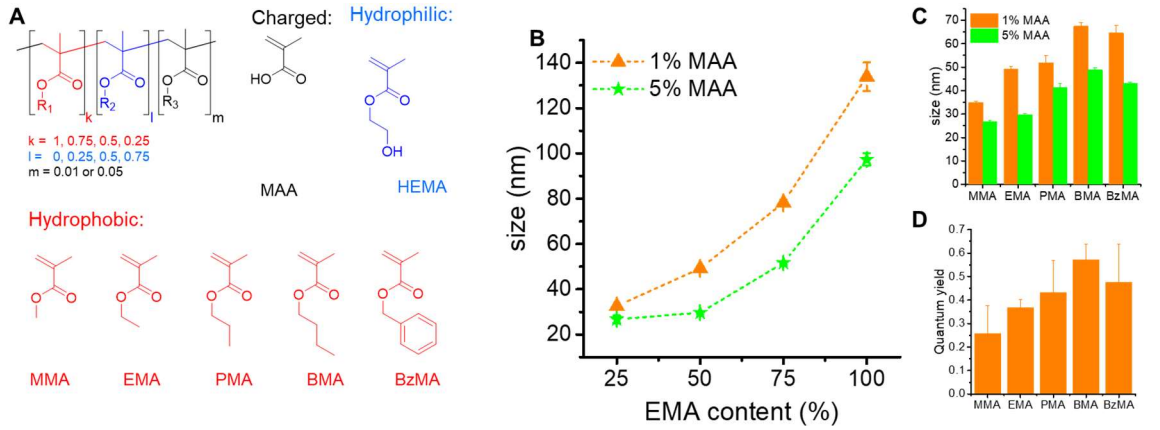

Figure 16: Influence of polymer hydrophobicity on NP formation. A) Some monomers used in the design of copolymers. Typically, one charged, one hydrophilic, and one hydrophobic monomer were combined in different ratios to synthesize the copolymer. B, C) Influence of copolymer composition on size of particles obtained through nanoprecipitation: (B) Influence of ratio of monomers for HEMA/EMA/MAA copolymers. (C) Influence of the type of hydrophobic monomer for copolymers with HEMA (50 mol%) and MAA. D) Fluorescence quantum yields of NPs made from different copolymers and loaded with 10 wt% of R18/F5-TPB. Influence of type of hydrophobic monomer for copolymers with HEMA (50 mol%) and MAA (1 mol%).

The impact on NPs size was attributed to a difference of surface tension of growing particles, which is greater in the case of hydrophobic polymers. Lower QYs are typically due to aggregation caused quenching (ACQ), suggesting higher dye aggregation when they were precipitated with more hydrophilic polymers. This could be explained by a difference between the speed of precipitation of the dye salt and the polymer. Indeed, the dye alone can precipitate and even form NPs. The precipitation of the dyes is presumably faster than the most hydrophilic polymers, leading to their clustering and hence a reduced QY. NPs formed with PLA, PLGA or PCL also showed different encapsulation efficiencies based on the polymer used and the hydrophobicity of the load[112,113], underlying the importance of these parameters on the formation of polymeric NPs through nanoprecipitation.

Block copolymer composition

The use of block copolymers for the preparation of NPs is a distinct case, where the nature of the hydrophilic and hydrophobic block, as well as their relative (and absolute) length have to be considered. In these systems the hydrophilic block is most often PEG and it often directly serves the stabilization of the particles through steric repulsion by forming a shell around the NPs.

As a consequence, increasing the size of the hydrophilic block should increase the size of the particles, with an exacerbated effect if the chains are fully extended. This effect is very clear in the case of NPs which were formed, then coated with PEG of different chain lengths, because the size of the core of the NPs remains constant. Rahme et al. have evidenced this phenomenon with gold NPs with a mean diameter of 15 nm which were coated with mPEG-SH. The resulting diameter of NPs varied from 25 to 90 nm for a PEG M_w of 1000 and 50 000 g.mol^{-1} respectively[114]. However, the case of block copolymer NPs obtained by precipitation is more complex because the modification of the hydrophilic block also influences the formation process of the NPs. Gu et al studied the formation of NPs with a block copolymer made of PLGA, PEG and an aptamer[27]. They found that reducing PEG M_w from 10 000 to 5000 g.mol^{-1} decreased the size of the NPs they obtained from 290 to 160 nm, whereas PLGA M_w had no influence on particle size. However, fully extended PEG chain of 5000 and 10000 g.mol^{-1} are 40 and 80 nm long respectively. Then

a difference of diameter > 80 nm cannot be explained uniquely by a change in size of the hydrophilic layer.

In another study, Zhu et al. formed nanoparticles by flash nanoprecipitation of a diblock polymer with a PEG moiety of 5000 $g.mol^{-1}$ and a hydrophobic block of 10000 $g.mol^{-1}$ made of PS or PLGA[113]. Therefore, the length of the PEG block as well as the size ratio of the two blocks were constant. Yet, the particles formed with PS had a diameter of 32 nm whereas with the PLGA they had a diameter of 62 nm. This has been attributed to a higher hydrophobicity of the PS block. Other studies have reported a similar trend when investigating the influence of the hydrophobic block. In view of these results, the ratio between the length of the PEG and hydrophobic block seems to have a negligible impact on the size of NPs obtained by precipitation, whereas it is known that it influences the geometry of objects obtained by self-assembly[62,115] (under thermodynamic control), and their size as it is the case for polymer micelles[116,117]. This demonstrate the importance of polymer chemistry of both blocks on the size of NPs during the nanoprecipitation process.

Several polymers are commonly used as insoluble moiety in block copolymers such as PLGA, PLA, PCL, PS, PMMA and PEMA (Figure 17). Their different hydrophobicity may be used to tune the size of the NPs obtained by nanoprecipitation.

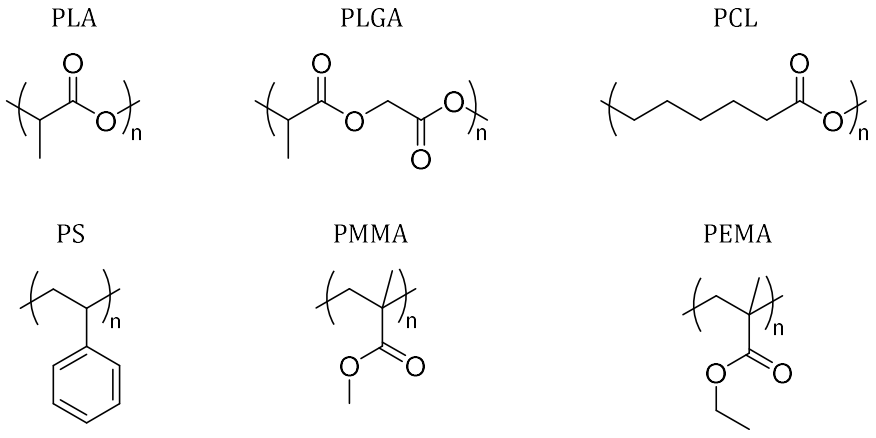

Figure 17: Commonly used hydrophobic blocks in amphiphilic polymers.

Nevertheless, in some cases the choice of the hydrophobic block used cannot be based only on the size of the NPs formed after precipitation. Indeed, their nature also influence other particle properties. Among the polymers presented, only PLA, PLGA and PCL are biodegradable, which is an important property for drug delivery systems because it allows to release the drug upon particle degradation. Moreover, the degradation rate of

the particles can be tuned by changing the nature of the hydrophobic polymer. For instance, PLGA 50-50 is known to be the fastest ratio for PLGA to decompose, while increasing the lactic acid amount allows to slow down the degradation process[118,119] (Glycolic acid amount is rarely superior to 50% due to the crystallinity of the polymer obtained[120]). The nature of the hydrophobic polymer also influences the encapsulation efficiency and the stability of NPs obtained by nanoprecipitation. PLGA-b-PEG for example, was found to be a better choice than PLA-b-PEG or PCL-b-PEG to form stable NPs encapsulating β-carotene. This was attributed to the high Tg of PLGA and its non-crystalline behavior[63,113]. Finally, the impact of polymer chemistry, including the nature of the hydrophobic block, also has a critical influence on the in vivo circulation time of NPs as demonstrated by d'Addio et al[14].

Charged groups

The presence of charged groups on the polymers can have a strong effect on the size of NPs obtained through nanoprecipitation. Several studies have shown that the simple presence of a small amount of charged groups, e.g. as end-groups of the polymer, leads to a significant reduction in particle size.[90,121,122] The amount, or percentage, of charged groups on the polymer chain is directly related to the obtained NP size. For example, increasing the amount of sulfonate groups to 5 mol% led to a reduction in particle size to less than 10 nm.[52] A further increase in the fraction of charged groups did not lead to a further reduction in size, which can be related either to the fact, that it would require formation of single-chain NPs, or due to changes in the overall solubility of the polymer. The strong effect of charged groups has been evidenced for various negatively (sulfonate, carboxylate) as well as positively (amine, trimethylammonium) charged groups.[52,90] It seems to apply to many types of polymer backbones and requires only small fractions of charged groups, typically below 10 mol%. However, the extent of size reduction depends on the type of charged group: Polymers containing one percent of sulfonate or ammonium salt groups lead to the formation of very small NPs (~10 nm), indicating that these groups provide very good electrostatic stabilization (Figure 18). In contrast the same amount of carboxylic acid groups gave larger NPs (>50 nm). This was attributed to partial deprotonation of acids in the precipitation conditions, reducing the effective amount of charges available for stabilization.

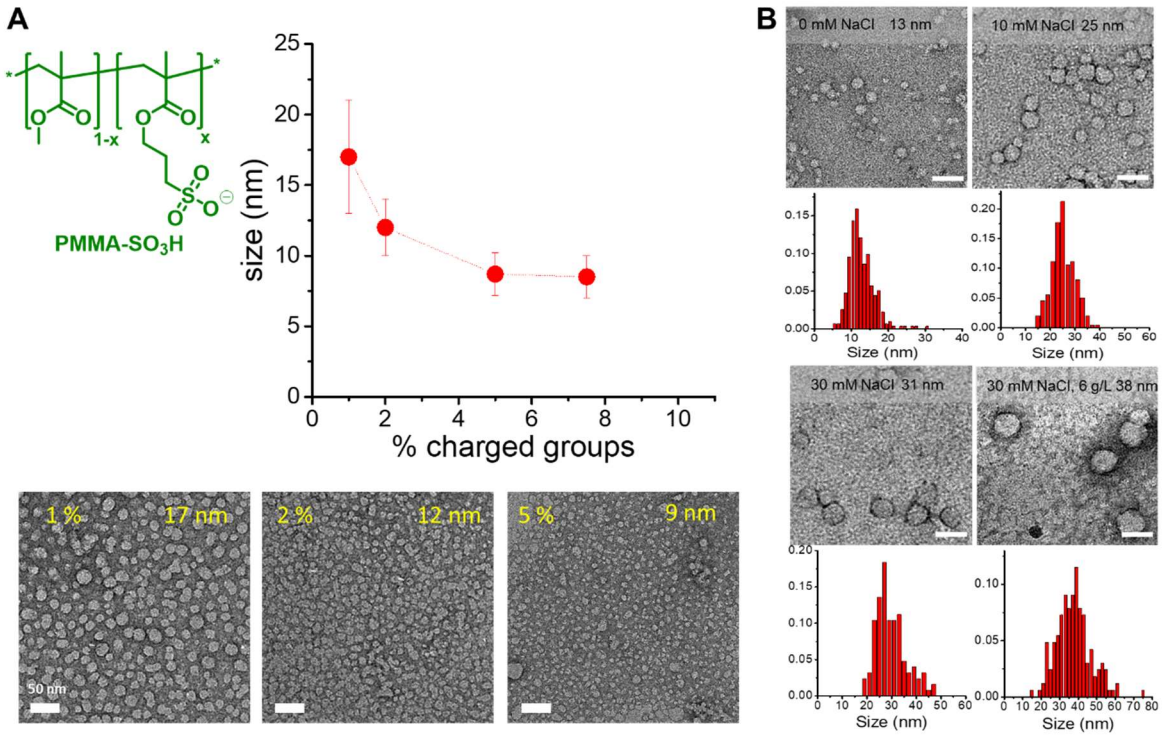

Figure 18: Influence of charged groups on NPs formed through nanoprecipitation. A) Size as obtained by TEM imaging depending on percentage of sulfonate groups in methacrylate polymers.[52] B) Influence of ionic force and concentration on the formation of NPs from sulfonate bearing methacrylate polymers (PEMA-SO_3 1%). TEM micrographs, mean sizes, and size histograms are given[123].

In case of NPs stabilized through electrostatic interactions, the aqueous medium used during precipitation has also a major influence on the size of the formed NPs. For example, in the case of carboxylate bearing polymers the presence of a buffer, or more generally the pH of the aqueous phase can change the particle size.[90,124] Particles made in phosphate buffer at pH 7.4 were markedly smaller than NPs made in MillliQ water,[52] and the size could be further reduced by using a borate buffer at pH 9.[124] The fact that electrostatic interactions can be screened through the presence of small ions can further be used to fine tune the particle size. Sulfonate bearing polymers gave increasingly bigger NPs when the NaCl concentration in the aqueous phase was increased.[123]

4 Objectives

Polymeric NPs are a promising tool for nanomedicine: their small size allows to access to the whole organism, the functionalization of their surface grants them stability and specificity, and their ability to encapsulate compounds make them versatile in the domains of imaging and therapy. Nanoprecipitation is among the most used process to

form NPs dedicated to biomedical applications. Indeed, it is easily scalable thanks to microfluidic devices and many parameters may be adjusted to tune the properties of the NPs. Adjusting these parameters requires a good control and understanding over the NPs formation process. Polymer chemistry has notably a marked influence on the formation of NPs. However, its precise role and interactions during nanoprecipitation are not elucidated yet.

In the first place, we wanted to better understand the influence of polymer chemistry during nanoprecipitation, particularly in respect to the mixing. This led us to study in more details the kinetics of particle formation with various polymers. We followed up by investigating the influence of polymer architecture on nanoprecipitation. For this, we synthesized different block copolymers and observed the size and encapsulation properties of the particles they formed. The final objective was to use the insights brought by these studies to formulate nanoparticles with unique properties thanks to the kinetically controlled aspect of nanoprecipitation.

Materials and methods

1 Materials

Ethyl methacrylate (EMA, 99%, Ref. 234893), methacrylic acid (MAA, 99%, Ref. 155721), 3-sulfopropyl methacrylate potassium salt (SO_3, 98%, Ref 251658), [2-(Methacryloyloxy) ethyl]trimethylammonium chloride solution (NMe_3, 80 wt% in water, Ref. 408,107), 2-(dimethylamino)ethyl methacrylate (NMe_2 98%, Ref 234907), 2-hydroxyethyl methacrylate (HEMA, 99%, Ref 477028), pentafluorophenyl methacrylate (PF5, 95%, Ref 741108), 2-Cyano-2-propyl benzodithiodate (97%, Ref 722987), N-Boc-hexanediamine (98%, Ref 79229), Sephadex LH-20 (Ref 17-0090-02) were purchased from Sigma-Aldrich. Azobis isobutyronitrile (Aldrich, 98%, Ref. 408107) was recrystallized twice from ethanol.

Triethylamine (TEA, 99%), was purchased from sigma Aldrich. Dimethylformamide (DMF, analytical grade), dimethylsulfoxide (DMSO, analytical grade), dichloromethane (DCM, analytical grade), methanol (MeOH, analytical grade), ethanol (EtOH, analytical grade) and acetonitrile (ACN, analytical grade) were purchased from Carlo Erba.

R18/F5-TPB was synthesized from rhodamine B octadecyl ester perchlorate (Sigma-Aldrich, >98.0%) and lithium tetrakis(penta fluorophenyl)borate ethyl etherate (Alfa Aesar, 97%) through ion exchange followed by purification through column chromatography according to the method previously described. MemBright-488 and the amine functionalized bodipy were kindly provided by Mayeul Collot.

Dulbecco's modified eagle medium (DMEM), fetal bovine serum (FBS), antibiotic solution (penicillin-strepomycine, Gibco-Invitrogen), L-Glutamine and trypsine were used for the culture of HeLa Cells. Cellular imaging was made using μ-Dish 35 mm, high Glass bottom plates from Ibidi.

2 Index of polymers

Many different polymers have been used during this thesis work. The goal of this section is to provide to the reader an overview of all the polymers along with the name and scheme used to refer to them. Polymers are presented in the order of appearance throughout the chapters.

PEMA-COOH x%

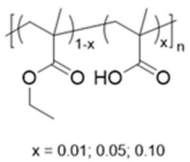

PEMA-HEMA

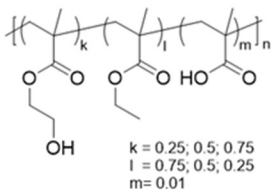

P(EMA-b-HEMA)

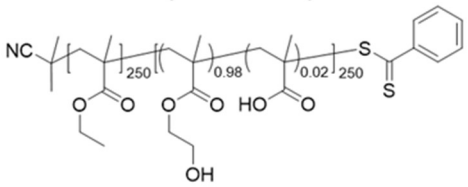

PLA

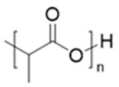

PLGA

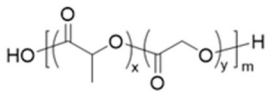

PEG-b-PLGA

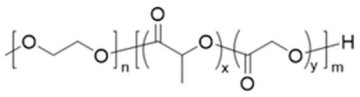

Bodipy functionalized PEMA-HEMA

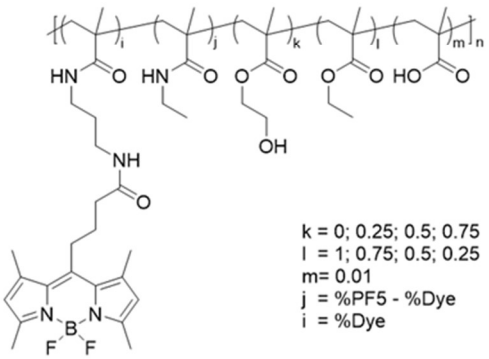

Rhodamine functionalized PEMA-HEMA

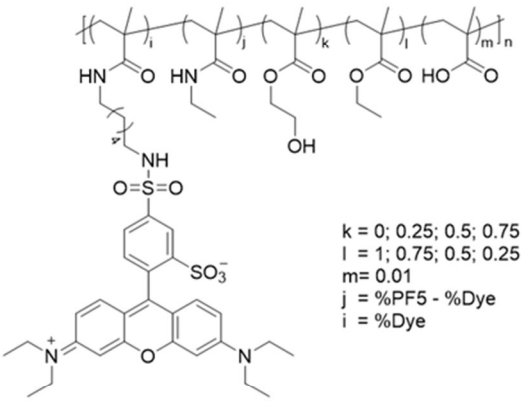

P1stat-COOH

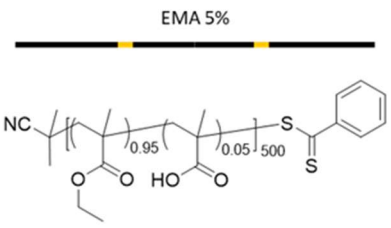

P2block-COOH

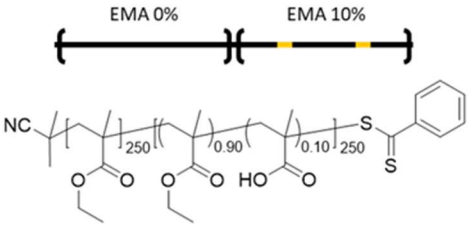

P3block-COOH

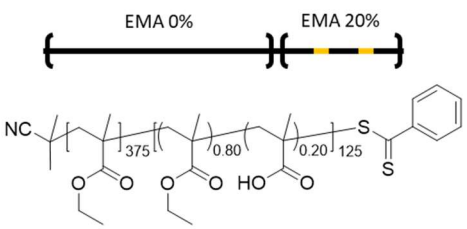

P4block-COOH

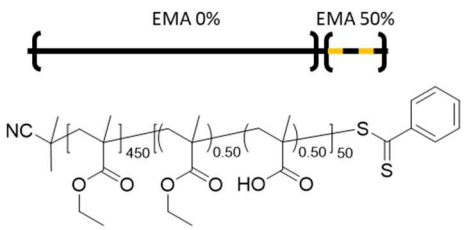

NMe_2 stat

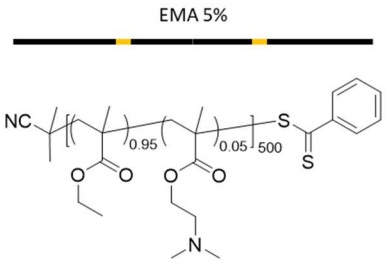

NMe_2 block

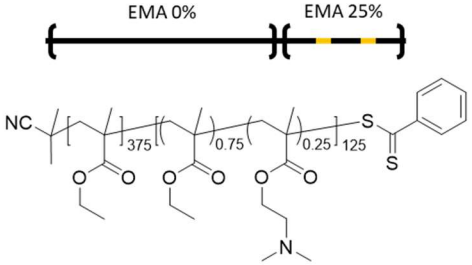

NMe_3^+ stat

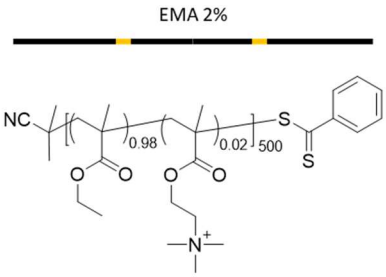

NMe_3^+ block

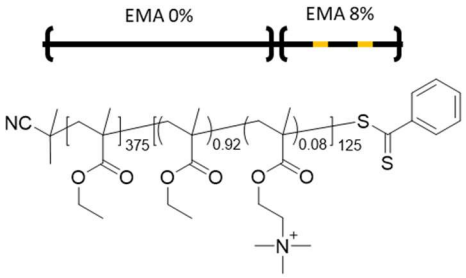

SO_3^- stat

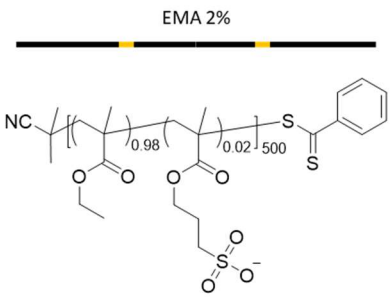

SO_3^- block

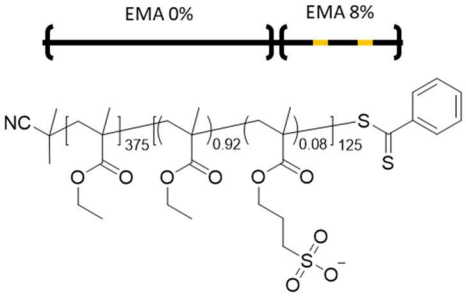

P5

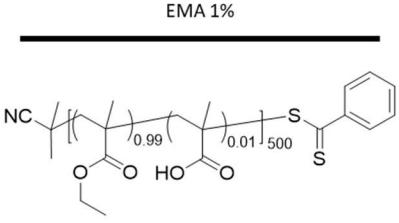

P6s

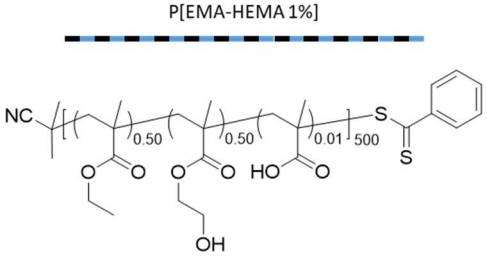

P7b

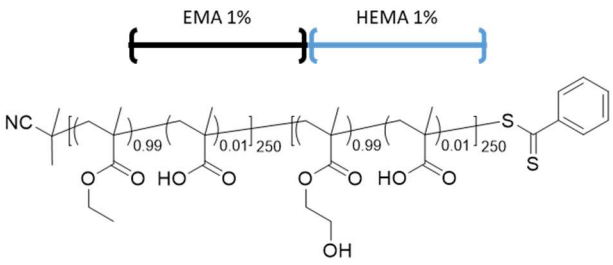

P8b

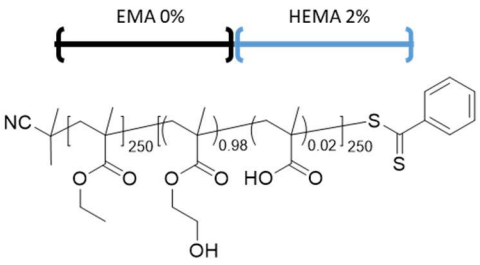

PEMA-COOH x%

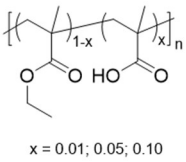

x = 0.01; 0.05; 0.10

x = 0.01
0.05
0.10
0.25

PEMA-NMe_3^+ x%

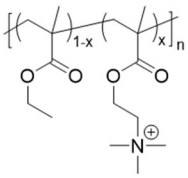

x = 0.01
0.05
0.10
0.25

Naphtalene functionalized PEMA-COOH 5%

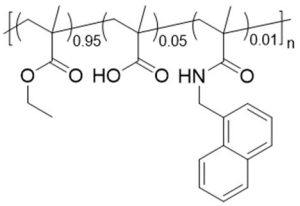

Pyrene functionalized PEMA-NMe_3^+ 5%

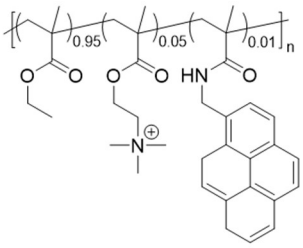

3 Methods

3.1 Polymerizations

In order to study the effects of polymer chemistry on nanoprecipitation, we needed to synthetize a library of various polymers. Therefore, we looked for a versatile and convenient polymer chemistry. Radical polymerization of methacrylates was chosen for the following reasons:

- There are many commercially available methacrylates comprising hydrophobic, hydrophilic, charged or fonctionalizable monomers.
- Polymer composition can be readily tuned by changing the monomer feeding ratio of polymerization reactions.
- Methacrylates are compatible with RAFT polymerization, allowing to control polymer architecture.

The following section describes the mechanisms of the polymerization reactions used and the general procedures of polymer synthesis. Details of the polymerizations and characterization of the obtained polymers can be found in the annexes.

3.1.1 Free radical polymerization

Free radical polymerization (FRP) is a chain polymerization process relying on radical reactions which can be described in four steps:

The first step is the generation of radicals typically by molecules called initiators. These are species that can undergo decomposition through heating, UV irradiation or Redox reactions, leading to the formation of radical species. The most common thermal initiator is azobisisobutyronitrile (AIBN), which decomposed into two radicals comprising a nitrile group and a molecule of N_2.

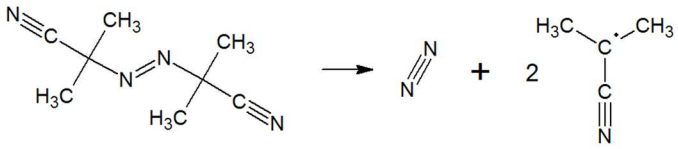

Figure 19: Generation of radicals by thermal decomposition of AIBN.

In FRP, radicals must be generated during the whole polymerization. As all radical polymerizations, the reaction has to be performed in the absence of oxygen, known to be a radical quencher. It is possible to conduct FRP in water (properly degassed) by using water soluble initiators.

The second step is the initiation, when a radical reacts with a monomer to start a new chain. In the case of vinylic monomers such as methacrylates, the radical reacts with one electron of the double bond, generating a new radical at the end of the polymer chain.

The third step is called propagation and corresponds to the addition of new monomer units to the polymer chain. This process lasts as long as there is a radical on the growing chain and monomers available.

The last step is the termination, which occurs when the polymer chain loses its radical. Then it becomes a dead chain unable to continue its growth. Termination reactions may occur for example through combination or disproportionation.

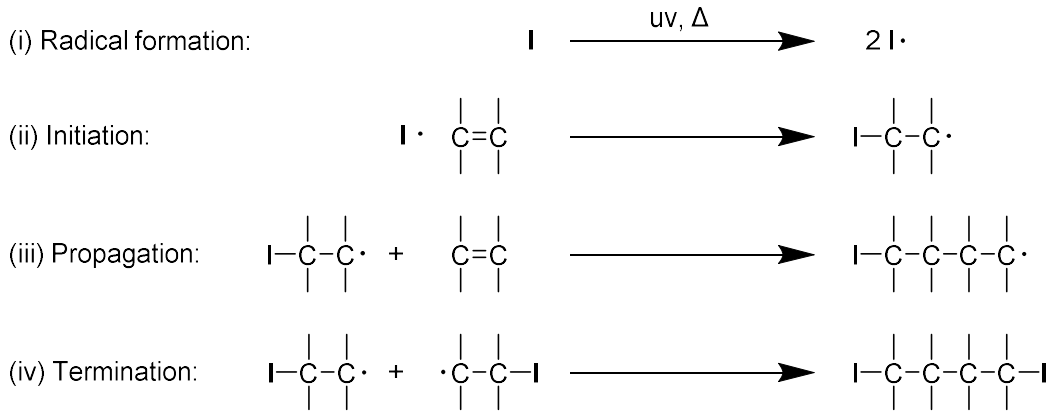

Figure 20: Mechanism of free radical polymerization process.

These four steps are represented in the scheme above (Figure 20). In FRP the control over the termination reactions and then over the chain length is relatively poor. Therefore polymer chains obtained by FRP usually have a high polydispersity index (PDI = M_w/M_n) laying between 1.5 and 3. The life time of a growing chain is also very short, typically less than a second[125]. In consequence, if monomers do not have the same reactivity, the composition of the polymer may vary between chains, especially for high conversion values.

3.1.1.1 General procedure for Free radical polymerization:

Monomers and AIBN (1 mol%) were dissolved in DMSO or DMF. Argon was bubbled in the solution for approximately 5 minutes then the flask was placed in a pre-heated oil bath at 70°C, under inert atmosphere. After 30 min the reaction was stopped by cooling and an aliquot was withdrawn to determine its conversion by NMR. When the desired conversion was reached, the polymers were precipitated in methanol or in a methanol/water mixture. Polymers that couldn't be precipitated in these conditions were purified by dialysis with standard regenerated cellulose membrane with MWCO 3.5 kDa and freeze dried. Otherwise polymers were collected by centrifugation, dissolved in ACN and precipitated a second time in the same medium. Then, they were dried under reduced pressure and characterized by NMR. Molar mass of the polymers was estimated using a SEC setup based on a Resolve and Reveal module from Malvern Panalytical and 3 PLgel Mixed-B columns in series (10 mm, l: 30 cm, d: 7.5 mm), with DMF containing 0.1 M LiBr as eluent. Combined refractive index and LALS and RALS (low and reverse angle light scattering) were used for detection and evaluation of the molar mass.

3.1.2 RAFT polymerization

Reversible addition-fragmentation chain transfer (RAFT) polymerization was used to obtain polymers with a defined architecture. This technique, developped in 1998, uses a molecule called chain transfer agent (CTA) to perform a living, controlled radical polymerization[126]. Ideally, the initiation step should be fast in order for polymer chains to grow simultaneously and have a low polydispersity. After initiation occurred, the growing polymer chains rapidly react with the CTA, which generates a stable radical at the end of the chains. This has the effect to convert a growing chain into a dormant one. This state is in equilibrium with a propagating state with a much larger amount of dormant chains, greatly reducing the radical concentration and so the probability of termination reactions and granting to RAFT polymerization its controlled and living character. However, this does not have a strong effect on the rate of polymerization, which remains similar as conventional radical polymerization[127].

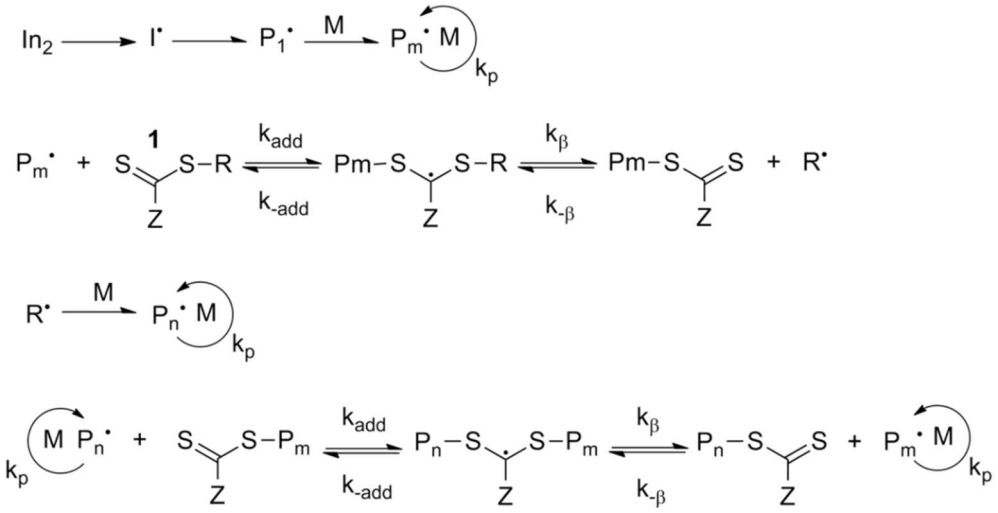

Figure 21: Mechanism of RAFT polymerization process.

The other tremendous asset of this technique is that the polymerization can be interrupted, the polymers purified, characterized and be used as a macro-RAFT agent on which other monomers can be added. Because the chain is ended with the CTA, polymers simply need to be dissolved in an appropriate solvent with monomers and a small amount of initiators to start the reaction again. This allows to readily create block copolymers or functionalize polymer chain ends[128].

3.1.2.1 General procedure for RAFT polymerization:

Monomers, AIBN and chain transfer agent (CTA) or macro-CTA were dissolved in DMF and put in a schlenk tube. After 3 freeze-pump-thaw cycles, reaction was set at 80°C under argon overnight. An aliquot was withdrawn to determine the conversion of the reaction by NMR. Polymers were purified by precipitation, dried under reduced pressure and characterized by NMR. Polymer synthetized on a small scale (< 100mg) were purified by size exclusion chromatography using a Sephadex™ LH-20 filled column. This product is a cross-linked dextran medium, which can be swollen in a wide variety of solvents and is used to separate compounds base on their molecular mass. Eluents used for purification were DCM-MeOH 50/50 vol. Molar mass of the polymers was estimated using a SEC setup based on a Resolve and Reveal module from Malvern Panalytical and 3 PLgel Mixed-B columns in series (10 mm, l: 30 cm, d: 7.5 mm), with DMF containing 0.1 M LiBr as eluent. Combined refractive index and LALS and RALS (low and reverse angle light scattering) were used for detection and evaluation of the molar mass.

3.2 Preparation of nanoparticles

Stock solutions of polymers at 10 $g.L^{-1}$ were prepared in ACN or in a mix ACN-MeOH 7:3 (for polymers with high amounts of MAA or HEMA groups). Stock solutions were diluted to 2 $g.L^{-1}$ in ACN before nanoprecipitation with addition of dye at the desired concentration.

3.2.1 Manual preparation

For manual nanoprecipitation, 50 µL of this solution were quickly added with a micro pipette to 450 µL of aqueous phase under shaking in an Eppendorf. The solution of NPs obtained was then diluted five times prior characterization.

3.2.2 Formation using microfluidic mixers

For preparation using microfluidics, we used an impact-jet (KM) mixer, whose structure consists of three steel plates, namely the inlet, mixing and outlet plates[129]. Both inlet fluid streams are split into 3 sub-streams thanks to microchannels of 120 µm. Then the alternated 6 sub-streams converge to a single pin hole of 300 µm, where they are mixed by frontal collision. In this case, the organic solution was mixed in a ratio 1:9 with Milli-Q water or phosphate buffer (20 mM, pH 7.4) at global volume flow rates of 2, 5, or 10 $mL.min^{-1}$, using two KDS Legato™ 100 Infuse Only Syringe Pumps from KD Scientific. Considering the geometry of the mixer, these volume flow rates correspond to flow speeds of 0.77, 1.93 and 3.86 $m.s^{-1}$. Samples were taken after about 30 s of stabilization at the given flow rates. The particle solutions were analyzed directly after suitable dilution, without purification in order to better visualize the effects of preparation conditions (Figure 32).

3.2.3 Stopped flow experiments

Stock solutions of fluorescent polymers were diluted to 0.5 $g.L^{-1}$ (with identical solvent) for stopped flow experiments. Bodipy and rhodamine functionalized polymers dissolved in ACN were loaded in a first syringe. A second syringe was loaded with MQ water. The volumes injected for each measurement were 101 µL and 905 µL for the syringe containing the polymer solution and water respectively. They were injected at a flow rate of 1 $mL.s^{-1}$ and 9 $mL.s^{-1}$ respectively. In these conditions the dead time given by

the supplier is 3.7 ms. For each run, 8000 values were recorded for a duration of 4 seconds, corresponding to a measurement every 0.5 ms. Excitation wavelength used for fluorescence measurements was 475 or 560 nm for bodipy or rhodamine excitation respectively. The emission of bodipy and rhodamine were collected using band pass filters (500-540 and 570-590 nm respectively) and a photomultiplier tube.

3.3 Characterization of particles

3.3.1 Dynamic Light Scattering (DLS)

A major characteristic of polymeric NPs is their size, which needs to be characterized consistently. DLS is an analytical technique to measure objects with a size between 1 nm and 1 µm. It is a convenient routine technique as it is fast, non-invasive and requires low quantities of materials. The size of particles is calculated from their Brownian motion that is the random movement of particles in solution coming from the collision with solvent molecules[130,131]. Brownian motion varies with the size of particles, smaller particles moving faster than larger ones. The rate of Brownian motion is related to the translational diffusion coefficient (*D*), which can be obtained through dynamic light scattering. The principle is the following: Laser light is directed on the sample and is scattered due to the presence of particles creating a speckle pattern (Figure 22). Diffusion of particles creates fluctuations of the scattered light, which modify the recorded signal. The speed of intensity fluctuations depends on the diffusion rates of particles. Within a very short period of time, the signal recorded will be almost identical to the original one: These signals are called "correlated". At longer time scales, the correlation decreases until the recorded pattern changes completely and there is no correlation with the original signal.

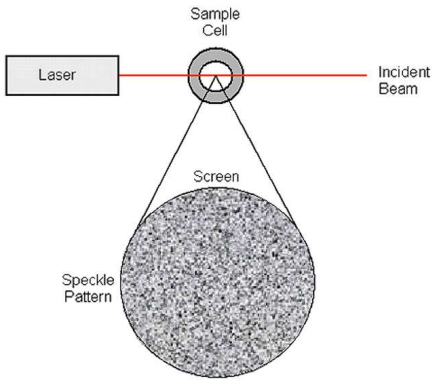

Figure 22: Schematic representation of a speckle pattern, from malvernpanalytical.com.

The value of the correlation coefficient can be plotted with time: For large particles the decay of the signal takes up to several milliseconds while for small particles it is only 10's of microseconds. The exponential decay of the correlation function is then fitted with a nonlinear fit algorithm from which is extracted the translational diffusion coefficient.

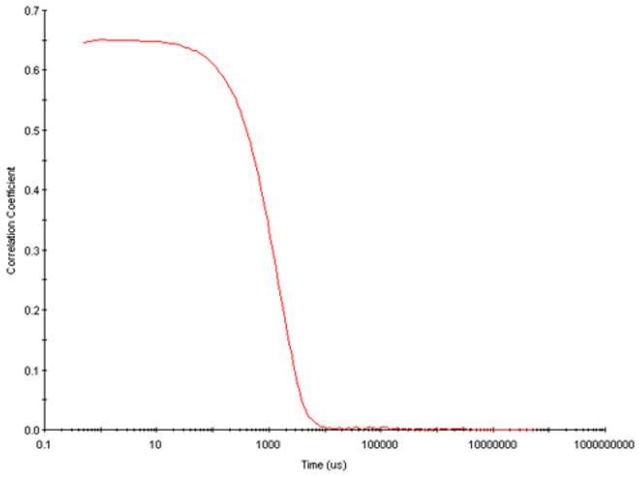

Figure 23: Typical correlogram from a sample containing large particles in which the correlation of the signal takes milliseconds to decay, from malvernpanalytical.com.

Finally, the hydrodynamic diameter D_h of the particles is calculated using the Stokes-Einstein equation (Equation 4):

$$D_h = \frac{kT}{3\pi\eta D} \qquad \text{(Equation 4)}$$

Where k is the Boltzmann constant, T the temperature and η the viscosity of the continuous phase.

Because DLS does not "directly" measure the size of the particles but deduces it from their movements, several aspects have to be kept in mind:

- DLS gives a hydrodynamic size of the measured objects. The presence of an ion layer or pendant polymer chains on the surface of a particle may reduce its movement speed and therefore increase the size (D_h) measured by DLS, with respect to its hard core diameter.
- DLS uses visible light (typically a laser with wavelength = 633 nm). Thus it is important not to have any fluorescent species able to emit (or absorb too strongly) light of this wavelength otherwise the measurement will be disturbed.

- The intensity of the scattering due to particles increases strongly with their diameter (proportional to d^6). For example, the intensity of light scattered by a particle of 50 nm is one million times superior to that of a particle of 5 nm. Therefore, a small population of large particles or aggregates may mask the signal coming from smaller particles.

Despite these minor drawbacks, DLS is used extensively as a routine measurement of NP size. Other techniques such as electron microscopy are often more costly and time consuming.

3.3.1.1 DLS measurements procedure

The size of the polymeric NPs was measured on a Zetasizer Nano series ZSP (Malvern Instruments S.A.). Each sample (500 µL in disposable PS cuvette) was measured 10 times with a run length of 10 s each. The volume average values, determined by the Zetasizer software (Malvern) based on Mie theory, were used. Mean values give the average over at least three independent preparations, error bars correspond to standard error of the mean.

3.3.2 ζ-potential

Particles in suspension in water usually carry electric charges at their surface. They may come from ionization of surface groups or adsorption of charged species. Particles bearing charges of identical sign will repel each other due to electrostatic repulsion. This repulsion effect is a main component of the DLVO theory, which describes from a thermodynamic point of view the stability of colloidal dispersions. Therefore, it is crucial to be able to characterize the charges present on the surface of particles. This is precisely the role of ζ-potential measurements.

Charged particles in solution will inevitably attract ions of opposite charge to their surface. Closest ions are strongly bounds to the particles and form a region called Stern Layer. Further, there is an outer layer called diffuse layer, made of ions loosely bound to the particle (Figure 24). ζ-potential is the potential at the external boundary of this layer, expressed in mV.

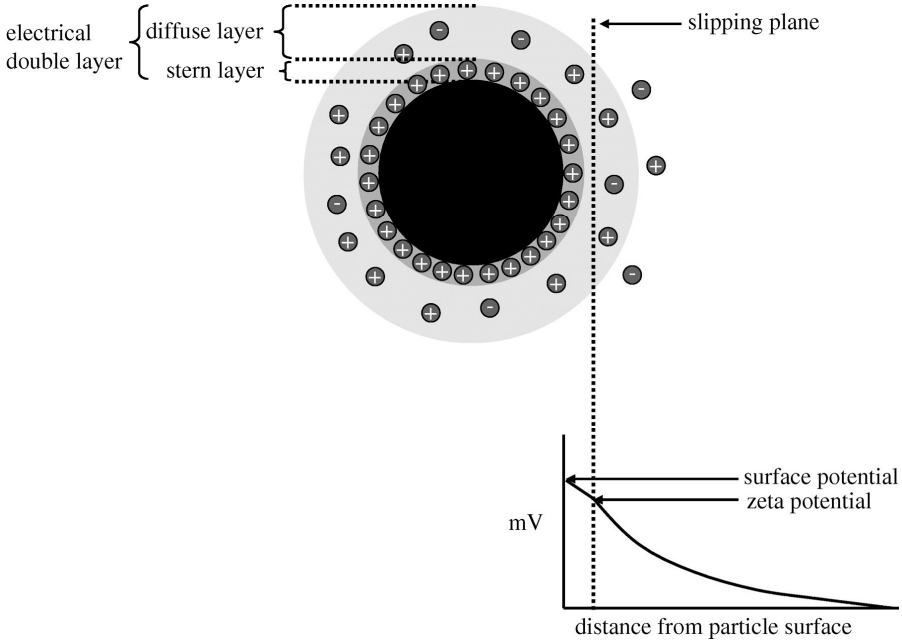

Figure 24: Representation of the electrical double layer and the ζ- potential, from ref[132].

In order to measure the ζ-potential, particles in solution are placed in a special cell equipped with two electrodes. An electric field is applied through the sample and the particles move accordingly to their surface charge. The setup uses a laser which is split into a reference beam and another one which is sent on the sample. The latter is scattered by the particles. Due to the displacement of the particles in solution the scattered light undergoes a Doppler effect, which modifies its frequency proportionally to the particles velocity. Both lasers (reference and scattered) are compared with a photodetector and the measurement of the Doppler shift allows to determine the electrophoretic velocity of the particles (ν). Then the electrophoretic mobility (μ) can be calculated with Equation 5:

$$\mu = \frac{v}{E} \qquad \text{(Equation 5)}$$

Where v is the observed electrophoretic velocity ($m.s^{-1}$) and E the electric field strength ($V.m^{-1}$). The ζ-potential is then calculated using the Henry equation (Equation 6):

$$\mu = \frac{2\varepsilon\zeta f(ka)}{3\eta} \qquad \text{(Equation 6)}$$

Where ε is the dielectric constant of the medium, ζ the ζ-potential, η the viscosity and f(ka) Henry's function. This function varies between 1 and 1.5 depending on the ratio between the particle radius and the double electrical layer thickness[132]. In our case the

Smoluchowski approximation, typically used for polar media, was employed corresponding to a value f(ka) = 1.5.

The ζ-potential value provides a good indication on the stability of a colloidal dispersion (when particles are stabilized by electrostatic repulsion). If the ζ-potential is too small, repulsion forces may be overcome by attractive forces (Van der Waals) and the particles will aggregate, leading to coagulation or flocculation. On the opposite, high ζ-potential (positive or negative) lead to strong electrostatic repulsion and consequently good colloidal stability. The following behaviour are expected depending on the magnitude of the ζ-potential:

- In range of 0-5 mV: Rapid aggregation
- In range of 5-20 mV: Particle have low stability
- In range 20-40 mV: Particle have decent stability
- Above 40 mV: Particles are highly stable

The ζ-potential is also used to characterize the surface charge of proteins. The latter is pH dependent due to the presence of many pH sensitive groups (carboxylic acids, amines, phosphonates etc). The particular case of the pH at which the mean ζ-potential of a protein is equal to zero is called the isoelectric point.

3.3.2.1 ζ-potential measurements procedure

The ζ-potential of the polymeric NPs was measured on a Zetasizer Nano series ZSP (Malvern Instruments S.A.). Each sample (1 mL in folded capillary cells DTS 1070) was prepared by diluting NPs in 1 mM solution of NaCl to control the conductivity. Three successive measurements per sample were made combining electrophoretic mobility and laser Doppler velocimetry. Every measurement had more than 10 runs carried out with an applied potential of ± 150 V.

3.3.3 Transmission electron microscopy

Transmission electron microscopy (TEM) uses the interaction between an electron beam and matter to create an image of a sample. This technique has high resolution, (down to 0.04 nm[133]) since electron wavelengths are very small (2.5 pm for a TEM working at 200 kV). Hence resolution limitation does not arise from electron wavelength

but from technical limitations of the microscope[134]. The image of the sample is projected on a CCD camera for recording, or a phosphorescent screen for direct observation.

Several steps are required for sample preparation before imaging. Firstly, a solution containing the sample to observe (e.g., proteins, viruses, nanoparticles) is prepared and a drop is deposited on a metallic grid covered with a thin carbon film. This film is ionized in a plasma chamber prior deposition to enhance sample adhesion. The drop is let still on the grid for roughly thirty seconds then water is removed with a blotting paper. Then, depending on its composition, the sample can be imaged directly or a staining agent can be added to improve the contrast between the objects and the background. In this case a drop of solution containing the staining agent is deposited on the sample, and removed in the same manner after ten to twenty seconds.

During imaging, electrons directly interact with the atoms composing the sample as the electron beam is passing through. The probability of interaction between an atom and an electron is proportional to Z^4 (with Z the atomic number of the atom). Thus, heavy atoms give a very good contrast and most metallic samples (e.g., gold nanoparticles Z=79) are readily imaged. On contrary, organic samples such as proteins or polymeric NPs are mainly composed of lighter atoms (hydrogen, carbon, nitrogen, oxygen with Z values < 8) so they will be poorly or not distinguishable from the background. In order to improve the contrast of these samples, staining agents made of heavy metals like osmium (Z=76), lead (Z=82) or uranium (Z=92) may be used. When deposited on the grid they form a dark, uniform background around the sample which appears brighter than its surroundings. This coloration is called negative staining. Sometimes the staining agent will accumulate only around the sample, resulting in a darker object, hence called positive staining (Figure 25).

TEM allows to take an actual picture of the objects imaged. In contrary to DLS, where the size of particles is deducted from their motion, TEM ensures a reliable measurement of the hard core particle diameter. For each sample, it is important to take images on different spots of the grid to ensure that the mean size measured is representative of the whole sample.

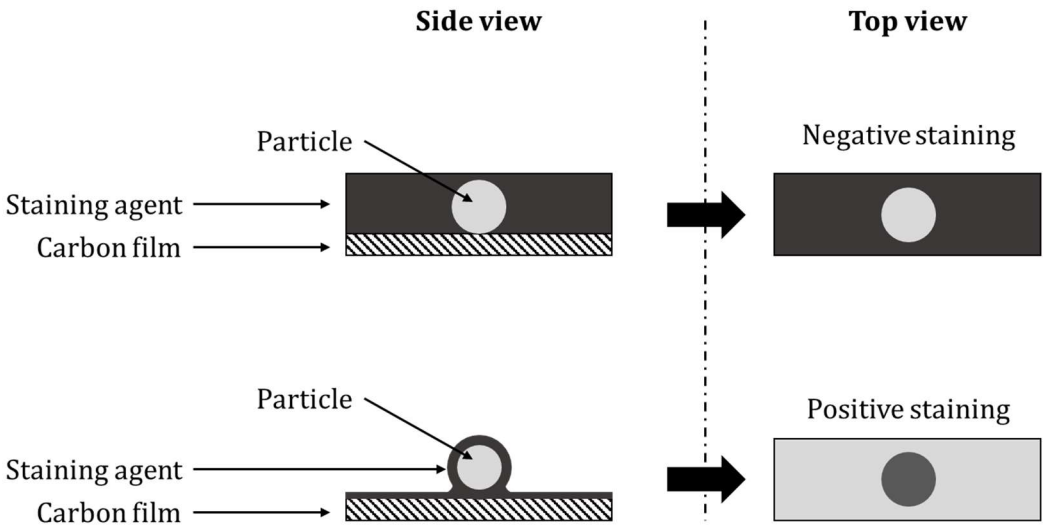

Figure 25: Schematic view of different staining modes possible in TEM.

3.3.3.1 TEM imaging procedure

Solutions of NPs (5 µL) were deposited onto carbon-coated copper-rhodium electron microscopy grids following air or amylamine glow-discharge. They were then treated for 20 s with a 2% uranyl acetate solution for staining. The obtained grids were observed using a Tecnai F20 Twin transmission electron microscope (FEI Eindhoven Holland) operating at a voltage of 200 kV. Images (2,048 * 2,048 pixels) were recorded using a US1000 camera (Gatan) and analyzed using the Fiji software. More than 200 particles were analyzed per condition and histograms of particle size were made to evaluate the dispersity of the sample. The software Fiji was used to treat the images recorded. The magnification used was between 20 000 and 50 000.

3.3.4 Fluorescence spectroscopy

There are many types of fluorescent or luminescent compounds, such as molecules, quantum dots, metal nano clusters or lanthanides and their absorption and emission properties need to be characterized precisely. We will focus here on molecular fluorescence: how it works, what are the main characteristics and how are they measured.

3.3.4.1 Characteristics of fluorescence

The first step in fluorescence is the absorption of a photon (Figure 26). The energy absorbed is proportional to the frequency of the photon and is equal to hν (with h the

Planck constant). According to quantum mechanics a molecule can only absorb a photon with an energy equal to the spacing between its various energy levels. Hence every molecule has its own absorption spectrum. After it has absorbed a photon, the molecule is in an excited state meaning that an electron has been promoted to an orbital with a higher energy level. This configuration is very unstable and the molecule rapidly comes back to its ground state by dissipating the energy absorbed. Several processes are involved in this transition such as internal conversion or vibrational relaxation. These are non-radiative and allow the electron to come back to the lowest vibrational state of the S1. The molecule then returns to the ground state by releasing the energy as heat. Fluorophores undergo this transition by emitting a photon of energy hν, equal to the difference between the S1 and a vibrational state of the S0. In some cases, the electron in the S1 state can encounter a spin-conversion, resulting in a molecule in the triplet state T1. The energy release from the T1 state is called phosphorescence. All of these transitions are represented in the Jablonski diagram[135].

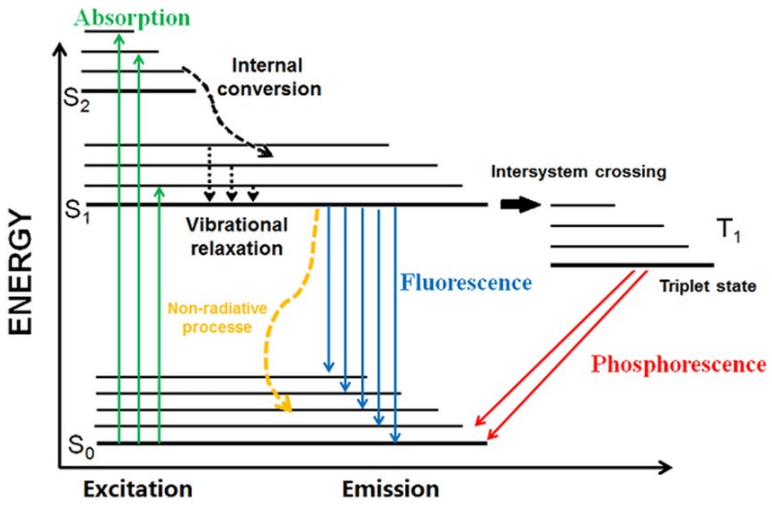

Figure 26: Jablonski diagram of fluorescence and phosphorescence, adapted from ref[136].

All of the non-radiative processes involved in the relaxation of a fluorescent molecule dissipate a part of the energy initially absorbed. This results in the emission of a less energetic photon, in consequence the emission spectra of the molecule is shifted to higher wavelengths compared to the absorption spectra. This difference, called Stokes shift, can vary a lot between different fluorophores. This property is used in fluorescence microscopy to separate the signal from the excitation source from the signal of the fluorophore by using a filter absorbing the excitation wavelength[137].

Because the first step of fluorescence is the absorption of a photon, the absorption coefficient of fluorescent dyes used in imaging is crucial. Absorbance is measured at a specific wavelength by sending a light beam through a solution containing the sample. A reference beam passes through a solution with the same components except the one characterized. The difference of intensity of the two beams allows to calculate the absorbance of the solution (Equation 7). The absorbance follows the Beer-Lambert law:

$$A_{(\lambda)} = \varepsilon_{(\lambda)} * l * c \qquad \text{(Equation 7)}$$

Where l is the optical path length, c the concentration of the sample in solution and ε the molar absorption coefficient, which represents the capacity of a species to absorb light at a given wavelength. It is an intrinsic value of the studied molecule at a given temperature in a specific solvent and it is expressed in $M^{-1}.cm^{-1}$.

Fluorescent objects are notably characterized by their quantum yield (QY), which is the ratio between the number of photons emitted and absorbed by a fluorophore (Equation 8):

$$\Phi = \frac{N(photons\ emitted)}{N(photons\ absorbed)} \qquad \text{(Equation 8)}$$

Where Φ is the QY. It does not depend on the excitation wavelength and is measured in a given solvent. The first step to determine a QY is to measure the absorbance of a solution of dye at a specific wavelength. Then the fluorescence of this solution is quantified using a fluorometer. A light beam with the same wavelength used in absorbance is sent on the sample and the photons emitted are counted thanks to an integration sphere[138]. This way the QY can be calculated for any fluorescent species. Because photons are emitted in all directions, the absolute quantification of the fluorescence is complicated. In practice, fluorescence is measured with a sensor placed at 90° from the excitation beam. The QY of a sample is measured by comparing its fluorescence signal to a standard for which the QY is known[139]. Rhodamine R101 is commonly used because its quantum yield is well characterized (considered here to be 100%)[140]. It is crucial that absorbance and emission measurements are conducted in the same conditions for the sample and the reference. Then the QY of the sample can be calculated following the equation 9[135]:

$$\Phi = \Phi_{ref} \frac{\eta^2.I.A_{ref}}{\eta^2_{ref}.I_{ref}.A} \quad \text{(Equation 9)}$$

Where η is the refractive indices of the solvent, I the integration of the intensity of fluorescence and A the absorbance at the excitation wavelength. Another commonly used value to characterize fluorescent species is their brightness (B), corresponding to the number of photons emitted in specific conditions of illumination (Equation 10). It is given by the product of the molar absorption coefficient and the QY.

$$B = \varepsilon * \Phi \quad \text{(Equation 10)}$$

Thus to be very bright, a fluorophore must have a good quantum yield but also have a high ε at the working wavelength. The brightness of a fluorescent object, such as a nanoparticle, can be enhanced by increasing the amount of fluorophores encapsulated. In this case, it is calculated taking into account the number of fluorophore (n) per particle (Equation 11):

$$B = \varepsilon_{fluorophore} * \Phi * n \quad \text{(Equation 11)}$$

However, at high concentrations dyes typically undergo quenching which reduces their quantum yield and therefore the brightness. This phenomenon, called aggregation caused quenching (ACQ), is due to π-π stacking of the fluorophores favored by their planar aromatic structures. This promotes non-radiative intermolecular energy transfer, thus reducing the QY. Although this can provide useful information, for instance on the dye organization within nanoparticles, ACQ is a major problem in the quest for brighter nano-objects. It is usually fought by preventing π-π stacking via the insertion of bulky groups[141] or polymer chains[142] on the fluorophores. In the case of ionic dyes, bulky counter ions have been used as spacers to increase the distance between dyes, thus reducing ACQ[143,144].

3.3.4.2 Förster resonance energy transfer

Förster Resonnance Energy Transfer (FRET) is a type of non-radiative energy transfer that can take place between two spatially close fluorophores. When excited, the fluorophore called donor may transfer its energy via a non-radiative process to the acceptor, which can subsequently return to its fundamental state by emitting a photon.

This transfer only happens if the three following conditions, illustrated in figure 27, are satisfied:

- 1. Fluorophores are near (<10 nm)
- 2. The emission spectrum of the donor overlaps with the absorption spectrum of the acceptor
- 3. The emission transition dipole of the donor and the transition absorption dipole of the acceptor are not orthogonal

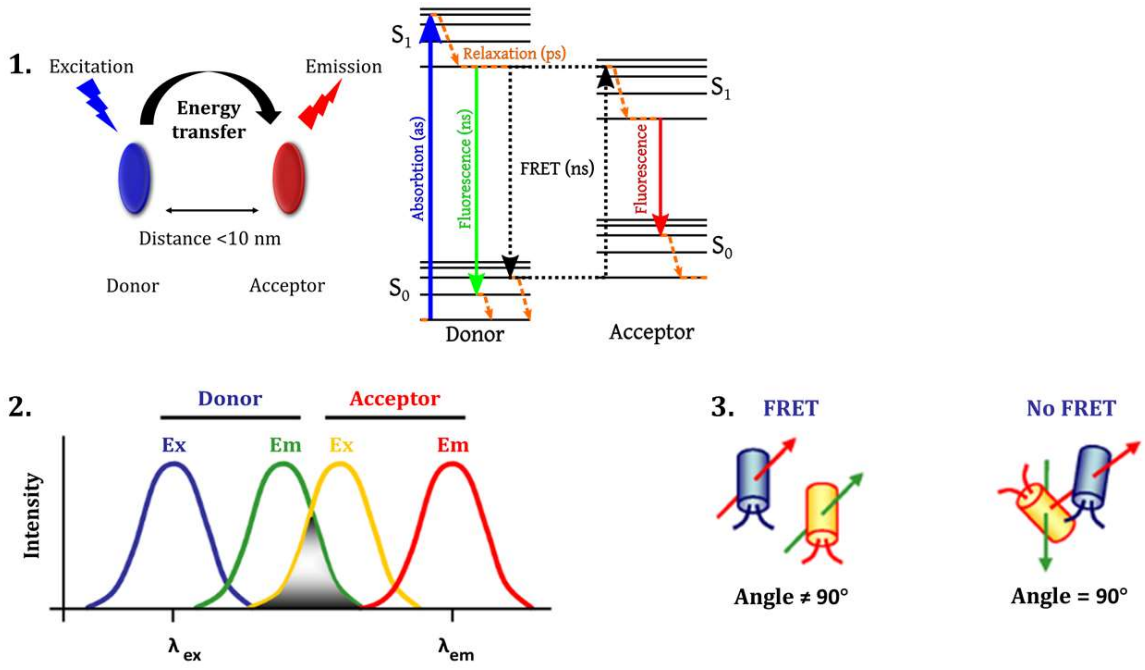

Figure 27: Schematic representation of the conditions required for FRET adapted from ref[135].

FRET is notably characterized by the FRET efficiency (E) which is the quantum yield of the energy transfer[136]. This is the ratio between the number of energy transfer events and the number of excited donor molecules. It depends on the distance between the donor and the acceptor, according to equation 12:

$$E = \frac{1}{1+(r/R_0)^6} \qquad \text{(Equation 12)}$$

Where r is the distance between the donor and the acceptor and R_0 the Förster distance. R_0 is defined for each donor-acceptor pair as the distance at which the energy transfer efficiency is 50%. It is notably impacted by the overlap integral of the emission spectrum of the donor and the absorption spectrum of the acceptor. The value of the Förster

distance for the FRET pair between the bodipy and the rhodamine used in this thesis work is R_0 = 6.2 nm (calculated with FPbase, according to Wu and Brand[145]). As the FRET efficiency is inversely proportional to the distance between the fluorophores to the power six, it tends to zero extremely rapidly if the fluorophores are not very close spatially (Figure 28).

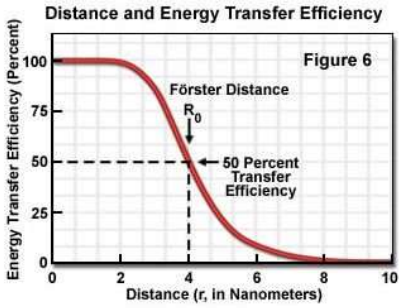

Figure 28: Efficiency of FRET depending on the distance between the two fluorophores[135].

In practice, fluorophores are used to label different objects and FRET can be seen as an on/off system describing if these objects are in contact or not. FRET is notably used in biology where proteins are labeled with fluorescent dyes so their interactions can be monitored by fluorescence. In this case the FRET efficiency is measured thanks to the decrease in the fluorescence emission of the donor (Equation 13) with the formula:

$$FRET_{efficiency} = 1 - \frac{Imax\ (D)}{Imax\ (D0)} \qquad \text{(Equation 13)}$$

Where Imax(D0) and Imax(D) are the maximum intensities of the donor alone and in the presence of the acceptor respectively.

3.3.4.3 UV-Vis and fluorescence spectroscopy procedure

Absorption and emission spectra were recorded on a Cary 5000 Scan ultraviolet–visible spectrophotometer (Varian) and on a FS5 Spectrofluorometer (Edinburgh Instruments), respectively. Emission spectra were recorded from a wavelength 10 nm higher than the excitation wavelength. Quantum yields were determined using a simplified relative method with rhodamine 101 in ethanol with peak absorbance below 0.1 as reference[139].

3.4 Other procedures

3.4.1 Cellular experiments

Hela cells (ATCC® CCL-2) were grown in Dulbecco's modified Eagle's medium with low (1 $g.L^{-1}$) glucose (DMEM, Gibco), supplemented with 10% fetal bovine serum (FBS, Dutscher), 1% Lglutamine (Lonza) and 1% penicillin–streptomycin (Lonza) at 37 °C in a humidified atmosphere containing 5% CO2. For investigating NP-cell interactions, cells were seeded in 35-mm-glass bottom culture dishes (ibidi) at a density of 100 000 cells per well. After letting the cells adhere for 18 h, the cell culture medium was removed, and the cells were rinsed twice with Opti-MEM, followed by incubation with a freshly prepared solution of the NPs diluted twentyfold in Opti-MEM. After 1 h of incubation, the NP suspension was removed and the cells were rinsed with Opti-MEM. Just before imaging, MemBright-488 (kindly provided by Mayeul Collot) was added to obtain a final concentration of 200 nM. Imaging was then performed using a Leica TSC SPE laser scanning confocal microscope with a 63x oil immersion objective. Images were recorded with a pixel width of 228 nanometers.

3.4.2 Nuclear Magnetic Resonance (NMR) spectroscopy

NMR spectra were recorded at 20 °C on a BrukerAvance III 400 spectrometer and were used to evaluate polymerization conversion and characterize the final polymers via ^{1}H and ^{19}F NMR spectroscopy.

3.4.3 Competitive reactions

Mixing times were determined following a procedure established by J-M. Commenge et al.[146] Briefly, an acidic and a basic solution are mixed with a small excess of basic solution. The basic solution contains potassium iodate which reacts with acid to form I_2 which then react with iodide to form I_3^-. This reaction only happens with inhomogeneous mixing, because this reaction is in competition with the acid-base reaction which is much faster. The amount of I_3^- is measured by absorbance (OD) and is correlated to the mixing time.

Stock solutions of potassium iodate (0.06 $mol.L^{-1}$), potassium iodide (0.32 $mol.L^{-1}$), boric acid (0.665 $mol.L^{-1}$), sodium hydroxide (1 $mol.L^{-1}$) and sulfuric acid (0.5 $mol.L^{-1}$) were prepared in degassed water. Solutions of sulfuric acid were made at 0.04 $mol.L^{-1}$ and

0.06 mol.L^{-1} (respectively for low and high speed of mixing). Basic solution was prepared by adding successively solutions of boric acid, sodium hydroxide, potassium iodide and potassium iodate to obtain a final concentration of 0.09 mol.L^{-1} of NaH_2BO_4, 0.032 mol.L^{-1} of potassium iodide and 0.006 mol.L^{-1} of potassium iodate. Both solutions were degassed by Argon bubbling for at least 10 minutes. Mixing time was determined with manual mixing and with microfluidic mixing (2, 5 and 10 mL/min).

After mixing, the absorbance was measured at 353 nm. From this, and taking into account the used concentrations, the segregation index X_S was calculated with equation 14, following procedures from the literature[146]:

$$X_S = \frac{Y}{Y_{segregated}} = \frac{\frac{2([I_2]+[I_3^-])}{[H^+]_0}}{\frac{6[IO_3^-]_0}{6\,[IO_3^-]_0+[H_2BO_3^-]_0}} \qquad \text{(Equation 14)}$$

Using described models, the absorbance can be further used to estimate mixing times with the equation 15. All experiments were performed in triplicate.

$$t_m = 0.33(OD)[H^+]^{-4.55}[KI]^{-1.5}[KIO_3]^{5.8}[NaOH]^{-2}[H_3BO_3]^{-2} \qquad \text{(Equation 15)}$$

3.4.4 CFD modeling

The Ansys Fluent software was used to model the flow at various flow rates, corresponding to the flow speeds calculated based on the mixer geometry. A geometry based on 6 converging entry channels of 120 µmx120µm width and a cylindrical outlet channel of 280 µm diameter and a length of 5 or 10 mm was used. A species model of acetonitrile and water was used to simulate the mixing.

Chapter II: Formation kinetics of polymeric nanoparticles by nanoprecipitation

As explained in chapter I, nanoprecipitation is a simple process for the synthesis of loaded polymeric NPs. It allows to readily encapsulate hydrophobic compounds by dissolving them together with polymers in a water-miscible organic solvent and mixing this solution with an aqueous phase. Under certain conditions, notably a composition in the Ouzo region, co-precipitation of the hydrophobic components then leads to the formation of nanoparticles. This process is kinetically controlled, meaning that particle properties rely strongly on the kinetics of their formation[75,147,148]. In the present chapter, we wanted to study the kinetics of polymer nanoprecipitation and how it is related to polymer chemistry.

Nanoprecipitation is a very rapid process, and so most kinetic information was obtained indirectly from models and studies of the influences of mixing times or other process parameters. Indeed, nanoprecipitation of polymers is notably influenced by the mixing step. However, others and we also found that it depends on polymer chemistry. In a first place, we studied these parameters and their relative importance qualitatively by forming dye-loaded NPs with various polymers, under different mixing conditions. Their effects were evaluated by comparing the size and QY of the particles obtained. In a second place, we aimed to characterize more quantitatively the kinetics of nanoprecipitation of different polymers by monitoring the formation of NPs through FRET using a stopped flow setup.

1 Effects of mixing and polymer chemistry on nanoprecipitation

The kinetically controlled nature of nanoprecipitation has the consequence that the way and speed of mixing of the two phases can strongly influence particle formation and through this size, size distribution, and loading. [96,97,149] Improved mixing leads in general to smaller NPs with narrower size distributions.[64,94] Related to this are various parameters that indirectly influence the kinetics of particle formation. Among these are the concentration of polymer and load,[80,150] and the organic solvent used.[151] While the former influences the diffusion distances, the latter influences the limit of solubility of the polymer in the water-solvent mixture. On the other hand, it was also observed that the

nature of the polymer can influence the synthesis and the properties of nanoparticles. Indeed, charged groups on the polymers have been shown to reduce particle size,[121–123,150] as well as hydrophilic groups.[152]

We thus wanted to evaluate the relative importance or influence of polymer chemistry and mixing for the preparation of loaded polymeric nanoparticles. For this, we compared nanoparticles prepared manually, corresponding to "slow mixing", to NPs prepared using an impact-jet mixer, which has been shown previously to yield particularly small nanoparticles, supposedly due to very efficient and fast mixing.[98] Then we determined for which polymer the mixing played an important role or not.

1.1 Design of the study

1.1.1 Polymers

As described previously, in the case of nanoprecipitation, it has been found that the hydrophobicity of the polymer chain, its architecture or the amount of charged groups can have an influence on the formation of NPs. To study these, we have chosen to work with methacrylate based polymers because many different monomers (hydrophobic, hydrophilic, charged…) are commercially available. We then synthetized two series of polymers containing ethyl methacrylate (EMA) as a hydrophobic monomer and various amount of methacrylic acid (MAA) or hydroxyethyl methacrylate (HEMA), respectively as charged and hydrophilic monomers. PEMA-HEMA polymers also contained 1 mol% of methacrylic acid to help the formation of stable particles (Figure 29). Moreover, we synthetized a block copolymer of EMA and HEMA. We used the same ratio of monomers as for the synthesis of statistical PEMA-HEMA 50-50, but monomers were split in a hydrophobic and a hydrophilic block.

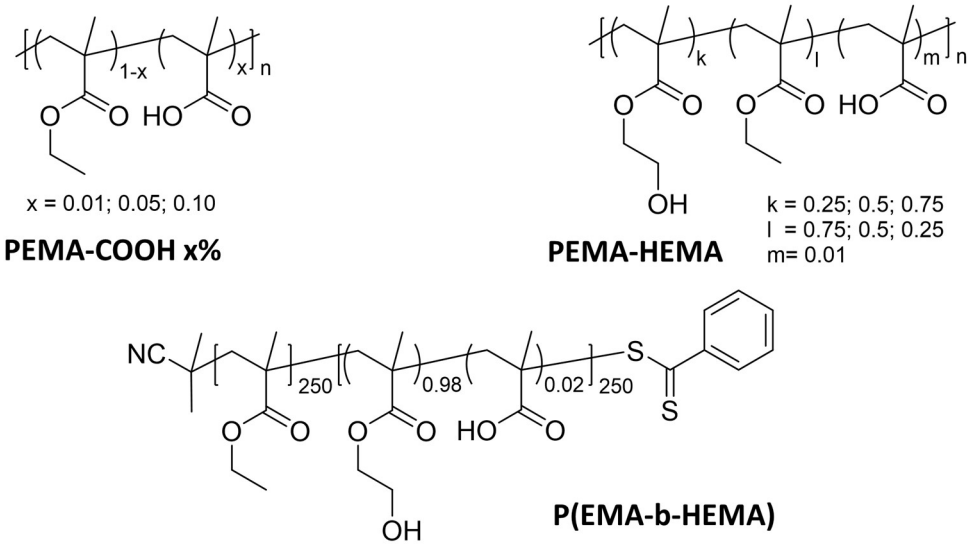

Figure 29: Structures of statistical (top) and block (bottom) polymethacrylates used in this study.

In order to extend the study to other types of polymers, commercially available polyesters were also used for the formation of particles. These polymers have a different backbone than polymethacrylates and are commonly used for medical applications due to their biocompatibility and biodegradability. We worked with acid terminated PLA and PLGA polymers as well as with a PEG-PLGA block copolymer. Both PLGA polymers had a LA:GA molar ratio of 50:50 (Figure 30).

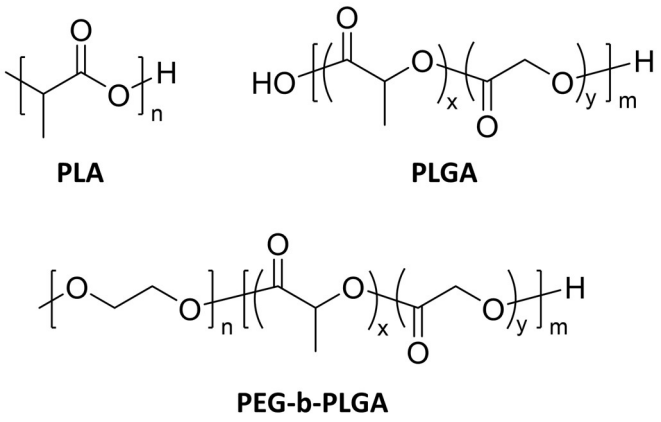

Figure 30: Structure of polyesters used in this study.

1.1.2 Mixing methods studied

Dye-loaded NPs were obtained by co-precipitation of polymers with a hydrophobic dye salt, R18/F5-TPB. Solutions of polymer were prepared at a concentration of 2 $g.L^{-1}$ in

acetonitrile with 5 wt% or 30 wt% of dye (relative to the polymer). For manual preparation, this solution was quickly added to a 9-fold volume excess of Milli-Q water or phosphate buffer (20 mM, pH 7.4) under shaking (Fig 31).

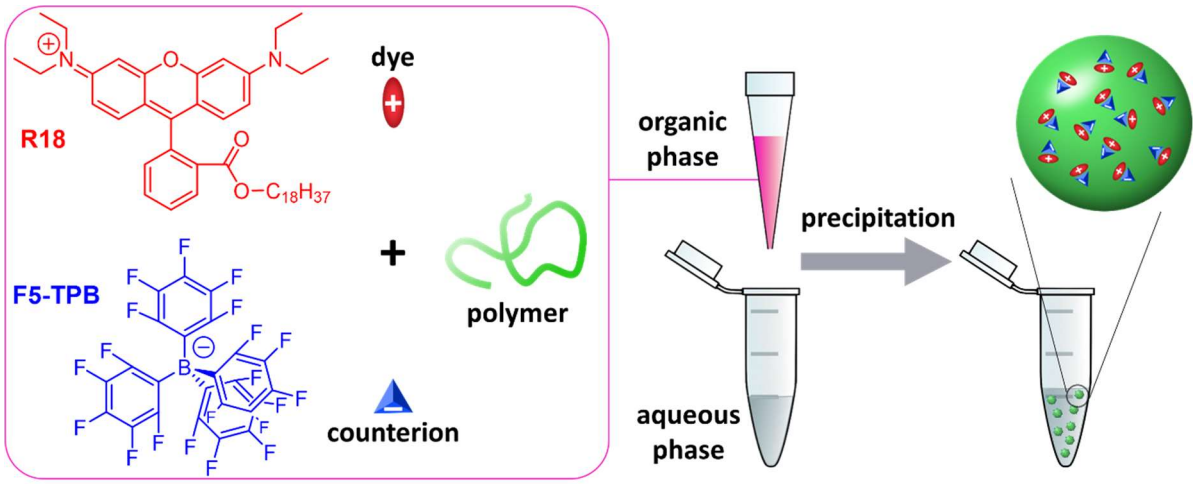

Figure 31: Structure of R18/F5-TPB dye salt and principle of manual nanoprecipitation.

For preparation using microfluidics, we used an impact-jet (KM) mixer, whose structure consists of three steel plates, namely the inlet, mixing and outlet plates (Figure 32). The organic solution was mixed in a ratio 1:9 with Milli-Q water or phosphate buffer (20 mM, pH 7.4) at global volume flow rates of 2, 5, or 10 mL.min^{-1}, using two automatic syringe drivers. Samples were taken after about 30 s of stabilization at the given flow rates.

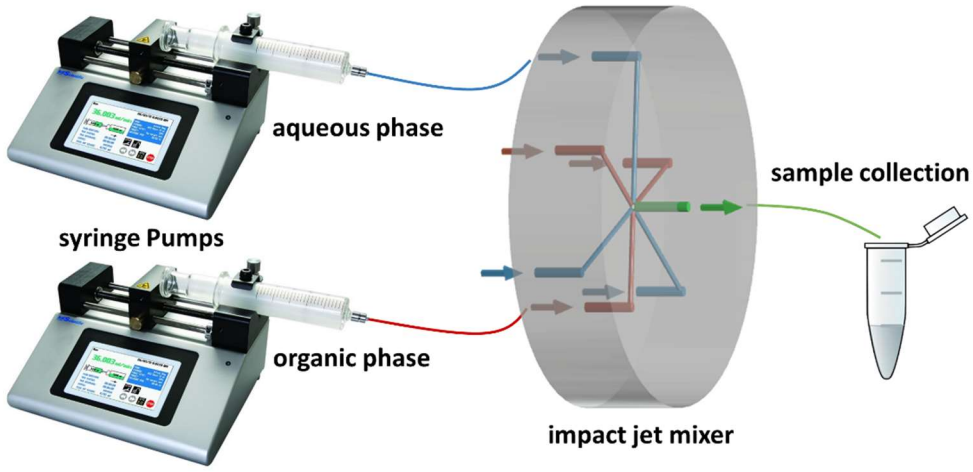

Figure 32: Scheme of the setup for nanoprecipitation using the impact jet mixer.

1.2 Mixing

In a first step, we aimed at characterizing the mixing of the two fluid phases in the two approaches we used for particle preparation, that is manual mixing and microfluidic mixing using an impact-jet mixer. One way to achieve this for the latter is to simulate the flow in the mixer using continuous flow dynamics (CFD). In our case, we modeled the mixing of acetonitrile and water in the mixer using the ANSYS Fluent software for the three used volume flow rates. The results are summarized in Figure 33 and Table 1 and show that increasing the flow speed leads to improved mixing, in particular when going from a global flow rate of 2 mL.min^{-1} to 5 mL.min^{-1}. The so called uniformity index (1 for highest uniformity) can be used to quantify the extent of mixing, indicating that in the case of 5 mL.min^{-1} very good mixing (uniformity index 0.96) is achieved after a residence time of 3 ms, while this value decreased to 1.4 ms at 10 mL.min^{-1} (uniformity index 0.95). In the case of 2 mL.min^{-1}, reaching corresponding mixing values requires > 15 ms.

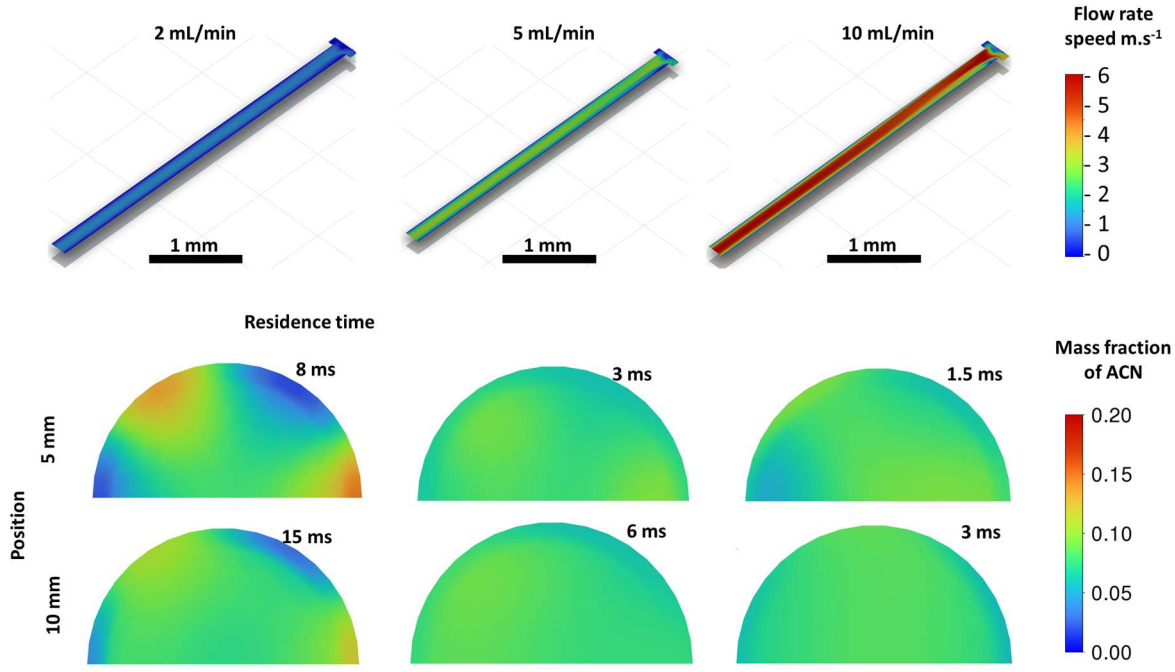

Figure 33: Simulation of fluid mixing between water and acetonitrile at different flow speeds: Top: velocity profiles along the symmetry plane for three global volume flow rates with a acetonitrile:water volume ratio of 1:9. Middle and bottom: Mass fraction profiles of acetonitrile for cross-sections situated at 5 (middle) and 10 (bottom) mm. The residence time values indicate the mean residence time of the fluid up to the given position in the mixer.

A second way, to achieve a comparison of the different mixing conditions is the use of competitive reactions, which allows relating the ratio of the obtained products to the speed of mixing.[146,153,154] Here, we chose the Villermaux-Dushman reaction, in which

neutralization of borate competes with the acid catalyzed redox reaction of iodate with iodide according to equation 16 and 17.

$$H_2BO_3^- + H^+ \leftrightarrow H_3BO_3 \qquad \text{(R1)} \qquad \text{(Equation 16)}$$

$$IO_3^- + 5I^- + 6H^+ \leftrightarrow 3I_2 + 3H_2O \qquad \text{(R2)} \qquad \text{(Equation 17)}$$

The reaction R1 is much faster than the reaction R2, therefore in the case of ideal mixing it consumes all of the H^+ ions which are in stoechiometric defect. However, in the case of poor mixing, local over-concentrations of acid can happen and the second reaction may take place. It generates I_2 which reacts with I^- according to the following equilibrium (equation 18):

$$I_2 + I^- \leftrightarrow I_3^- \qquad \text{(Equation 18)}$$

The concentration of triiodide ions can then easily be measured by UV-Vis. This can be used to determine a so-called segregation index or to obtain the mixing time. Our choice was motivated by the simple quantification of product ratios through absorbance measurements and the fact that this reaction has been previously used to characterize similar mixers.[129,146,155] The obtained segregation indices X_S (X_S = 0 for perfect micromixing, X_S = 1 for infinitely slow mixing) for the impact-jet mixer showed that increasing the flow rate effectively led to better, that is, faster mixing (Figure 34). The speed of manual mixing was of the same order of magnitude as mixing at the lowest flow rate used here (2 mL.min^{-1}). However, at high flow-rates (5 and 10 mL.min^{-1}) mixing in the impact-jet mixer lead to clearly improved mixing. Further quantification of the mixing based on a model proposed for this reaction yields micromixing times of tens of ms for manual and slow micro-fluidic mixing (27 ± 5 ms and 28 ± 3 ms). For faster flow, the obtained micromixing times were of the order of a few ms (2 ± 1 ms for 5 mL.min^{-1}) or even below 1 ms (for 10 mL.min^{-1}). Thus, the measured values were in reasonably good quantitative agreement with the simulated ones (considering a uniformity index of 0.9 – 0.95). Furthermore, the measured values are comparable to previous evaluations, which found very fast mixing under these conditions.[129,155] Measurements in other types of impinging jet or multi-inlet-vortex mixers yielded mixing times in the low ms range,[154,156] which is consistent with the results obtained here.

These results suggest that the two mixing schemes provide effectively two different time schemes for mixing of the aqueous and organic phases: very fast mixing in the case of the impact-jet mixer and significantly slower mixing for manual mixing using a pipette and a shaker, for which mixing was at least one order of magnitude slower.

Mixing type	Flow rate (mL.min^{-1})	Mixing time[1)] (ms)	Residence time[2)] (ms)	Uniformity index[2)]
Manual	-	27 ± 5	-	-
Impact Jet	2	28 ± 4	8	0.87
Impact Jet	5	2 ± 1	3	0.96
Impact Jet	10	<1	1.4	0.95

Table 1: Characteristic values of different mixing methods. 1) as obtained from the Villermaux-Dushman reaction. 2) as obtained from CFD simulation.

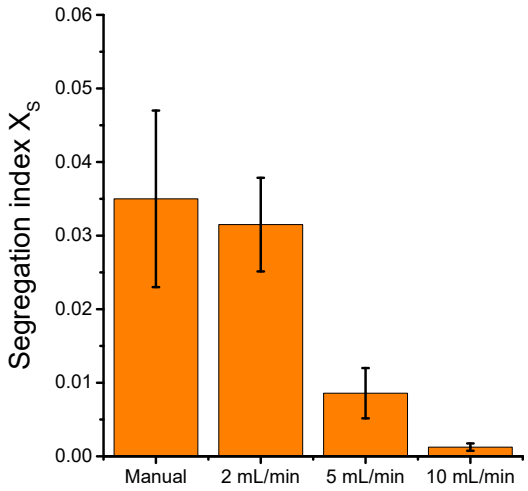

Figure 34: Segregation indices for various mixing conditions either manually or using the impact-jet mixer as obtained using the Villermaux-Dushman reaction. Experiments were performed in triplicate and error bars give the standard deviation.

1.3 Turbidimetry

The driving force of particle formation in nanoprecipitation is the insolubility of the polymer and the load in the final mixture obtained after mixing the organic and the aqueous phases. In a second step, we therefore determined the limit of solubility of the different polymers. For this, we used turbidimetry experiments, in which small quantities

of an aqueous phase (Milli-Q water or phosphate buffer) were added to solutions of the polymers at 2 $g.L^{-1}$ in acetonitrile, while measuring the transmittance. We considered that the solubility limit was reached when the measured transmittance at 400 nm dropped below 80%.

In the case of the ethyl methacrylate polymers with different percentages of charges, the solubility limit was reached between 6 and 12 vol% water, as expected for copolymers with a high amount of hydrophobic monomers (Figure 35A). Increasing the amount of methacrylic acid groups only slightly shifted the solubility limit to higher water fractions. Interestingly, the solubility limit further decreased to less than 3% when phosphate buffer was used as the aqueous phase. The reason for this behavior could either be related to salting-out in the presence of an electrolyte[157] or to a change in the protonation state of the carboxylic acid groups on the polymers. Performing the same experiment with 20 mM NaCl solution gave a solubility limit of 7% aqueous phase for PEMA-COOH 5%, indicating that both may contribute.

Increasing the fraction of hydrophilic monomers in statistical copolymers led to a continuous (and practically linear) increase in the solubility limit, up to a water fraction of over 50 vol% for the copolymer bearing 75 mol% of HEMA monomers (Figure 35B), in good agreement with previous observations.[152] In sharp contrast, the block copolymer p(EMA-b-HEMA), which has a molar ratio between the two monomers of 50%, reached its solubility limit below 10 vol% of water, indicating that, under the conditions studied here, the hydrophobic block has a crucial impact on polymer solubility. A similar behavior was observed for PLGA and the PLGA-PEG block copolymer, where the solubility limits were practically independent of the presence of the PEG block (Figure 35C). The obtained values were in good agreement with results obtained by others[151] and showed that, in general, the polyesters had a somewhat higher solubility than the hydrophobic methacrylates, in particular the PLA. Again, the solubility limit was lower when phosphate buffer was used as the aqueous phase. Performing the same type of experiments using DLS with the dye salt R18/F5-TPB alone yielded a solubility limit of about 6 vol% of water.

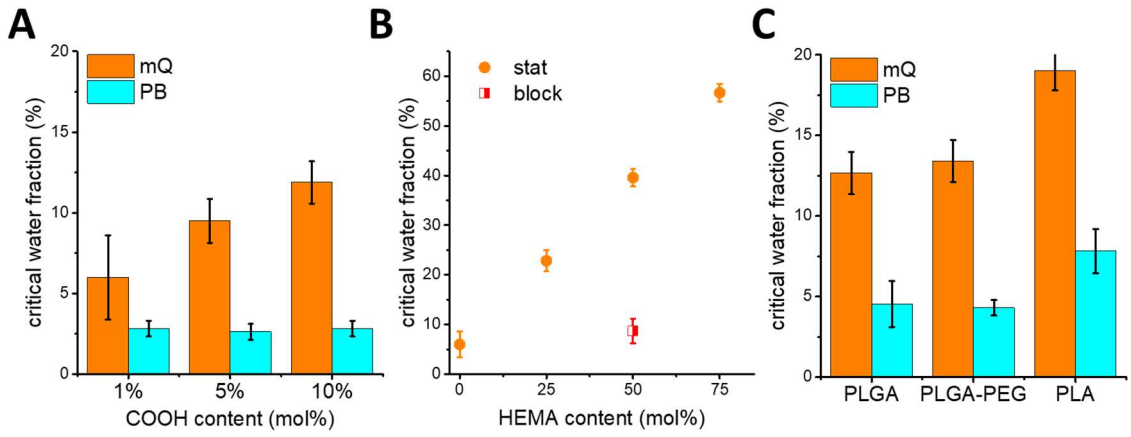

Figure 35: Limits of solubility of the different polymers as obtained from turbidimetry measurements by adding an aqueous phase to a 2 g L^{-1} solution of the polymers in acetonitrile. A) PEMA-COOH with different fractions of COOH groups. B) P(EMA-HEMA) with different EMA/HEMA ratios either as statistical or block copolymers. C) Different polyesters. Given is the highest fraction of aqueous phase in the mixture before the transmittance decreased below 80%. mQ: Milli-Q water, PB: phosphate buffer 20 mM, pH 7.4. Mean values are triplicates of three independent measurements, error bars give the standard error of the mean.

1.4 Nanoparticles from Methacrylate Polymers

To evaluate the relative influence of polymer chemistry and speed of mixing on synthesis of NPs through nanoprecipitation, we started from methacrylate polymers having different types and amounts of side groups and architectures. In all cases 30 wt% (relative to the polymer) of the hydrophobic dye salt R18/F5-TPB were added to the organic phase. Microfluidic mixing using an impact jet mixer was used as fast mixing and manual addition using a micropipette under shaking as "slow" mixing. First, we applied this protocol to PEMA polymers bearing 1, 5, or 10 mol% of COOH groups. As observed previously, the particle size decreased strongly with increasing amount of charges.[158] However, for these polymers fast mixing in the impact-jet mixer did not lead to the formation of smaller NPs than manual mixing (Figure 36). Indeed, it was rather the slower manual mixing that yielded smaller particles according to DLS. A closer look on the particle sizes using TEM revealed no significant differences in the particle size distributions between particles made through fast or slower mixing. A particular case was PEMA-COOH 1%, as the preparation of particles at the highest flow rates led to the formation of aggregates, we decreased the flow rates accordingly to avoid formation of aggregates. The ζ-potential was clearly negative for both ways of mixing, e.g. for PEMA-COOH 5% - 21 mV for manual and -27 mV for preparation with the impact jet mixer.

Quantum yield measurements of the corresponding dye-loaded NPs also showed very similar values, with in some cases a slightly lower value for the particles made using microfluidics.

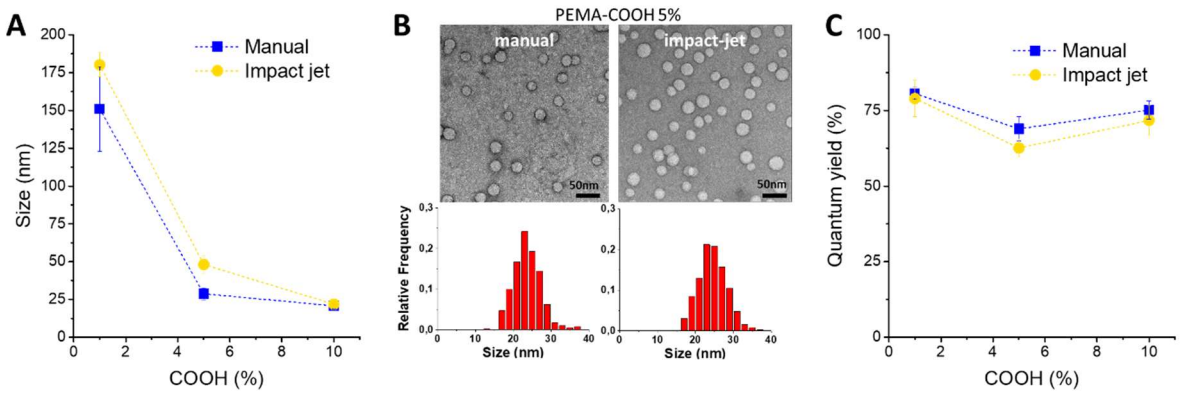

Figure 36: Sizes from DLS (A), TEM micrographs and histograms (B), and quantum yield (C) of NPs made from PEMA-COOH with different COOH fractions either manually or using an impact-jet mixer. NPs contained 30 wt% dye (R18/F5-TPB). Nanoprecipitation was performed in phosphate buffer. The used flow rates were 5 mL.min^{-1} except for PEMA-COOH 1%, where 2 mL.min^{-1} was used in order to avoid aggregate formation. For DLS and QY mean values from three independent preparations are given. Error bars correspond to standard error of the mean. For TEM histograms at least 200 particles were analyzed per condition.

Quantum yields provide a qualitative information on the encapsulation of fluorescent dyes. Indeed, it was shown that improper encapsulation is responsible of a decrease in the QY of the NPs[143]. Here the high QYs measured (close to 70%) for all the polymers and mixing methods suggest a homogeneous encapsulation of the dyes within the particles.

Next, we varied the overall hydrophobicity of the polymer by using copolymers of EMA and HEMA with varying fractions of the two monomers. As expected from previous results,[152] we observed a decrease in particle size, as well as a decrease in QY with increasing fraction of hydrophilic groups in the polymer (Figure 37). For HEMA contents starting from 25%, particles prepared through fast mixing using the impact-jet mixer showed significantly lower sizes in DLS. TEM images confirmed a significant shift of the particle size distribution to smaller sizes for preparation using microfluidics compared to manual preparation. Indeed, both the mean values of the particle sizes as well as the sizes of the largest particles were significantly lower for the former. The ζ-potential was again clearly negative in both cases (e.g. -30 mV and -20 mV for EMA/HEMA 25/75, respectively, for manual and impact jet mixing). At the same time, we observed significantly higher QYs for the particles prepared through microfluidics, starting from 25% of HEMA content. Mixing thus has a distinctive influence on particle formation in the case of these polymers.

Interestingly, the effect of mixing was strongly reduced when a block copolymer of the same composition was used (Figure 38).

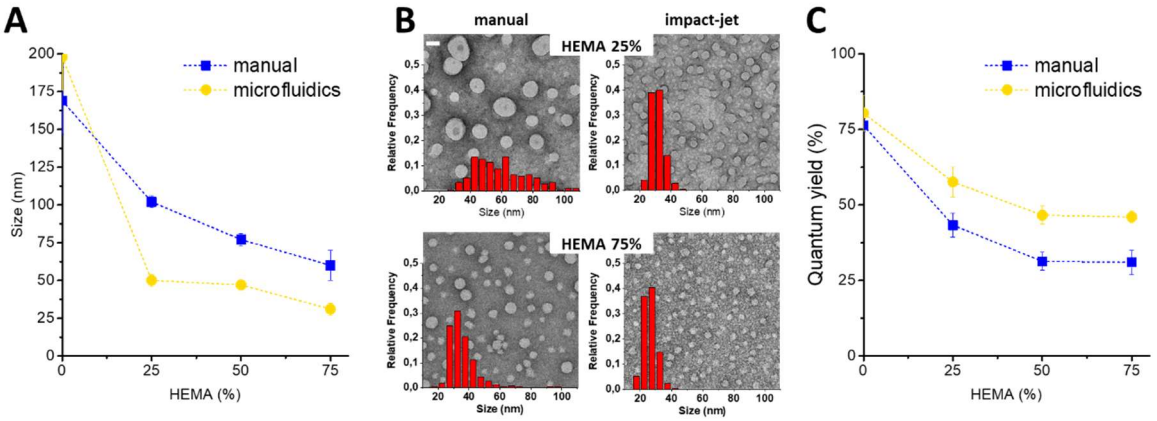

Figure 37: Sizes from DLS (A), TEM micrographs and histograms (B), and quantum yield (C) of NPs made from EMA-HEMA copolymers with different HEMA fractions either manually or using an impact-jet mixer. NPs contained 30 wt% dye (R18/F5-TPB). Nanoprecipitation was performed in Milli-Q water. The used flow rates were 10 mL.min^{-1} except for EMA 100%, where 2 mL.min^{-1} was used in order to avoid aggregate formation. For DLS and QY mean values from three independent preparations are given. Error bars correspond to standard error of the mean. For TEM histograms at least 200 particles were analyzed per condition.

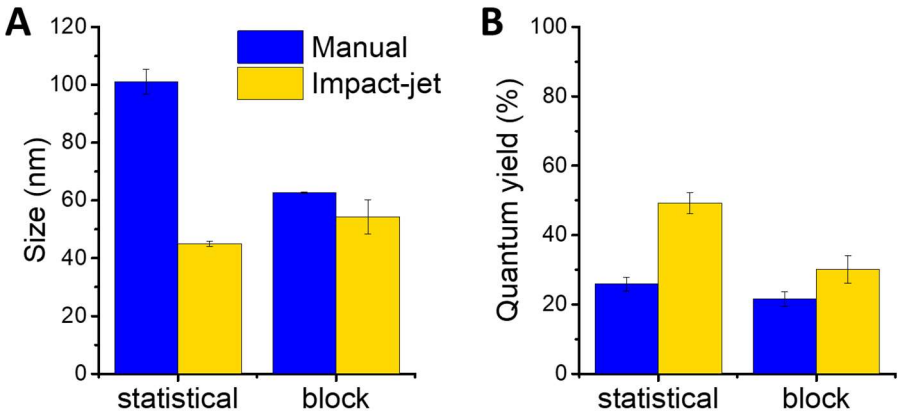

Figure 38: Size (A) and QY (B) of NPs of EMA/HEMA (50/50) statistical and block copolymers, with 10 wt% dye (R18/F5-TPB) prepared using the impact-jet mixer and manual nanoprecipitation in Milli-Q water. Mean values from three independent preparations are given. Error bars correspond to standard deviation. The flow rates used were 10 mL.min^{-1}.

1.5 Nanoparticles from Polyesters

In a next step we extended our study to biodegradable polyesters frequently used in the assembly of nanoparticles for biomedical applications: PLGA and PLA, as well as a

PLGA-PEG block copolymer. In the case of the latter, NPs between 37 and 43 nm have been obtained, whatever the conditions of assembly, indicating that mixing had no significant influence on NP formation for this polymer. Nevertheless, for this polymer NPs made through fast mixing using the impact-jet mixer showed higher QYs than those prepared manually. In the case of acid terminated PLGA a clear influence of mixing was observed for NPs prepared in Milli-Q water, as observed previously,[98] while this effect was much less expressed in phosphate buffer. For PLA, finally, fast microfluidic mixing gave clearly smaller NP sizes and higher QYs whatever the aqueous phase.

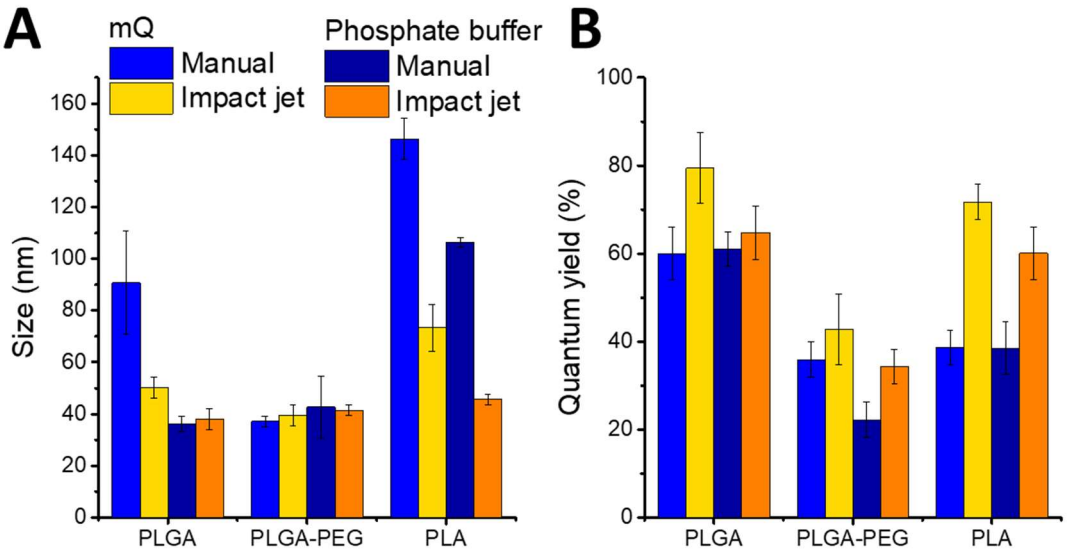

Figure 39: Size (A) and QY (B) of NPs of PLGA, PLGA-PEG and PLA, with 5 wt% dye (R18/F5-TPB) prepared using the impact-jet mixer and manual nanoprecipitation in Milli-Q water or phosphate buffer. Mean values from three independent preparations are given. Error bars correspond to standard deviation. The flow rates used were 5 mL.min^{-1}.

1.6 Discussion

In order to differentiate the relative effects of polymer chemistry and mixing on the formation of loaded polymer NPs, we tested several aspects of polymer chemistry in two types of mixing: manual mixing, resulting in a mixing time of several tens of milliseconds, and microfluidics based mixing using an impact jet mixer, which resulted in mixing times on the microsecond timescale. We can first distinguish the polymers considering, whether the size of the formed NPs depends on mixing or whether it is independent of the type and speed of mixing. The latter group includes the charged EMA based polymers without HEMA, the EMA/HEMA block copolymer, but also PLGA and PLGA-PEG, when precipitated

in phosphate buffer. A common point between all these is that their limit of solubility in the considered aqueous phase lies below 6% of water fraction. Among the systems, where mixing matters, we find the EMA/HEMA copolymers, PLA, but also PLGA when precipitated in Milli-Q water. For all of these the limit of solubility lay above a water fraction of 6%. Overall this indicates that the most "hydrophobic" polymers are insensitive to mixing, while mixing plays a decisive role in case of the less hydrophobic ones. It should also be noted that charged groups play an important role: On the one hand, the only polymer that is insensitive to mixing, while having a solubility limit above 6 vol% water is the PLGA-PEG block copolymer (in case of precipitation in MillliQ water), which does not have charged groups. On the other hand, the systems being the least sensitive to mixing are those, where charge effects are supposed to be the most important, e.g. PEMA-COOH in phosphate buffer.

A possible explanation for these observations is that in case of the most hydrophobic polymers a very small amount of water is sufficient to induce phase separation or at least deswelling of the chains. This would lead to the formation of single chain primary particles that then aggregate with other polymer chains in a diffusion controlled process.[81,159] In view of the small amount of water needed, and the much faster diffusion of water compared to polymer chains, the diffusion of the polymers or primary particles would then always be the rate determining step. Particle growth will then be mainly limited by the stabilization of the particles, notably through the build-up of a sufficient surface charge. In case of a higher solubility limit, the diffusion of water would become more important with respect to polymer diffusion, in which case the way and speed of mixing gains increasing importance. Indeed, it has been found previously that in these conditions the relative rates of diffusion of the polymers and their reorganization become decisive for particle formation.[160,161]

The influence (or its absence) of mixing on the encapsulation of the load was monitored here through the fluorescence QY. Decreasing QY can be linked to increasing aggregation of the dye molecules. In practically all cases, the influence of mixing on the QY overlapped with the influence on particle size. This could be explained by the fact that in case of the most hydrophobic polymers "phase separation" occurs very rapidly, followed by adhesion of dye salt to the polymer, rather than that dye aggregation in solution can occur.

Interestingly, the limit of solubility of the dye salt alone was found to be close to the critical value of 6 vol% of water.

2 Monitoring nanoprecipitation

In a next step, we were interested to quantitatively measure the kinetics of NP formation and in particular, how they were affected by changes in polymer chemistry. Indeed, examples of the direct monitoring of nanoprecipitation are scarce, principally due to the observation difficulty of this phenomenon[162]. The rapid formation of NPs requires a setup with high temporal resolution coupled with instruments able to detect objects at a nanometric scale. Rapid mixing can be obtained with the use of microfluidic mixers[163] or with stopped flow devices, commonly used for kinetic studies[164,165]. Both systems have been coupled with SAXS or SANS[165–167] to study nano-size objects such as proteins[168] or detect the formation of polymeric[169] or inorganic[170–172] NPs. However, to the best of our knowledge, no study focused on the role of polymer chemistry in nanoprecipitation. Our approach is to use fluorescence spectroscopy, and in particular the FRET phenomenon, to observe the formation of particles during precipitation[173]. Firstly, fluorescent polymers are dissolved in organic solution, where no FRET should be observed due to the distance between dyes. Then, during precipitation, polymer chains aggregate, reducing the distance between dyes and resulting in the appearance of FRET. The evolution of the FRET efficiency during the precipitation of polymers should therefore allow visualizing chain association (Figure 40).

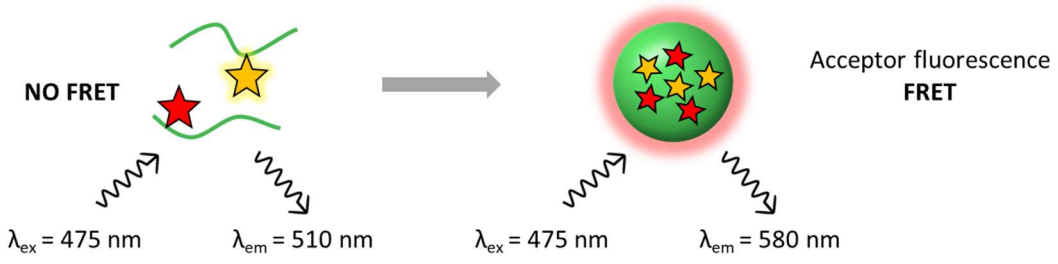

Figure 40: Basic scheme for monitoring particle formation using FRET.

This experiment has been performed with a stopped flow setup: this device performs a rapid mixing of solutions, which are injected into an observation cell. Then the flow is stopped and measurements are performed with a high temporal resolution. The advantages of this approach is that fluorescence spectroscopy is a very sensitive

technique and FRET can only occur if the dyes are very close (< 10nm), allowing fine detection of the assembly of polymer chains. This study was performed on different polymers bearing either the donor or the acceptor dye.

2.1 Synthesis of fluorescent polymers

A first step was therefore to synthesize different polymers labelled separately with a suitable donor-acceptor pair. The study has been performed on a series of polymethacrylates containing different amounts of hydrophilic groups, which is statistical PEMA-HEMA polymers. Four polymers have been synthetized containing EMA and 0, 25, 50 or 75 mol% of HEMA with 1 mol% of methacrylic acid. To limit differences between polymers, we opted for a post-functionalization approach. In order to functionalize these polymers with fluorescent dyes, 1 mol% of an activated ester monomer, pentafluorophenyl methacrylate (PF5), has been added during polymerization (Figure 41). This monomer is able to react with primary amines to form an amide bound. Therefore, it can be used for post-synthesis functionalization of polymers with amine-bearing fluorophores[174]. For more clarity, MAA and PF5 percentage will be omitted in the name of polymers. For example, a polymer with the following composition: 49% EMA, 49% HEMA, 1% MAA and 1% PF5 will be noted PEMA-HEMA 50-50.

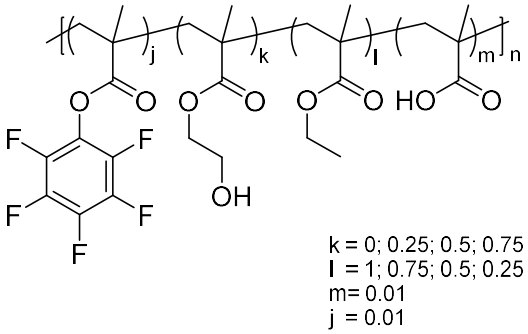

Figure 41: General structure of the functionalizable polymers used in this study.

In total, four polymers have been synthetized, namely PEMA-HEMA 100-0, 75-25, 50-50 and 25-75. The polymerization conversion was kept relatively low to avoid strong variations in the composition of the polymer chains. Polymers have been purified by two successive precipitations in H_2O/MeOH mixtures (the ratio was adjusted for each polymer composition) and characterized by NMR. The percentage of active ester per polymer chain has been measured in NMR by adding trifluoroethanol as standard in the deuterated

solvent (1 mg.mL^{-1}). This molecule has two aliphatic protons and three fluorine atoms, hence it allows to establish a ratio between ^{1}H and ^{19}F NMR integrations and calculate the amount of PF5 monomer in polymers chains. This procedure is detailed below for the PEMA polymer, whose NMR spectra can be found in the protocols section at the end of the manuscript.

The ^{1}H integration signal of trifluoroethanol around 4 ppm ($A_{standard}$) is divided by the integration signal of the CH_2 groups of the polymer chain ($A_{polymer}$) to obtain the molar ratio of the two species (Equation 19). Both account for two carbons so their ratio directly leads to the molar ratio between trifluoroethanol and repeating units of polymers. Deconvolution has been used because the chemical shift of the two signal is close.

$$\frac{n_{Standard}}{n_{Polymer}} = \frac{A_{Standard}}{A_{Polymer}} \qquad \text{(Equation 19)}$$

Then the ^{19}F integration of the trifluoroethanol at -77 ppm ($I_{standard}$, divided by 3 because it integrates for 3 fluorine atoms) is divided by the integration signal at -165 ppm from the pentafluorophenyl groups (I_{PF5}, divided by 2 because it integrates for 2 fluorine atoms). This ratio gives the molar ratio between trifluoroethanol and the functionalizable groups in the polymer chain (Equation 20):

$$\frac{n_{Standard}}{n_{PF5}} = \frac{\frac{I_{Standard}}{3}}{\frac{I_{PF5}}{2}} \qquad \text{(Equation 20)}$$

Finally, the quotient of these two ratio gives the percentage of PF5 groups in polymer chains (Equation 21). Here:

$$\frac{n_{PF5}}{n_{Polymer}} = \frac{\frac{A_{Standard}}{A_{Polymer}}}{\frac{I_{Standard}/3}{I_{PF5}/2}} = \%_{PF5} \qquad \text{(Equation 21)}$$

For example, in the case of the PEMA polymer, we obtain:

$$PF5\ fraction = \frac{204685/2657890}{\frac{3/3}{0.27/2}} = 0.0104 = 1.04\%$$

Therefore, the PEMA polymer contains 1.04% of PF5 groups. The same protocol has been repeated for all polymers. The percentage of PF5 groups for each polymer is given in table

2. Two polymers, the PEMA-HEMA 75-25 and 25-75, have a relatively high amount of PF5 compared to the feeding ratio of the monomer, which was 1%. In both cases, the conversion of polymerization reactions of these polymers was relatively high. In fact, we usually try to keep the conversion below 25% but for these polymers it reached 36% and 42% respectively. Hence, the high content of PF5 may come from a difference in the reactivity of the monomers which affect the composition of polymers for high conversion rates.

Polymer	Conversion of polymerization reaction (%)	PF5 content in polymer chains (%)
PEMA	26	1.04
PEMA-HEMA 75-25	36	2.25
PEMA-HEMA 50-50	26	1.10
PEMA-HEMA 25-75	42	1.91

Table 2: Reactions conversions of polymers synthesis and percentage of functionalizable groups per polymer chains.

These polymers have then been functionalized with an amine bearing bodipy or rhodamine, to make eight fluorescent polymers (Figure 42).

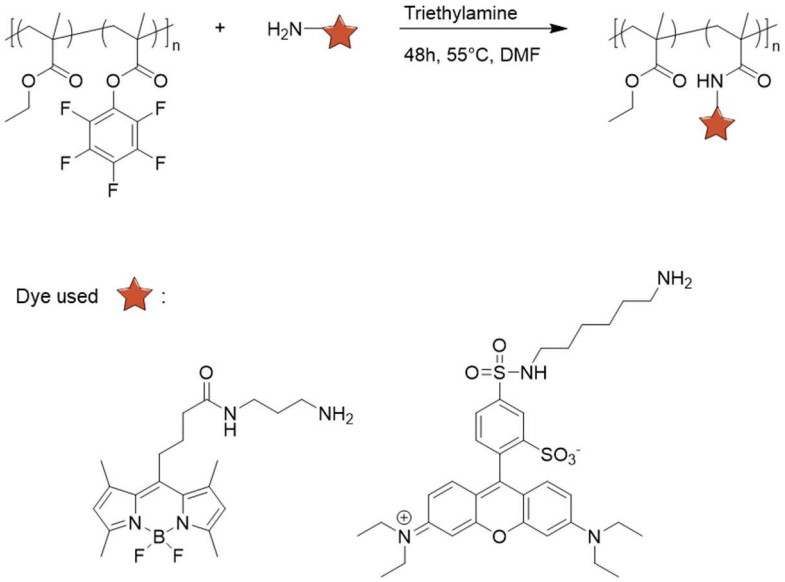

Figure 42: Method for the functionalization of polymers with a fluorescent dye and chemical structures of fluorescent dyes used to functionalize polymers (Left: bodipy, right: rhodamine).

Briefly, polymers were dissolved in DMF, and 3 equivalents of fluorophore (in respect to PF5 amount) were added together with triethylamine. Reactions were set at 55°C for 48h prior addition of 40 equivalents of ethylamine. This large excess of ethylamine was used

to cap unreacted sites. Reactions were quenched by precipitation, followed by purification on steric exclusion chromatography.

Thereby, every polymer has been functionalized separately either with a FRET donor (bodipy) or acceptor (rhodamine) fluorophore. Each polymer couple was made with the same batch of functionalizable polymer, ensuring they have the same composition, molecular weight and dispersity. The amount of functionalized sites has been estimated by UV-Vis analysis of polymer solutions. The fluorophore concentration has been calculated using the Beer-Lambert law (with ε_{bodipy} = 80000 L.mol^{-1}.cm^{-1} and $\varepsilon_{rhodamine}$ = 100000 L.mol^{-1}.cm^{-1}) and it has been divided by the polymer concentration to obtain the molar fraction of dyes per polymer chain ($\%_{Dye}$). This value has been compared with the molar fraction of PF5 groups ($\%_{PF5}$) calculated by NMR to determine the efficiency of the coupling reaction ($\%_{Functionalization}$) as given in equation 22:

$$\%_{Functionalization} = \frac{\%_{Dye}}{\%_{PF}} = \frac{\frac{C_{Dye}}{C_{Poly}}}{\%_{PF5}} = \frac{\frac{\frac{A}{l*\varepsilon}}{C_{Poly}}}{\%_{PF5}} \qquad \text{(Equation 22)}$$

Where C_{Dye} and C_{Poly} are the molar concentrations of fluorophore and polymer in solution respectively, A the absorbance obtained in UV-Vis measurements, ε the molar extinction coefficient of the dye and l the length of the cuvette (1 cm).

Table 3 shows the percentage of functionalizable sites that have reacted with a fluorophore for each coupling reaction. The mean value of functionalized sites with the bodipy is slightly higher than the one with rhodamine for all the polymers. This may be due to the smaller size of the bodipy, reducing steric hindrance when the molecule approaches a polymer chain. The molar percentage of dye per polymer chain is also given, as measured by absorbance ($\%_{Dye}$).

Polymer	Functionalized sites with bodipy (%)	Functionalized sites with rhodamine (%)	% Bodipy	% Rhodamine
PEMA	36	25	0.37	0.26
PEMA-HEMA 75-25	33	21	0.74	0.54
PEMA-HEMA 50-50	42	28	0.46	0.31
PEMA-HEMA 25-75	39	22	0.75	0.42

Table 3: Efficiency of the coupling reaction between polymers and fluorescent dyes and molar percentages of dye per polymer chain.

We further wanted to estimate the number of dyes per polymer chain. The molecular weight measurements of these polymers have not been performed yet, hence we will use the value measured for a polymer synthetized in similar conditions that is the PEMA-COOH 5%. This polymer has a molecular weight M_n = 127 000 g.mol^{-1}, corresponding approximately to 1100 monomers per chain. The molar percentage of dye per polymer is comprised between 0.26 and 0.74 %. Hence, roughly estimated, there are between 3 and 8 dyes per polymer chain.

In this way, a series of four statistical polymers with various hydrophobicities have been synthesized. They are composed of a hydrophobic monomer (ethyl methacrylate) and contain 0, 25, 50 or 75% of a hydrophilic monomer (hydroxyethyl methacrylate). All polymers were functionalized separately with a bodipy and a rhodamine dye, making four polymer couples to monitor particles formation by FRET (Figure 43).

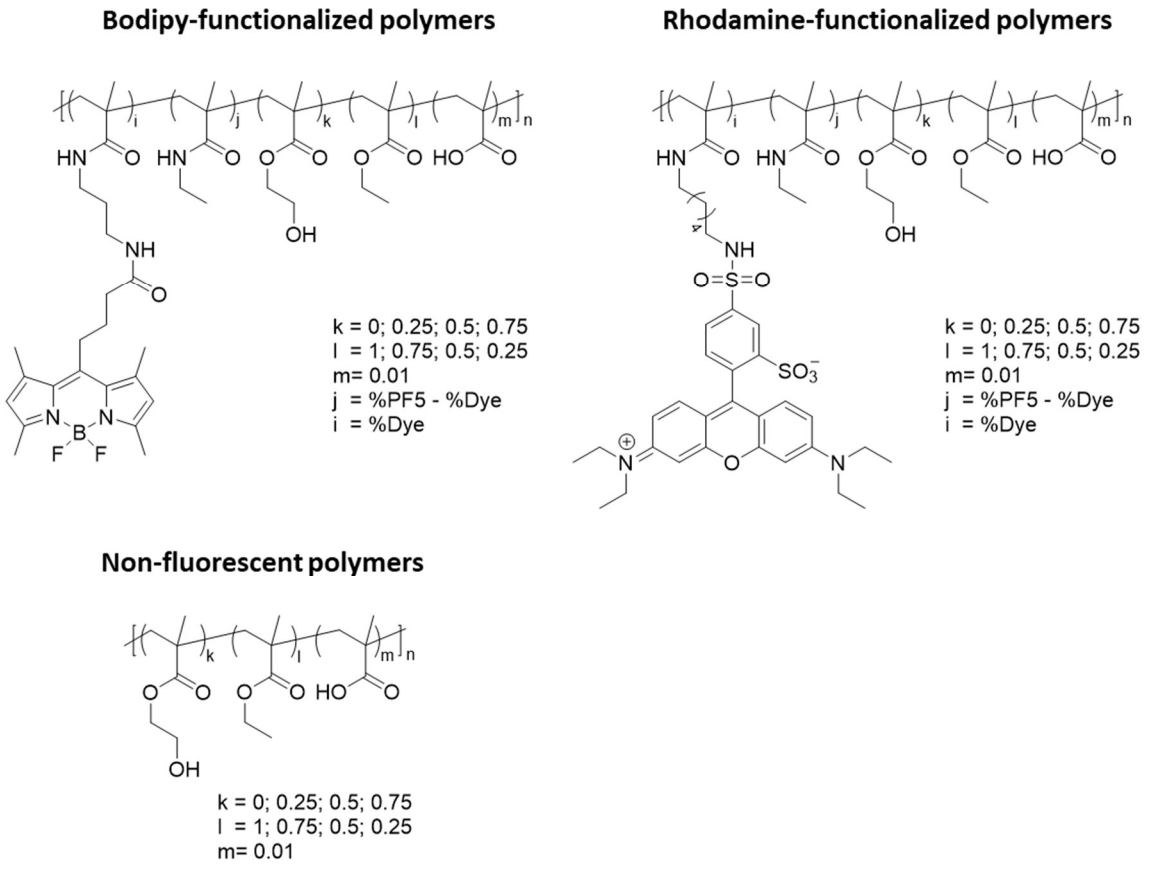

Figure 43: Chemical structures of bodipy or rhodamine-functionalized polymers and non-fluorescent polymers used in this study.

Stock solution of polymers were prepared at 2 g.L^{-1}, then their absorbance was measured and adjusted in order to have the same amount of dyes in all the experiments.

Indeed, the polymers had different coupling efficiencies with dyes, and then making stock solutions at the same polymer concentration do not ensure there is the same amount of dye in all solutions. However, analysis of FRET experiments is simplified with the same number of donor and acceptor dyes. Therefore, stock solutions of fluorescent polymers at 2 $g.L^{-1}$ were mixed with solutions of their non-fluorescent analogues at 2 $g.L^{-1}$ to adjust the absorbance of all solutions at the same value. Normalized absorption and emission spectra of polymer solutions are given in figure 44A. Moreover, the fluorescence signal of a polymer dissolved in organic solution and precipitated in water has been recorded to visualize the change of its emission spectra due to the apparition of FRET (Figure 44B). A strong decrease of the fluorescence emission of the donor is visible at 510 nm, while the increase of the signal at 580 nm correspond to the fluorescence emission of the acceptor.

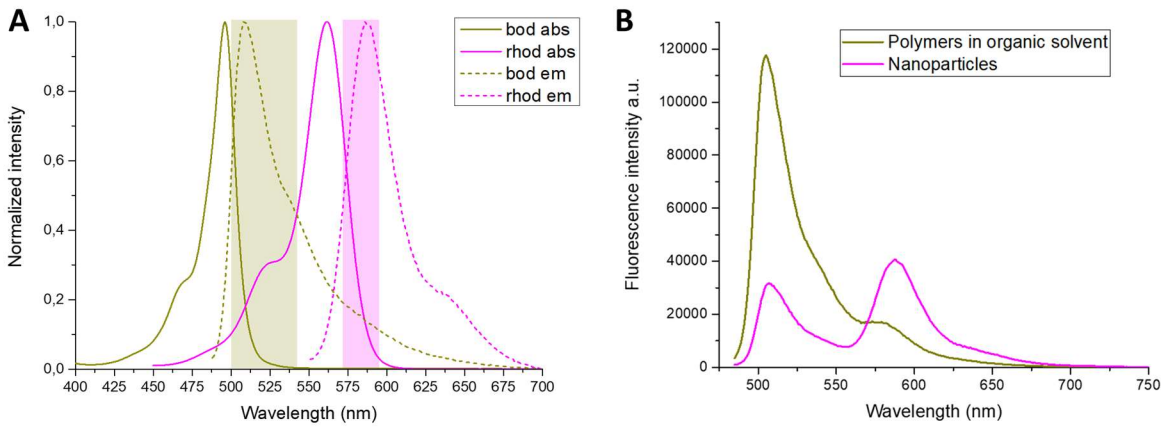

Figure 44: (A) Normalized spectra of absorption and emission of fluorescent polymers (PEMA-HEMA 75-25 was used for this figure) functionalized with bodipy and rhodamine. The rectangles correspond to the observation windows of the band-pass filters (500-540 and 570-590nm).(B) Emission of polymer (PEMA-HEMA 25-75) in organic solution and in water after nanoprecipitation.

2.2 Stopped flow experiments

2.2.1 Description of the stopped flow setup

The central part of the stopped flow setup is the observation cell. Reactions take place in this chamber and are monitored via diverse means. In our case, it was used to observe the nanoprecipitation of polymer chains thanks to fluorescence measurements. The polymer solution and the water phase are initially contained in two syringes. When the pistons are actuated, the solutions are mixed and directed toward the observation cell. A stop-valve placed after the cell then stops the stream and the measurement starts. The functioning of the setup is represented in Figure 45.

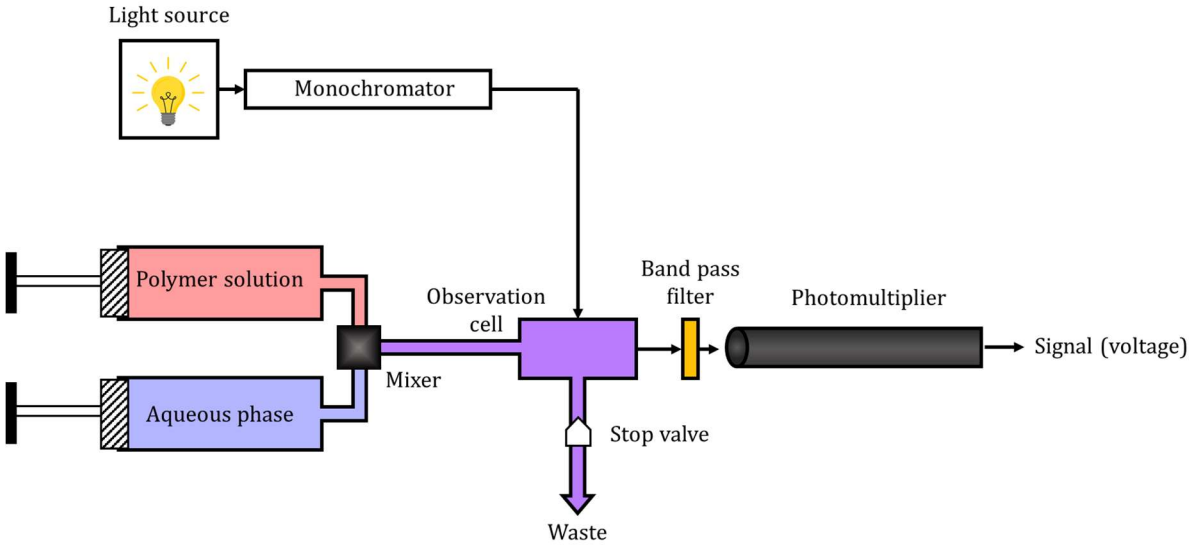

Figure 45: Scheme of the elements composing the stopped flow setup.

2.2.2 Acquisition parameters

The precipitation was performed by mixing the organic and the aqueous phases in a 1:9 ratio. The dead time given by the constructor is 3.7 ms. This correspond to the time taken by the solution to reach the observation cell after mixing. Hence the first value recorded corresponds to t=3.7 ms (and not t=0 ms). In order to observe the emission of bodipy-functionalized polymers, the corresponding band pass filter (500-540 nm) and an excitation wavelength of 475 nm were used.

2.3 Results

2.3.1 Nanoprecipitation of fluorescent polymers

In order to perform FRET experiments, solutions of bodipy and rhodamine functionalized polymers were mixed in a 1:1 ratio for a final polymer concentration of 0.5 $g.L^{-1}$. The raw data obtained after stopped flow measurements are presented first followed by the calculation of the FRET efficiency. As a reminder, the FRET efficiency is calculated following equation 13:

$$FRET_{efficiency} = 1 - \frac{Imax\ (D)}{Imax\ (D0)} \qquad \text{(Equation 13)}$$

Where Imax(D0) and Imax(D) are the maximum intensities of the donor alone and in the presence of the acceptor respectively. In order to record the signal of the donor alone,

bodipy-functionalized polymers were mixed with non-fluorescent polymers in a 1:1 ratio, giving polymer solutions at 0.5 $g.L^{-1}$ with the same amount of donor dye than experiments in presence of acceptor dye (Figure 46).

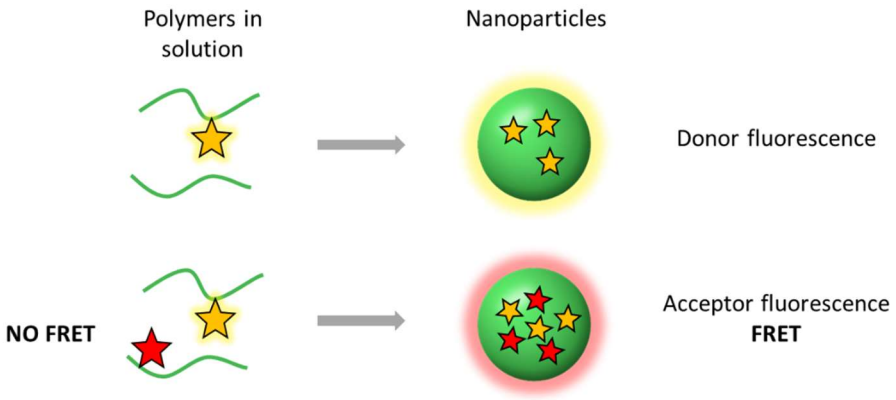

Figure 46: Scheme representing the fluorescence signal emitted by NPs when the donor dye is precipitated alone (top) and in the presence of acceptor (bottom).

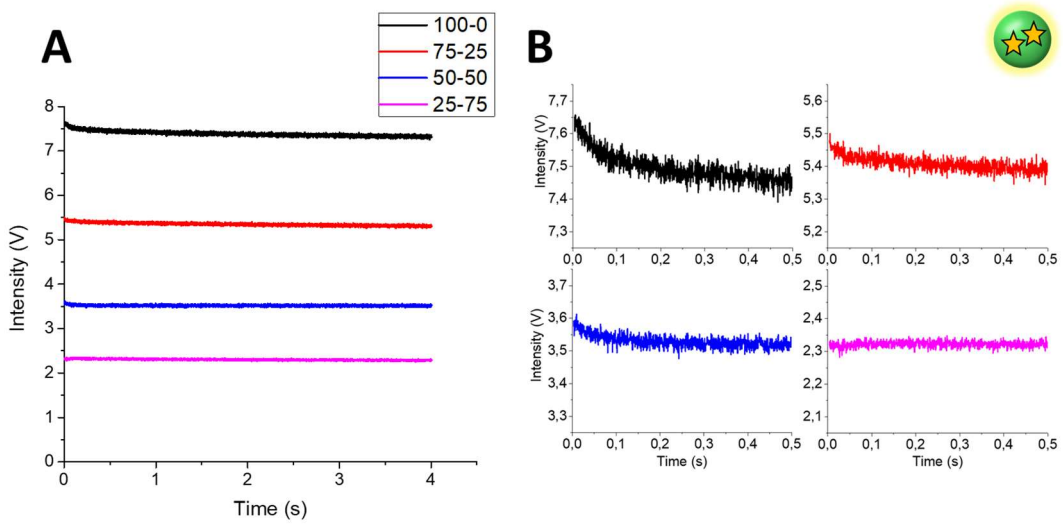

*Figure 47: Donor-polymers signals during precipitation measured between 500-540 nm with a photomultiplier coupled with a stopped flow setup. λex = 475 nm, colors correspond to the different polymers: **PEMA** (noted **100-0**), **PEMA-HEMA 75-25**, **PEMA-HEMA 50-50**, **PEMA-HEMA 25-75**. A) Signals over four second range. B) Zoom on each signal at short times.*

The signals of the donor polymers when they were precipitated in the absence of acceptor were recorded in a first place. The intensities of the donor signals were globally constant over time for each polymer (Figure 47). The PEMA polymer and to a minor extend PEMA-HEMA 75-25 and 50-50 polymers showed a small decrease of the signal at short times. However, the intensity of the signals varied a lot between the different polymers despite the same amount of fluorophore in every polymer solution. The signal

was the strongest with the most hydrophobic polymer (PEMA) while its intensity decreased when the percentage of HEMA in the polymer chains increased. This could be explained by a difference in the QY of the dyes depending on their environment. Indeed, higher QY of hydrophobic dyes have been observed when the latter were encapsulated in more hydrophobic polymers[13].

In the next step, bodipy and rhodamine-functionalized polymers have been precipitated together. This resulted in a decrease of the signal of the donor dyes over time (Figure 48).

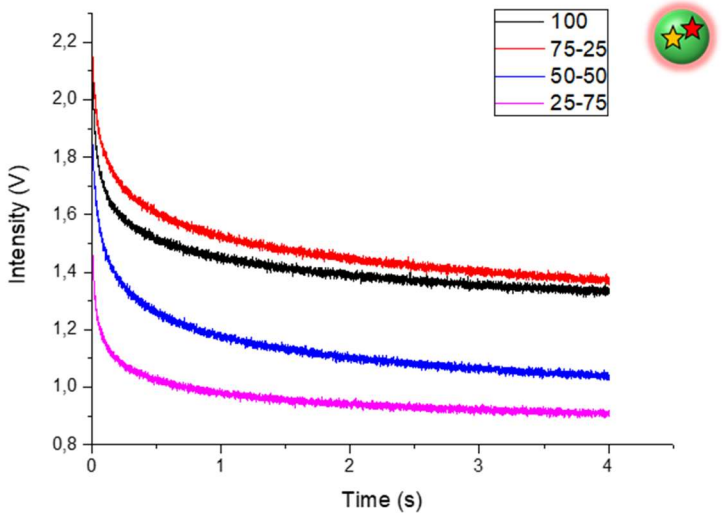

Figure 48: Donor-polymers signals during co-precipitation with acceptor-functionalized polymers measured between 500-540 nm with a photomultiplier coupled with a stopped flow setup. λex = 475 nm, colors correspond to the different polymers: ***PEMA*** *(noted* ***100-0****),* ***PEMA-HEMA 75-25****,* ***PEMA-HEMA 50-50****,* ***PEMA-HEMA 25-75****.*

The decrease of the intensity of the donor signal can be attributed to the appearance of FRET as polymer chains assemble. It is sharp in the early stage of precipitation and becomes slower after approximately 200 ms. The FRET efficiency during precipitation has been calculated for all polymers based on these signals and the intensity of the donor-functionalized polymers alone (Figure 49). The FRET efficiency increased during the precipitation of the polymers, rapidly during the first 200 ms and then at a slower rate. When the amount of HEMA in polymer chains was increased, both the initial and the final values of FRET efficiency decreased gradually.

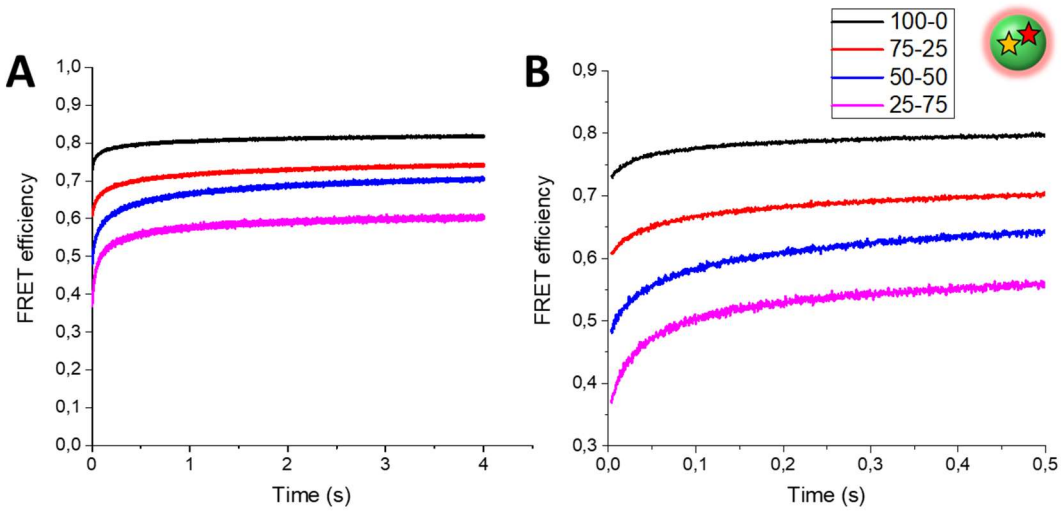

Figure 49: FRET efficiency during nanoprecipitation of polymers. Colors correspond to the different polymers: ***PEMA*** *(noted* ***100-0****),* ***PEMA-HEMA 75-25****,* ***PEMA-HEMA 50-50****,* ***PEMA-HEMA 25-75****. A) FRET efficiency over four second range. B) Zoom on FRET efficiency at short times.*

Focusing on the early stage of precipitation allows a better visualization of the evolution of the FRET efficiency between polymers (Figure 49B); hence, we used the first 500 ms of the each measurement to compare the obtained results. The total increase of FRET efficiency appears to be higher for the more hydrophilic polymers. For instance, it increased from 73 to 80% for the PEMA polymer within the first 500 ms, whereas for the PEMA-HEMA 25-75 it went from 37 to 56%.

2.3.2 Influence of polymer concentration

We further investigated the influence of polymer concentration on the evolution of FRET efficiency. We have chosen the polymer with the highest FRET increase, that is PEMA-HEMA 25-75, to perform these experiments. Polymer solutions were prepared at 1 $g.L^{-1}$ and diluted at 0.5, 0.25 and 0.125 $g.L^{-1}$. Unfortunately, the solution at 0.25 $g.L^{-1}$ gave inconsistent results, so this experiment has been excluded from the series and will be repeated later. The intensity of the signals corresponding to the donor polymers precipitated alone increased gradually with the concentration of polymers, as expected for an increased amount of donor dyes (Figure 50A). These signals were stable over time except at the beginning of the measurement where they slightly increased. This increase was more marked when polymer solutions were more concentrated. When precipitated with the acceptor (rhodamine) functionalized polymers, the signals of the donor dyes

decreased over time as observed previously: the decrease was sharp during the first hundreds of milliseconds and then slower until the end of the measurements (Figure 50B).

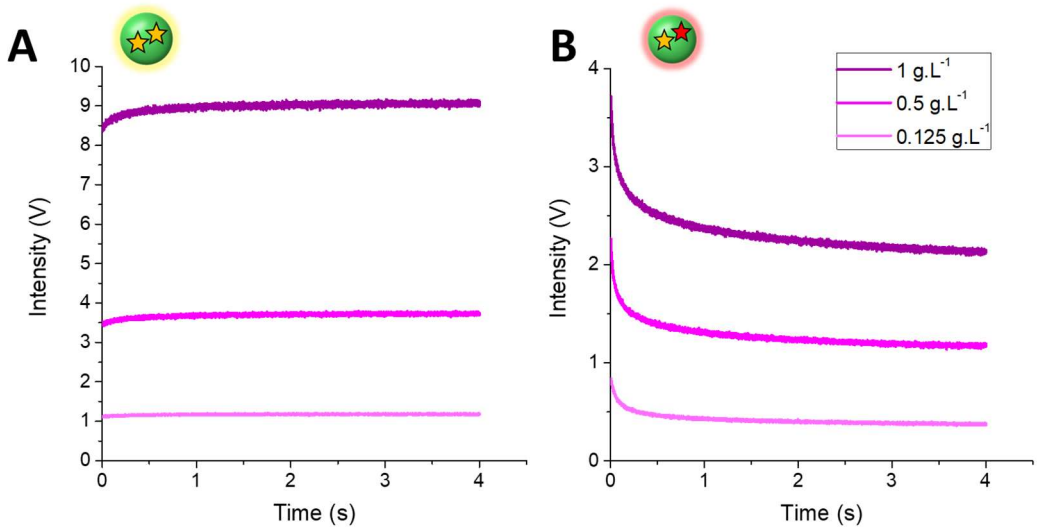

*Figure 50: Donor-polymer signals of **PEMA-HEMA 25-75** during co-precipitation (A) alone and (B) with acceptor-functionalized polymers measured between 500-540 nm with a photomultiplier coupled with a stopped flow setup. λex = 475 nm, colors correspond to the different polymer concentrations: **1 g.L-1**, **0.5 g.L-1** and **0.125 g.L-1**.*

The FRET efficiency was again plotted during the first 500 ms of the measurements (Figure 51). The initial FRET efficiency increased with polymer concentration, as did the final one.

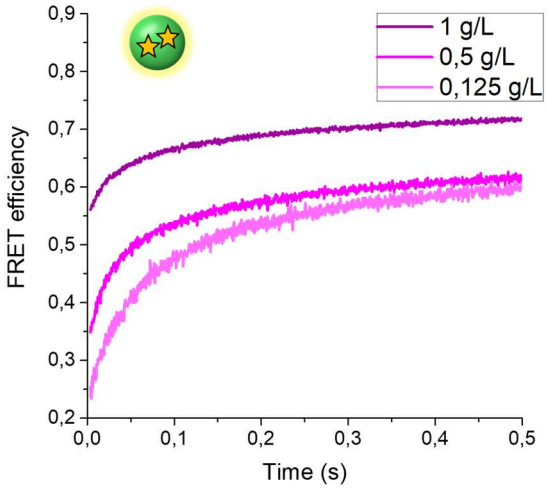

*Figure 51: FRET efficiency vs time during nanoprecipitation of the **PEMA-HEMA 25-75** polymer as obtained from stop-flow experiments. Colors correspond to the different polymer concentrations: **1 g.L-1**, 0.5 g.L-1 and **0.125 g.L-1**.*

A further major difference observed between the measurements was the total increase of FRET efficiency, which was greater when the polymer concentration was decreased.

Indeed, it increased from 59 to 72% and from 25 to 60% when the polymer concentration was 1 $g.L^{-1}$ and 0.125 $g.L^{-1}$ respectively.

2.3.3 Encapsulation of fluorescent dyes

In a next step, we were interested to observe how polymer chemistry influences the encapsulation of hydrophobic dyes. For this purpose, we used two hydrophobic dye salts able to undergo FRET, R18/F5-TPB and CY5/F12-TPB (Figure 52 A and B). We have chosen these dyes because they are readily encapsulated in NPs during precipitation[143,175]. In this FRET couple the rhodamine plays the role of the donor dye, therefore the signal recorded during the precipitation was the emission of the rhodamine. This was achieved by using a band pass filter with an observation window between 570 and 590 nm and with an excitation wavelength at 560 nm (Figure 52 C).

The experiment relies on the same principle than the monitoring of polymer nanoprecipitation but focused on dye encapsulation: In this case, the fluorescent dyes are not covalently bound to polymer chains. Therefore, the polymers used were not fluorescent. The fluorescence signal of the donor dye (rhodamine) was recorded alone and in the presence of the acceptor (cyanine 5) during precipitation. Dyes have been co-precipitated with the most hydrophobic and the most hydrophilic polymer of the previous series, **PEMA** (noted **100-0**) and **PEMA-HEMA 25-75** respectively. Polymers were mixed with 4 wt% of R18 and 1 wt% of CY5 before measurements. This way the loading of the particles corresponded to 5% of the polymer mass and the ratio between the donor and acceptor was 4:1. The experiment was also conducted without polymer to observe the precipitation of the dyes alone.

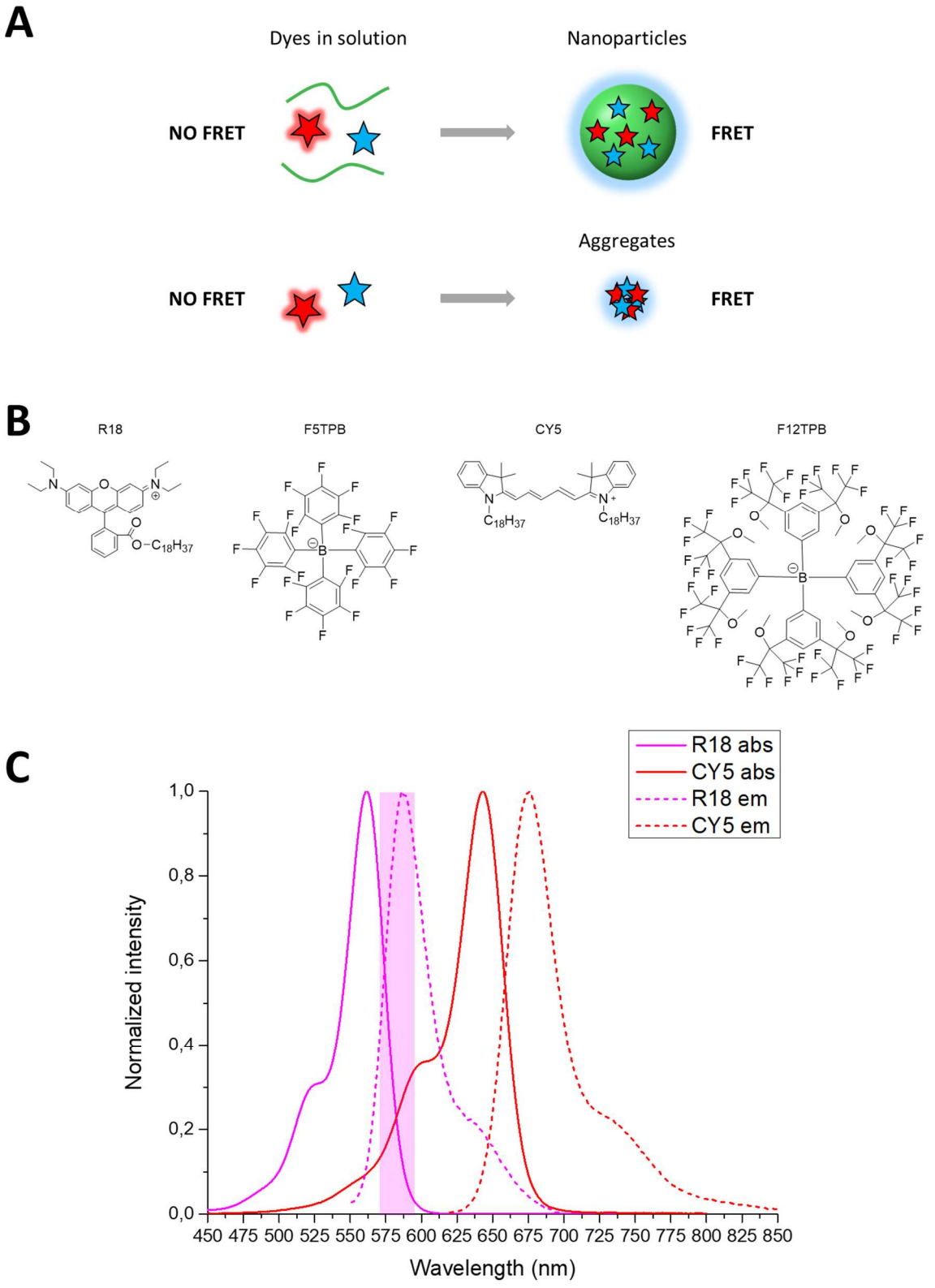

Figure 52: (A) Scheme representing the co-precipitation of hydrophobic dyes with polymer (top) or alone (bottom). (B) Chemical formula of fluorescent dyes and counterions used for these experiments. (C) Normalized spectra of absorption and emission of fluorescent dyes used for encapsulation. The rectangle corresponds to the observation windows of the band-pass filter.

In the case of R18 precipitated with polymers in absence of acceptor, a higher intensity of the signal was recorded compared to R18 precipitated alone (Figure 53A). Again, the intensity of the signals slightly varied in the beginning of the measurements before remaining stable. The reduction in the emission intensity of R18 precipitated alone is due to the aggregation caused quenching phenomenon, which cause a strong decrease in the dye quantum yield, as observed previously[176]. This effect is reduced when the dye is precipitated with polymers, leading to more intense signals. In the next step, the CY5 was added in the solutions and the evolution of R18 emission was recorded during the precipitation (Figure 53B).

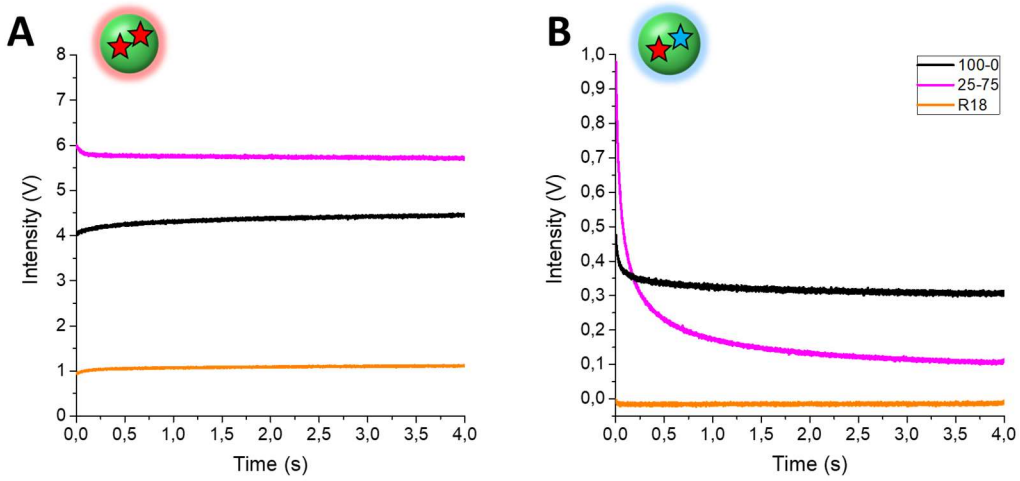

*Figure 53: Donor dye signals vs time during nanoprecipitation (A) alone and (B) in the presence of acceptor dye, measured between 570-590 nm with a photomultiplier coupled with a stopped flow setup. λex = 560 nm, colors correspond to the different polymers: **PEMA** (noted **100-0**), **PEMA-HEMA 25-75** and **no polymer**.*

When the dyes were precipitated without polymer, no emission from the rhodamine could be observed at all. The signal recorded was within the noise observed in control experiment in the absence of fluorophores (for this reason, its value is sometime negative). In the presence of polymer the emission of R18 decreased, strongly in the first 500 ms recorded and at a slower rate until the end of the measurement. This decrease was notably bigger and prolonged in the case of the PEMA-HEMA 25-75 polymer compared to the PEMA. The FRET efficiency was again plotted during the first 500 ms of the measurements. For the dyes alone it was equal to 100% and did not vary during the experiment. However, in the presence of polymers, it increased from 83 to 98% for the PEMA-HEMA 25-75 and from 88 to 93% for the PEMA (Figure 54).

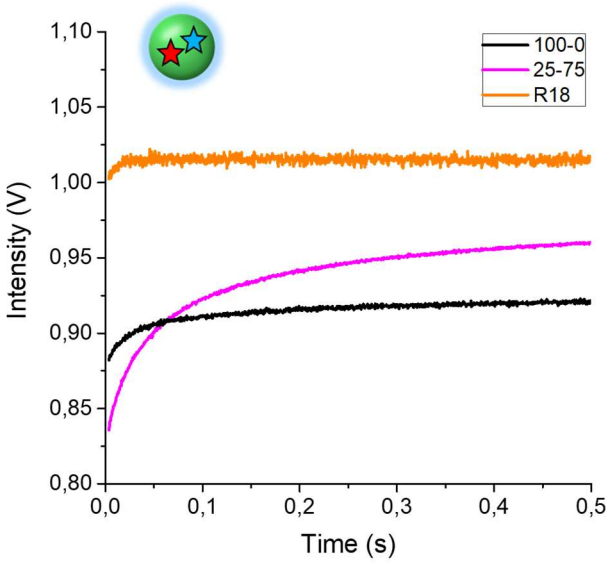

Figure 54: FRET efficiency of R18/CY5 dyes during precipitation. Colors correspond to the different polymers: ***PEMA*** *(noted* ***100-0****),* ***PEMA-HEMA 25-75*** *and* ***no polymer****.*

2.4 Discussion

In order to monitor the kinetics of NPs formation and study the influence of polymer chemistry, we synthetized a series of polymers with various amounts of hydrophilic monomers (HEMA). These polymers were functionalized with fluorescent dyes forming a FRET pair to study their nanoprecipitation via fluorescence measurements. Indeed, while no FRET was observed for mixtures of these polymers in organic solution, FRET occurred upon nanoprecipitation. To follow this quantitatively, the nanoprecipitation of the polymer bearing the donor dye was realized alone and in the presence of the acceptor using a stop-flow apparatus. The signals recorded allowed to calculate the FRET efficiency of the system during the precipitation and major differences were observed between the polymers.

The first noticeable difference is between the fluorescence signals of the polymers bearing the donor dye precipitated alone. The most hydrophobic polymers had a stronger signal, which was explained by a difference of the quantum yield of the dyes. This indicates that already at the beginning of the recording (after 3.7 ms), the dyes had a different

environment that strongly affects their emission properties. In some cases, the signal slightly varied during the beginning of the measurements and quickly stabilized suggesting no further evolution of the system.

A second result is the strong initial FRET efficiency and the evolution of the FRET efficiency during the measurements (the decrease of the donor signal in presence of acceptor is directly correlated to the FRET efficiency; therefore it is not discussed further). For all polymers, the FRET efficiency increases rapidly at the beginning of the measurements, before undergoing a slow growth between roughly 0.5 and 4 seconds. We believe that these two steps arise from different phenomena. The first is presumably due to the assembly of the polymer chains resulting in the apparition of FRET. The second phase could be due to a maturation phenomenon of the particles. Indeed, after their assembly polymer chains still have a little mobility[177], which could allow the dyes on the chains to reorganize inside the particles. Hence, we decided to focus our attention on the first 500 milliseconds of measurements to compare polymers. It should be noted that for every polymer a substantial part of the precipitation seems to happen during the dead time of 3.7 ms. Moreover, we did not investigate further the differences in the final value of FRET efficiencies. Indeed, this phenomenon could find multiple sources, such as a difference in quantum yield of dyes or simply an observation time too short for all particles to reach their final values of FRET efficiency. (Here the signal became unstable after about five seconds, presumably due to pressure variations in the system, which made a direct extension to longer times difficult.)

For each polymer, the increase of the FRET efficiency was calculated between its initial and final value (at 500 ms) and expressed as a percentage of its maximum (Equation 23):

$$FRET\ increase = \frac{F_{500} - F_{3.7}}{F_{500}} \qquad \text{(Equation 23)}$$

Where F_{500} and $F_{3.7}$ are the values of FRET efficiency at 500 and 3.7 ms respectively. For example, for the PEMA polymer, the FRET increase during precipitation is equal to $\frac{80-73}{80} = 0.0875$ or 9%. This polymer had the lowest FRET efficiency increase, with only 9% in the observation window. This value increased gradually with the percentage of HEMA in the polymers, up to 44% for the PEMA-HEMA 25-75. Therefore, the less hydrophobic was the polymer, the bigger was the increase of FRET observed, suggesting that the addition of

hydrophilic groups in the polymer composition slows down the precipitation. In order to quantify the precipitation rates of the polymers, one can determine the time for the FRET efficiency to reach 90% of its maximum, noted t (90%) in Table 4.

Polymer	FRET efficiency at 3,7 ms (%)	FRET efficiency at 500 ms (%)	FRET increase (%)	t (90%)
PEMA	73	80	9	< 3.7
PEMA-HEMA 75-25	61	70	13	16.7
PEMA-HEMA 50-50	49	64	23	74.2
PEMA-HEMA 25-75	37	56	34	93.7

Table 4: Increase of FRET efficiency and time to reach 90% of its maximal value during the first 500 ms of nanoprecipitation kinetic measurements for the different polymers.

The influence of polymer chemistry on precipitation then clearly appears, with the most hydrophobic polymer precipitating within few milliseconds, while the less hydrophobic precipitates in roughly 100 ms. The same calculations may be applied to the precipitation of polymer solutions at various concentrations (Table 5). In this case, increasing the concentration of polymer reduced the time required to reach 90% of the FRET efficiency, suggesting a faster association of polymer chains, which is in good agreement with a diffusion controlled process requiring the encounter of primary aggregates.

Concentration ($g.L^{-1}$)	FRET efficiency at 3,7 ms (%)	FRET efficiency at 500 ms (%)	FRET increase (%)	t (90%)
1	56	72	22	62.2
0,5	35	62	44	139
0,125	25	60	58	184

Table 5: Increase of FRET efficiency and time to reach 90% of its maximal value during the first 500 ms of nanoprecipitation kinetic measurements for different concentration of the PEMA-HEMA 25-75 polymer.

In order to study the encapsulation of fluorescent dyes we performed similar experiments with two dyes forming a FRET pair, which were not covalently attached to the polymers, but co-precipitated with non-fluorescent polymers, or alone. In the latter case, the FRET efficiency measured at 3.7 ms is already 100%, meaning that aggregates are already formed when the measurement starts. Dye aggregation is then extremely fast and happens during the dead time of the experiment. However, when precipitated with polymer, this process is slowed down. The polymer chemistry also affected the evolution

of the FRET efficiency, with more hydrophobic polymers chains showing a faster FRET increase during nanoprecipitation. This suggest that the dyes interact with polymer chains during the early phase of nanoprecipitation, as predicted by Cheng et al[72]. However, the precipitation rates of the dyes remained relatively fast (Table 6).

Polymer	FRET efficiency at 3,7 ms (%)	FRET efficiency at 500 ms (%)	FRET increase (%)	t (90%)
No polymer	100	100	0	< 3.7
PEMA	88	92	4	< 3.7
PEMA-HEMA 25-75	84	96	13	15.2

Table 6: Increase of FRET efficiency and time to reach 90% of its maximal value during the first 500 ms of nanoprecipitation kinetic measurements during the encapsulation of R18/F5-TPB and CY5/F12-TPB dyes.

3 Conclusion

The influence of polymer chemistry on nanoprecipitation kinetics has been studied in two ways. This study revealed that, depending on polymer chemistry, the formation of particle may (or may not) be influenced by the mixing parameters. This has been correlated to the solubility limit of polymers in the aqueous phase. Polymers having a solubility limit below 6 vol% of water formed similar NPs independently of the mixing conditions. However, polymers with a higher solubility limit were sensitive to mixing. Indeed, particles formed with these polymers had better quantum yields and smaller sizes in the case of a fast mixing. However, the precipitation rate of polymers was unknown so their solubility limit was used as a comparative factor.

Then we studied quantitatively the precipitation of a series of fluorescent polymers thanks to a stopped flow setup. Major differences in their kinetic of precipitation, monitored via FRET efficiency, were observed. The increase of the FRET efficiency was significantly smaller for the most hydrophobic polymers, meaning that only the end of the precipitation process was witnessed. The time required to reach 90% of maximal FRET efficiency was taken as indicator of the precipitation time. This time increases from less than 3.7 ms to approximately 100 ms for the most and the less hydrophobic polymer respectively (PEMA and PEMA-HEMA 25-75). These time scales are coherent with the results of the first part. Indeed, particles formed with the PEMA polymer, which has a

short precipitation time, were not influenced by the mixing. On contrary, particles formed with PEMA-HEMA 25-75, which has a higher precipitation time were strongly influenced by the mixing.

The kinetics of hydrophobic dyes precipitation has also been studied and it appeared that the presence of polymers slows down their aggregation rate. Moreover, the latter was slightly impacted by the nature of the polymer. This suggest that dye-dye aggregation is perturbed by the presence of polymers and that dyes preferentially associate with polymer chains. Finally, several additional aspects are still to be investigated. For example, it would be interesting to perform stopped flow experiments with polyesters and block polymers as these polymers are commonly used for the synthesis of biocompatible NPs.

Chapter III: Influence of Polymer Architecture on Assembly of Dye-Loaded Nanoparticles through Nanoprecipitation

In the previous chapter, we observed, as seen before, that polymer chemistry can have a strong influence on the formation of NPs via nanoprecipitation. In particular, the presence of charged and hydrophilic groups affects the size and QY of the formed nanoparticles as well as the kinetics of nanoprecipitation. Over the last two decades, block copolymers have been widely used to form nanocarrier loaded with drugs or contrast agents. Thermodynamically controlled self-assembly of block copolymers can lead to various morphologies of nano-objects such as micelles, rods or vesicles[115,178,179]. The resulting structure, size, and properties directly depend on the polymer architecture and in particular on the absolute and relative length of the two blocks. [116,180] This approach has now been extended through the use of polymerization induced self-assembly.[181,182]

Nanoprecipitation on the other hand is a widely used example of the kinetically controlled assembly of loaded NPs. Indeed, kinetic trapping of the load presents an efficient, yet easy, way to encapsulate a compound of interest by co-precipitation with a polymer.[64,65] However, in this case the influence of polymer architecture, e.g. the distribution of charged or hydrophilic groups along the chain, is not as clear as in the case of self-assembled systems, partially due to the effects of the numerous process parameters on particle properties[183]. This lead to different affirmations that may, in appearance, look contradictory about the role of the hydrophobic block nature[113,184], or its length[63,185]. The study of block copolymer precipitation remains then of great interest. In particular, it was rarely applied to charged groups and their distribution along the polymer chains.

Here, we studied in detail the influence of the polymer architecture on the formation of dye-loaded polymer nanoparticles through nanoprecipitation. More specifically we synthetized two series of hydrophobic copolymers, one containing hydrophilic groups, and the other charged groups, and we studied how the repartition of these groups on the polymer chains affects NP properties. Statistical and block copolymers were obtained through reversible addition-fragmentation chain transfer (RAFT) polymerization. To evaluate their capacity to form loaded NPs, these polymers were co-precipitated with a hydrophobic fluorescent dye, a rhodamine B derivative with a bulky hydrophobic

counterion, as described before. We analyzed in detail the NP size, which is directly influenced by polymer chemistry, and fluorescence, which depends on encapsulation efficiency and organization of dyes inside NPs.

1 Case of charged polymers

Charged species are commonly used to stabilize polymeric NPs through electrostatic repulsion. The particle size seems to be particularly sensitive to charged groups, which allow to precisely control the particle size, [121,122,150] down to that of single proteins.[158] This was attributed to their ability to stabilize growing particles against aggregation.[186] These results have been achieved with either a single charge at the end of the chain, limiting the number of charges, or a statistical distribution of the charges throughout the polymer chain. It seemed therefore very promising to combine the strong influence of charged groups on nanoprecipitation with a precise control of their positioning along the chain as obtained in block copolymers.

1.1 Polymers studied

In order to study the influence of the polymer architecture on formation of dye-loaded particles through nanoprecipitation, we varied the distribution of charged groups along the copolymer chains. In all cases ethyl methacrylate (EMA) was used as the hydrophobic monomer, making up ≥95 mol% of the polymer. Four types of charged monomers were used. The weakly acidic methacrylic acid (MAA, pKa = 4.6) and the weakly basic 2-(dimethylamino)ethyl methacrylate (NMe_2, pKa = 8.4), whose charge state depends on the pH, were used at 5 mol% in total. Two other monomers, bearing permanent charges, the 3-sulfopropyl methacrylate (SO_3^-) and the 2-(methacryloyloxy)ethyl] trimethylammonium (NMe_3^+), were used at 2 mol% at total, due to the stronger effect of these groups on particle size.[150] While the percentage of the two hydrophobic and charged monomers was kept constant (95 and 5 mol% and 98 and 2 mol%, respectively, for weak and strong charged groups), we varied their distribution along the polymer chain using RAFT polymerization, going from statistical to block copolymers (Figure 55). The overall degree of polymerization (DPn) aimed for was 500, i.e. 475 EMA and 25 MAA or NMe_2 monomers per chain, or 490 EMA and 10 SO_3^- or NMe_3^+ monomers per chain. The

charged monomers were distributed either randomly throughout the full 500 monomers (statistical polymer), or only within the last 250, 125 or 50 monomers of the chain.

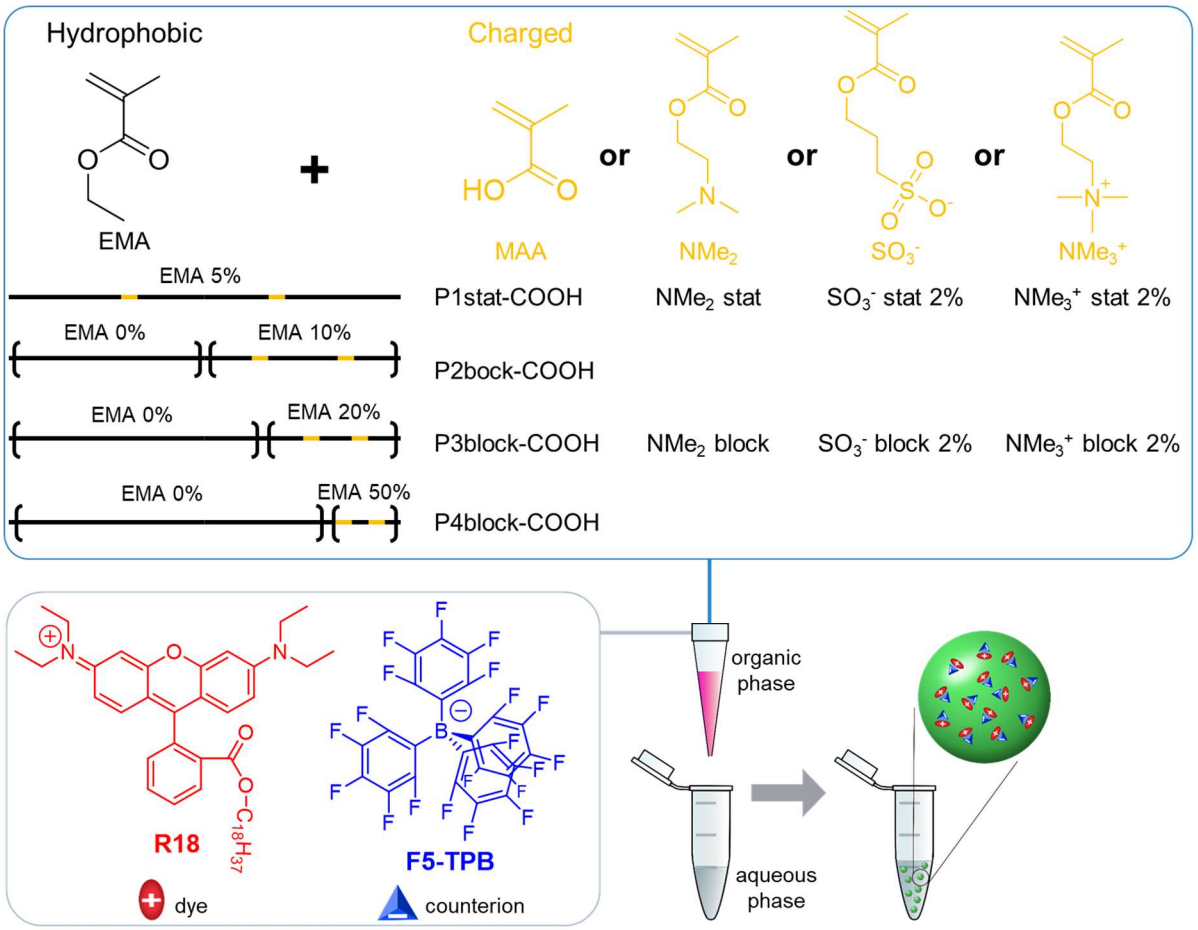

Figure 55: Architectures of polymers and structure of dye-salt used in this study. Percentages are the molar fraction of charged monomer in a given block. Schematic representation of nanoprecipitation.

For synthesis of block copolymers, the polymers synthesized in a first step were used as macro-RAFT agent for polymerization of the second block. Polymers were characterized by ^{1}H NMR spectroscopy after every polymerization step. In case of the PEMA-COOH copolymers, ^{1}H NMR showed generally good conversion upon polymerization of the second block (Table 7). However, due to the absence of clear specific peaks, chain extension and quantification of MAA integration are difficult to quantify. The copolymerization parameters for EMA and MAA (r_1 = 0.7 (0.8), r_2= 0.6 (1.0), second based on Q and e values)[187], suggest a relatively faithful incorporation of the monomers in the polymers. The obtained polymer molecular weights were found to be of the same order of magnitude, around 30 000 g.mol^{-1}, for all PEMA-COOH polymers according to SEC measurements, with low PDIs (<1.2), in good agreement with what is expected for

controlled polymerizations (Table 7).[188] The only exception was P4b-COOH, which has the strongest variation in polarity between the blocks, presumably perturbing the measurements. The obtained molecular weights can be further compared to the theoretical M_n calculated based on the achieved conversion. For example, for polymer P1stat-COOH the calculated M_n is DPn*M_{ave}*conversion = 500*112.6*0.88 = 49 544 g.mol^{-1}, which is of the same order as the measured value (with M_{ave} the average molecular weight of repeating units taking into account monomer feeding ratio; here for 95 mol% of EMA and 5 mol% of MAA, M_{ave} = 0.95*114 + 0.05*86 = 112.6 g.mol^{-1}). The lower M_n values observed for the other polymers of the PEMA-COOH series might be due to a deswelling of the polymers with relatively polar fragments.

Quantification of the integration of the different monomers and observation of chain extension was more readily achieved for the NMe_2, SO_3^- and NMe_3^+ monomers, which can be identified more clearly by NMR. Taking the NMe_2 containing polymers as example, we found 6 mol% of the NMe_2 monomer in the statistical copolymer, based on the signal of the two methyl groups bound to the amine. In order to ensure proper integration and follow-up of the NMe_2 monomers in the block copolymers, we started these with the synthesis of the NMe_2 containing block. NMR analysis of the first block gave 23 mol% of the NMe_2 monomer, in good agreement with the aimed 20 mol%. Chain extension with EMA led to a decrease in the relative intensity of the signal of the amine bound methyl groups, and gave a final fraction of NMe_2 monomer of 2 mol%. In the case of the NMe_3^+ monomers, NMR indicated about 9 mol% of NMe_3^+ monomer after polymerization of the first block, which decreased to about 1 mol% after chain extension (the former was based on the CH_2 groups between amine and carbonyl, and the latter on the methyl groups, due to overlaps with solvents). For the SO_3^- monomer containing polymers, the signals of CH_2 α and β to the sulfonate group could be detected easily in the first block indicating 9 mol% of SO_3^- monomer (8 mol% expected). In the final polymer, the signal of the corresponding peaks were too weak to be integrated and calculate a reliable percentage of charged groups. Though copolymerization data was not available for these three monomers with EMA, literature data shows that sulfoethyl methacrylate undergoes nearly ideal copolymerization with EMA, [187,189] which could also be supposed for our SO_3^- monomer. Together these results suggest that we could effectively synthesize EMA based polymers

with a good control of the amounts of different types of charged groups, with different distribution patterns along the chains.

Polymer	Composition [1]	DPn aimed	Conversion (%) [2]	Mn (g.mol^{-1}) [3]	Mn/Mw
P1s-COOH	EMA 5%	500	88	49 000	1.05
P2b-COOH	[EMA]-b-[EMA 10%]	250-250	84-95	27 000	1.12
P3b-COOH	[EMA]-b-[EMA 20%]	375-125	87-95	34 000	1.10
P4b-COOH	[EMA]-b-[EMA 50%]	450-50	82-66	28 000	1.43
NMe_2 stat	EMA 5%	500	81	47 000[4]	N/A
NMe_2 block	[EMA]-b-[EMA 20%]	375-125	94-77	61 000[4]	N/A
SO_3^- stat	EMA 2%	500	75	43 000[4]	N/A
SO_3^- block	[EMA]-b-[EMA 8%]	375-125	97-82	63 000[4]	N/A
NMe_3^+ stat	EMA 2%	500	93	53 000[4]	N/A
NMe_3^+ block	[EMA]-b-[EMA 8%]	375-125	97-96	65 000[4]	N/A

Table 7: Overview of synthetized polymers. 1) Percentages are the molar fraction of charged monomers in a given block. 2) Conversion of polymerization reaction for each block, as obtained by NMR. 3) Molecular weights were obtained by SEC, except for 4, where they were estimated based on the DPn calculated with NMR conversion values. Na) These measurements have not been performed yet due to problems with the set-up.

1.2 Nanoparticles properties

Nanoparticles were formed through nanoprecipitation: Solutions of polymer and dye salt in acetonitrile (containing 5% methanol) were added quickly to a nine-fold excess of an aqueous solution (Milli-Q water or phosphate buffer, 20 mM, pH 7.4) under shaking. Phosphate buffer was used to ensure that carboxylic groups were effectively deprotonated. For the series of COOH bearing polymers, the resulting NP sizes as measured by DLS are given in Figure 56A, with and without 10 wt% of R18/F5-TPB. The statistical copolymer P1stat-COOH, gave small NPs of 19 and 22 nm, respectively, without and with dye, in good agreement with previous results.[13] Surprisingly, increasing segregation of charges along the polymer chain by confining the same number (or global fraction) of charged groups progressively at one end of the polymer chain, led to a strong increase in particle size, going from 22 nm for the statistical polymer to over 300 nm for the polymer with the strongest charge separation (P4b-COOH). Analysis of the NPs by TEM (Figure 57) confirmed the particle sizes and trends and showed a relatively narrow size distribution of NPs, except for P4b-COOH due to the appearance of very large particles > 150 nm. The somewhat smaller average sizes obtained by TEM can be attributed to the

fact that DLS measures the hydrodynamic diameter, gives a volume averaged distribution and that larger particles scatter much stronger.[130] At the same time, confining the charged groups at the end of the chain led to an increasingly negative ζ-potential of the obtained NPs, going from -22 mV for P1stat-COOH to close to -40 mV for P4b-COOH (Figure 56B).

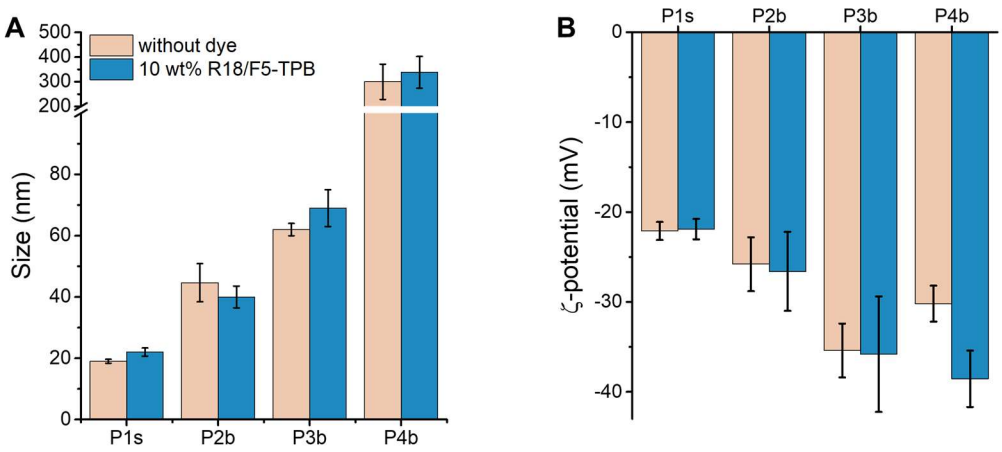

Figure 56: Sizes (A) and ζ-potentials (B) of nanoparticles from different COOH bearing polymers, as determined by DLS. The sizes, given as volume weighted average, and ζ-potentials are the mean of at least three independent preparations, either without or with 10 wt% of R18/F5-TPB; error bars correspond to standard error of the mean. P1s: EMA 5%; P2b: [EMA]-b-[EMA 10%]; P3b: [EMA]-b-[EMA 20%]; P4b: [EMA]-b-[EMA 50%], where the percentage gives the molar fraction of MAA in the corresponding block.

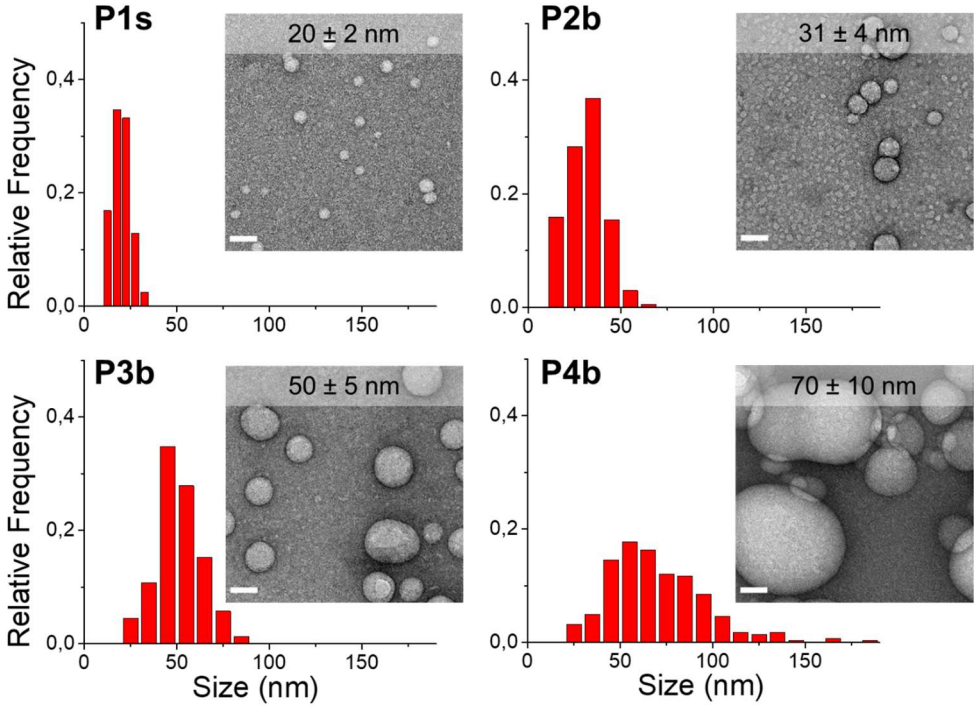

Figure 57: Size distributions and micrographs of NPs made from different COOH bearing polymers and loaded with 10 wt% of R18/F5-TPB as obtained using TEM. Mean value and standard deviation of the size are given on the images. At least 100 NPs were measured for each sample. Scale bars: 50 nm. P1s: EMA 5%; P2b: [EMA]-b-[EMA 10%]; P3b: [EMA]-b-[EMA 20%]; P4b: [EMA]-b-[EMA 50%], where the percentage gives the molar fraction of MAA in the corresponding block.

Next, we extended this analysis to other types of charged groups, dimethyl amine, sulfonate, and trimethyl ammonium (Figure 58). NPs made using polymers bearing statistically distributed NMe_2 groups had sizes of about 80 nm, indicating that these groups are less efficient in reducing the particle size than COOH groups in the same conditions of pH. When concentrating the NMe_2 groups in the first quarter of the polymer chain, the size of obtained particles increased strongly to over 150 nm. Nanoparticles made with statistical polymers bearing SO_3^- and NMe_3^+ groups had sizes below 10 nm, as observed previously.[158] Again, concentrating the charged groups at one end of the chain led to a strong increase in particle size, giving NPs with mean sizes of 30 and 60 nm, respectively. The ζ-potential was governed by the type of charged groups, giving a negative surface charge for SO_3^- and a positive one for NMe_2 and NMe_3^+ groups. In the case of SO_3^- the absolute value of the surface charge became again slightly more negative when block copolymers were used.

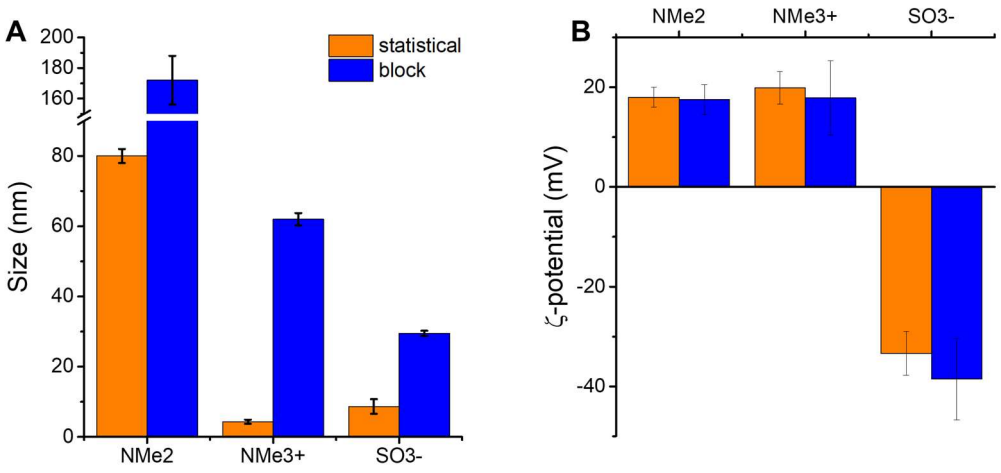

Figure 58:Sizes (A) and ζ-potentials (B) of nanoparticles from polymers bearing different types of charged groups distributed statistically or concentrated at one end of the chain (block), as determined by DLS. The sizes, given as the volume weighted average, and ζ-potentials are the mean of at least three independent preparations, with 10 wt% of R18/F5-TPB; error bars correspond to standard error of the mean.

The influence of polymer architecture on encapsulation properties was investigated with the fluorescent NPs, which were loaded with 10 wt% (relative to the polymer) of the hydrophobic dye salt R18/F5-TPB as model compound. After nanoprecipitation of polymers bearing COOH groups, all NPs had an absorbance at the maximum of the rhodamine peak (λ_{max} = 565 nm) between 0.3 and 0.35, close to the expected value (A = 0.36, Figure 59A, Table 8). The shapes of the absorption spectra were very similar, with,

nevertheless, a slight decrease in the height of the shoulder at 535 nm for the most segregated polymers (P3b and P4b).

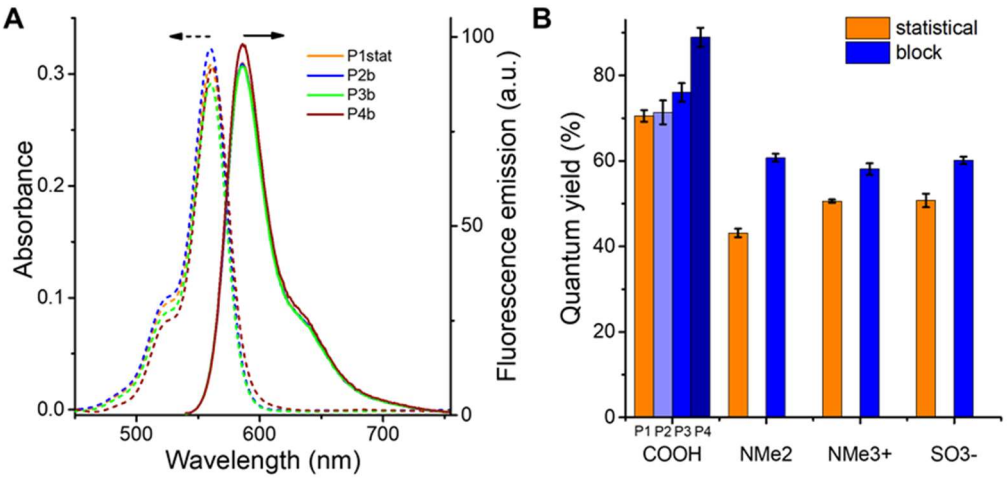

Figure 59: (A) Absorbance and fluorescence spectra of R18/F5-TPB loaded NPs made from polymers bearing 5 mol% COOH, distributed in different ways along the chain. P1stat: EMA 5%; P2b: [EMA]-b-[EMA 10%]; P3b: [EMA]-b-[EMA 20%]; P4b: [EMA]-b-[EMA 50%], where the percentage gives the molar fraction of MAA in the corresponding block. (B) Quantum yields of these NPs and NPs made of statistical and block polymers with dimethyl amine, sulfonate, and trimethyl ammonium charged groups. Loading with R18/F5-TPB corresponded to 10 wt% with respect to the polymer. The values give the average of at least three independent preparations; error bars correspond to standard error of the mean.

The obtained NPs were then subjected to dialysis for 24 h. Monitoring of the absorbance over this period did not show any significant changes for NPs made from the different polymers, except for the copolymer P4b with the strongest charge segregation (Table 8, Figure 60). In fact, DLS measurements revealed that NPs made with polymer P4b, were not stable during dialysis, in contrary to the other formulations, where NP sizes were not affected.

Polymer	Absorbance at λ_{max} [1]	Encapsulation efficiency (%)[2]	Loss after dialysis (%)[3]
P1s-COOH	0.33	84	0
P2b-COOH	0.35	97	2
P3b-COOH	0.34	96	3
P4b-COOH	0.31	86	32

Table 8: Encapsulation and dye leakage of R18/F5-TPB loaded NPs. 1) Directly after NP preparation. 2) Relative to theoretical absorbance. 3) Determined after 24h of dialysis compared to non-dialyzed reference sample.

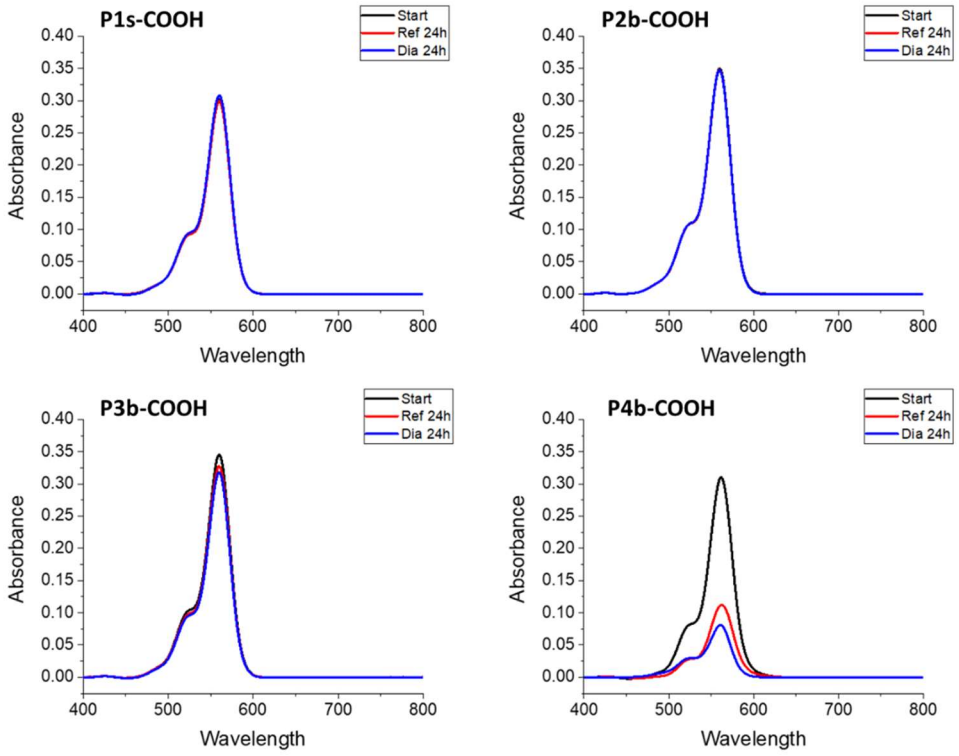

Figure 60: Absorbance spectra of COOH series NPs after nanoprecipitation (black curves) and after dialysis (blue curves). Red curves give the spectra of NPs after 24 h without dialysis.

For all COOH bearing polymers the fluorescence quantum yields of NPs were very high with values between 70 and 90% and only a slight increase with increasing concentration of charged groups at the chain end. Polymers with other charged groups showed a similar trend, with good encapsulation as observed by absorbance measurements, and a slight increase in the QYs when going from statistical to block polymers (Figure 59B, Figure 61). However, the achieved QYs in these cases were somewhat lower, presumably due to interactions of these charged groups with the dye salt, as observed previously.[190] Together these results suggest that the dye is encapsulated nearly quantitatively inside the NPs, that most of the particle formulations are stable, and that these polymers can be used to obtain very bright fluorescent nanoparticles.[191]

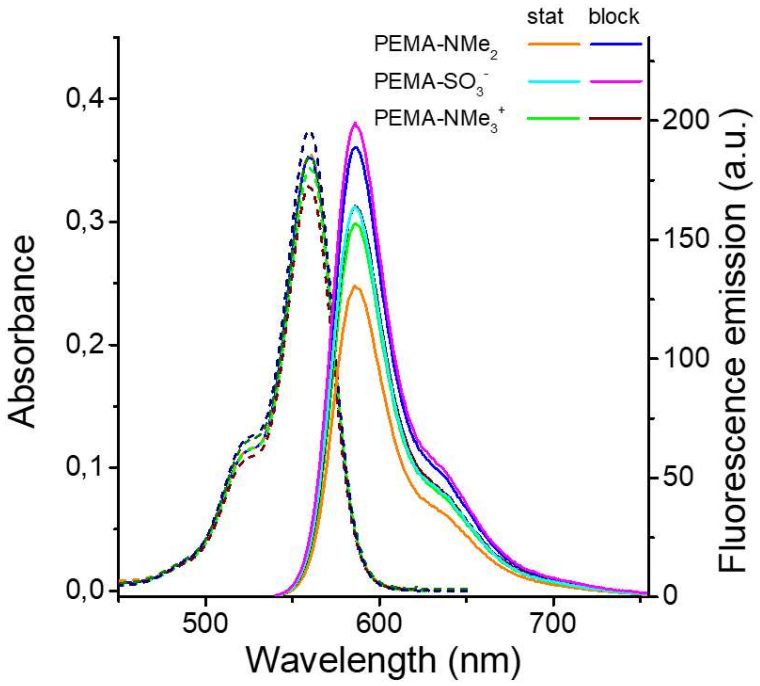

Figure 61: Absorbance and fluorescence spectra of R18/F5-TPB loaded NPs made from polymers bearing NMe_2, SO_3^- and NMe_3^+ groups, distributed in different ways along the chain.

1.3 Interaction of nanoparticles with cells

Furthermore, the interaction of the NPs made from the different polymers bearing COOH groups with cancerous mammalian KB cells was studied. For this, the cells were incubated with dye-loaded NP solutions for 3 h prior to imaging through confocal microscopy. The mass concentration in terms of NPs, and so also in terms of dye-salt, were kept constant. In the case of the statistical polymer P1stat, a high number of bright fluorescent spots were observed inside the cells, predominantly in the perinuclear region (Figure 62A). Fluorescent spots were also observed in the case of the block copolymers P2b and P3b, however, their brightness decreased with increasing segregation of the charged groups. In the case of nanoparticles made from P4b, showing the strongest concentration of the charges at the chain end, practically no fluorescent spots were observed inside the cells. The tendency of decreased internalization of NPs when going from P1stat to P4b was also confirmed by quantitative analysis of the overall fluorescence intensity per cell (Figure 62B).

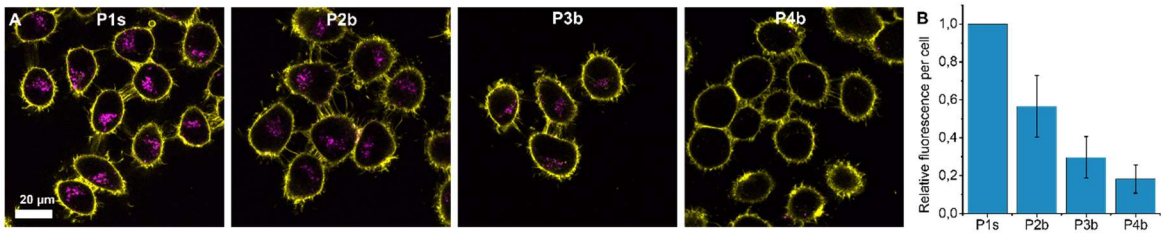

Figure 62: Interactions with cells of nanoparticles formed from PEMA-COOH with different polymer architectures: (A) Fluorescence micrographs of KB cells incubated for 3 h with nanoparticles loaded with 10 wt% of R18/F5-TPB. Yellow color represents the MemBright-488 channel (λ_{ex} 488 nm, λ_{em} 495-560 nm), magenta gives the NP channel (λ_{ex} 561 nm, λ_{em} 570-610 nm). The scale bar corresponds to 20 µm. (B) Fluorescence intensity per cell as measured on the micrographs normalized to the value for P1s. At least 50 cells were measured per condition, values give the average over 3 independent experiments, error bars correspond to standard deviation of the mean.

1.4 Discussion

Here, we compared nanoprecipitation of copolymers of hydrophobic and charged methacrylates, which had the same overall composition (95 mol% hydrophobic EMA and 5 mol% methacrylic acid or NMe_2, or 98 mol% EMA and 2 mol% SO_3^- and NMe_3^+), but varied in their architecture. We found that the more segregated the charges were along the polymer chain, the bigger the resulting particle sizes. At the same time, the ζ-potential of the NPs had a tendency to become increasingly more negative. Nanoprecipitation is a kinetically controlled process, in which particle growth stops when the integration of new polymer chains or the aggregation of NPs becomes sufficiently slow. A possible mechanism leading to a strong decrease in growth rate is the repulsion between like-charged groups, as suggested by theoretical and experimental results.[121,122,150,192] Smaller NPs imply earlier stabilization of NPs during the nanoprecipitation process. The results obtained here indicate that statistically distributed charged groups along polymer chains are more effective in stabilizing growing NPs, and this is valid for groups derived from weak and strong acidic and basic groups. A possible explanation is that the homogeneity of the coverage of the NP surface with charged groups is more important than the overall number of charged groups per surface area. This is in good agreement with the measured less negative ζ-potential of NPs made from the statistical copolymer for COOH and SO_3^- groups, and its continuous decrease with increasing charge segregation (the fact that this was not observed for positively charged groups might come from the tendency of negative charges to adsorb on surfaces in contact with water.[193]). We assume that with increasing

segregation of the charged groups at the end of the chain, the formed NPs would have more clusters of charged groups on the NP surface, or even strongly charged chain ends dangling from the surface. However, due to hydrophobic patches in-between the charges, these latter are less effective in stabilizing small particles. In contrast, random polymers ensure homogeneous charge distribution on the surface of small NPs and thus their efficient stabilization. Moreover, polymer P4b can be considered as an amphiphilic polymer, similar to those used for preparation of polymeric micelles.[194,195] However, in this case, the polar block is too small compared to the apolar part, which can explain so large NPs size and their poor colloidal stability.

When co-precipitating these polymers with a hydrophobic dye salt the polymer architecture had no significant influence on encapsulation, and dialysis experiments did not reveal any dye leakage. All dye-loaded NPs exhibited good to very good QYs, with only a small increase with increasing charge segregation. Altogether these results evidence good incorporation of the dye inside polymeric NPs and allowed to use the NPs for cellular labelling. The interactions of the NPs with cells depended again strongly on the distribution of the charges on the used polymer. However, as both, surface charge and size of the NPs (and so also their molar concentration), varied simultaneously, the origin of the differences in interaction with cells cannot be determined unambiguously.

2 Case of hydrophilic polymers

In this part the influence of polymer architecture on the formation of NPs was studied with polymers bearing hydrophilic groups. The intense use of hydrophilic/hydrophobic block copolymers used for NP preparation and the results obtained in the first chapter with the P(EMA-b-HEMA) block copolymer encouraged us to deepen our researches on this system. We found particularly interesting to be able to work with polymers with the same overall composition, but different architectures, as it is the case with PEMA-HEMA copolymers. Indeed, such experiments are not easily possible with PEG stabilized amphiphilic polymers.

2.1 Polymers studied

In this study, the series of polymers synthetized contains 50 mol% of EMA and 50 mol% of HEMA as hydrophobic and hydrophilic monomer respectively. In addition, 1 mol% of methacrylic acid was added to help the formation of small NPs (this percentage

is latter voluntarily omitted in the name of the polymers). RAFT polymerization was employed for the synthesis of every polymer. The DPn aimed for polymer chains was 500, that is 250 EMA and 250 HEMA monomers per chains. One polymer without HEMA (PEMA, DPn = 500) was also synthetized to emphasize differences due to the incorporation of hydrophilic groups. Schematic representation of the polymers used is provided in Figure 63.

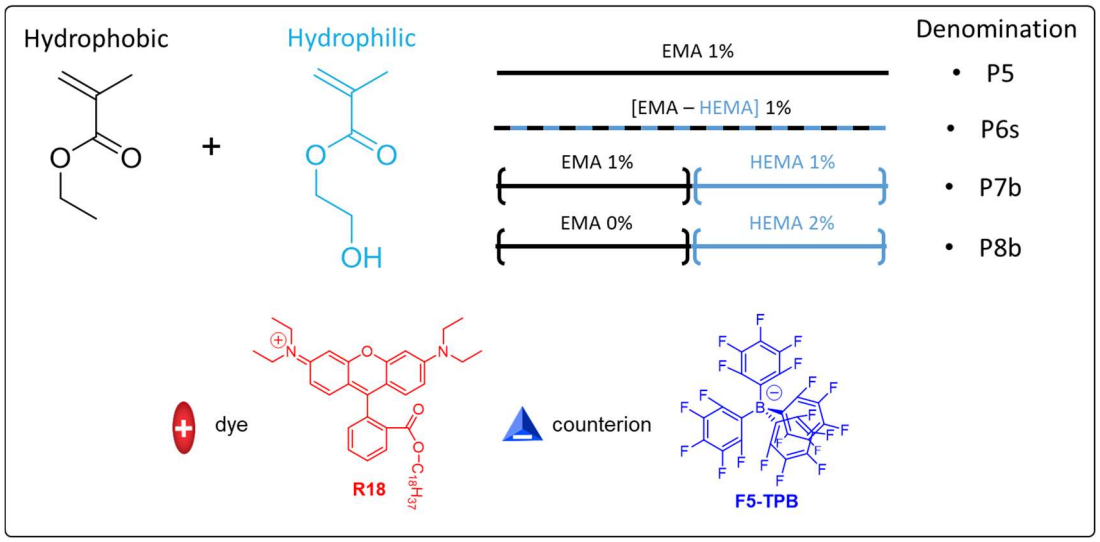

Figure 63: Architectures of polymers and formula of the dyes used in this study. Percentages are the molar fraction of methacrylic acid in a given block.

As explained in the first part, incorporation of MAA in polymer chains could not be observed by ^{1}H NMR. Block copolymers were made using the PEMA block as macro-RAFT agent so the apparition of HEMA peaks in NMR confirmed the presence of the second block (Figure 64). Moreover, these polymers were purified using precipitation in MeOH/Water mixtures in which the PEMA and P(EMA-b-HEMA) copolymers are insoluble due to the PEMA moiety. However, this is not the case of PHEMA which is soluble in this mixture. Therefore the precipitation step should remove unreacted HEMA monomers or PHEMA homopolymers. The combination of these results therefore let us conclude that chain extension was indeed successful.

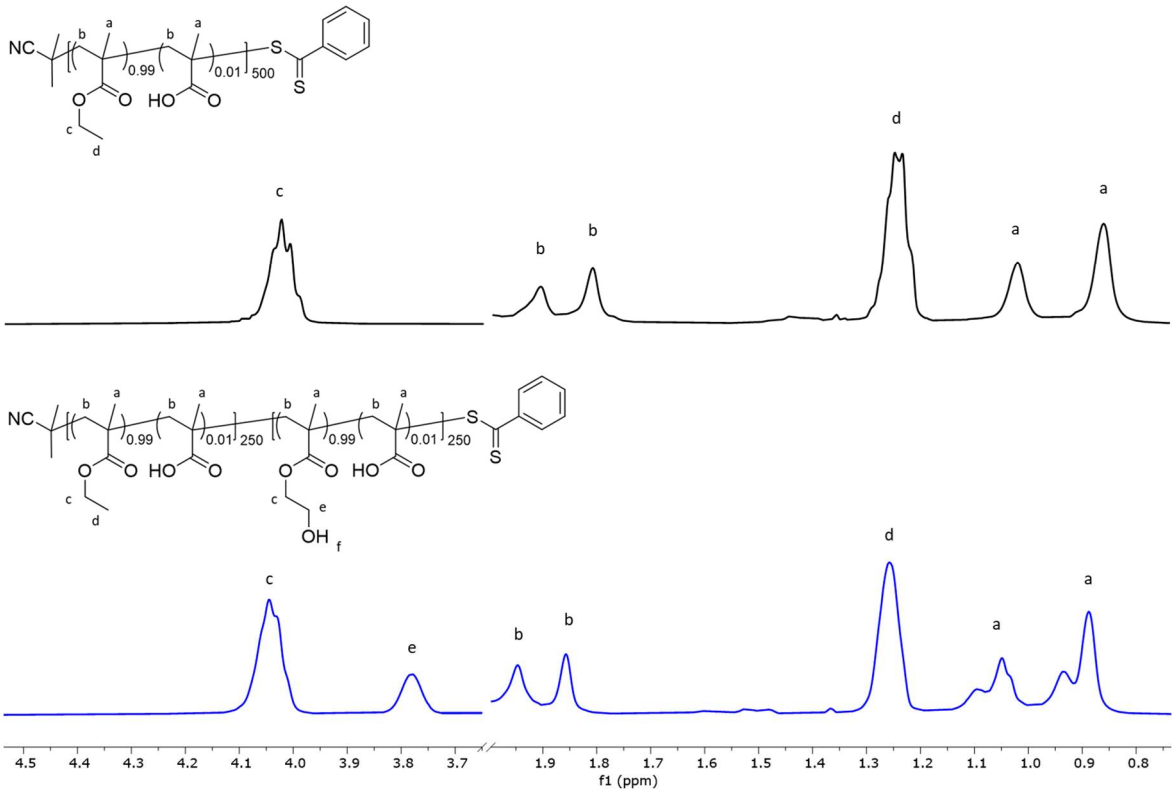

Figure 64: ^{1}H NMR of P7b polymer after 1st block (black, in $CDCl_3$) and 2nd block (blue, in acetone d_6) synthesis.

Polymer molecular weights were determined by SEC measurements. The polymers P6s and P7b had abnormally high PDI values for controlled polymerization, whereas the polymer P8b signals did not permit a proper analysis of its molecular weight (Table 9). We believe that the presence of HEMA and particularly the strong amphiphilic character of this polymer disturbed the measurements.

Polymer	Composition [1]	DPn aimed	Conversion (%) [2]	Mn (g.mol^{-1}) [3]	Mn/Mw
P5	EMA 1%	500	78	30 000	1.28
P6s	EMA-HEMA 1%	500	78	29 000	1.54
P7b	[EMA 1%]-b-[HEMA 1%]	250-250	71-73	19 000	1.92
P8b	[EMA]-b-[HEMA 2%]	250-250	84-95	N/A	N/A

Table 9: Overview of synthetized polymers. 1) Percentages are the molar fraction of methacrylic acid in a given block. 2) Conversion of polymerization reaction for each block, as obtained by NMR. 3) Molecular weights were obtained by SEC. N/A) This measurement did not allowed M_n determination.

2.2 Nanoparticles properties

Nanoparticles were formed through nanoprecipitation, as previously: Solutions of polymer and dye salt in acetonitrile (containing 5% methanol) were added quickly to a nine-fold excess of Milli-Q water under shaking. Polymers containing 50 mol% HEMA formed NPs between 60 and 50 nm while the polymer without HEMA gave bigger NPs around 130 nm. These results are in agreement with previous studies showing that increasing the fraction of hydrophilic groups in the polymer led to a decrease in NP size.[13] The architecture of the polymer, on the other hand, only slightly decreased the particle size in the case of block copolymers, as measured by DLS. When precipitated without dyes, block copolymers yielded slightly smaller NPs. However, the statistical PEMA-HEMA polymer (P6s) and the hydrophobic PEMA (P5) polymer formed much smaller particles in this case (Figure 65A).

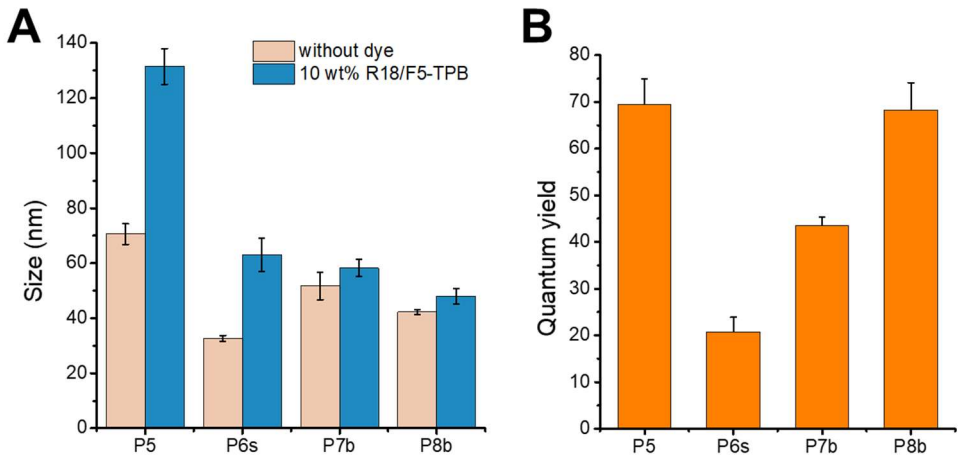

Figure 65: (A) Size determined by DLS and (B) Quantum yields of nanoparticles from HEMA polymers series with 10 wt% of R18/F5-TPB. The sizes are given as volume weighted average, and quantum yields are the mean of at least three independent preparations. Error bars correspond to standard error of the mean. P5: EMA 1%; P6s: EMA-HEMA 1%; P7b: [EMA 1%]-b-[HEMA 1%]; P8b: [EMA]-b-[HEMA 2%], where the percentage gives the molar fraction of MAA in the corresponding block.

Dye-loaded NPs were further analyzed by TEM (Figure 66). All showed lower average sizes as obtained by DLS, presumably due to stronger scattering of the larger particles[196]. Images of polymer P5 are composed of large and very polydispersed NPs. The polymer P6s showed an important amount of small NPs with a mean diameter of 30 nm but also a significant amount of larger particles with a diameter > 50 nm. Only the latter were detected in DLS, again due to enhanced scattering of bigger particles. According to the size of NPs made without R18/F5-TPB (mean size of 31 nm measured by DLS, later confirmed

by TEM), we think that the population of smaller particles is possibly not dye loaded. Mean particle size of block copolymer are in good agreement with DLS measurements.

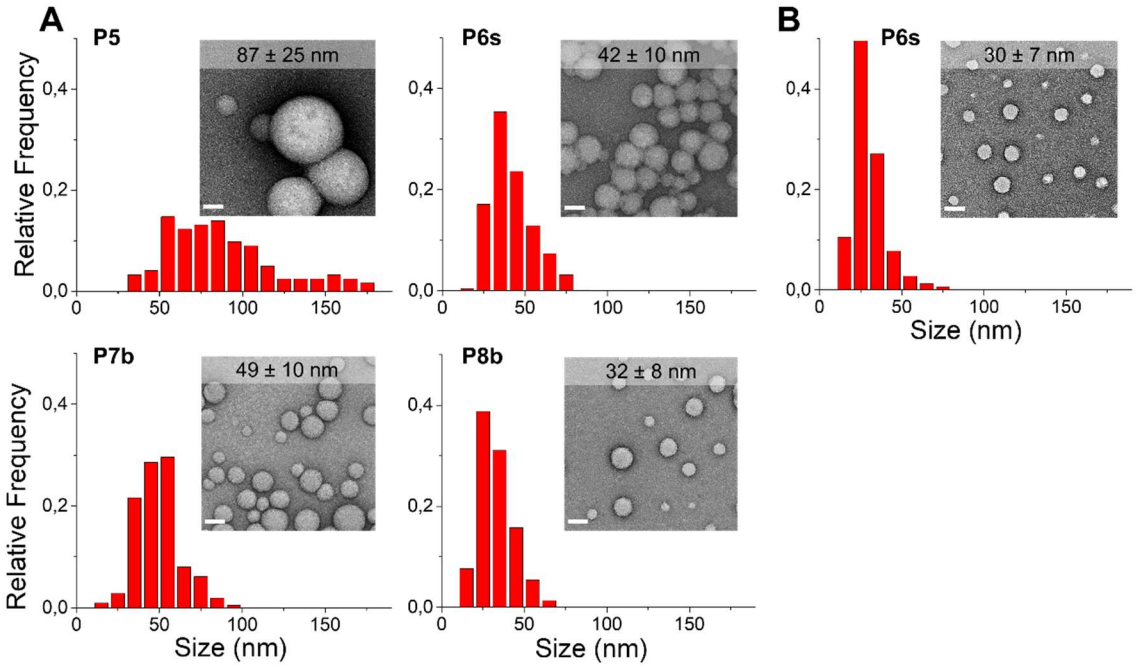

Figure 66: Size distributions and micrographs of NPs made from different HEMA bearing polymers (A) loaded with 10 wt% of R18/F5-TPB (B) without dye, as obtained using TEM. Mean value and standard deviation of the size are given on the images. At least 100 NPs were measured for each sample. Scale bars: 50 nm. P5: EMA 1%; P6s: EMA-HEMA 1%; P7b: [EMA 1%]-b-[HEMA 1%]; P8b: [EMA]-b-[HEMA 2%], where the percentage gives the molar fraction of MAA in the corresponding block.

After nanoprecipitation, all NPs had an absorbance at the maximum of the rhodamine (565 nm) between 0.3 and 0.35 except for the statistical polymer P6s that was around 0.25, but for which the shoulder at 530 nm was relatively more intense (Figure 67). Comparison of these values with the expected value (A = 0.36) suggest that no significant losses of rhodamine due to formation of dye aggregates occurred (with exception for P6s). No major change in absorbance was recorded after dialysis for 24 h, suggesting that the dye is effectively encapsulated in NPs[191]. At the same time, the architecture of the polymer had a drastic influence on the quantum yield: NPs formed with the statistical polymer had the lowest QY, while the highest QY was obtained with the block polymer with the most hydrophobic chain (Figure 65B). A decrease in quantum yield of dyes inside NPs is typically due to aggregation caused quenching supporting the possibility of dye clustering inside NPs, which is also in agreement with the increase in the intensity of the shoulder in absorbance.

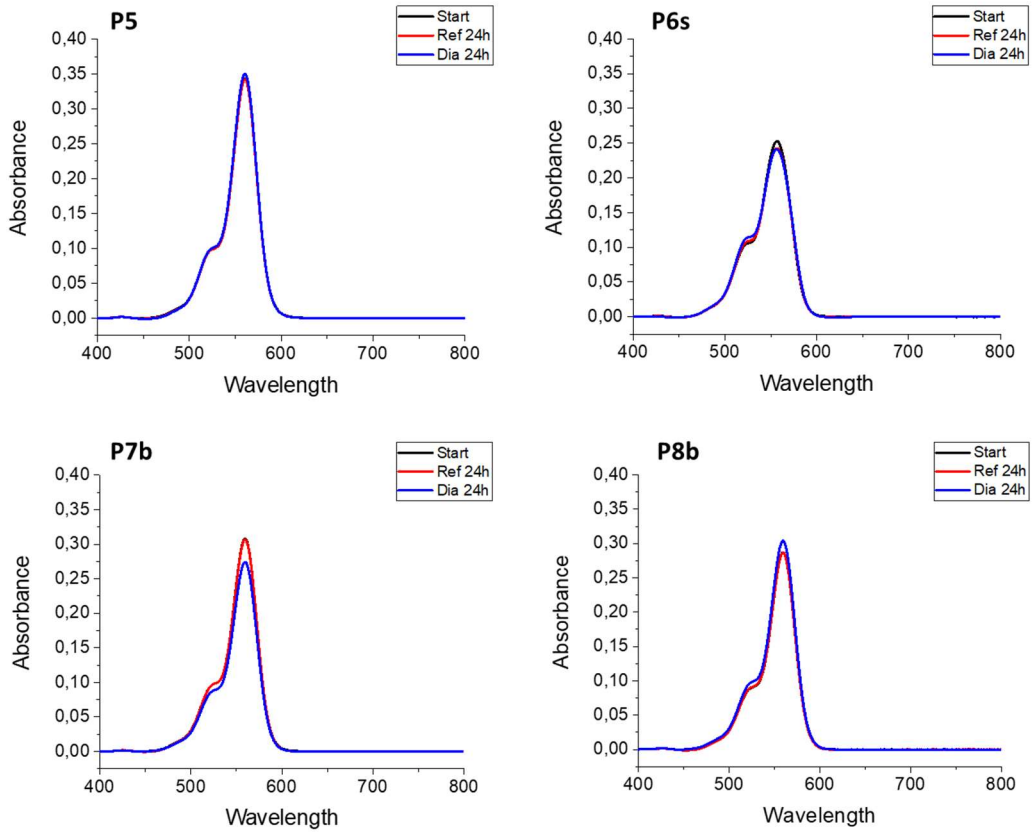

Figure 67: Absorbance spectra of HEMA series NPs after nanoprecipitation with R18/F5TPB (black curves) and after dialysis (blue curves). Red curves give the spectra of NPs after 24 h without dialysis.

Seeing that the architecture of polymers seems to have only a slight impact on NP size but a strong one on dye encapsulation, we decided to investigate this point in more details. For this, we used the statistical polymer P6s and the block copolymer P8b to encapsulate a series of dyes with different hydrophobicities. The dyes used were derivatives of the R18/F5-TPB dye, which have a shorter alkyl chain on the rhodamine of respectively 12, 8 and 4 carbon atoms, making them less hydrophobic, as it can be seen from their co-migration on TLC (Figure 68).

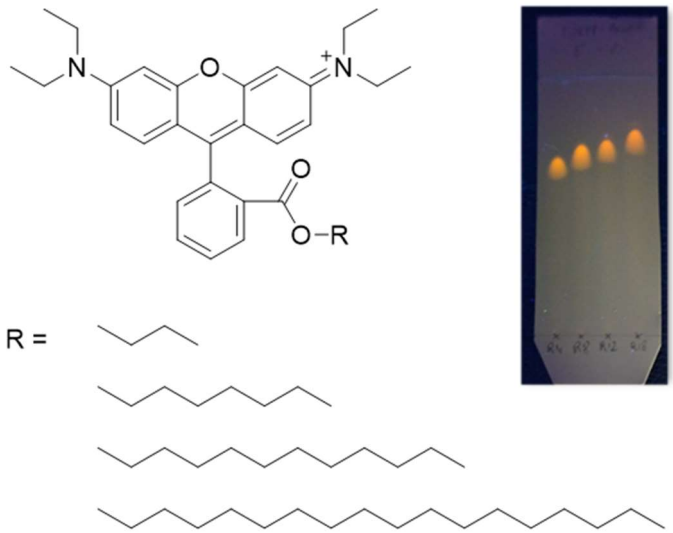

Figure 68: Structure of R18/F5-TPB derivative dyes used to study encapsulation properties of polymers P6s and P8b. Picture of TLC of the dyes eluted in DCM/MeOH 9-1 mixture. Rf R4 = 0.68; Rf R8 = 0.74; Rf R12 = 0.76; Rf R18 = 0.81.

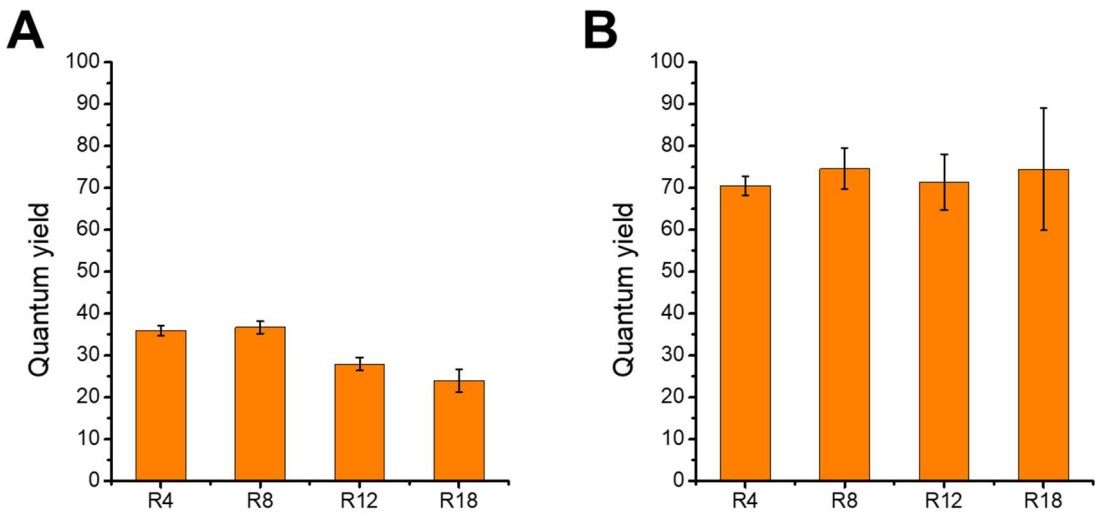

Figure 69: Quantum yields of NPs formed with (A) the statistical copolymer P6s and (B) the block copolymer P8b. Error bars correspond to standard error of the mean performed on two independent measurements.

As observed previously, particles formed with the statistical polymer have smaller QYs (Figure 69). However when the hydrophobicity of the dye was decreased, the QY increased from 24% with R18/F5-TPB to 36% with R8 and R4/F5-TPB. Even though this value does not approach the QYs obtained with the block polymer, this represents an increase of particle fluorescence of 50% (absorption was unchanged). When formed with the block copolymer, no such trend was observed for the QY of the particles, which remained constant around 70%. We further studied the encapsulation efficiency of NPs by dialyzing them overnight in water in presence of Tween 80. The decrease in

absorbance of particle solutions (compared to non-dialyzed solution after 24h) was interpreted as dye loss due to improper encapsulation (Figure 70).

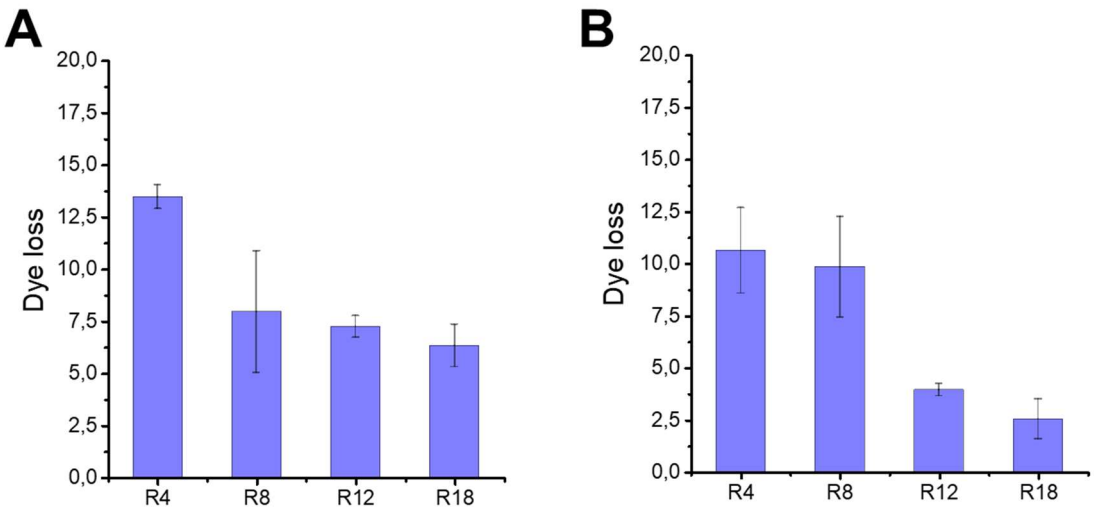

Figure 70: Dye loss after NPs dialysis in tween 80 solution for (A) the statistical copolymer P6s and (B) the block copolymer P8b. Error bars correspond to standard error of the mean performed on two independent measurements.

The statistical polymer had a dye loss of approximately 7% for all dyes except for the R4/F5-TPB, where it was significantly higher, up to 14%. On the other hand, the block copolymer had a dye loss around 10% for the R4 and R8 dyes that decreased strongly when the hydrophobicity of the dye increased, down to 2.5% with R18/F5-TPB.

2.3 Discussion

Here, we compared nanoprecipitation of different polymers containing hydrophilic groups, which had the same overall composition, but varied in the architecture. The results obtained showed that polymer architecture influences the properties of the formed particles such as size and especially quantum yield. The formed NPs were stable over time, indicating that the different properties observed for varying polymer architecture arise from the nanoprecipitation step itself.

Smaller particles were obtained with the statistical polymer, but only when precipitation was performed without dye. During co-precipitation with the hydrophobic R18/F5-TPB dye, NPs of different size are observed in TEM, a majority with a diameter similar to NPs without dye (30 nm), and a smaller amount with bigger diameter around 60 nm. On the contrary, size of NPs formed with bloc copolymers P3 and P4 was barely influenced by the presence of dye. This can result from different precipitation rates of

polymers. In fact, one should keep in mind that the dye salt has also its own precipitation rate. Hence, if the polymer precipitate after the dye, particle formed would have a hydrophobic core formed from dye aggregate, surrounded by polymer. Those particles would have a bigger diameter than the polymer precipitated alone, and this is what we observe in the case of the polymer P6s, which is the most hydrophilic polymer of the series. Indeed, in the previous chapter its solubility limit measured was 40 vol% whereas the block copolymer P8b had a solubility limit of 10 vol%. Polymer P7b and P8b, which have a very hydrophobic block, presumably precipitate faster, explaining the small influence of dye co-precipitation on the size of NPs formed with these polymers.

The low quantum yields of particles formed with polymer P6s corroborate this sequential precipitation mechanism, by evidencing dye aggregation in NPs. Co-precipitation of polymer P6s with more hydrophilic dyes (R4 and R8/F5-TPB) led to higher quantum yields (35%) than with the hydrophobic R18/F5-TPB dye. At the same time, the less hydrophobic dye R4 was poorly encapsulated in this polymer. In the case of the block copolymer P8b, both the R4 and R8 dyes were not encapsulated correctly. This suggest that the reduced hydrophobicity of these dyes may have a negative impact on their encapsulation.

3 Conclusion

In order to study the impact of polymer architecture on kinetically controlled processes of assembly of NPs, we synthetized two series of copolymers bearing charged or hydrophilic groups through RAFT polymerization. This allowed in the first case to vary the distribution of charged groups along the polymer chains going from statistical to block copolymers. Nanoprecipitation of these polymers to form dye-loaded NPs revealed a strong influence of polymer architecture on the particle properties. Indeed, statistical polymers were more effective than block copolymers to obtain small dye-loaded NPs, which was attributed to more efficient stabilization of growing particles. The resulting differences in size and surface charge had, in turn, a strong effect on the interactions of the particles with cells.

In the second part, we have studied how the block architecture influences the properties of particles made of polymers containing hydrophilic groups. The size of dye loaded NPs was weakly influenced by the architecture of polymers, whereas the latter had a marked influence on the encapsulation of the hydrophobic dyes. This was attributed to the relative precipitation kinetics of the dye and polymer chains.

These results show the importance of an appropriate polymer design for controlling particle formation. In particular, they reveal that, despite their versatility, block copolymers are not always the most optimal choice for the assembly of polymer NPs, in the case of charged polymers. They also point out that matching precipitation rates between the load and the polymer is crucial to achieve proper encapsulation.

Chapter IV: Protein-like nanoparticles

One of the major applications of polymeric NPs is their use as nano-carriers for drugs and contrast agents. The role of the particles is often to deliver the drug in specific regions of the body or more generally in biological systems. In nature, the role of nano-containers is notably performed by proteins[197], which surpass NPs in many points. Indeed, NPs usually have a bigger size, a simpler structure and often suffer from non-specific interactions in biological media. A unique feature of proteins is the complexity of their surface, which grant them a good stability in various conditions of pH or ionic strengths, allows specific interactions and minimizes non-specific ones[198]. This is possible thanks to the presence of hydrophilic and charged groups on their surface and notably the fact that the latter has positively and negatively charged areas[199] (Figure 71).

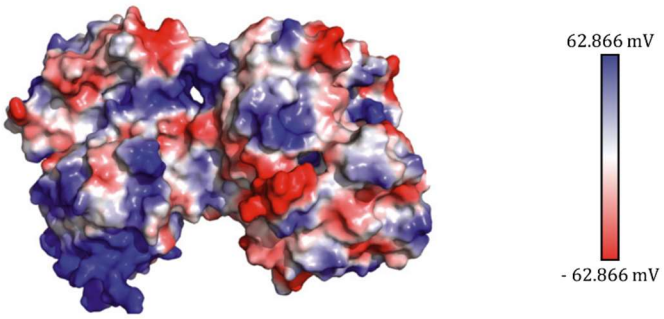

Figure 71: Surface potential on human lactoferrin, reproduced from Baker[200].

Inspired by proteins properties, we wanted to create NPs with oppositely charged groups on their surfaces. Such mixed charge NPs have been obtained by functionalizing the surfaces of gold NPs with mixtures of positively and negatively charged thiol ligands[201]. In the case of polymer based NPs, different charged groups have been combined within the same polymer, sometimes in masked form, yielding polymer ampholytes[202]. Moreover, surfaces with unique design have been obtained as in the case of molecularly imprinted NPs, obtained thanks to polymerization precipitation[203,204]. However, as charge pairing can occur between the opposite charges, it remains difficult to achieve availability of both charges on the surface. This is exemplified by polyelectrolyte complex NPs, in which two polyelectrolytes of opposite charge are combined, and by polyplexes, which are NPs formed between cationic polymers and nucleic acids, as well as by the association of oppositely charged NPs[205,206]. Upon NP formation, opposite charges are pairing up, leading to more hydrophobic ion pairs that

are typically contained inside the NPs, while the shell is formed exclusively by the charges in excess, with the stability depending on the amount and sign of the surface charge[207,208].

In order to create mixed charge polymeric NPs, we have chosen to assemble polymers of opposite charge by nanoprecipitation. Indeed, based on the concepts presented before, we hypothesized that using polymer hydrophobicity as driving force to assemble NPs would allow to trap polymer chains in a kinetically frozen state, avoiding charge pairing. Moreover, the kinetic control of particle formation has the further advantage to simplify encapsulation of functional compounds, including drugs and contrast agents. We made two series of oppositely charged polymers comporting 1, 5, 10 or 25 mol% of charged groups that we mixed before precipitation to obtain mixed charge NPs. We then studied the effects of charge percentage, polymer ratio, and precipitation medium on the size of the NPs. ζ-potential and particle stability were also investigated, in various conditions of pH or ionic strengths. We were interested to see if particles efficiently presented both type of charges on their surface but also if we could form small (<20 nm) and fluorescent NPs, stable in a large spectrum of environments. Such NPs, exhibiting properties similar to proteins, would be good candidates for the formation of new nanocarriers.

1 Assembly of oppositely charged polymers

We decided to work with poly(ethyl methacrylate) polymers comporting either methacrylic acid (noted PEMA-COOH in the following) or [2-(Methacryloyloxy)ethyl]-trimethylammonium chloride (noted PEMA-NMe_3^+) as charged groups. These charged groups have already been used independently for the formation of polymeric NPs[209–211] and such NPs can readily encapsulate hydrophobic compounds such as dye salts to make them fluorescent[90]. Moreover, varying the amount of charges on the polymer chain allowsd to control the size of the particles formed by nanoprecipitation[13]. Hence, this couple appeared to us as an easily tunable and versatile system suitable for this project.

1.1 Two series of oppositely charged polymers

PEMA-COOH and PEMA-NMe_3^+ polymers were made through free radical polymerization, so the charged monomers were distributed statistically along the polymer chains. The mole fraction of the charged (or ionizable) monomers in the feed was varied from 1 to 25% (Figure 72).

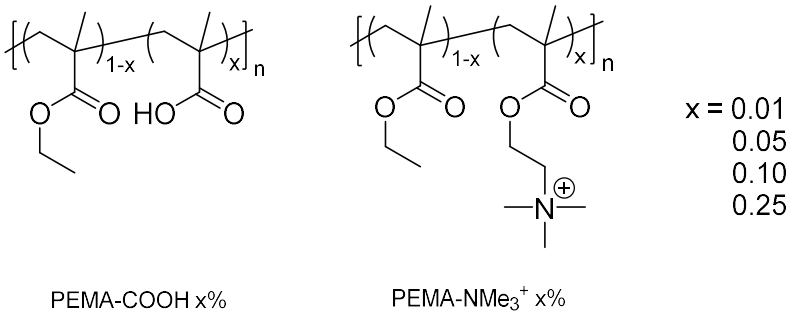

Figure 72: Structures of the polymers bearing COOH or NMe_3^+ groups used to form NPs. x corresponds to the molar fraction of charged monomer.

In order to avoid strong variations in the composition of the polymer chains, the conversion of polymerization reactions was kept relatively low. Polymers with only 1% of charged groups could be precipitated in MeOH. However, for higher charge percentages, addition of water was necessary to decrease polymer solubility and perform precipitation. Larger amounts of water were notably required for higher charge percentages. This indicates qualitatively that the composition of polymers was changing according to the monomer feeding ratios.

NMR spectroscopy was used to characterize polymers and, when it was possible, quantify the proportion of charged monomers. The amount of NMe_3^+ groups was determined by comparing the signal of the nine protons from the trimethyl ammonium group (δ = 3.5 ppm) with the signal of the methyl group on the polymer backbone (δ = 1 ppm) (Figure 73). However, the carboxylic acid bearing monomer could not be quantified by NMR due to the absence of characteristic peak (Table 10).

Polymer	% charged group	Conversion (%)	% charged group measured by NMR
PEMA-MAA	1	31	N/A
PEMA-MAA	5	37	N/A
PEMA-MAA	10	10	N/A
PEMA-MAA	25	25	N/A
PEMA-NMe_3^+	1	27	0.8
PEMA-NMe_3^+	5	30	3.2
PEMA-NMe_3^+	10	31	7.2
PEMA-NMe_3^+	25	36	24

Table 10: Conversion of polymerization reactions and amount of charged groups per polymer chain as determined by ^{1}H NMR spectroscopy.

Molecular weight of the polymer chains was determined by SEC for the two polymers bearing 5% of charges that is PEMA-COOH 5% and PEMA-NMe_3^+ 5%. The value obtained for the molecular weight (Mn) were 127 000 $g.mol^{-1}$ (PDI 1.31) for the PEMA-COOH and 151 000 $g.mol^{-1}$ (PDI 1.74) for the PEMA-NMe_3^+.

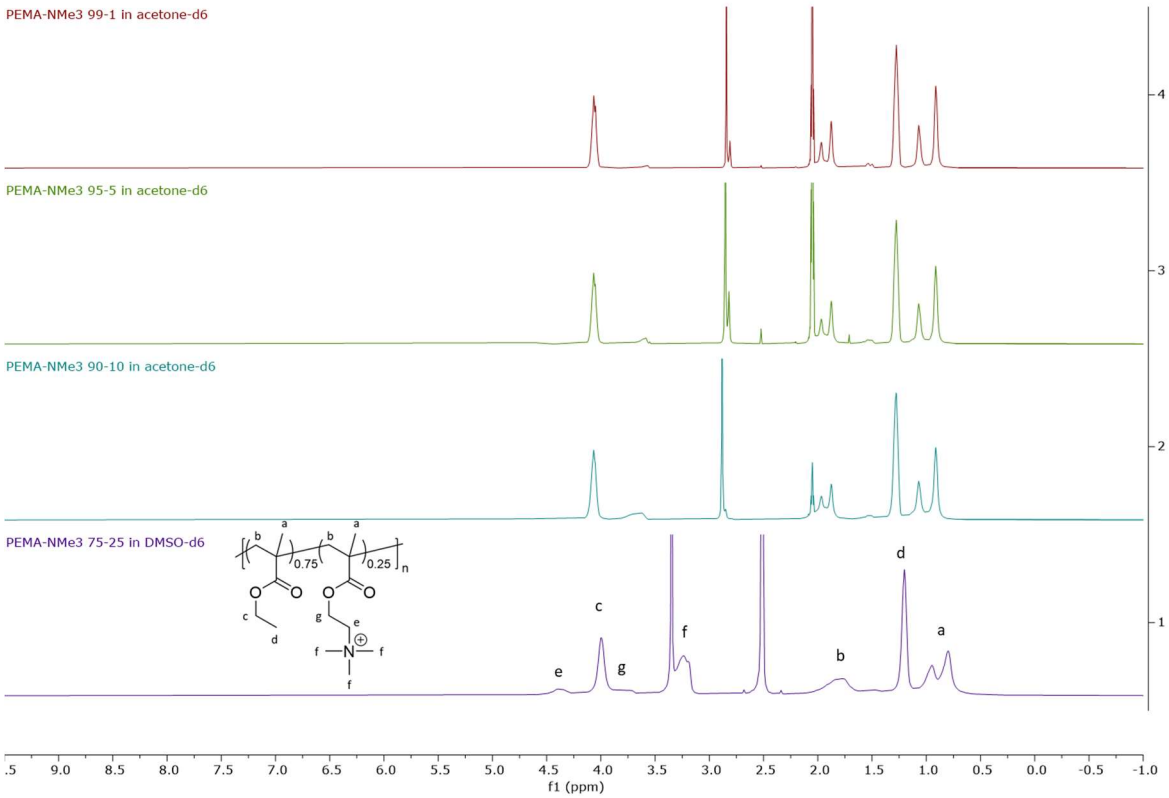

Figure 73: Stacked NMR spectra of the PEMA-NMe_3^+ polymers with different amount of charged groups. Solvent used for NMR are given in spectra names. The increase of the percentage of NMe_3^+ groups can be observed with the apparition of a characteristic peak at 3.5 ppm.

In this way, we obtained two series of oppositely charged polymers, with various charge percentages. Stock solutions of polymers at 10 $g.L^{-1}$ are usually prepared in acetonitrile, however polymers with a charge percentage ≥ 10% could not be dissolved in this solvent. In consequence, stock solutions were prepared in acetonitrile containing 30 vol% of methanol, and were further diluted to 2 $g.L^{-1}$ in acetonitrile before particle formation.

1.2 Preparation of nanoparticles

The protocol for preparation of NPs described in the methods section was adapted for the formation of particles with polymer blends. Solutions of the two polymers with the same charge fraction of either COOH or NMe_3^+ groups, that is with the same percentage of charges, but opposite sign, were first mixed at the desired ratio in acetonitrile. This ratio is named polymer ratio (noted also COOH/NMe_3^+ ratio) and corresponds to the ratio of the two polymers in the solution, and, in first approximation, to the molar ratio of COOH and NMe_3^+ groups. E.g. a polymer ratio of 75:25 for a charge fraction of 5% corresponds to a solution containing 75 mol% PEMA-COOH 5% and 25 mol% PEMA-NMe_3^+ 5%. In the present work we used 7 polymer ratios, going from 0:100 (only PEMA-NMe_3^+ polymer), over 10:90, 25:75, 50:50, 75:25, 90:10 to 100:0 (only PEMA-COOH). The following table schematically represents five of the polymer ratios used in this study (Table 11).

COOH/NMe_3^+ ratio	100:0	75:25	50:50	25:75	0:100
Composition	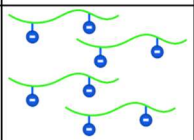	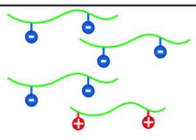	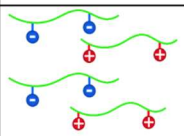	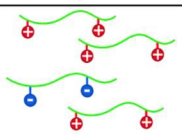	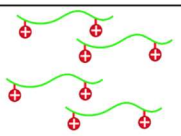

Table 11: Schematic representation of polymer ratios used for the formation of mixed charge NPs.

Mixed polymer solutions were then added quickly and under shaking to a nine-fold excess of an aqueous solution, followed by a second dilution in the desired medium. In the case of dye-loaded NPs, 10 wt% (relative to the polymer) of a hydrophobic dye salt, R18/F5-TPB, was added to the polymer solution prior precipitation (Figure 74).

PEMA-NMe_3^+ polymers are always positively charged in water due to the quarternary ammonium groups, which are present as chlorine salt. The extent or fraction of negative charges of PEMA-COOH polymers depends on the pH, controlling the deprotonation of carboxylic acid functions in water. In Milli-Q water, only a fraction of these groups is efficiently deprotonated. For this reason, we decided in some experiments to neutralize the carboxylic acids prior to NP formation. For neutralization of the COOH bearing polymers, the corresponding amount of NaOH (1 M in methanol) was added to the mixture of the polymers before particle assembly.

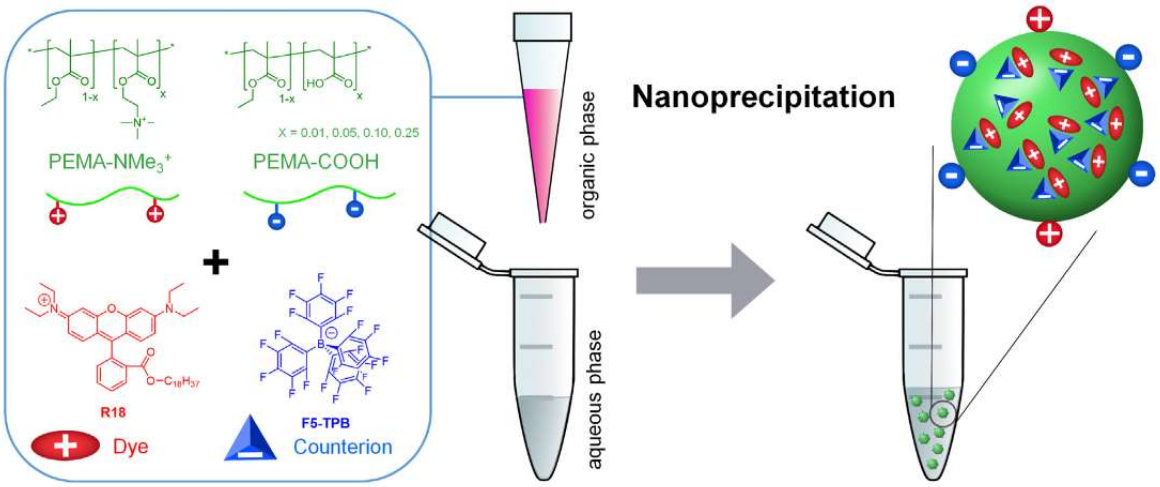

Figure 74: Principle of nanoprecipitation using oppositely charged polymers. Chemical structures of polymers and dye salt used in this study.

1.3 Titration of the PEMA-COOH polymer

In order to further characterize polymers containing methacrylic acids, we decided to quantify the amount of acid functions thanks to a back-titration. This would allow to determine with a different method than NMR the percentage of acid groups per polymer chain. A known amount of polymer was dissolved in an aqueous solution containing a known quantity of NaOH (greater than the quantity of methacrylic acids). Then this solution was titrated with a solution of HCl. Back titration was used notably because the polymer chains are much more soluble in water when they are charged. This way we ensure that chains remain completely soluble at least until the equivalence point. Only PEMA-COOH polymers with ≥ 25% of charged groups could be titrated this way. The amount of charged groups determined with this method was 26%, which is very close to 25% corresponding to the monomer feeding ratios used for the polymerization reaction.

2 Characterization of nanoparticles

2.1 Size

Nanoprecipitation without neutralization of the COOH groups led to the formation of very small NPs with sizes of <25 nm, for most of the polymer ratios independently of the fractions of charged groups (Figure 75). Only the polymer ratio COOH/NMe_3^+ 90:10 led to a strong increase in particle size (> 250 nm) and DLS results suggested formation of

aggregates. This was accompanied by the appearance of a turbidity visible by eye. In other cases, no such turbidity was observed.

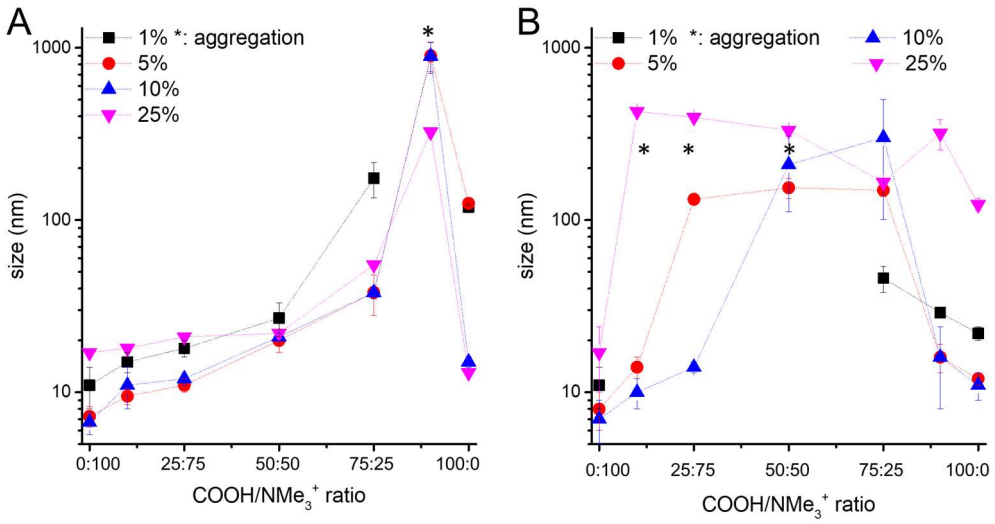

Figure 75: Sizes of mixed polymer NPs for different charge fractions on the polymers and different polymer (COOH/NMe_3^+) ratios, as obtained in mQ water, without (A) and with (B) neutralization of the COOH bearing polymer.

In the case of PEMA-COOH polymers neutralized with NaOH prior precipitation, larger particles or aggregates were formed with polymers ratios close to 50:50. Some polymer association was even observed in acetonitrile by turbidimetry. This didn't lead to the formation of NPs but rather the pairing of few polymer chains, so that they were pre-organized before the precipitation. Mixtures of polymers with a large excess of either COOH or NMe_3^+ groups (mainly for ≥ 90:10 and ≤ 10:90) still gave small NPs below 25 nm for polymers with 5 or 10% charge fraction.

Large particles or aggregates are obtained when the particles formed in the early stage of nanoprecipitation are not stable enough to prevent their growth by aggregation. For charged NPs, this typically correspond to a weak electrostatic repulsion between their surfaces due to a low ζ-potential. In case of neutralized PEMA-COOH polymers, nanoprecipitation with PEMA-NMe_3^+ formed large particles when the two polymers were used in similar ratios, that is when the number of opposite charges were similar. In this case, we believe that an excess of one of the two types of charges is required to form small mixed charge NPs by precipitation. Without neutralization of PEMA-COOH, aggregation took place at a 90:10 COOH/NMe_3^+ ratio. We suppose that this ratio corresponds to the conditions where the number of opposite charges is equal. Indeed, as mentioned earlier,

in Milli-Q water only a small fraction of carboxylic acids is deprotonated, shifting the aggregation ratio toward a higher PEMA-COOH content.

We then studied particle formation with an aqueous phase at pH 7.4 (20 mM phosphate buffer) and in 30 mM NaCl for polymers bearing 5 or 10% of charges (Figure 76). In the presence of NaCl, the particle sizes were larger than in pure Milli-Q water over the whole range of ratios, and the maximum sizes remained at 90:10, as in the case of Milli-Q water. NPs formed with polymers having 5% of charged groups had a bigger increase in size than the series made with 10% charged polymers. At pH 7.4 the maximum particle sizes shifted to a COOH/NMe_3^+ ratio of 50:50 between charged groups, as in the case of neutralized PEMA-COOH in Milli-Q water, but with larger particle sizes. Polymers bearing 5% of charged groups notably formed much larger particles in phosphate buffer (PB) whenever the PEMA-NMe_3^+ polymer was used in excess whereas this effect was diminished with 10% charged polymers.

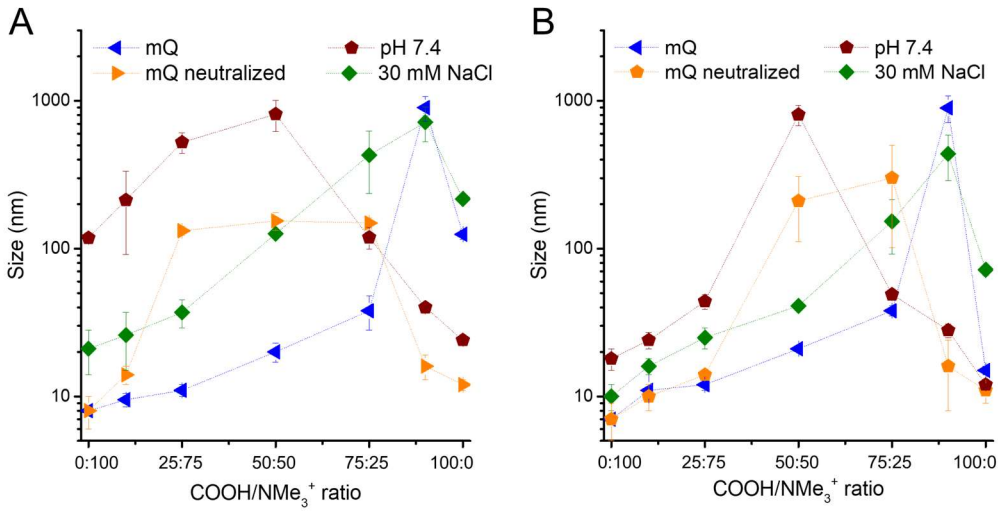

Figure 76:Size of mixed polymer NPs for polymers with charge fractions of (A) 5% or (B) 10% in different polymer ratios, obtained in different precipitation media: (i) mQ water, (ii) mQ water with prior neutralization of polymer, (iii) phosphate buffer (20 mM, pH 7.4), and (iv) 30 mM NaCl.

It appears clearly that the presence of salt in water during precipitation is responsible for an increase in the size of the NPs. This is due to a screening effect of the salt on the charges of the polymer chains, reducing the repulsion forces between particles and favoring aggregation processes[212]. This is a well-known effect that has been used previously in our group to control the size of charged particles obtained by nanoprecipitation[52]. Increasing the pH of the aqueous solution to 7.4 had a similar effect on NP sizes than neutralizing the PEMA-COOH polymer prior precipitation. The fact that

particle sizes increased for polymer ratios close to 50:50 let think that carboxylic acids functions are efficiently deprotonated in PB. The small increase in NP sizes formed with 10% charged polymers is probably due to the effect of ions present in PB, similarly to NaCl experiments. This effect was more marked with polymers bearing only 5% of charged groups, possibly because bearing less charges, particles stability was more affected by the presence of ions.

The series of NPs made from PEMA-COOH 5% and PEMA-NMe_3^+ 5% in MQ water were further analyzed by TEM (Figure 77). Size distributions were narrow with the full width at half maximum below 8 nm, even in cases where DLS gave PDI values > 0.3. Somewhat larger NPs were observed for the PEMA-COOH 5% alone (100:0), in line with DLS.

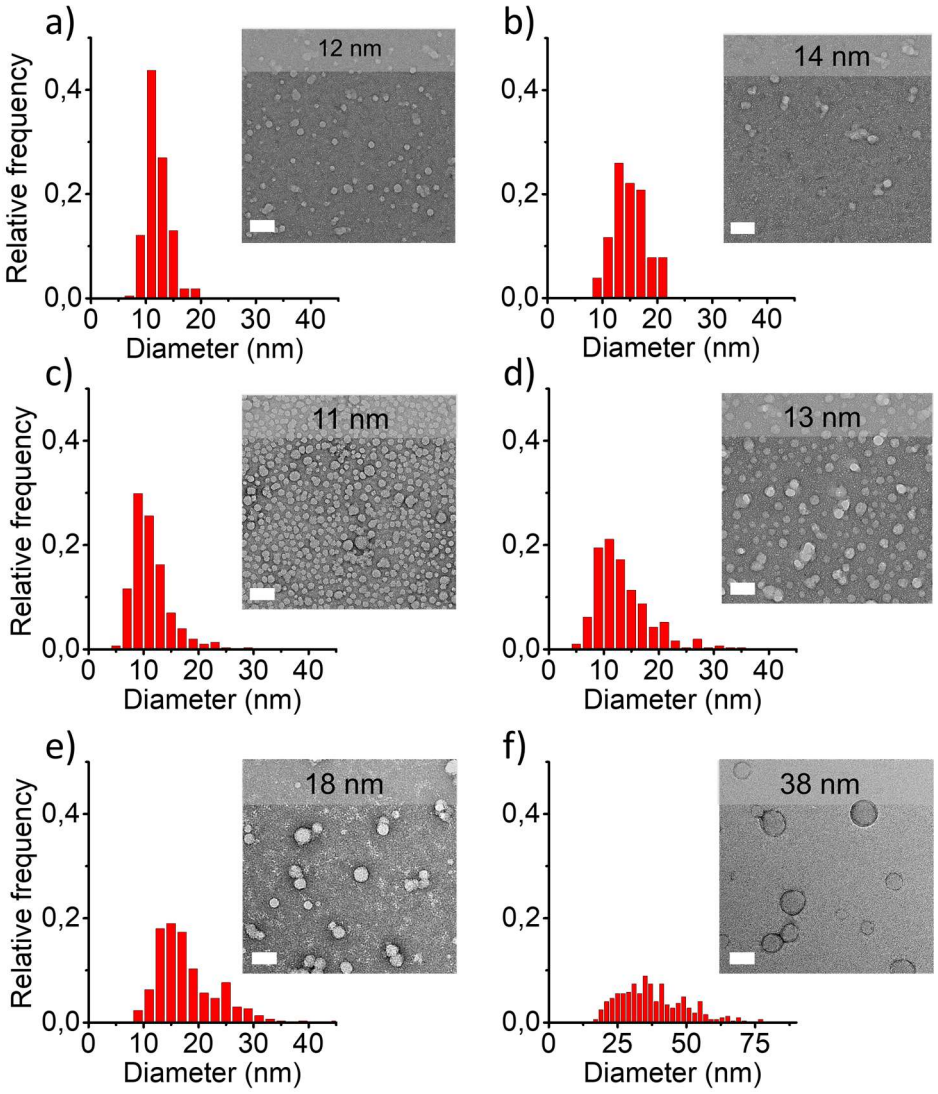

Figure 77: TEM images of mixed polymer NPs for polymers bearing 5% of charged groups and different COOH/NMe_3^+ mixing ratios (from a to f : 0:100, 10:90, 25:75, 50:50, 75:25, 100:0). Mean values of the sizes are given on the images. The size distributions are shown newt to the images. For each condition at least 200 NPs were measured. Scale bars: 50 nm.

Among the many formulations and conditions tested for nanoprecipitation, several led to the formation of very small NPs with a diameter between 10 and 20 nm. Although these particles are still bigger than the majority of proteins, they approach the size of larger ones like antibodies[213]. Bigger particles or aggregates were obtained when the same amount of oppositely charged groups was used. In MQ water, this corresponded to a ratio COOH/NMe_3^+ 90:10, whereas when PB or NaOH were used to neutralize the PEMA-COOH polymer, aggregation took place around a 50:50 ratio.

We further wanted to verify, whether both kinds of polymers are combined within the same NP. To achieve this, we synthesized PEMA-COOH 5% and PEMA-NMe_3^+ 5% polymers bearing about 1 mol % of a naphthalene or a pyrene group, respectively. These two fluorophores can undergo Förster resonance energy transfer (FRET) if they are sufficiently close (Förster radius 2.9 nm[214]), which can be realized only within the same NP (Figure 78A). Starting from a 1:1 mixture of the two polymers in the organic phase, we first simply diluted the solution ten-fold with acetonitrile. Upon illumination at 293 nm, the wavelength where the ratio of naphthalene to pyrene absorbance is highest, we observed fluorescence emission in the regions 320–355 nm and 375–425 nm, corresponding to naphthalene and pyrene emission, respectively, with similar intensities (Figure 78B). Given that the absorbance of pyrene at this excitation wavelength remains relatively high, significant acceptor emission is probably related to its direct excitation rather than FRET. When the same 1:1 mixture of polymers was used for nanoprecipitation (addition to nine-fold excess of water), a strong emission of pyrene was observed, indicating efficient FRET from naphthalene to pyrene. On the other hand, when NPs were prepared separately with the naphthalene and pyrene bearing polymers, and the particle solutions were mixed after nanoprecipitation, the relative intensities of the two bands were similar to those observed in organic solution - indicating that no FRET occurred in this system. Taken together these results show that under the conditions used here for mixed nanoprecipitation, both types of polymers are present in the same NP.

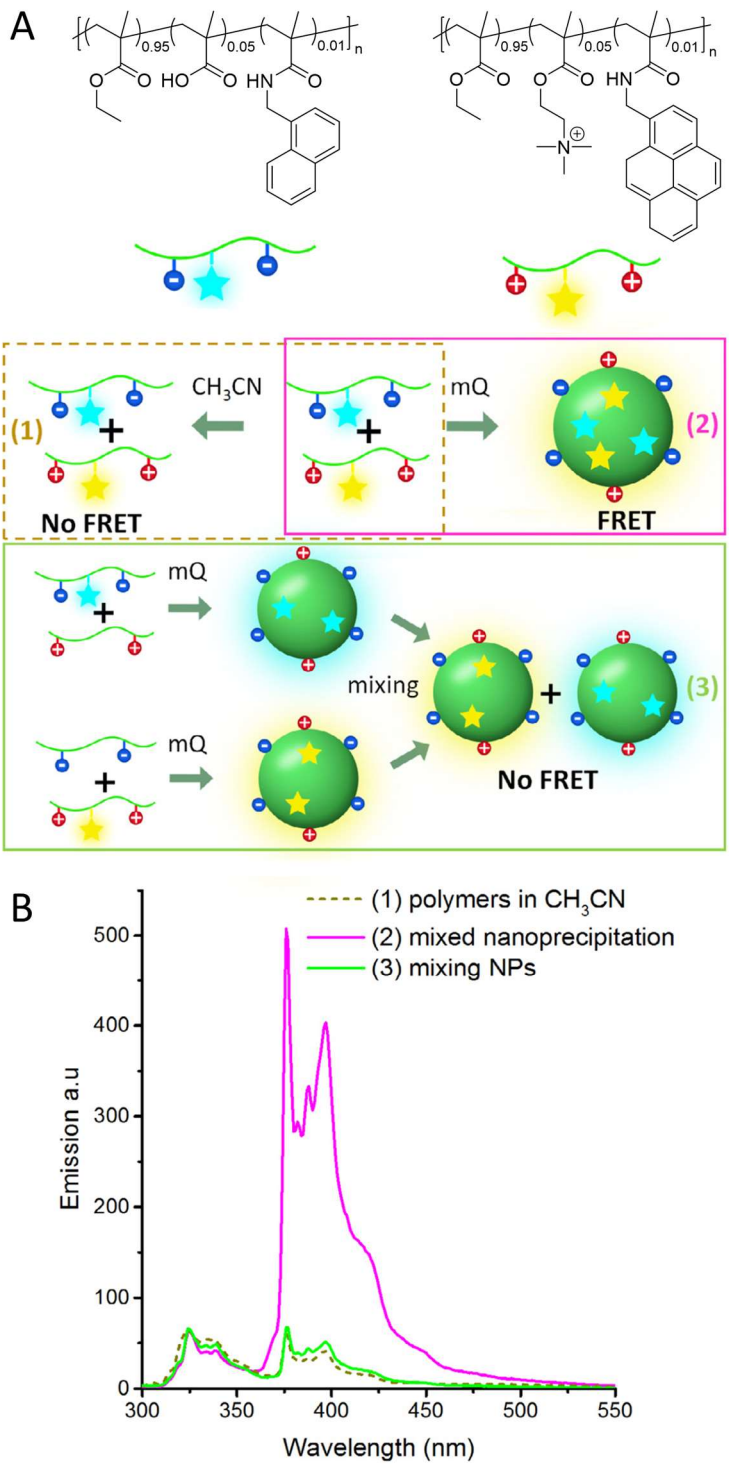

Figure 78: FRET between polymers in the particles. (A) Schematic view of PEMA-COOH 5% - Naphthalene and PEMA-NMe_3^+ 5%-Pyrene, and of the different experiments: (1) Polymers diluted in acetonitrile. (2) Nanoprecipitation using a 50:50 ratio of the two polymers. (3) Nanoprecipitation using one labeled and one non-labeled polymer followed by mixing of the two types of NPs. (B) Corresponding emission spectra obtained upon excitation at 293 nm (emission was normalized with respect to the peak at 325 nm)

2.2 ζ-potential

In order to further characterize the NPs and understand their properties, we studied their surfaces thanks to ζ-potential measurements, which were performed for NPs formed with polymers bearing 5 and 10% of charges (Figure 79). For low COOH/NMe_3^+ ratios, the particles formed had a positive ζ-potential, whereas the latter was negative for high ratios. The PEMA-COOH to PEMA-NMe_3^+ ratio, at which crossing from positive to negative ζ-potential occurred, depended on the conditions of nanoprecipitation. At pH 7.4 or after neutralization of the PEMA-COOH, the surface charge switched at a polymer ratio of about 50:50. In Milli-Q water in the absence of neutralization, the change in sign occurred between COOH to NMe_3^+ ratios of 90:10 and 100:0. Both values corresponded well to the range of ratios at which the largest particle sizes were observed or aggregation occurred. This indicates that the systems became unstable or formed very large NPs when the net surface charge was approaching zero, and, at the same time, that a clearly positive or negative net surface charge is required to form small NPs through nanoprecipitation. These results are in good agreement with results from simulations underlining the importance of charge stabilization in the formation of NPs through nanoprecipitation[215].

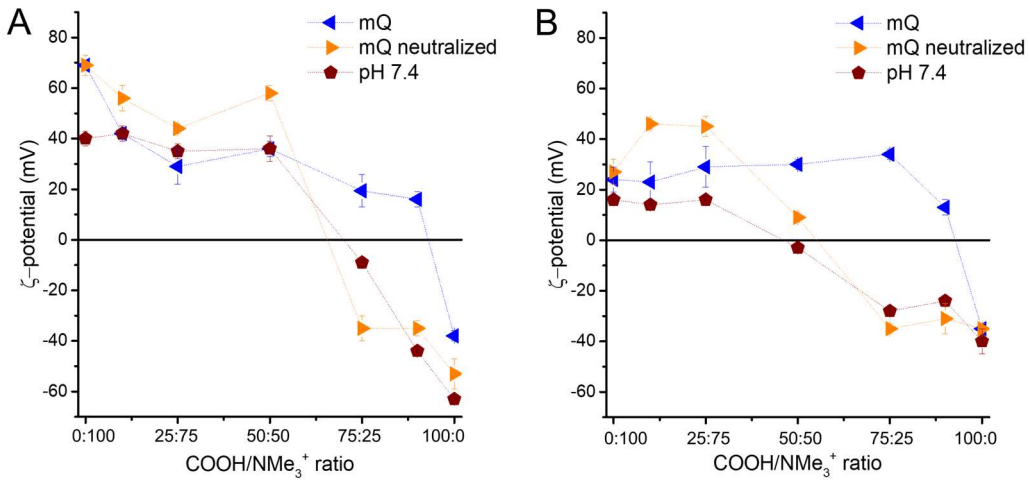

Figure 79: ζ-potential of mixed polymer NPs for polymers with charge fractions of (A) 5% or (B) 10% in different polymer ratios, obtained in different precipitation media: (i) mQ water, (ii) milli-Q water with prior neutralization of polymer, (iii) phosphate buffer (20 mM, pH 7.4).

In a next step, the availability of the charged groups on the surface of the NPs was studied. For this, NPs were prepared using PEMA-COOH 5% and PEMA-NMe_3^+ 5%, without prior neutralization, at different polymer ratios. The obtained NP solutions were

titrated with either NaOH (0.01 M) or HCl (0.01 M) and the ζ-potential was determined at different pH values (Figure 80A). Before addition of acid or base, the NP solutions had pH values around 5.5, presumably due to deprotonation of part of the carboxylic acid groups.

When NPs were prepared from the PEMA-COOH polymer only (ratio 100:0), the ζ-potential remained negative over the entire studied pH range. However, the value changed gradually from -5 mV at pH < 4 to -40 mV at pH 7, followed by a slight decrease to -45 mV at pH > 11 as shown in Figure 80. The observed change in surface charge agrees well with the expected deprotonation of the carboxylic acid groups with increasing pH. After precipitation in MQ water, the ζ-potential of these particles was close to -20 mV. This value is far from the -45 mV obtained when the pH was increased, meaning that initially a rather high amount of carboxylic acids on the surfaces are still protonated.

In the case of a COOH/ NMe_3^+ ratio of 75:25, the particles initially displayed a ζ-potential of about + 25 mV. Addition of HCl led to its increase to about + 32 mV at pH < 4. Upon addition of NaOH, the ζ-potential decreased sharply with increasing pH and became negative at a pH between 6.5 and 7, followed by a further decrease to -30 mV at pH > 9. These particles had hence an isoelectric point, as proteins usually have, which lay here between 6.5 and 7. NPs prepared with higher amounts of PEMA-NMe_3^+ (ratios 50:50 and 25:75) also showed a decrease of the ζ-potential with increasing pH, however, the ζ-potential remained positive up to a pH close to 12. Performing the same type of experiment with NPs made from PEMA-COOH and PEMA-NMe_3^+ 10% in a ratio 75:25 showed again a charge reversal, this time at pH 7. The change of potential with pH was more abrupt in the latter case.

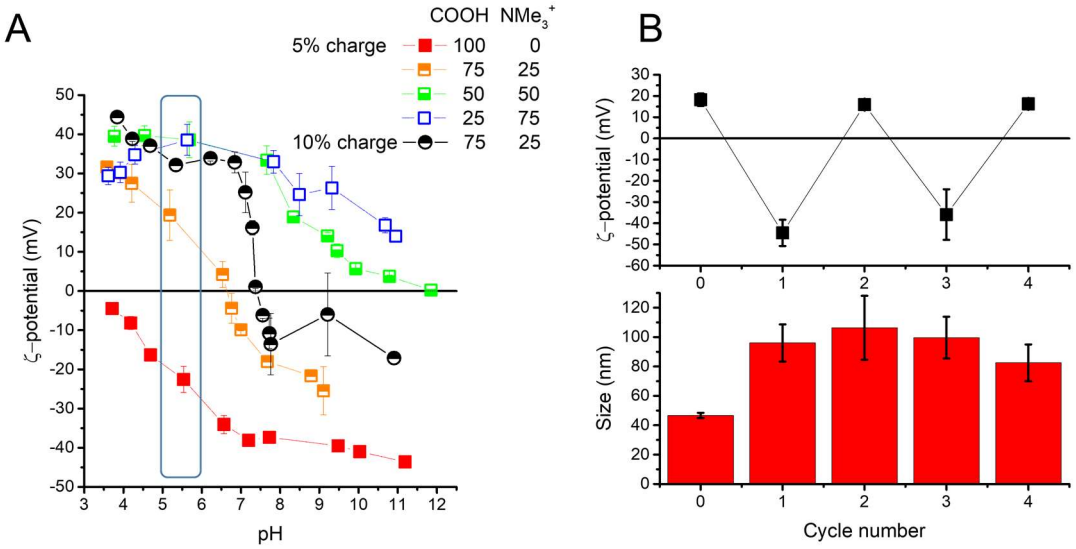

Figure 80: (A) Response of particles to pH changes: isoelectric points and (B) charge reversal. NPs were initially formed in MQ water. Points in the box are the initial value of pH and ζ-potential of the particles after being formed in MQ water.

The results of the titrations revealed that both types of charged groups seemed indeed to be present on particle surfaces. Here, the changes in the surface charge were simply due to the protonation/ deprotonation of the carboxylic acid groups, while the NMe_3^+ groups can be assumed to remain charged over the whole pH range studied. With increasing amount of PEMA-NMe_3^+ the ζ-potential vs pH curves were progressively shifted towards higher potentials and higher pH values. Only in the case of a COOH/NMe_3^+ ratio of 75:25 we observed an actual charge inversion in the studied pH range, and thus these NPs had what corresponds to an isoelectric point. However, comparison with the curves for polymer ratios 100:0 and 50:50 suggested that it should be possible to assemble further NP systems with charge reversal at polymer ratios in this range, with an isoelectric point increasing with increasing amount of PEMA-NMe_3^+. On the other hand, increasing the charge fraction on the polymer to 10% led to a steeper transition between positive and negative ζ-potential. Together these results suggest that mixed nanoprecipitation allows fine tuning the surface charge of NPs through a combination of positive and negative charges on the surface.

We then wanted to know, whether inversion of the surface charge was a reversible process. For this, NPs of PEMA-COOH and PEMA-NMe_3^+ 5% in a 75:25 ratio (ζ-potential + 20 mV) were added alternatively to 20 mM NaOH and HCl solutions (Figure 80B). This resulted indeed in repeated inversion of the ζ-potential, going to around -40 mV in NaOH

and to + 20 mV in HCl. Upon the first charge inversion, we observed an increase in the size, probably due to some association of NPs. However, no further aggregation was observed, and the charge inversion could be carried out over at least 4 cycles.

2.3 Fluorescence of nanoparticles

Fluorescent NPs were made by adding 10wt% (relative to the polymers) of a hydrophobic dye salt (R18/F5-TPB) to the polymer solutions used for particle preparation, followed by nanoprecipitation as before. Here, absorption spectra of the obtained NP solutions were nearly identical for most polymer ratios (Figure 81A). Only the 90:10, and to a minor degree the 75:25 ratios, showed lower dye absorbance values, indicating a loss of part of the dye-salt. For the other formulations the observed absorbance is within 10% of the expected value, indicating a high (>90%) yield for the nanoprecipitation. This value was calculated with the Beer-Lambert law (Equation 24), based on the concentration and molar extinction coefficient (ε) of the dye in the solution of NPs.

$$A_{th} = \frac{C_m}{M*d} * \varepsilon * l \qquad \text{(Equation 24)}$$

With C_m the mass concentration of dye in the solution before precipitation (in $g.L^{-1}$), M the molecular weight of the dye salt, d the dilution factor during particle preparation (10 times during precipitation and 5 times before absorbance measurements), and l the length of the cuvette used for measurements (1 cm). This way,

$$A_{th} = \frac{0.2}{1375*50} * 120000 * 1 = 0.35$$

Fluorescence emission was clearly higher for particles made from the PEMA-COOH polymer only (100:0), corresponding to a higher fluorescence QY (66%) (Figure 81B and C). Apparently, the presence of even a small amount of PEMA-NMe_3^+ decreased the QY to about 45%, but a further addition had no major influence. A possible explanation is that the trimethylammonium groups displaced some of the dye from the hydrophobic counterion F5-TPB, which was thus not available anymore for preventing dye aggregation, leading to reduced QYs.

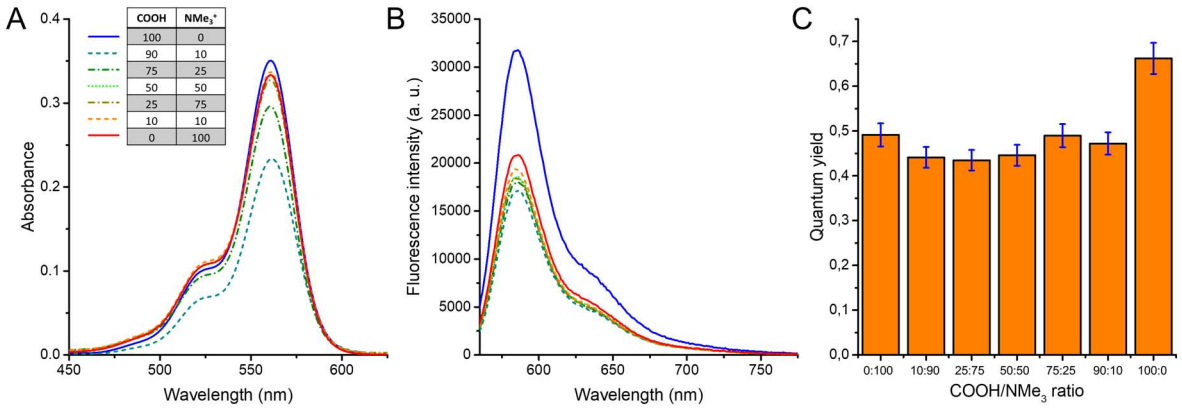

Figure 81: Mixed polymer NPs based on PEMA-COOH 5% and PEMA-NMe_3^+ 5% with different COOH/NMe_3^+ ratios encapsulating 10 wt% (relative to the polymer) of R18/F5-TPB. (A) Absorbance, (B) fluorescence spectra, and (C) fluorescence quantum yields (QY, reference Rhodamine 101) of the different NPs.

Overall, these results suggest that encapsulation can be achieved readily into these mixed polymer, mixed charge NPs and that very small particles of still very high brightness can be obtained.

3 Behavior of the nanoparticles

The fate of NPs in biological environments depends notably on their stability and their interactions with the various biomolecules present. Non-specific interactions of particles with proteins leads to the formation of a protein corona, which affects their properties such as cellular uptake or drug release capacity and clearance from blood circulation by the reticuloendothelial system[216] [217]. The study of the interaction of particles with cells and their stability in various conditions of aqueous media (pH, ionic strength…) gives precious indications on their possible in vivo behavior. Here we tested the stability and behavior of NPs in biological environments in order to evaluate their suitability for biomedical applications.

3.1 Cell internalization

The influence of the composition of these NPs on their interaction with cells was evaluated using fluorescence microscopy. We chose the series of PEMA-COOH and PEMA-NMe_3^+ 5% NPs made from four different polymer ratios: 0:100, 25:75, 50:50 and 100:0. The sizes of these NPs lay in a similar range (between 11 and 8 nm according to TEM), but their ζ- potential varied between + 40 and – 30 mV. NPs were added to HeLa cells, followed

by incubation for 1 h and imaging through confocal microscopy (Figure 82). In the case of pure PEMA-COOH and PEMA-NMe_3^+ NPs, corresponding to ratios 100:0 and 0:100, numerous (15 to 20 per cell), brightly fluorescent spots were observed inside the cells, indicating a good internalization of the NPs. The appearance of the spots and previous results suggest that these correspond to endosomes or lysosomes containing several particles each[175,218]. For NPs made from polymer blends, both the number and the brightness of the spots decreased markedly, suggesting that internalization of NPs bearing both types of charges was reduced. Increasing the charge fraction, by using NPs made from pure PEMA-COOH 10% (ratio 100:0), led to a further clear reduction of the number and intensity of the observed fluorescent spots.

Reduced cell uptake may arise from an increase of the stability of the NPs in the biological medium. Indeed, particles can aggregate and flocculate in the cell culture environment, which leads to sedimentation onto cell surfaces. More stable particles will have less interaction with cells and are less likely to be internalized. Therefore, a possible explanation of these results is that the stability of the NPs increases in the cell culture medium when both charges are present on their surface as it is the case for the particles made from COOH/NMe_3^+ 25:75 and 50:50 polymer ratios. Reduced internalization was also observed when the amount of charges on the polymer was increased from 5 to 10%, which could also lead to an increase of the stability of particles.

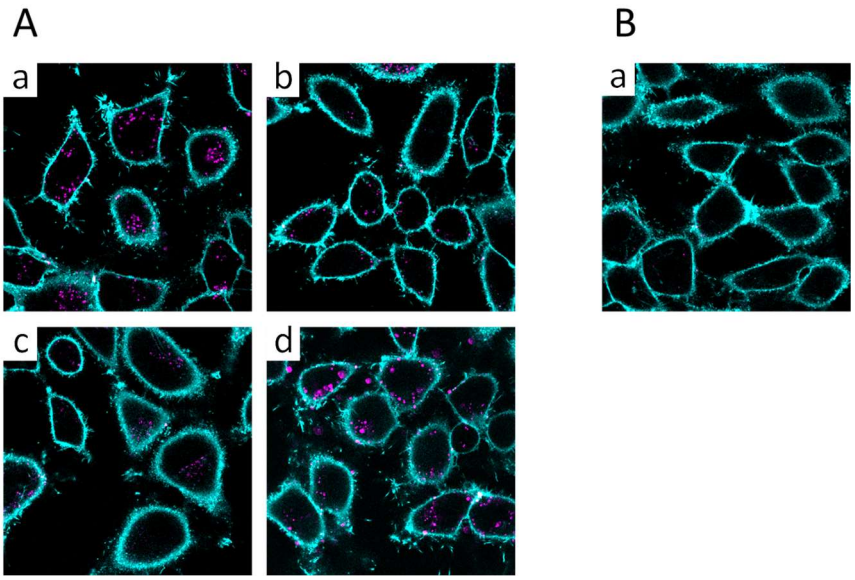

Figure 82: Fluorescence micrographs of HeLa cells incubated with different NPs loaded with 10 wt% of R18/F5-TPB for 1 h. (A) NPs based on PEMA-COOH 5% and PEMA-NMe_3^+ 5% with different mixing ratios (from a to d: 0:100, 25:75, 50:50, 100:0). (B) PEMA-COOH 10% NPs.

3.2 Stability in saline solutions

In the previous sections, we have seen that it was possible to obtain small NPs with a pH responsive surface and an isoelectric point, similarly to proteins. We further wanted to know if the particles formed could also mimic the stability of proteins in biological media. We decided to study particles formed with polymers having a high charge percentage that is 10 and 25% of charged groups per polymer chain. Indeed, increasing the amount of charged groups should result in a better electrostatic stabilization. The reduced cell internalization of particles made of polymers with 10% of charged groups comforted this idea. We formed particles without neutralizing the PEMA-COOH polymer because all NPs formed in this condition had a small diameter (except for the 90:10 ratio which was therefore not tested here).

The stability of the particles was studied in different aqueous solutions: NaCl (20 mM), PB (20 mM, pH = 7.4) and PBS (1x, pH = 7.4). PBS was chosen because its pH and ion concentration match those of the human body, therefore it is a good model to test the NP stability. PB and NaCl solutions were then used to independently study the influence of the pH and the presence of salt on the stability of the NPs. Stability measurements were performed with dye loaded (10 wt%) NPs, which allowed to observe if the suspension underwent aggregation or sedimentation during the experiment.

Particles were formed in MQ water and diluted five times in MQ water, NaCl, PB or PBS solutions. The size of the particles was measured two minutes and at least 24h after dilution. The numbers in the following tables are the diameter of the particles measured after 2 minutes in solution while the color of the cells indicate the stability of the particles after 24 h based on the increase in size:

Green: The size remained constant
Yellow: The size increased less than 2 times original diameter
Orange: The size increased more than 2 times original diameter
Red: Particles were not stable and no mean size can be measured

For example, particles formed with the PEMA-COOH 10% in MQ water and diluted five times in NaCl exhibited a diameter of 45 nm two minute after the dilution. However, after

24h they were completely aggregated, hence the corresponding case in the table is colored in red.

Particles formed with polymers having 10% of charged groups were stable for any polymer ratio in MQ water. In PB and PBS, none of the particles containing the PEMA-NMe_3^+ polymer were stable contrary to the particles formed exclusively with PEMA-COOH. Finally, the ratio between the two polymers used for the formation of the NPs had a marked influence on the stability of particles in the NaCl solution (Table 12).

COOH/NMe_3^+	100:0	90:10	75:25	50:50	25:75	10:90	0:100
MQ	51		18	11	11	6	8
NaCl	45		92	25	14	11	11
PB	42		1046	773	108	75	76
PBS	43		1225	1333	1005	796	962

Table 12: Size and stability of particles made from PEMA-COOH and PEMA-NMe_3^+ polymers with 10% of charged groups.

In order to explain these stability results, it is important to have in mind what groups are present on the surface of the NPs. In the case of COOH/NMe_3^+ 100:0 ratio, the only groups present on the surface of the particles are COOH and COO^-. Based on the results obtained in the ζ-potential section, when particles were titrated, we can assume that a large amount of carboxylic acids are in protonated form (COOH) before dilution in the medium tested. When diluted in NaCl solution, particles were not stable presumably due to a screening of charges by small ions. However, they were very stable when diluted in PB, which contain 20 mM of phosphate salts. This increase in stability may come from the higher pH of the PB, deprotonating a part of COOH groups initially present on the surface of the NPs. This would result in an increase of the amount of charges and hence of NP stability. The same phenomenon could take place in PBS, where particles are stable despite a salt concentration of approximately 150 mM.

Particles made from all of the other polymer ratios (from COOH/NMe_3^+ 75:25 to 0:100) have initially a positive ζ-potential when formed in MQ water. All of them are fairly stable in NaCl solution except the ones made with the COOH/NMe_3^+ 75:25 ratio. These particles actually have the smallest ζ-potential of this series, due to the higher amount of PEMA-COOH polymer. Based on this observation and the behaviour of the NPs exclusively made

from the PEMA-COOH polymer, it seems that the presence of NaCl affects the stability of particles with a low ζ-potential. However, when the latter is increased, very small or no effect of NaCl is observed on the stability of the particles.

Particles containing the PEMA-NMe_3^+ polymer were not stable in PB and PBS solutions. They suffered from aggregation or a large increase in size. Two phenomena can contribute to this: In case of PEMA-NMe_3^+ polymer excess (ratios 25:75, 10:90 and 0:100), the multivalent phosphate ions could associate to these positively charged groups, causing a charge inversion and a destabilization. In PBS the combined effect of phosphate ions and high salinity of the medium directly led to the sedimentation of the dispersion. In case of an excess of PEMA-COOH, transfer into a buffer could lead to deprotonation and thus a ζ-potential approaching 0 mV, which would again favor aggregation.

We then studied particles formed with polymers bearing 25% of charged groups. The increased amount of charges made the particles generally more stable, however, the global trends in stability were similar (Table 13).

COOH/NMe_3^+	100:0	90:10	75:25	50:50	25:75	10:90	0:100
MQ	24		28	20	13	13	17
NaCl	149		1289	26	21	18	19
PB	25		1766	1118	27	21	16
PBS	25		1444	1245	33	24	15

Table 13: Size and stability of particles made from PEMA-COOH and PEMA-NMe_3^+ polymers with 25% of charged groups.

Interestingly particles formed only with PEMA-COOH were also very sensitive to salt. This probably means that they initially have a similar amount of charged groups on their surface compared to particles made with polymers bearing 10% of charges. These particles were stable once diluted in PB and PBS, as observed with the particles made from 10% charged polymers. Again, particles made from the COOH/NMe_3^+ 75:25 and 50:50 ratio were not stable in PB or PBS, we assume for the same reasons given previously. Particles formed with an excess of PEMA-NMe_3^+ polymer were stable in all studied conditions.

In a next step, we wanted to test the stability limits of this system by increasing the concentration of NaCl in the aqueous solutions tested. To this end, particles were formed

in MQ water and diluted two times in Tris buffer (10 mM, pH = 7.4). This buffer was used to avoid the presence of phosphate ions, which supposedly have a negative impact on the stability of the particles. Then the particles were diluted twice in NaCl solutions of various concentration and their size was measured after one hour. For example, to study the stability of NPs in a solution at 150 mM of NaCl, 250 µL of particles were diluted in 250 µL of NaCl solution at 300 mM.

None of the particles made from the polymers with 10% of charges were stable in NaCl solutions with a concentration ≥ 150 mM, except those made from PEMA-COOH only. However, when polymers with 25% of charges were used, several formulations led to the formation of small and stable particles (Table 14).

$COOH/NMe_3^+$	100:0	90:10	75:25	50:50	25:75	10:90	0:100
0 mM	27	150	1730	57	25	21	21
150 mM	25	212	1360	228	25	18	17
500 mM	26	288	1740	229	29	18	16
1000 mM	39	483	1530	391	32	20	16

Table 14: Size of particles made from polymers with 25% of charges one hour after addition in NaCl solutions of different concentrations.

For nanoparticles made from mixtures of particles bearing 25% of charged groups, practically no change in particle size was observed at least up to a NaCl concentration of 1 M in comparison to the reference (0 mM of NaCl). The only exceptions were the particles formed with the $COOH/NMe_3^+$ 90:10 and 50:50 ratios, for which large particles were observed. In the case of the $COOH/NMe_3^+$ 75:25 ratio, aggregates were formed even in the control experiment (0 mM of NaCl). All other polymer ratios showed a very high stability, indicating that it was effectively possible to achieve stable mixed charge polymer NPs.

The present results show that several conditions are required to obtain stable mixed charge NPs. Firstly, one of the two type of charges should be in excess in order to ensure a high ζ-potential and hence a high stability. If the number of opposite charges happens to be equivalent during the formation of the particles or due to a pH change, particle aggregation may take place. Secondly, increasing the amount of charges on the polymers used to form the particles leads to an increase of their stability. This trend has been observed when particles were incubated in with cells and in different aqueous solutions.

Finally, the most stable particles were obtained with polymers having 25% of charged groups.

4 Conclusion

In this study, two series of positively or negatively charged polymers (PEMA-NMe_3^+ and PEMA-COOH) bearing 1 to 25% of charged groups were synthetized. Polymers were combined in different ratios prior to nanoprecipitation and particles were formed in various aqueous media. The size, ζ-potential and stability of the particles was studied for seven different polymer ratios (COOH/NMe_3^+ = 100:0, 90:10, 75:25, 50:50, 25:75, 10:90 and 0:100) in various conditions of pH and ionic strengths and the influence of the neutralization of the carboxylic acids was studied extensively. The encapsulation of a hydrophobic dye has also been realized and the interaction of particles with cells was monitored via fluorescence microscopy.

The particles obtained effectively had both kind of charges on their surfaces. Particles formed without neutralization of the COOH groups appear to be the most versatile formulations. Increasing the number of charges per polymer chains from 10 to 25% yielded NPs with a better stability in various aqueous media. Some of these were even stable up to at least 1M NaCl.

In the present work, we have aimed at mimicking proteins properties with synthetic polymeric NPs. The size and the surface properties of the particles synthetized, notably the presence of an isoelectric point, let think that the approach we used is very promising. The fabrication of stable NPs in biological media is a great challenge for drug delivery systems. The most common strategy currently used is to PEGylate the surface of NPs, with the inconvenience to reduce the availability of the particle surface. Moreover, the frequent use of PEGylated systems generates an increase of PEG allergies and the development of anti-PEG antibodies[219–221]. Thus finding an alternative technology for particle stabilization becomes crucial. We believe that the system we developed is very promising in that sense, because it allows to form very small loaded NPs with an excellent stability in saline solutions. Moreover, this approach allows fine tuning of particle surfaces simply by changing the polymer ratios used for particle formation.

These results remain only the preliminary steps of the creation of new nanocarriers. The stability of the particles should now be investigated further in biological media, for example with fluorescence correlation microscopy. This technique could allow the study of the interaction between particles and proteins and the comparison of the behaviour of our particles with classic stealth NPs. This could be realizable thanks to the encapsulation of fluorescent dyes, similarly to those used in this study. Finally, another important work to do would be to implement targeting properties to the particles. Functionalization of the particles could be further achieved using the groups present on their surface. Indeed, we observed that nanoprecipitation allows the presence of different functions on the surface of the particles, which could be coupled with appropriate targeting moieties. These are challenging perspectives, however, combined with recently developed concepts of (co)nanoprecipitation[222,223], this study may pave the way to polymer nanoparticles with a stability, and functionality approaching those of proteins.

General conclusion

The aim of this thesis work was to study the influence of the polymer chemistry on the formation of nanoparticles obtained through nanoprecipitation. This aspect is of prime importance for the design of novel polymeric NPs in order to meet the needs of biomedical applications.

We started with the study of the kinetics of formation of nanoparticles and how these are influenced by polymer chemistry. We evidenced that the properties of NPs may (or may not) depend on the mixing stage, depending on polymer chemistry. The most hydrophobic polymers were not influenced by mixing whereas polymer with a higher solubility limit formed smaller NPs in the case of fast mixing. This was presumably linked to the relative rates of mixing and polymer nanoprecipitation kinetics. Therefore, in a next step we studied the kinetics of particle formation by monitoring the assembly of polymer chains with a stopped flow setup. We have shown that the assembly rate of polymer chains is highly impacted by the nature of the polymer. The precipitation of the most hydrophobic polymer studied happened on a time scale of few milliseconds but this time increased to 100 milliseconds range with a more hydrophilic polymer. Moreover, the kinetics of dye encapsulation has also been studied, which allowed to show that they associate with polymer chains in the early stage of nanoprecipitation.

Block copolymers are widely used for the preparation of loaded NPs. However, in the case of nanoprecipitation, the influence of polymer architecture is not perfectly clear. We were interested to study this point through the formation of dye-loaded NPs. On one hand, the study of the repartition of charged groups along the polymer chain revealed that statistical polymers show better performances than their block analogues to form small and monodisperse NPs. Therefore, despite their versatility, block copolymers are not always the most optimal choice for the assembly of polymer NPs. On the other hand, in the case of hydrophilic polymers, the block architecture allowed to increase the quantum yield of dye loaded NPs. Varying the hydrophobicity of the dye has shown that the relative hydrophobicity of the polymer and the load have an important impact on particle formation and that the polymer used should be chosen meticulously to perform an efficient encapsulation.

Finally, we have taken advantage of the kinetic aspect of nanoprecipitation to form mixed charge NPs via the co-precipitation of polymers bearing oppositely charged groups. The particles formed had both kind of charges available on their surface and exhibited an isoelectric point thanks to the presence of weakly acidic groups. Moreover, they had an exceptional stability in saline solutions. Their size, surface properties and stability hence approach the characteristics of proteins. Therefore, these particles are a good candidate for the development of new PEG-free and surfactant-free nanocarriers dedicated to biomedical applications.

The insights brought by this thesis work are principally based on polymethacrylate chemistry. Additional stopped flow experiments could be considered with polyester such as PLGA or PEG-PLGA polymers to gather information on these widely used polymers. Further experiments on the stability of mixed charge NPs are another possible research focus. Their stability in biological media or in vivo should be investigated in details to evaluate their interaction with these environments as well as the possibility to functionalize their surfaces. These challenging points are essential for making new nanocarriers, however, we believe that the particle we synthetized are a great starting point in this end.

The complexity of polymeric NPs keeps increasing thanks to innovative research to modify their structure and interactions: Janus NPs, molecularly imprinted NPs, biocompatible and targeting NPs, all are now far from simple polymeric nanospheres. These advances have been possible thanks to the apparition of new materials, methods and processes combined of course with the ingenuity of researchers. With this thesis work, we have shown that nanoprecipitation is not just a convenient method for the preparation of NPs. The kinetic control it offers is a valuable resource, which may be used to form unique nanostructures. A good understanding of its mechanism and of the influence of polymer chemistry on the formation of NPs is the key to design new materials with this process. One day, it may allow to push further the researches dedicated to the development of nanocarriers, improving their properties and functionalities to the level of artificial proteins.

Résumé de thèse

Des nombreuses avancées dans le secteur biomédical sont dues aux progrès réalisés dans le domaine des nanomatériaux qui possèdent des propriétés uniques dues à leur taille variant de quelques nm à plusieurs centaines de nm[4]. Les nanoparticules polymériques (NPs) font partie de cette grande famille. Leur matrice en polymère est capable d'encapsuler de nombreux composés tels que des principes actifs[224] ou des agents de contraste[6]. Le principal objectif des NPs est de servir de véhicules afin de protéger, transporter et éventuellement relarguer leur charge. Leur taille, forme et propriétés de surface ont des effets considérables sur ces fonctions[8–10]. Une encapsulation efficace du composé d'intérêt est également de la plus grande importance. Différentes méthodes sont employées pour former des nanoparticules polymériques[12]. Il est possible de réaliser des émulsions comportant les composés à encapsuler ainsi que les monomères puis de les polymériser pour obtenir des nanoparticules. D'autres techniques consistent à employer des polymères afin de les assembler sous forme de nanoparticules par auto-assemblage ou nanoprécipitation. Dans tous les cas, afin de pouvoir contrôler les propriétés des nanoparticules formées, il est important de comprendre précisément leur mécanisme de formation, c'est-à-dire les interactions chimiques et physiques qui vont conduire à leur formation.

Une des techniques les plus couramment utilisées pour la formation de NPs encapsulant d'autres composés est la nanoprécipitation[66]. Dans la majorité des cas, les polymères ainsi que la charge à encapsuler sont dissous dans un solvant organique miscible à l'eau. Cette solution est ensuite ajoutée sous agitation dans une grande quantité d'eau et les polymères, hydrophobes, précipitent pour former des nanoparticules en intriquant la charge dans la matrice polymérique formée. Ce processus est contrôlé cinétiquement, ainsi les conditions utilisées lors de la nanoprécipitation ont une grande influence sur les propriétés des nanoparticules.[64,68,73] Parmi ces conditions, la chimie des polymères et la phase de mélange jouent un rôle important.

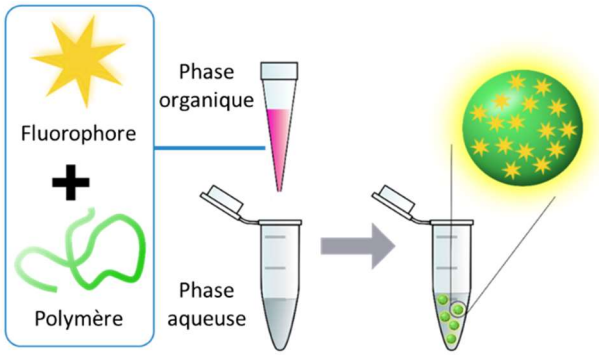

Figure 83: Représentation de la formation de nanoparticules fluorescentes par la méthode de nanoprécipitation.

Les objectifs de cette thèse sont d'étudier la nanoprécipitation et en particulier l'influence de la chimie des polymères sur la formation, l'encapsulation et les propriétés des particules obtenues. Dans ce but de nombreux polymères ont été synthétisés et co-précipités avec un colorant organique fluorescent (Figure 83). Les nanoparticules fluorescentes sont largement employées en imagerie médicale ou en bio-imagerie pour leur grande brillance[6]. La fluorescence des particules est également un outil très utile pour caractériser l'encapsulation et le comportement des particules en milieu biologique. Ces connaissances serviront à concevoir des particules de petite taille, stables en milieu biologique et fonctionnelles grâce à leurs propriétés d'encapsulation.

1 Cinétique de formation des nanoparticules obtenues par nanoprécipitation

La nanoprécipitation des polymères est notamment influencée par la phase de mélange et la chimie des polymères[13,225]. Dans un premier temps, nous avons étudié ces paramètres qualitativement en formant des nanoparticules chargées en fluorophores avec différents polymères et en variant la méthode de mélange. Leur influence a été évaluée en comparant la taille et le rendement quantique des particules obtenues. Dans un second temps, nous avons souhaité caractériser quantitativement la cinétique de précipitation de différents polymères en suivant la formation des nanoparticules grâce à une méthode par blocage de flux (stopped-flow).

Effets du mélange et de la chimie des polymères sur la nanoprécipitation :

Dans cette partie, nous avons voulu évaluer l'importance relative de la chimie des polymères et de l'étape de mélange pendant la préparation de nanoparticules obtenues par nanoprécipitation. Pour cela, nous avons comparé les nanoparticules préparées manuellement, correspondant à un mélange « lent » (environ 30 ms) à celles préparées en utilisant un mélangeur micro-fluidique (< 3 ms). Nous avons ensuite déterminé pour différents polymères (Figure 84) quelles étaient les formulations où les propriétés des particules étaient influencées par le mélange.

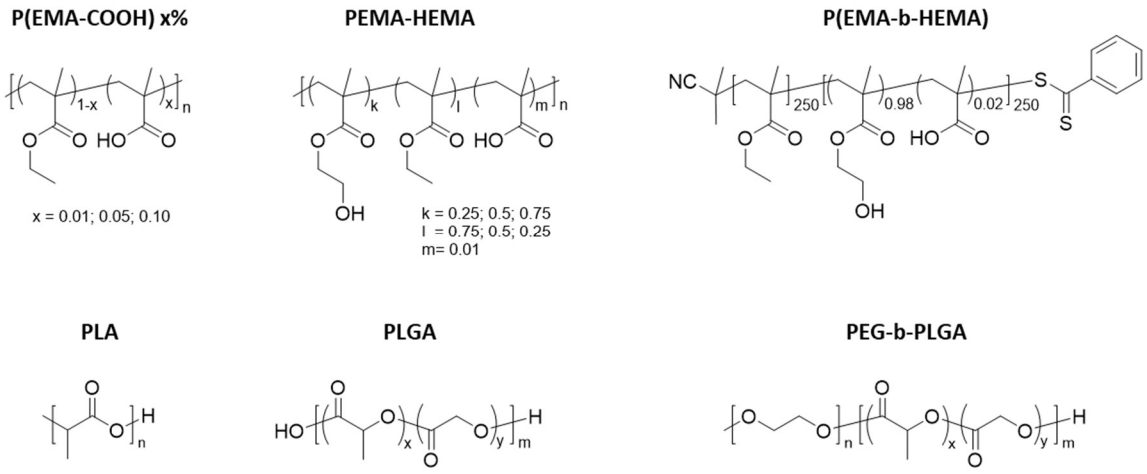

Figure 84: Formules des polymères étudiés lors de la formation de particules chargées en fluorophores par précipitation "manuelle" ou réalisée avec un mélangeur micro-fluidique.

La taille et le rendement quantique des particules formées avec les polymères les plus hydrophobes, qui sont les P(EMA-COOH), le polymère à blocs P(EMA-b-HEMA) et les PLGA n'étaient pas influencés par les conditions de mélange utilisées. En revanche, les polymères statistiques contenant le monomère hydrophile HEMA ainsi que le PLA ont formé des particules plus petites (Figure 85A) et avec un rendement quantique plus élevé lorsque le mélange était plus rapide. Ces résultats ont été corrélés avec la limite de solubilité des polymères (Figure 85B), qui a été mesurée par turbidimétrie, et qui correspond au volume d'eau à partir duquel les chaines de polymères devenaient insolubles. En effet, le premier groupe de polymères, non influencés par le mélange, avaient tous une limite de solubilité inférieure à 6 vol%. Une explication possible est que ces polymères précipitent si rapidement que la vitesse de mélange n'influence pas la formation des particules.

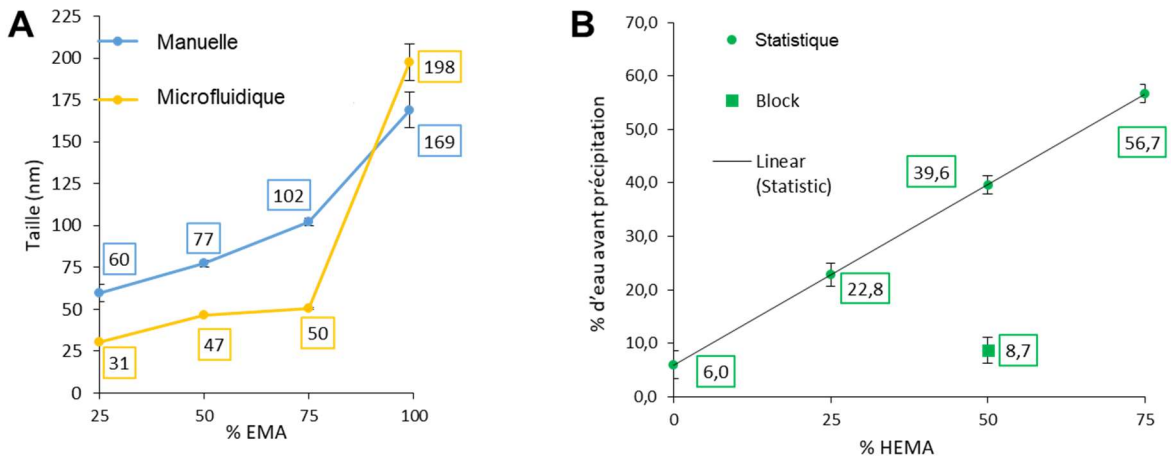

Figure 85: (A) Taille des nanoparticules formées avec 30% en masse de fluorophore et (B) limite de solubilité des copolymères utilisés pour leur formation en fonction du ratio des deux monomères (EMA-HEMA) composant les polymères.

Observation du phénomène de nanoprécipitation :

La cinétique de précipitation des polymères est un point clé du mécanisme de formation des NPs obtenues par nanoprécipitation. Ce phénomène est complexe à observer et quantifier à cause des infimes échelles de temps et de taille mises en jeu. Un protocole a été mis en place afin d'observer cette cinétique, reposant sur l'utilisation de polymères fluorescents et de l'apparition d'un phénomène de « Förster resonance energy transfer » (FRET) durant la précipitation (Figure 86). Ce phénomène se traduit par une modification de la fluorescence d'un couple de fluorophores lorsque ceux-ci se trouvent spatialement proches (<10 nm)[226]. Plusieurs couples de polymères fluorescents ont été synthétisés afin d'observer la formation des nanoparticules en suivant l'évolution de la fluorescence (apparition du phénomène de FRET). Les polymères ont été fonctionnalisés séparément avec un bodipy en tant que donneur ou une rhodamine en tant qu'accepteur. L'observation de la nanoprécipitation des polymères a été réalisée à l'aide d'une méthode par blocage de flux. Cet équipement permet l'étude de la cinétique de réactions chimiques grâce à un mélange très rapide des réactifs, envoyés par la suite dans une cellule de mesure. Dans le cadre de cette étude, ce système a été adapté pour suivre la formation des particules en observant la fluorescence du milieu de précipitation.

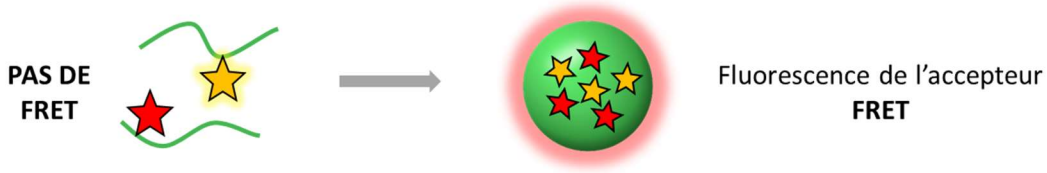

Figure 86: Schéma représentant le principe de l'observation de formation des nanoparticules utilisant le FRET.

Une série de quatre polymères plus ou moins hydrophiles (comprenant différents pourcentages de méthacrylate d'hydroxyéthyle) a été synthétisée, puis ces polymères ont été fonctionnalisés avec les fluorophores formant le couple FRET (Figure 87A). L'efficacité de FRET au cours du temps a été calculée pendant la nanoprécipitation de chaque polymère, dès les premiers instants de la précipitation (le montage comprend un temps mort de 3,7 ms).

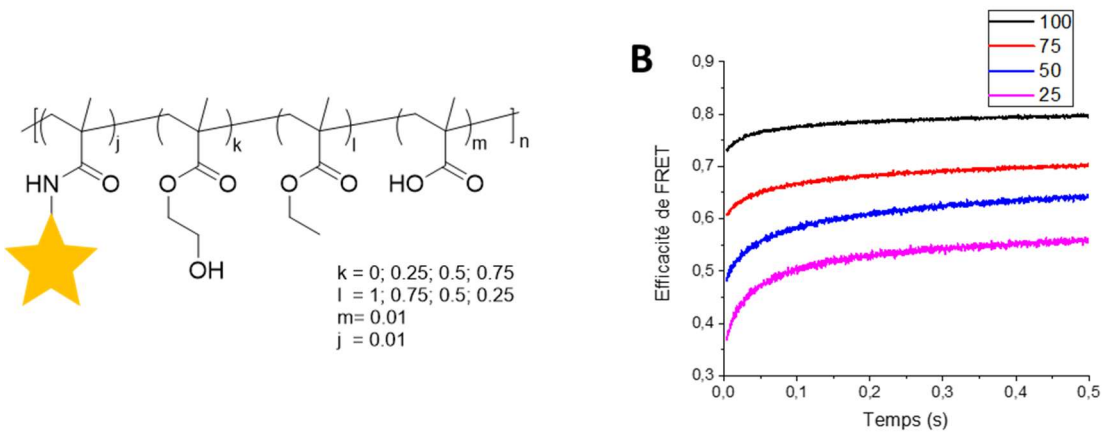

Figure 87: A) Structure des polymères fluorescents utilisés lors de cette étude. B) Evolution de l'efficacité de FRET durant les premières 500 ms de la mesure.

La figure 87B montre l'évolution de l'efficacité de FRET (normalisée) pour chaque polymère. La légende correspond au pourcentage de monomère hydrophobe (méthacrylate d'éthyle). La plus grande augmentation de FRET a été observée pour les polymères les moins hydrophobes, signifiant que dans les autres cas, seulement la fin du phénomène de précipitation a été enregistrée. Afin d'avoir un point de comparaison entre les polymères, nous avons décidé de noter le temps à partir duquel l'efficacité de FRET atteint 90% de sa valeur finale. Pour le polymère le plus hydrophobe, cela se produit pendant le temps mort de l'expérience, soit moins de 3,7 ms. Cependant, dans le cas du polymère le plus hydrophile, environ 100 ms secondes sont nécessaires à atteindre cette valeur. Ainsi, la cinétique de nanoprécipitation de ces polymères a été mesurée

quantitativement et les résultats obtenus corroborent avec ceux de la première partie. En effet, la taille des particules formées avec le polymère ayant le temps de précipitation le plus court n'était pas influencée par le mélange à l'opposé de celles formée avec le polymère ayant un temps de précipitation plus long.

2 Influence de l'architecture des polymères sur la formation de nanoparticules obtenues par nanoprécipitation

Cas des polymères chargés

Des précédents travaux réalisés au sein de notre équipe ont montré que l'ajout de monomères hydrophiles ou chargés dans la composition des polymères influence drastiquement la formation des NPs[13]. L'augmentation du nombre de charges a tendance à fortement réduire leur taille, tandis que l'introduction de groupements hydrophiles a un effet similaire mais elle modifie également leurs propriétés d'encapsulation. Cependant ces études ont exclusivement été menées sur des polymères statistiques. Afin d'étudier l'influence de l'architecture des polymères sur leur précipitation, plusieurs polyméthacrylates ont été synthétisés, contenant divers groupements chargés afin d'assurer la stabilité des particules (Figure 88). Ces derniers ont été répartis de manière différente le long des chaînes de polymères grâce à la polymérisation contrôlée RAFT (Reversible Addition-Fragmentation chain Transfer).

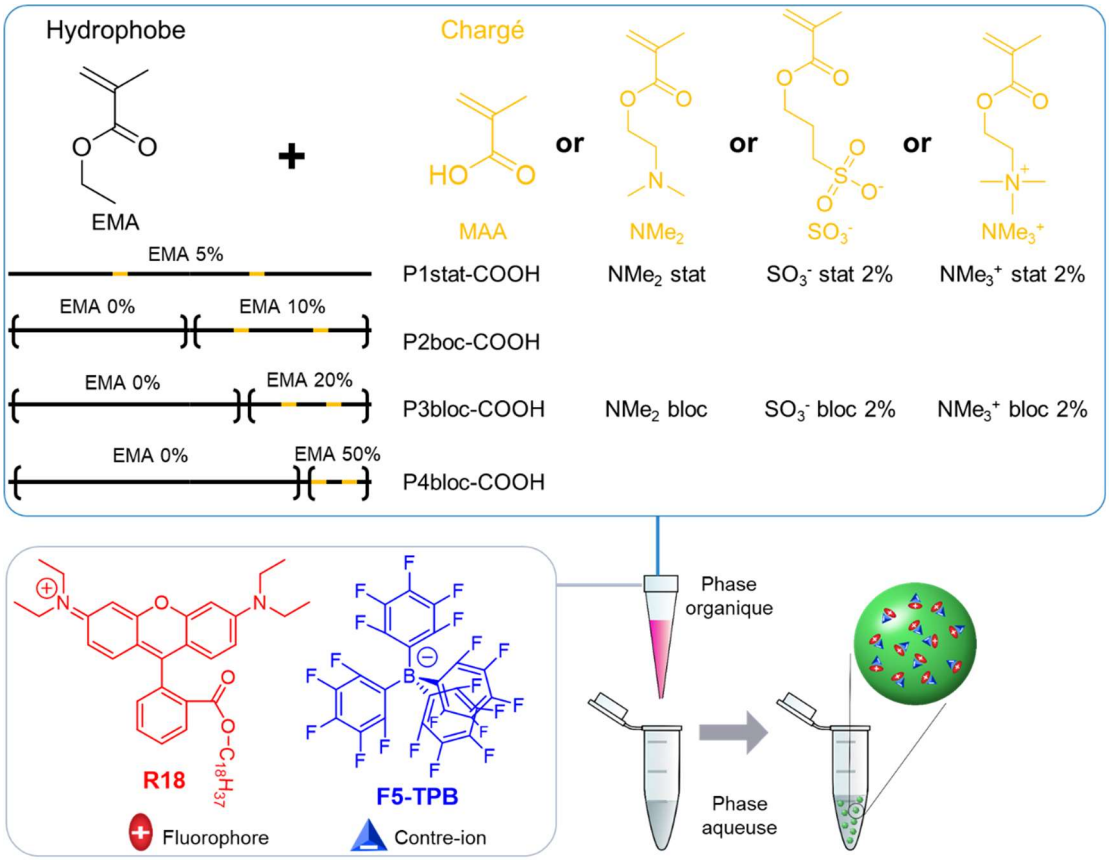

Figure 88: Schéma des polymères synthétisés et structure du fluorophore utilisé dans cette étude. Les pourcentages représentent la fraction molaire des monomères chargés dans un bloc donné. Représentation schématique de la nanoprécipitation avec un colorant fluorescent.

Dans le cadre des polymères comportant l'acide méthacrylique, la taille des particules est affectée par la ségrégation des charges, augmentant de 25 à plus de 300 nm lorsque celles-ci sont concentrées en bout de chaine tandis que leur fluorescence reste inchangée. De plus, la concentration des charges en bout de chaine a eu comme conséquence de fortement limiter l'internalisation des particules dans des cellules HeLa (Figure 89). Cela atteste d'une modification importante des propriétés de surface des particules qui ont été caractérisées par leur potentiel zêta.

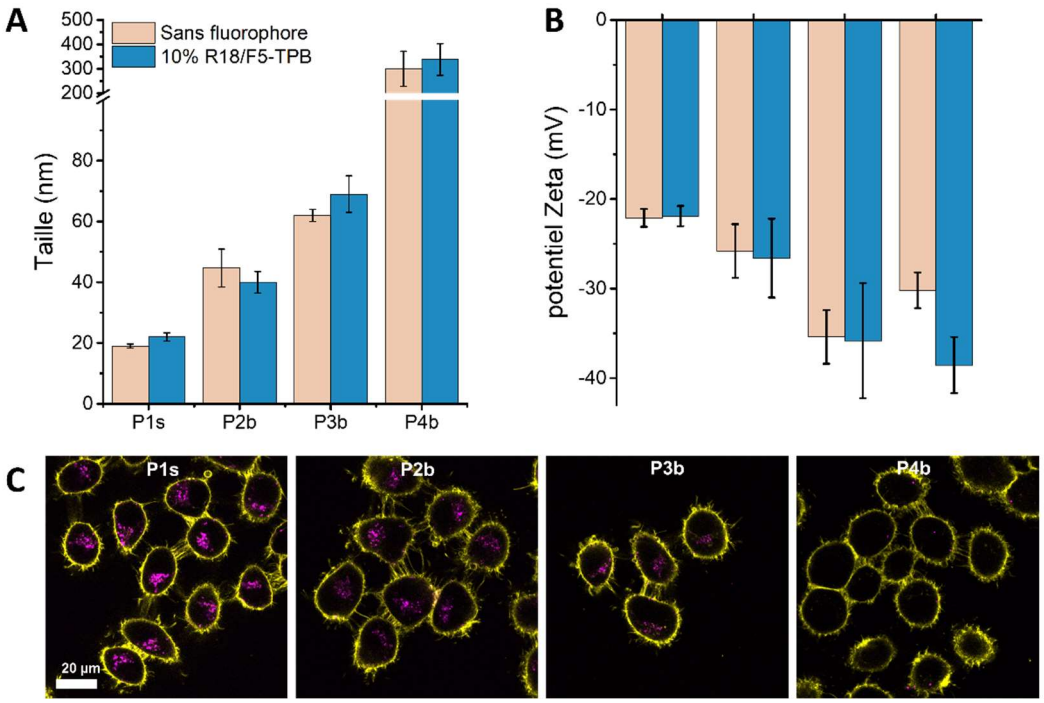

Figure 89: Taille (A) et potentiel zêta (B) des nanoparticules formées à partir des polymères comportant des groupements acides COOH, déterminés par DLS. C) Image des nanoparticules internalisées dans des cellules HeLa obtenues par microscopie de fluorescence. P1s: EMA 5%; P2b: [EMA]-b-[EMA 10%]; P3b: [EMA]-b-[EMA 20%]; P4b: [EMA]-b-[EMA 50%], où les pourcentages correspondent à la fraction molaire de monomères chargés pour un bloc donné. Les particules ont été formées avec 10% en masse de fluorophore ou sans, les barres d'erreur correspondent à l'écart type de la moyenne des mesures.

Cette étude a ensuite été étendue à des polymères comportant d'autres types de groupements chargés. De nouveau, concentrer les charges sur une partie des chaines de polymères a conduit à une augmentation de la taille des particules. Le potentiel zêta est de manière logique influencé par le type de charge : Il a été mesuré négatif pour les particules stabilisées par les groupements SO_3^- et positif avec les groupements NMe_2 et NMe_3^+ (Figure 90). Le rendement quantique de ces particules était encore une fois peu influencé par la distribution des charges sur les chaines de polymères.

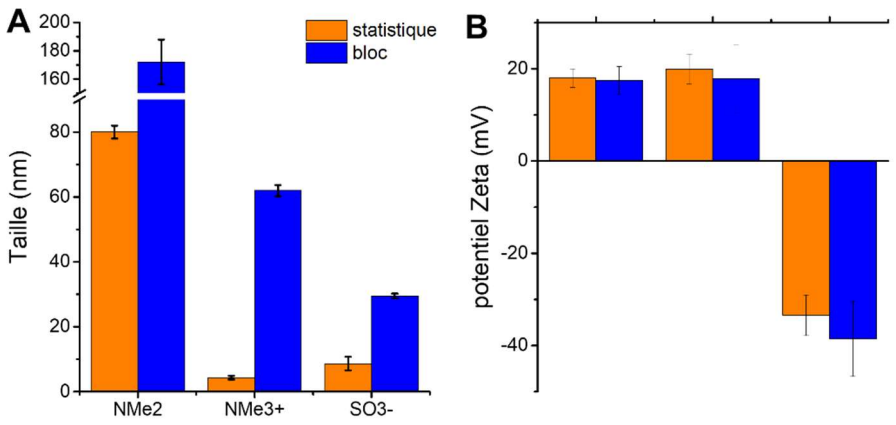

Figure 90: Taille (A) et potentiel zêta (B) des particules formées avec les polymères comportant d'autres types de charges, réparties statistiquement ou concentrées sur une partie de la chaine, determinés par DLS. Les particules ont été formées avec 10% en masse de fluorophore, les barres d'erreur correspondent à l'écart type de la moyenne des mesures.

Cas des groupements hydrophiles

L'étude de l'influence de l'architecture des polymères a également été menée sur des polymères comportant des groupes hydrophiles. Pour cela, quatre polymères ont été synthétisés: Le premier, entièrement hydrophobe, est uniquement composé de méthacrylate d'éthyle et sert de comparaison afin d'observer l'influence des groupes hydrophiles. Les trois autres polymères sont composes à 50% de méthacrylate d'éthyle et de méthacrylate d'hydroxéthyle, un monomère hydrophile. De plus, tous les polymères contiennent 1% d'acide méthacrilique afin de former des particules stables. L'architecture des polymères a été variée en répartissant les groupements HEMA de manière statistique ou sous forme de bloc (Figure 91).

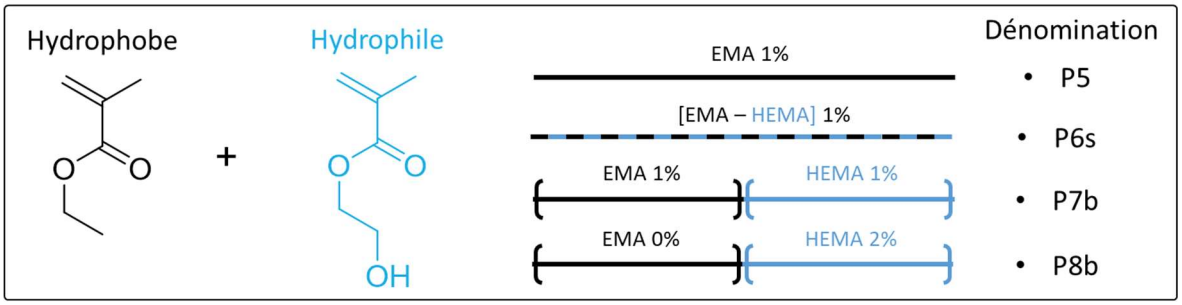

Figure 91: Architecture des polymères utilisés dans cette étude. Les pourcentages représentent la fraction molaire d'acide méthacrylique dans un bloc donné.

Cette série de polymères a été affectée de manière différente par leur architecture. Alors que la taille des particules obtenues varie peu, leur rendement quantique augmente de 20 à 73% lorsque le polymère utilisé comporte un bloc hydrophobe (au lieu de répartir les groupes hydrophobes de manières statistique le long de la chaine) (Figure 92). Cela a été attribué à une variation dans la cinétique de précipitation du polymère. En effet une différence trop importante entre la cinétique de précipitation du colorant et des chaînes de polymères peut être responsable d'une faible encapsulation ou à contrario d'une forte agrégation du fluorophore.

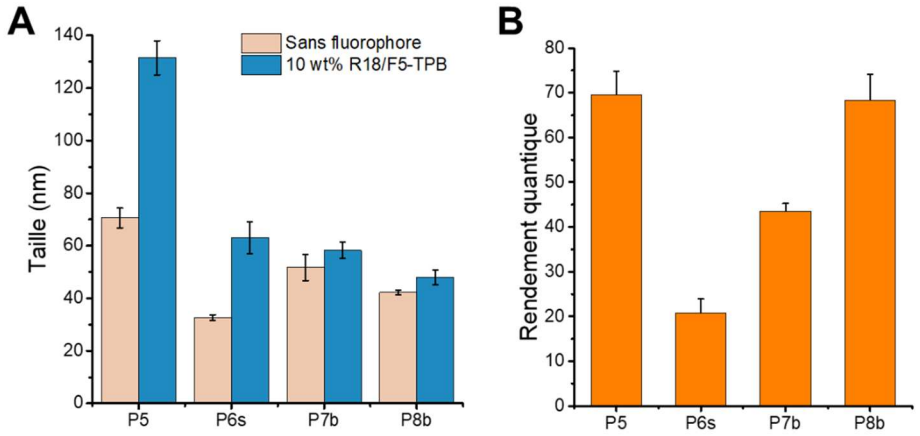

Figure 92: (A) Taille et (B) rendement quantique des particules formées avec la série de polymères HEMA. Les particules fluorescents ont été formées avec 10% en masse de fluorophore, les barres d'erreur correspondent à l'écart type de la moyenne des mesures. P5: EMA 1%; P6s: EMA-HEMA 1%; P7b: [EMA 1%]-b-[HEMA 1%]; P8b: [EMA]-b-[HEMA 2%], où les pourcentages représentent la fraction molaire des monomères chargés dans un bloc donné.

Ces deux études montrent l'importance d'un design de polymère approprié pour contrôler la formation des particules obtenues par nanoprécipitation. Elles ont notamment révélé que malgré leur popularité, les copolymères à blocs ne sont pas toujours le choix optimal pour la formation de nanoparticules, dans le cas des polymères chargés. Elles soulignent également qu'il est crucial de faire correspondre la vitesse de precipitation des polymères avec celle de la charge à encapsuler afin d'optimiser l'encapsulation.

3 Formation de particules avec des polymères de charges opposées.

Une des principales application des nanoparticules polymériques est l'administration de médicaments, où leur rôle est de transporter et relarguer un principe actif à un endroit

spécifique du corps[5,227]. Dans le corps humain, ce rôle de transporteur est notamment assuré par les protéines, qui surpassent les nanoparticules sur plusieurs points. En effet ces dernières ont généralement une taille plus grande, une structure plus simple et souffrent d'interactions non-spécifiques en milieu biologique. Une particularité des protéines est la complexité de leur surface qui leur confère une grande stabilité dans divers conditions des pH ou de forces ioniques. Elle permet également de réaliser des interactions spécifiques tout en minimisant celles non-spécifiques[198].

Inspirés par la surface des protéines, portant des groupements chargés positivement et négativement, nous avons cherché à créer des nanoparticules avec les mêmes caractéristiques. Pour ce faire, nous avons choisi d'assembler des polymères portant des charges opposées par nanoprécipitation. En effet, en s'appuyant sur les concepts évoqués précédemment, nous avons émis l'hypothèse qu'utiliser l'hydrophobicité des polymères en tant que force motrice pour assembler les particules permettrait de piéger les chaines de polymères dans un état cinétiquement gelé, évitant ainsi le couplage des charges. De plus, le contrôle cinétique de la formation des particules a l'avantage supplémentaire de faciliter l'encapsulation de composés d'intérêt, tels que des principes actifs ou des agents de contraste. Ainsi, deux séries de polymères statistiques portant de 1 à 25% de groupements chargés positivement ou négativement ont été synthétisées. Le méthacrylate d'éthyle a été choisi comme principal constituant hydrophobe des chaînes de polymères. L'acide méthacrylique et le [2-(méthacryloyloxy)éthyl] triméthylammonium ont été utilisés comme monomères chargés négativement et positivement respectivement (Figure 93).

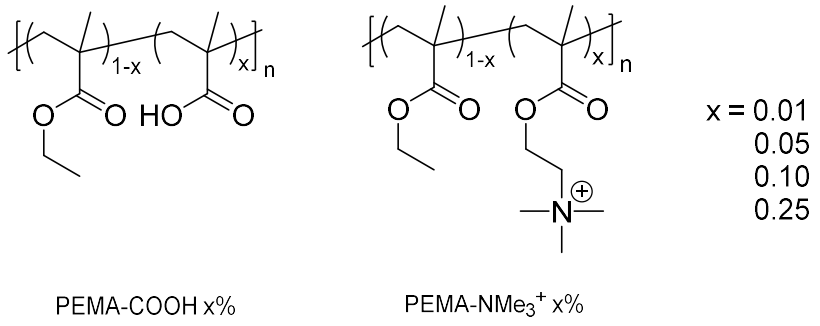

Figure 93: Formules des polymères utilisés pour la formation de nanoparticules portant des charges opposées.

La co-précipitation de ces polymères dans différents ratios avec un colorant hydrophobe a permis d'obtenir des particules fluorescentes dont la taille et le potentiel

zêta ont été mesurés. Ce dernier est sensible au pH dû à la présence d'acides carboxyliques à la surface des particules. Cela confère à certaines particules un point isoélectrique à l'instar des protéines. Le potentiel zêta de ces particules a été inversé en les exposant successivement à des milieux acides ou basiques (Figure 94). Cela indique que les deux groupements utilisés (COOH et NMe_3^+) sont présents sur la surface des nanoparticules.

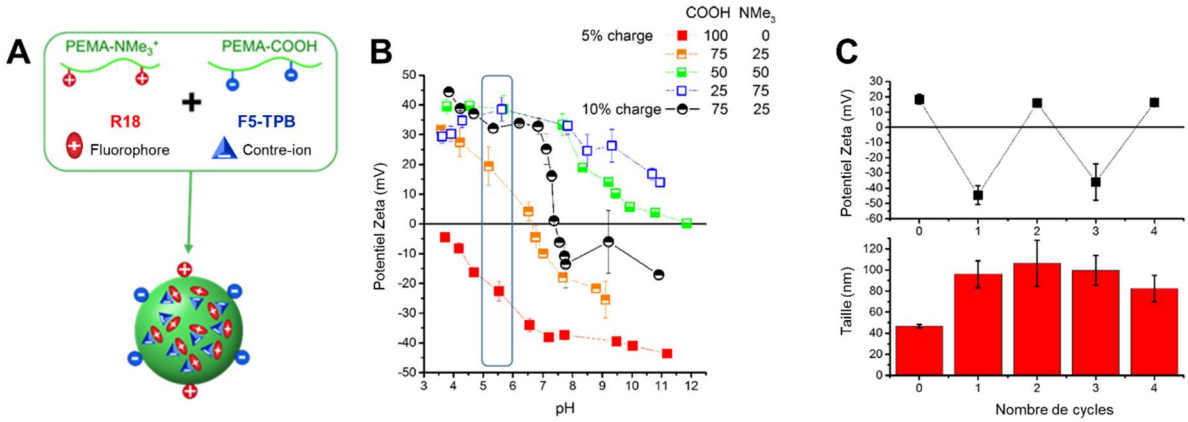

Figure 94: (A) Principe de co-précipitation de polymères de charges opposées. (B) Potentiel zêta des particules formées avec différents ratios de polymères en function du pH. (C) Taille et potentiel zêta des particules formées avec les polymères PEMA-COOH 5% et PEMA-NMe_3^+ 5% dans un ratio 75:25 lors de l'inversion de charges de leur surfaces.

La stabilité de ces particules a également été étudiée en détails dans diverses solutions aqueuses: Un tampon phosphate à pH 7,4 (20 mM), un tampon phosphate salin à pH 7,4 (20 mM) contenant en plus 150 mM de sels et dans des solutions de NaCl à différentes concentrations. Les particules les plus stables étaient celles formées avec les polymères possédant 25% de groupements chargés par chaine. De plus, ces particules ne sont stables que si un type de charge est excédentaire par rapport à l'autre. Dans ces conditions, des particules de petites taille (< 25 nm) sont restées stables dans une solution allant jusqu'à une concentration de 1M de NaCl.

4 Conclusion

A travers cette thèse, l'influence de la chimie des polymères sur la formation et les propriétés des particules obtenues par nanoprécipitation a été étudiée en détails. La cinétique de précipitation des nanoparticules, au cœur du mécanisme de leur formation, a été observée pour différents polymères. Ces résultats mettent en évidence la rapidité extrême de la précipitation des chaînes de polymères ainsi que l'influence de leur chimie sur ce processus. De plus, l'architecture des polymères a été étudiée et un modèle basé

sur le mécanisme de formation des particules a permis de rationaliser les résultats obtenus avec ces polymères. La notion de limite de solubilité des polymères a notamment été introduite et a permis d'homogénéiser les tendances obtenues entre des polymères de natures très différentes. Enfin, un nouveau type de nanoparticules a été mis au point avec une surface comprenant deux types de charges et un potentiel zêta ayant un point isoélectrique. Ces caractéristiques confèrent une grande stabilité aux particules et ouvrent le chemin vers la formation de protéines artificielles. Ensemble, ces résultats montrent la richesse des possibilités offertes par la chimie des polymères et par le contrôle cinétique de leur assemblage dans le design de nanomatériaux.

References

[1] L. Zhang, F. Gu, J. Chan, A. Wang, R. Langer, O. Farokhzad, *Clin. Pharmacol. Ther.* **2008**, *83*, 761–769.

[2] J. K. Patra, G. Das, L. F. Fraceto, E. V. R. Campos, M. del P. Rodriguez-Torres, L. S. Acosta-Torres, L. A. Diaz-Torres, R. Grillo, M. K. Swamy, S. Sharma, S. Habtemariam, H.-S. Shin, *J. Nanobiotechnology* **2018**, *16*, 71.

[3] S. Soares, J. Sousa, A. Pais, C. Vitorino, *Front. Chem.* **2018**, *6*, 360.

[4] M. Vert, Y. Doi, K.-H. Hellwich, M. Hess, P. Hodge, P. Kubisa, M. Rinaudo, F. Schué, *Pure Appl. Chem.* **2012**, *84*, 377–410.

[5] B. Begines, T. Ortiz, M. Pérez-Aranda, G. Martínez, M. Merinero, F. Argüelles-Arias, A. Alcudia, *Nanomaterials* **2020**, *10*, 1403.

[6] A. Reisch, A. S. Klymchenko, *Small* **2016**, *12*, 1968–1992.

[7] S. Indoria, V. Singh, M.-F. Hsieh, *Int. J. Pharm.* **2020**, *582*, 119314.

[8] J. W. Hickey, J. L. Santos, J.-M. Williford, H.-Q. Mao, *J. Controlled Release* **2015**, *219*, 536–547.

[9] R. Ridolfo, S. Tavakoli, V. Junnuthula, D. S. Williams, A. Urtti, J. C. M. van Hest, *Biomacromolecules* **2021**, *22*, 126–133.

[10] F. Esmaeili, M. H. Ghahremani, B. Esmaeili, M. R. Khoshayand, F. Atyabi, R. Dinarvand, *Int. J. Pharm.* **2008**, *349*, 249–255.

[11] M. Elsabahy, K. L. Wooley, *Chem. Soc. Rev.* **2012**, *41*, 2545.

[12] J. P. Rao, K. E. Geckeler, *Prog. Polym. Sci.* **2011**, *36*, 887–913.

[13] V. Rosiuk, A. Runser, A. Klymchenko, A. Reisch, *Langmuir* **2019**, *35*, 7009–7017.

[14] S. M. D'Addio, W. Saad, S. M. Ansell, J. J. Squiers, D. H. Adamson, M. Herrera-Alonso, A. R. Wohl, T. R. Hoye, C. W. Macosko, L. D. Mayer, C. Vauthier, R. K. Prud'homme, *J. Controlled Release* **2012**, *162*, 208–217.

[15] M. R. N. Lima, D. I. Devore, J. Kohn, *J. Colloid Interface Sci.* **2022**, *623*, 247–256.

[16] D. G. Rudmann, *Toxicol. Pathol.* **2013**, *41*, 310–314.

[17] I. H. Plenderleith, *Can. Fam. Physician Med. Fam. Can.* **1990**, *36*, 1827–1830.

[18] P. F. Peddi, S. Peddi, E. S. Santos, D. Morgensztern, *Expert Rev. Anticancer Ther.* **2014**, *14*, 857–863.

[19] F. E. Stuurman, B. Nuijen, J. H. Beijnen, J. H. M. Schellens, *Clin. Pharmacokinet.* **2013**, *52*, 399–414.

[20] P. Fasinu, V. Pillay, V. M. K. Ndesendo, L. C. du Toit, Y. E. Choonara, *Biopharm. Drug Dispos.* **2011**, *32*, 185–209.

[21] H. Wang, J. Yu, X. Lu, X. He, *Nanomed.* **2016**, *11*, 103–106.

[22] P. P. Desai, A. A. Date, V. B. Patravale, *Drug Discov. Today Technol.* **2012**, *9*, e87–e95.

[23] E.-K. Lim, T. Kim, S. Paik, S. Haam, Y.-M. Huh, K. Lee, *Chem. Rev.* **2015**, *115*, 327–394.

[24] Y. Liu, G. Yang, T. Baby, Tengjisi, D. Chen, D. A. Weitz, C. Zhao, *Angew. Chem. Int. Ed.* **2020**, *59*, 4720–4728.

[25] J. Hu, J. He, M. Zhang, P. Ni, *Polym. Chem.* **2015**, *6*, 1553–1566.

[26] Q. Hu, P. S. Katti, Z. Gu, *Nanoscale* **2014**, *6*, 12273–12286.
[27] F. Gu, L. Zhang, B. A. Teply, N. Mann, A. Wang, A. F. Radovic-Moreno, R. Langer, O. C. Farokhzad, *Proc. Natl. Acad. Sci.* **2008**, *105*, 2586–2591.
[28] G. Yan, A. Li, A. Zhang, Y. Sun, J. Liu, *Nanomaterials* **2018**, *8*, 85.
[29] J. Yao, M. Yang, Y. Duan, *Chem. Rev.* **2014**, *114*, 6130–6178.
[30] J. T. Alander, I. Kaartinen, A. Laakso, T. Pätilä, T. Spillmann, V. V. Tuchin, M. Venermo, P. Välisuo, *Int. J. Biomed. Imaging* **2012**, *2012*, 1–26.
[31] W. Schlegel, *Radiat. Prot. Dosimetry* **2010**, *139*, 321–326.
[32] J. Wang, G. Zhang, Q. Li, H. Jiang, C. Liu, C. Amatore, X. Wang, *Sci. Rep.* **2013**, *3*, 1157.
[33] A. Kusumi, T. A. Tsunoyama, K. M. Hirosawa, R. S. Kasai, T. K. Fujiwara, *Nat. Chem. Biol.* **2014**, *10*, 524–532.
[34] B. N. G. Giepmans, S. R. Adams, M. H. Ellisman, R. Y. Tsien, *Science* **2006**, *312*, 217–224.
[35] J. Zhang, R. E. Campbell, A. Y. Ting, R. Y. Tsien, *Nat. Rev. Mol. Cell Biol.* **2002**, *3*, 906–918.
[36] K. A. Kelly, M. A. Hollingsworth, R. E. Brand, C. H. Liu, V. K. Singh, S. Srivastava, A. D. Wasan, D. Yadav, D. K. Andersen, *Pancreas* **2015**, *44*, 1185–1194.
[37] S. Sim, N. Wong, *Biomed. Rep.* **2021**, *14*, 42.
[38] R. Hardman, *Environ. Health Perspect.* **2006**, *114*, 165–172.
[39] R. Alford, H. M. Simpson, J. Duberman, G. C. Hill, M. Ogawa, C. Regino, H. Kobayashi, P. L. Choyke, *Mol. Imaging* **2009**, *8*, 7290.2009.00031.
[40] B. C. Heng, G. K. Das, X. Zhao, L.-L. Ma, T. T.-Y. Tan, K. W. Ng, J. S.-C. Loo, *Biointerphases* **2010**, *5*, FA88–FA97.
[41] M. Riehl, M. Harms, B. Göttel, H. Kubas, D. Schiroky, K. Mäder, *Eur. J. Pharm. Sci.* **2019**, *132*, 27–33.
[42] J. Maillard, K. Klehs, C. Rumble, E. Vauthey, M. Heilemann, A. Fürstenberg, *Chem. Sci.* **2021**, *12*, 1352–1362.
[43] J. Kalra, V. Krishna, B. S. V. Reddy, A. Dhar, V. V. K. Venuganti, A. Bhat, in *Nanoparticles Anal. Med. Devices*, Elsevier, **2021**, pp. 175–210.
[44] J. Kim, N. Lee, T. Hyeon, *Philos. Trans. R. Soc. Math. Phys. Eng. Sci.* **2017**, *375*, 20170022.
[45] S. Chen, H. Miao, X. Jiang, P. Sun, Q. Fan, W. Huang, *Biomaterials* **2021**, *275*, 120916.
[46] I. Khalin, C. Severi, D. Heimburger, A. Wehn, F. Hellal, A. Reisch, A. S. Klymchenko, N. Plesnila, *Dynamic Tracing Using Ultra-Bright Labelling and Multi-Photon Microscopy Identifies Endothelial Uptake of Poloxamer 188 Coated Poly(Lactic-Co-Glycolic Acid) Nano-Carriers* in Vivo, Bioengineering, **2020**.
[47] R. Ferrari, M. Lupi, F. Falcetta, P. Bigini, K. Paolella, F. Fiordaliso, C. Bisighini, M. Salmona, M. D'Incalci, M. Morbidelli, D. Moscatelli, P. Ubezio, *Nanotechnology* **2014**, *25*, 045102.
[48] S. Bhargava, J. J. H. Chu, S. Valiyaveettil, *ACS Omega* **2018**, *3*, 7663–7672.
[49] K. Li, Y. Jiang, D. Ding, X. Zhang, Y. Liu, J. Hua, S.-S. Feng, B. Liu, *Chem. Commun.* **2011**, *47*, 7323.

[50] H. Zhang, Y. Sun, T. Zhou, Q. Yu, Z. Yang, Z. Cai, H. Cang, *Int. J. Polym. Mater. Polym. Biomater.* **2019**, *68*, 1079–1088.
[51] E. Zhang, V. Zhukova, A. Semyonkin, N. Osipova, Y. Malinovskaya, O. Maksimenko, V. Chernikov, M. Sokolov, L. Grigartzik, B. A. Sabel, S. Gelperina, P. Henrich-Noack, *Eur. J. Pharm. Biopharm.* **2020**, *150*, 131–142.
[52] A. Reisch, D. Heimburger, P. Ernst, A. Runser, P. Didier, D. Dujardin, A. S. Klymchenko, *Adv. Funct. Mater.* **2018**, *28*, 1805157.
[53] V. N. Kilin, H. Anton, N. Anton, E. Steed, J. Vermot, T. F. Vandamme, Y. Mely, A. S. Klymchenko, *Biomaterials* **2014**, *35*, 4950–4957.
[54] P. A. Lovell, F. J. Schork, *Biomacromolecules* **2020**, *21*, 4396–4441.
[55] J. M. Asua, *Prog. Polym. Sci.* **2002**, *27*, 1283–1346.
[56] F. M. Pavel, *J. Dispers. Sci. Technol.* **2004**, *25*, 1–16.
[57] A. Guyot, F. Chu, M. Schneider, C. Graillat, T. F. McKenna, *Prog. Polym. Sci.* **2002**, *27*, 1573–1615.
[58] M. D. Tzirakis, R. Zambail, Y. Z. Tan, J. W. Chew, C. Adlhart, A. Honciuc, *RSC Adv.* **2015**, *5*, 103218–103228.
[59] F. D'Agosto, J. Rieger, M. Lansalot, *Angew. Chem. Int. Ed.* **2020**, *59*, 8368–8392.
[60] B. Karagoz, L. Esser, H. T. Duong, J. S. Basuki, C. Boyer, T. P. Davis, *Polym Chem* **2014**, *5*, 350–355.
[61] J. K. Kim, S. Y. Yang, Y. Lee, Y. Kim, *Prog. Polym. Sci.* **2010**, *35*, 1325–1349.
[62] L. Zhang, A. Eisenberg, *J. Am. Chem. Soc.* **1996**, *118*, 3168–3181.
[63] K. M. Pustulka, A. R. Wohl, H. S. Lee, A. R. Michel, J. Han, T. R. Hoye, A. V. McCormick, J. Panyam, C. W. Macosko, *Mol. Pharm.* **2013**, *10*, 4367–4377.
[64] S. M. D'Addio, R. K. Prud'homme, *Adv. Drug Deliv. Rev.* **2011**, *63*, 417–426.
[65] C. J. Martínez Rivas, M. Tarhini, W. Badri, K. Miladi, H. Greige-Gerges, Q. A. Nazari, S. A. Galindo Rodríguez, R. Á. Román, H. Fessi, A. Elaissari, *Int. J. Pharm.* **2017**, *532*, 66–81.
[66] E. Lepeltier, C. Bourgaux, P. Couvreur, *Adv. Drug Deliv. Rev.* **2014**, *71*, 86–97.
[67] R. Botet, *J. Phys. Conf. Ser.* **2012**, *352*, 012047.
[68] X. Yan, J. Bernard, F. Ganachaud, *Adv. Colloid Interface Sci.* **2021**, *294*, 102474.
[69] F. Ganachaud, J. L. Katz, *ChemPhysChem* **2005**, *6*, 209–216.
[70] E. Middha, P. N. Manghnani, D. Z. L. Ng, H. Chen, S. A. Khan, B. Liu, *Mater. Chem. Front.* **2019**, *3*, 1375–1384.
[71] J. Schneider, L. D. Süss, F. Müller-Plathe, *J. Chem. Eng. Data* **2020**, *65*, 1264–1272.
[72] J. C. Cheng, R. D. Vigil, R. O. Fox, *J. Colloid Interface Sci.* **2010**, *351*, 330–342.
[73] Y. Liu, G. Yang, D. Zou, Y. Hui, K. Nigam, A. P. J. Middelberg, C.-X. Zhao, *Ind. Eng. Chem. Res.* **2020**, *59*, 4134–4149.
[74] T. Nicolai, O. Colombani, C. Chassenieux, *Soft Matter* **2010**, *6*, 3111.
[75] B. K. Johnson, R. K. Prud'homme, *Phys. Rev. Lett.* **2003**, *91*, 118302.
[76] J. W. Mullin, in *Ullmanns Encycl. Ind. Chem.*, American Cancer Society, **2003**.
[77] W. S. Saad, R. K. Prud'homme, *Nano Today* **2016**, *11*, 212–227.
[78] C. E. Mora-Huertas, H. Fessi, A. Elaissari, *Adv. Colloid Interface Sci.* **2011**, *163*, 90–122.
[79] D. Horn, J. Rieger, *Angew. Chem. Int. Ed.* **2001**, *40*, 4330–4361.

[80] F. Lince, D. L. Marchisio, A. A. Barresi, *J. Colloid Interface Sci.* **2008**, *322*, 505–515.
[81] A. D. Lavino, N. Di Pasquale, P. Carbone, D. L. Marchisio, *Chem. Eng. Sci.* **2017**, *171*, 485–494.
[82] C. Gauer, Z. Jia, H. Wu, M. Morbidelli, *Langmuir* **2009**, *25*, 9703–9713.
[83] E. E. Dormidontova, *Macromolecules* **1999**, *32*, 7630–7644.
[84] A. Nikoubashman, V. E. Lee, C. Sosa, R. K. Prud'homme, R. D. Priestley, A. Z. Panagiotopoulos, *ACS Nano* **2016**, *10*, 1425–1433.
[85] N. Li, A. Nikoubashman, A. Z. Panagiotopoulos, *J. Chem. Phys.* **2018**, *149*, 084904.
[86] H. S. Choi, W. Liu, P. Misra, E. Tanaka, J. P. Zimmer, B. I. Ipe, M. G. Bawendi, J. V. Frangioni, *Nat. Biotechnol.* **2007**, *25*, 1165–1170.
[87] L. Shang, K. Nienhaus, G. U. Nienhaus, *J. Nanobiotechnology* **2014**, *12*, 5.
[88] T. Kopac, *Int. J. Biol. Macromol.* **2021**, *169*, 290–301.
[89] G. Kumar, N. Shafiq, S. Malhotra, *Crit. Rev. Ther. Drug Carrier Syst.* **2012**, *29*, 149–182.
[90] A. Reisch, A. Runser, Y. Arntz, Y. Mély, A. S. Klymchenko, *ACS Nano* **2015**, *9*, 5104–5116.
[91] J. Aubry, F. Ganachaud, J.-P. Cohen Addad, B. Cabane, *Langmuir* **2009**, *25*, 1970–1979.
[92] S. Galindo-Rodriguez, E. Allemann, H. Fessi, E. Doelker, *Pharm. Res.* **2004**, *21*, 1428–1439.
[93] G. Bovone, L. Cousin, F. Steiner, M. W. Tibbitt, *Macromolecules* **2022**, *55*, 8040–8048.
[94] S. Ding, N. Anton, T. F. Vandamme, C. A. Serra, *Expert Opin. Drug Deliv.* **2016**, *13*, 1447–1460.
[95] H. Fessi, F. Puisieux, J. Ph. Devissaguet, N. Ammoury, S. Benita, *Int. J. Pharm.* **1989**, *55*, R1–R4.
[96] R. Karnik, F. Gu, P. Basto, C. Cannizzaro, L. Dean, W. Kyei-Manu, R. Langer, O. C. Farokhzad, *Nano Lett.* **2008**, *8*, 2906–2912.
[97] C. E. Markwalter, R. K. Prud'homme, *J. Pharm. Sci.* **2018**, *107*, 2465–2471.
[98] H. Chen, A. E. Celik, A. Mutschler, A. Combes, A. Runser, A. S. Klymchenko, S. Lecommandoux, C. A. Serra, A. Reisch, *Langmuir* **2022**, *38*, 7945–7955.
[99] L. M. Liz-Marzán, M. A. Correa-Duarte, I. Pastoriza-Santos, P. Mulvaney, T. Ung, M. Giersig, N. A. Kotov, in *Handb. Surf. Interfaces Mater.*, Elsevier, **2001**, pp. 189–237.
[100] R. Evans, D. H. Napper, *Kolloid-Z. Z. Für Polym.* **1973**, *251*, 409–414.
[101] C. Cruje, D. B. Chithrani, *Rev. Nanosci. Nanotechnol.* **2014**, *3*, 20–30.
[102] I. Oral, L. Grossmann, E. Fedorenko, J. Struck, V. Abetz, *Polymers* **2021**, *13*, 3675.
[103] F. Zhang, L. Cao, W. Yang, *Macromol. Chem. Phys.* **2010**, *211*, 744–751.
[104] J. H. Adair, E. Suvaci, J. Sindel, in *Encycl. Mater. Sci. Technol.*, Elsevier, **2001**, pp. 1–10.
[105] T. Tadros, in *Colloid Interface Sci. Pharm. Res. Dev.*, Elsevier, **2014**, pp. 29–54.
[106] F. Matter, A. L. Luna, M. Niederberger, *Nano Today* **2020**, *30*, 100827.
[107] Y. Gao, M. R. Chowdhury, J.-T. Liang, P. Dhar, *J. Appl. Polym. Sci.* **2015**, *132*, n/a-n/a.

[108] J. G. J. L. Lebouille, R. Stepanyan, J. J. M. Slot, M. A. Cohen Stuart, R. Tuinier, *Colloids Surf. Physicochem. Eng. Asp.* **2014**, *460*, 225–235.
[109] C. Zhao, S. Melis, E. P. Hughes, T. Li, X. Zhang, P. D. Olmsted, E. Van Keuren, *Langmuir* **2020**, *36*, 13210–13217.
[110] R. H. Ansary, M. B. Awang, M. M. Rahman, *Trop. J. Pharm. Res.* **2014**, *13*, 1179.
[111] M. L. T. Zweers, G. H. M. Engbers, D. W. Grijpma, J. Feijen, *J. Controlled Release* **2004**, *100*, 347–356.
[112] Á. Ábrahám, G. Gyulai, T. Tóth, B. Szvoboda, J. Mihály, Á. Szabó, É. Kiss, *Express Polym. Lett.* **2022**, *16*, 960–977.
[113] Z. Zhu, *Biomaterials* **2013**, *34*, 10238–10248.
[114] K. Rahme, L. Chen, R. G. Hobbs, M. A. Morris, C. O'Driscoll, J. D. Holmes, *RSC Adv* **2013**, *3*, 6085–6094.
[115] T. Smart, H. Lomas, M. Massignani, M. V. Flores-Merino, L. R. Perez, G. Battaglia, *Nano Today* **2008**, *3*, 38–46.
[116] T. Zinn, L. Willner, R. Lund, V. Pipich, M.-S. Appavou, D. Richter, *Soft Matter* **2014**, *10*, 5212–5220.
[117] S. C. Owen, D. P. Y. Chan, M. S. Shoichet, *Nano Today* **2012**, *7*, 53–65.
[118] H. K. Makadia, S. J. Siegel, *Polymers* **2011**, *3*, 1377–1397.
[119] E. Vey, C. Rodger, J. Booth, M. Claybourn, A. F. Miller, A. Saiani, *Polym. Degrad. Stab.* **2011**, *96*, 1882–1889.
[120] A. Little, A. M. Wemyss, D. M. Haddleton, B. Tan, Z. Sun, Y. Ji, C. Wan, *Polymers* **2021**, *13*, 2458.
[121] C. Zhang, V. J. Pansare, R. K. Prud'homme, R. D. Priestley, *Soft Matter* **2011**, *8*, 86–93.
[122] K. Roger, M. Eissa, A. Elaissari, B. Cabane, *Langmuir* **2013**, *29*, 11244–11250.
[123] S. Egloff, A. Runser, A. Klymchenko, A. Reisch, *Small Methods* **2021**, *5*, 2000947.
[124] N. Melnychuk, S. Egloff, A. Runser, A. Reisch, A. S. Klymchenko, *Angew. Chem. Int. Ed.* **2020**, *59*, 6811–6818.
[125] G. G. Odian, *Principles of Polymerization*, Wiley-Interscience, Hoboken, N.J, **2004**.
[126] G. Moad, E. Rizzardo, S. H. Thang, *Polymer* **2008**, *49*, 1079–1131.
[127] Y. K. Chong, J. Krstina, T. P. T. Le, G. Moad, A. Postma, E. Rizzardo, S. H. Thang, *Macromolecules* **2003**, *36*, 2256–2272.
[128] T. Berki, A. Bakunts, D. Duret, L. Fabre, C. Ladavière, A. Orsi, M.-T. Charreyre, A. Raimondi, E. van Anken, A. Favier, *ACS Omega* **2019**, *4*, 12841–12847.
[129] H. Nagasawa, N. Aoki, K. Mae, *Chem. Eng. Technol.* **2005**, *28*, 324–330.
[130] K. Fischer, M. Schmidt, *Biomaterials* **2016**, *98*, 79–91.
[131] P. A. Hassan, S. Rana, G. Verma, *Langmuir* **2015**, *31*, 3–12.
[132] M. Kaszuba, J. Corbett, F. M. Watson, A. Jones, *Philos. Trans. R. Soc. Math. Phys. Eng. Sci.* **2010**, *368*, 4439–4451.
[133] J. Rodenburg, *Nature* **2018**, *559*, 334–335.
[134] *Transmission Electron Microscopy*, Springer New York, New York, NY, **2008**.
[135] J. R. Lakowicz, Ed. , in *Princ. Fluoresc. Spectrosc.*, Springer US, Boston, MA, **2006**, pp. 1–26.

[136] B. Valeur, M. N. Berberan-Santos, *Molecular Fluorescence: Principles and Applications*, Wiley, **2012**.
[137] M. J. Sanderson, I. Smith, I. Parker, M. D. Bootman, *Cold Spring Harb. Protoc.* **2014**, *2014*, pdb.top071795.
[138] L. Porrès, A. Holland, L.-O. Pålsson, A. P. Monkman, C. Kemp, A. Beeby, *J. Fluoresc.* **2006**, *16*, 267–273.
[139] C. Würth, M. Grabolle, J. Pauli, M. Spieles, U. Resch-Genger, *Anal. Chem.* **2011**, *83*, 3431–3439.
[140] T. Karstens, K. Kobs, *J. Phys. Chem.* **1980**, *84*, 1871–1872.
[141] F. Würthner, *Chem Commun* **2004**, 1564–1579.
[142] S. Huang, K. Wang, S. Wang, Y. Wang, M. Wang, *Adv. Mater. Interfaces* **2016**, *3*, 1600259.
[143] B. Andreiuk, A. Reisch, E. Bernhardt, A. S. Klymchenko, *Chem. – Asian J.* **2019**, *14*, 836–846.
[144] C. Severi, S. Lahtinen, J. Rosenberg, A. Reisch, T. Soukka, A. S. Klymchenko, *Aggregate* **2022**, *3*, DOI 10.1002/agt2.130.
[145] P. G. Wu, L. Brand, *Anal. Biochem.* **1994**, *218*, 1–13.
[146] J.-M. Commenge, L. Falk, *Chem. Eng. Process. Process Intensif.* **2011**, *50*, 979–990.
[147] B. K. Johnson, R. K. Prud'homme, *Aust. J. Chem.* **2003**, *56*, 1021.
[148] W. S. Saad, R. K. Prud'homme, *Nano Today* **2016**, *11*, 212–227.
[149] J. Bresseleers, M. Bagheri, C. Lebleu, S. Lecommandoux, O. Sandre, I. A. B. Pijpers, A. F. Mason, S. Meeuwissen, C. F. van Nostrum, W. E. Hennink, J. C. M. van Hest, *Polymers* **2020**, *12*, 2572.
[150] A. Reisch, A. Runser, Y. Arntz, Y. Mély, A. S. Klymchenko, *ACS Nano* **2015**, *9*, 5104–5116.
[151] G. Bovone, L. Cousin, F. Steiner, M. W. Tibbitt, *Macromolecules* **2022**, *55*, 8040–8048.
[152] V. Rosiuk, A. Runser, A. Klymchenko, A. Reisch, *Langmuir* **2019**, *35*, 7009–7017.
[153] J. R. Bourne, *Org. Process Res. Dev.* **2003**, *7*, 471–508.
[154] B. K. Johnson, R. K. Prud'homme, *AIChE J.* **2003**, *49*, 2264–2282.
[155] L. Falk, J.-M. Commenge, *Chem. Eng. Sci.* **2010**, *65*, 405–411.
[156] Y. Liu, C. Cheng, Y. Liu, R. K. Prud'homme, R. O. Fox, *Chem. Eng. Sci.* **2008**, *63*, 2829–2842.
[157] A. M. Hyde, S. L. Zultanski, J. H. Waldman, Y.-L. Zhong, M. Shevlin, F. Peng, *Org. Process Res. Dev.* **2017**, *21*, 1355–1370.
[158] A. Reisch, D. Heimburger, P. Ernst, A. Runser, P. Didier, D. Dujardin, A. S. Klymchenko, *Adv. Funct. Mater.* **2018**, *28*, 1805157.
[159] J. C. Cheng, R. D. Vigil, R. O. Fox, *J. Colloid Interface Sci.* **2010**, *351*, 330–342.
[160] R. F. Pagels, J. Edelstein, C. Tang, R. K. Prud'homme, *Nano Lett.* **2018**, *18*, 1139–1144.
[161] A. Nikoubashman, V. E. Lee, C. Sosa, R. K. Prud'homme, R. D. Priestley, A. Z. Panagiotopoulos, *ACS Nano* **2016**, *10*, 1425–1433.

[162] B. L. Sanchez-Gaytan, F. Fay, S. Hak, A. Alaarg, Z. A. Fayad, C. Pérez-Medina, W. J. M. Mulder, Y. Zhao, *Angew. Chem. Int. Ed.* **2017**, *56*, 2923–2926.
[163] C.-Y. Lee, C.-L. Chang, Y.-N. Wang, L.-M. Fu, *Int. J. Mol. Sci.* **2011**, *12*, 3263–3287.
[164] A. Gomez-Hens, D. Perez-Bendito, *Anal. Chim. Acta* **1991**, *242*, 147–177.
[165] I. Grillo, *Curr. Opin. Colloid Interface Sci.* **2009**, *14*, 402–408.
[166] E. Ilhan-Ayisigi, B. Yaldiz, G. Bor, A. Yaghmur, O. Yesil-Celiktas, *Colloids Surf. B Biointerfaces* **2021**, *201*, 111633.
[167] R. Graceffa, R. P. Nobrega, R. A. Barrea, S. V. Kathuria, S. Chakravarthy, O. Bilsel, T. C. Irving, *J. Synchrotron Radiat.* **2013**, *20*, 820–825.
[168] K. N. Toft, B. Vestergaard, S. S. Nielsen, D. Snakenborg, M. G. Jeppesen, J. K. Jacobsen, L. Arleth, J. P. Kutter, *Anal. Chem.* **2008**, *80*, 3648–3654.
[169] S. Luo, S. Liu, J. Xu, H. Liu, Z. Zhu, M. Jiang, C. Wu, *Macromolecules* **2006**, *39*, 4517–4525.
[170] B. Abécassis, F. Testard, O. Spalla, P. Barboux, *Nano Lett.* **2007**, *7*, 1723–1727.
[171] M. Herbst, E. Hofmann, S. Förster, *Langmuir* **2019**, *35*, 11702–11709.
[172] X. Chen, J. Schröder, S. Hauschild, S. Rosenfeldt, M. Dulle, S. Förster, *Langmuir* **2015**, *31*, 11678–11691.
[173] B. L. Sanchez-Gaytan, F. Fay, S. Hak, A. Alaarg, Z. A. Fayad, C. Pérez-Medina, W. J. M. Mulder, Y. Zhao, *Angew. Chem. Int. Ed.* **2017**, *56*, 2923–2926.
[174] S. Bou, A. S. Klymchenko, M. Collot, *Mater. Adv.* **2021**, *2*, 3213–3233.
[175] B. Andreiuk, A. Reisch, M. Lindecker, G. Follain, N. Peyriéras, J. G. Goetz, A. S. Klymchenko, *Small* **2017**, *13*, 1701582.
[176] I. Shulov, S. Oncul, A. Reisch, Y. Arntz, M. Collot, Y. Mely, A. S. Klymchenko, *Nanoscale* **2015**, *7*, 18198–18210.
[177] J. X. Liu, N. Bizmark, D. M. Scott, R. A. Register, M. P. Haataja, S. S. Datta, C. B. Arnold, R. D. Priestley, *JACS Au* **2021**, *1*, 936–944.
[178] Y. Mai, A. Eisenberg, *Chem. Soc. Rev.* **2012**, *41*, 5969.
[179] H. Feng, X. Lu, W. Wang, N.-G. Kang, J. Mays, *Polymers* **2017**, *9*, 494.
[180] S. S. Kulthe, Y. M. Choudhari, N. N. Inamdar, V. Mourya, *Des. Monomers Polym.* **2012**, *15*, 465–521.
[181] N. J. W. Penfold, J. Yeow, C. Boyer, S. P. Armes, *ACS Macro Lett.* **2019**, *8*, 1029–1054.
[182] M. J. Derry, L. A. Fielding, S. P. Armes, *Prog. Polym. Sci.* **2016**, *52*, 1–18.
[183] R. C. Hayward, D. J. Pochan, *Macromolecules* **2010**, *43*, 3577–3584.
[184] R. F. Pagels, J. Edelstein, C. Tang, R. K. Prud'homme, *Nano Lett.* **2018**, *18*, 1139–1144.
[185] M. S. Verma, S. Liu, Y. Y. Chen, A. Meerasa, F. X. Gu, *Nano Res.* **2012**, *5*, 49–61.
[186] T. I. Morozova, V. E. Lee, A. Z. Panagiotopoulos, R. K. Prud'homme, R. D. Priestley, A. Nikoubashman, *Langmuir* **2019**, *35*, 709–717.
[187] J. Brandrup, E. H. Immergut, *Polymer Handbook*, Wiley-Interscience, New York, **1989**.
[188] R. Whitfield, N. P. Truong, D. Messmer, K. Parkatzidis, M. Rolland, A. Anastasaki, *Chem. Sci.* **2019**, *10*, 8724–8734.
[189] D. A. Kangas, R. R. Pelletier, *J. Polym. Sci. [A1]* **1970**, *8*, 3543–3555.

[190] A. Combes, K.-N. Tang, A. S. Klymchenko, A. Reisch, *J. Colloid Interface Sci.* **2022**, *607*, 1786–1795.
[191] B. Andreiuk, A. Reisch, E. Bernhardt, A. S. Klymchenko, *Chem. – Asian J.* **2019**, *14*, 836–846.
[192] N. Li, A. Nikoubashman, A. Z. Panagiotopoulos, *Langmuir* **2019**, *35*, 3780–3789.
[193] K. Roger, B. Cabane, *Angew. Chem. Int. Ed.* **2012**, *51*, 5625–5628.
[194] H. Cabral, K. Miyata, K. Osada, K. Kataoka, *Chem. Rev.* **2018**, *118*, 6844–6892.
[195] K. Kataoka, A. Harada, Y. Nagasaki, *Adv. Drug Deliv. Rev.* **2001**, *47*, 113–131.
[196] C. E. Barnett, *J. Phys. Chem.* **1942**, *46*, 69–75.
[197] A. Kessel, N. Ben-Tal, *Introduction to Proteins*, Chapman And Hall/CRC, **2018**.
[198] B. Ma, T. Elkayam, H. Wolfson, R. Nussinov, *Proc. Natl. Acad. Sci.* **2003**, *100*, 5772–5777.
[199] K. L. Shaw, G. R. Grimsley, G. I. Yakovlev, A. A. Makarov, C. N. Pace, *Protein Sci.* **2001**, *10*, 1206–1215.
[200] H. M. Baker, E. N. Baker, *Biochem. Cell Biol.* **2012**, *90*, 320–328.
[201] X. Liu, H. Li, Y. Chen, Q. Jin, K. Ren, J. Ji, *Adv. Healthc. Mater.* **2014**, *3*, 1439–1447.
[202] M. Zhang, X. Chen, C. Li, X. Shen, *J. Controlled Release* **2020**, *319*, 46–62.
[203] J. Xu, P. X. Medina-Rangel, K. Haupt, B. Tse Sum Bui, in *Methods Enzymol.*, Elsevier, **2017**, pp. 115–141.
[204] J. Xu, F. Merlier, B. Avalle, V. Vieillard, P. Debré, K. Haupt, B. Tse Sum Bui, *ACS Appl. Mater. Interfaces* **2019**, *11*, 9824–9831.
[205] P. Bansal, A. P. Deshpande, M. G. Basavaraj, *J. Colloid Interface Sci.* **2017**, *492*, 92–100.
[206] K. Ita, *Eur. J. Pharm. Sci.* **2020**, *150*, 105358.
[207] I. Insua, *Eur. Polym. J.* **2016**, 18.
[208] P. González-Monje, A. Ayala García, D. Ruiz-Molina, C. Roscini, *J. Colloid Interface Sci.* **2021**, *589*, 500–510.
[209] R. López-Muñoz, M. E. Treviño, G. Morales, J. A. Valdez-Garza, R. Díaz de León, H. Saade, F. J. Enríquez-Medrano, R. G. López, *J. Nanomater.* **2019**, *2019*, 1–9.
[210] R. López-Muñoz, M. E. Treviño, F. Castellanos, G. Morales, O. Rodríguez-Fernández, S. Saavedra, A. Licea-Claverie, H. Saade, F. J. Enríquez-Medrano, R. G. López, *J. Biomater. Sci. Polym. Ed.* **2021**, *32*, 1107–1124.
[211] M. Williams, N. J. W. Penfold, J. R. Lovett, N. J. Warren, C. W. I. Douglas, N. Doroshenko, P. Verstraete, J. Smets, S. P. Armes, *Polym. Chem.* **2016**, *7*, 3864–3873.
[212] M. S. Bannon, A. López Ruiz, K. Corrotea Reyes, M. Marquez, Z. Wallizadeh, M. Savarmand, C. A. LaPres, J. Lahann, K. McEnnis, *Part. Part. Syst. Charact.* **2021**, *38*, 2100016.
[213] H. P. Erickson, *Biol. Proced. Online* **2009**, *11*, 32–51.
[214] I. Berlman, *Energy Transfer Parameters of Aromatic Compounds*, Elsevier Science, Saint Louis, **2014**.
[215] T. I. Morozova, V. E. Lee, A. Z. Panagiotopoulos, R. K. Prud'homme, R. D. Priestley, A. Nikoubashman, *Langmuir* **2019**, *35*, 709–717.
[216] L. Brannon-Peppas, J. O. Blanchette, *Adv. Drug Deliv. Rev.* **2004**, *56*, 1649–1659.

[217] K. Obst, G. Yealland, B. Balzus, E. Miceli, M. Dimde, C. Weise, M. Eravci, R. Bodmeier, R. Haag, M. Calderón, N. Charbaji, S. Hedtrich, *Biomacromolecules* **2017**, *18*, 1762–1771.
[218] A. Reisch, P. Didier, L. Richert, S. Oncul, Y. Arntz, Y. Mély, A. S. Klymchenko, *Nat. Commun.* **2014**, *5*, 4089.
[219] G. T. Kozma, T. Shimizu, T. Ishida, J. Szebeni, *Adv. Drug Deliv. Rev.* **2020**, *154–155*, 163–175.
[220] L. Hong, Z. Wang, X. Wei, J. Shi, C. Li, *J. Pharmacol. Toxicol. Methods* **2020**, *102*, 106678.
[221] B. Cabanillas, N. Novak, *Allergol. Int.* **2021**, *70*, 313–318.
[222] Z. Sun, B. Wu, Y. Ren, Z. Wang, C. Zhao, M. Hai, D. A. Weitz, D. Chen, *ChemPlusChem* **2021**, *86*, 49–58.
[223] X. Yan, J. Bernard, F. Ganachaud, *Adv. Colloid Interface Sci.* **2021**, *294*, 102474.
[224] S. M. D'Addio, R. K. Prud'homme, *Adv. Drug Deliv. Rev.* **2011**, *63*, 417–426.
[225] A. Nikoubashman, V. E. Lee, C. Sosa, R. K. Prud'homme, R. D. Priestley, A. Z. Panagiotopoulos, *ACS Nano* **2016**, *10*, 1425–1433.
[226] R. M. Clegg, in *Lab. Tech. Biochem. Mol. Biol.*, Elsevier, **2009**, pp. 1–57.
[227] A. Duro-Castano, M. Talelli, G. Rodríguez-Escalona, M. J. Vicent, in *Smart Polym. Their Appl.*, Elsevier, **2019**, pp. 439–479.

Annexes

1 List of presentations

Poster: « Controlling size and fluorescence of dye-loaded polymer nanoparticles through polymer design », Vitalii Rosiuk, Anne Runser, Antoine Combes, Yuliia Koval, Denis Dujardin, Andrey S. Klymchenko, Andreas Reisch.
48ème Colloque international du groupe français d'études et d'applications des polymères (GFP), Mulhouse, du 25 au 29 Novembre 2019.

Communication orale: « Influence of polymer architecture on fluorescent nanoparticle properties », Antoine Combes, Andrey S. Klymchenko, Andreas Reisch.
49ème Journées d'Etudes des Polymères (JEPO2021), Ile de Porquerolles, du 3 au 8 octobre 2021.

Poster: « Protein-like particles through nanoprecipitation of mixtures of polymers of opposite charge », Antoine Combes, Khanh-Nam Tang, Andrey S. Klymchenko, Andreas Reisch.
Microscopy For Biology (MiFoBio), Presqu'île de Giens, du 5 au 12 Novembre 2021.

Communication orale: « Protein-like particles through nanoprecipitation of mixtures of polymers of opposite charge », Antoine Combes, Khanh-Nam Tang, Andrey S. Klymchenko, Andreas Reisch.
Les journées du campus d'Illkirch, faculté de pharmacie Illkirch-Graffenstaden, 23 Mai 2022.

Communication orale: « Protein-like particles through nanoprecipitation of mixtures of polymers of opposite charge », Antoine Combes, Khanh-Nam Tang, Andrey S. Klymchenko, Andreas Reisch.
Nano in Bio, Le Gosier, du 30 mai au 5 Juin 2022.

Communication orale: « How to control formation of polymer nanoparticles through polymer chemistry », Antoine Combes, Andrey S. Klymchenko, Andreas Reisch.
"Mise au Vert 2022", Inserm UMR_S 1121 / 3Bio / Spartha Medical Seminar, Mittelwihr, le 8 et 9 Novembre 2022.

2 List of publications

« Protein-like particles through nanoprecipitation of mixtures of polymers of opposite charge », Antoine Combes, Khanh-Nam Tang, Andrey S. Klymchenko, Andreas Reisch.
Journal of Colloid and Interface Science, (2022), 607, 1786-1795.
https://doi.org/10.1016/j.jcis.2021.09.080

« Assembly of Fluorescent Polymer Nanoparticles Using Different Microfluidic Mixers », Huaiyou Chen, Ali Emre Celik, Angela Mutschler, Antoine Combes, Anne Runser, Andrey S. Klymchenko, Sébastien Lecommandoux, Christophe A. Serra, Andreas Reisch
Langmuir, (2022), 38, 26, 7945-7955.
https://doi.org/10.1021/acs.langmuir.2c00534

« Enhancing Near Infrared II Emission of Gold Nanoclusters via Encapsulation in Small Polymer Nanoparticles », Lucie Haye, P. Iyanu Diriwari, Abdallah Alhalabi, Thibault Gallavardin, Antoine Combes, Andrey S. Klymchenko, Niko Hildebrandt, Xavier Le Guével, Andreas Reisch.
Advanced Optical Materials, (2022) ; 2201475
https://doi.org/10.1002/adom.202201474

3 Protocols

The ^{1}H NMR chemical shifts are reported relative to residual solvent signals. Data are presented as follows: chemical shift (ppm), multiplicity (s = singlet, d = doublet, t = triplet, q = quartet, dd = doublet of doublets, m = multiplet), coupling constant J (Hz) and integration. Integration signals were rounded to the number of corresponding protons except when they allowed to calculate the ratio of monomers in the polymer chains.

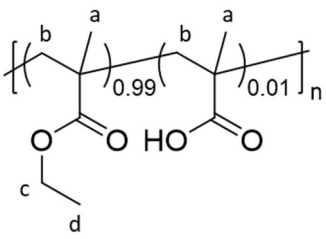

PEMA-MAA 99-1: Monomers were dissolved in DMSO at a concentration of 2M. 19.8 mL of EMA (39.6 mmol, 99 eq) and 0.2 mL of MAA (0.4 mmol, 1 eq) solutions were placed in a 50 mL round bottom flask. 1.68 mL of AIBN at 40 mg.mL^{-1} (0.41 mmol, 1 eq) were added and the mixture was flushed with argon during 5 min. It was then heated at 70 °C under inert atmosphere for 30 min and an aliquot was taken and analyzed using ^{1}H NMR spectroscopy. The ratio between the intensities of the O-CH_2- signals from the monomer and the polymer showed 20% of conversion. The mixture was then precipitated in 150 mL of MeOH/Water 9:1 mixture. The polymer was collected after centrifugation and redissolved in ACN before a second precipitation in 100 mL of methanol. The obtained polymer was dried under vacuum to give 852 mg of white solid (overall yield 14%). ^{1}H NMR (400 MHz, $CDCl_3$) δ (ppm): 4.03 (m, 2H), 1.91-1.82 (m, 2H), 1.24 (m, 3H), 1.03-0.88 (m, 3H).

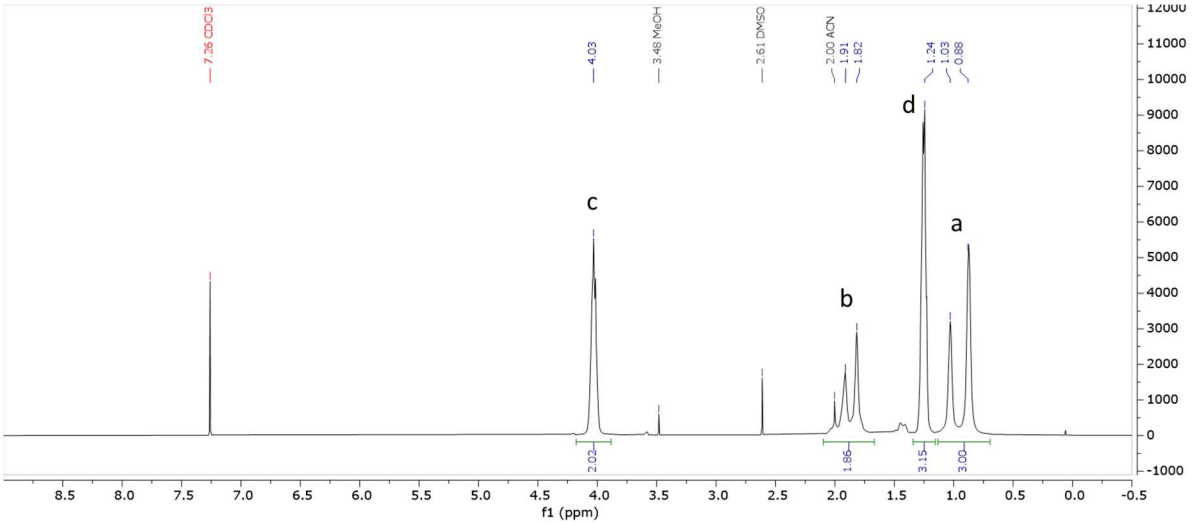

Figure 95: ^{1}H NMR spectrum of PEMA-MAA 99-1.

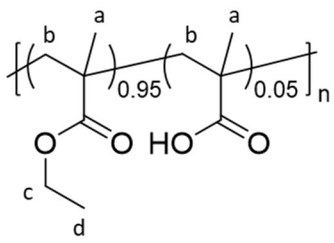

PEMA-MAA 95-5: Monomers were dissolved in DMSO at a concentration of 2M. 19mL of EMA (38 mmol, 95 eq) and 1 mL of MAA (2 mmol, 5 eq) solutions were placed in a 50 mL round bottom flask. 1.68 mL of AIBN at 40 $mg.mL^{-1}$ (0.41 mmol, 1 eq) were added and the mixture was flushed with argon during 5 min. It was then heated at 70 °C under inert atmosphere for 30 min and an aliquot was taken and analyzed using ^1H NMR spectroscopy. The ratio between the intensities of the O-CH_2- signals from the monomer and the polymer showed 37% of conversion. The mixture was then precipitated in 150 mL of MeOH/Water 9:1 mixture. The polymer was collected after centrifugation and redissolved in ACN before a second precipitation in 100 mL of methanol. The obtained polymer was dried under vacuum to give 1.15 g of white solid (overall yield 25%). ^1H NMR (400 MHz, $CDCl_3$) δ (ppm): 4.04 (m, 2H), 1.91-1.82 (m, 2H), 1.25 (m, 3H), 1.03-0.88 (m, 3H). Molecular weight determined by SEC: M_n = 127200 g/mol, PDI = 1.31

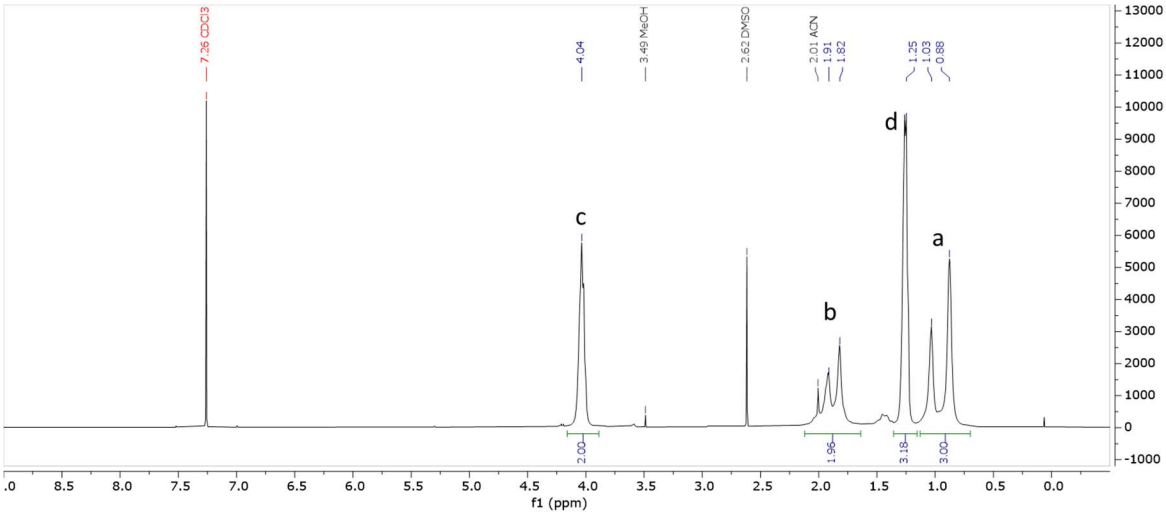

Figure 96: ^1H NMR spectrum of PEMA-MAA 95-5.

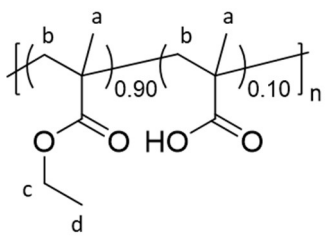

PEMA-MAA 90-10%: Monomers were dissolved in DMSO at a concentration of 2M. 72mL of EMA (144 mmol, 90 eq) and 8 mL of MAA (16 mmol, 10 eq) solutions were placed in a 100 mL round bottom flask. 3.36 mL of AIBN at 40 $mg.mL^{-1}$ (0.8 mmol, 0.5 eq) were added and the mixture was flushed with argon during 5 min. It was then heated at 70 °C under inert atmosphere for 30 min and an aliquot was taken and analyzed using ^1H NMR spectroscopy. The ratio between the intensities of the O-CH_2- signals from the monomer and the polymer showed 10% of conversion. The

mixture was then precipitated in 500 mL of MeOH/Water 9:1 mixture. The polymer was collected after centrifugation and redissolved in ACN before a second precipitation in 200 mL of MeOH/Water 9:1 mixture. The obtained polymer was dried under vacuum to give 1.25 g of white solid (overall yield 7%). ^{1}H NMR (400 MHz, $CDCl_3$) δ (ppm): 4.04 (m, 1.74H), 1.91-1.82 (m, 2H), 1.25 (m, 2.74H), 1.03-0.88 (m, 3H).

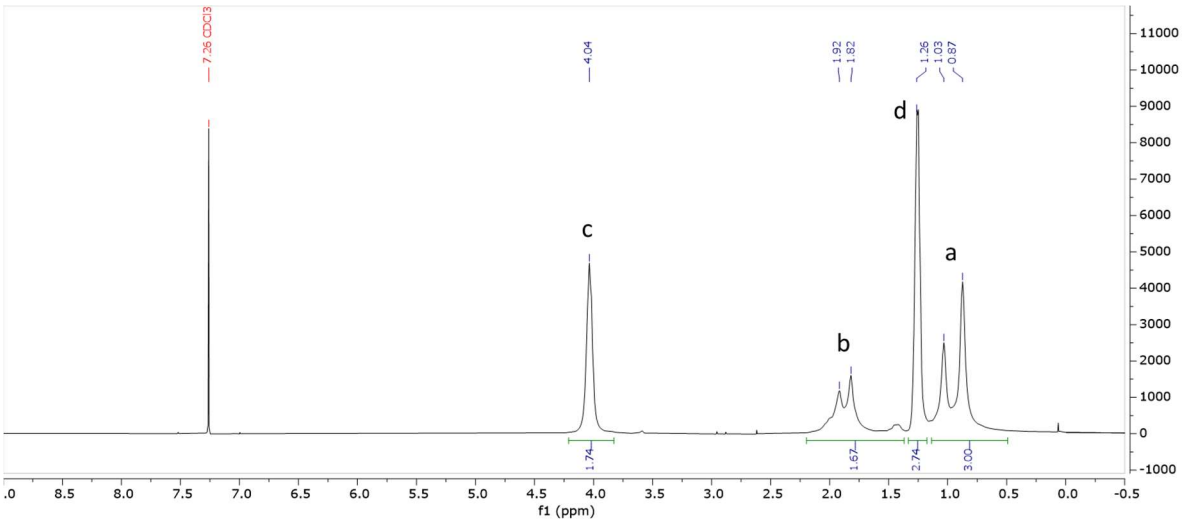

Figure 97: ^{1}H NMR spectrum of PEMA-MAA 90-10.

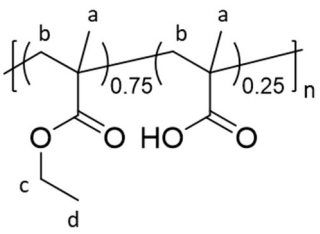

PEMA-MAA 75-25: Monomers were dissolved in DMSO at a concentration of 2M. 60mL of EMA (120 mmol, 75 eq) and 20 mL of MAA (40 mmol, 25 eq) solutions were placed in a 100 mL round bottom flask. 3.36 mL of AIBN at 40 mg.mL^{-1} (0.8 mmol, 0.5 eq) were added and the mixture was flushed with argon during 5 min. It was then heated at 70 °C under inert atmosphere for 30 min and an aliquot was taken and analyzed using ^{1}H NMR spectroscopy. The ratio between the intensities of the O-CH_2- signals from the monomer and the polymer showed 25% of conversion. The mixture was then precipitated in 500 mL of MeOH/Water 1:1 mixture. The polymer was collected after centrifugation and redissolved in ACN before a second precipitation in 200 mL of cold MeOH/Water 6:4 mixture. The obtained polymer was dried under vacuum to give 2.6 g of white solid (overall yield 15%). ^{1}H NMR (400 MHz, $CDCl_3$) δ (ppm): 4.01 (m, 1.51H), 1.91-1.80 (m, 2H), 1.24 (m, 2.43H), 1.00-0.84 (m, 3H).

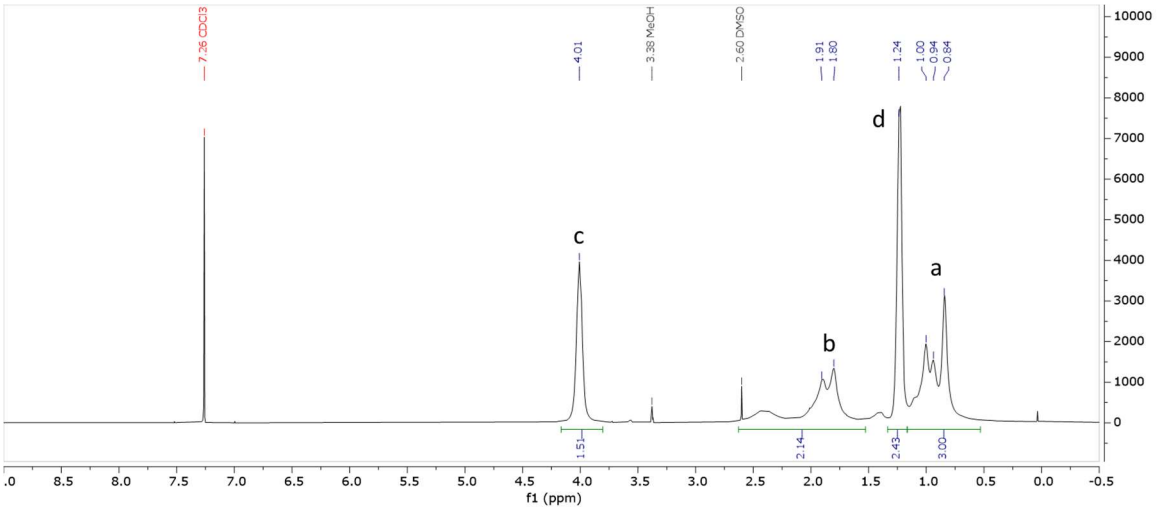

Figure 98: ^{1}H NMR spectrum of PEMA-MAA 75-25.

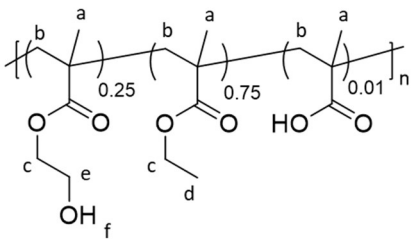

PEMA-HEMA-MAA 75-25-1: Monomers were dissolved in DMSO at a concentration of 2M. 22.35 mL of EMA (44.7 mmol, 75 eq), 7.35 mL of HEMA (14.7 mmol, 25 eq) and 0.3 mL of MAA (0.6 mmol, 1 eq) solutions were placed in a 50 mL round bottom flask. 2.52 mL of AIBN at 40 mg.mL^{-1} (0.6 mmol, 1 eq) were added and the mixture was flushed with argon during 5 min. It was then heated at 70 °C under inert atmosphere for 50 min and an aliquot was taken and analyzed using ^{1}H NMR spectroscopy. The ratio between the intensities of the O-CH_2- signals from the monomer and the polymer showed 52% of conversion. The mixture was then precipitated in 200 mL of cold MeOH/Water 75:25 mixture. The polymer was collected after centrifugation and redissolved in ACN before a second precipitation in identical medium. The obtained polymer was dried under vacuum to give 2.87 g of white solid (overall yield 40%). ^{1}H NMR (400 MHz, $CDCl_3$) δ (ppm): 4.07 (m, 2H), 3.84 (m, 0.51H), 1.91-1.82 (m, 2H), 1.25 (m, 2.56H), 1.04-0.88 (m, 3H).

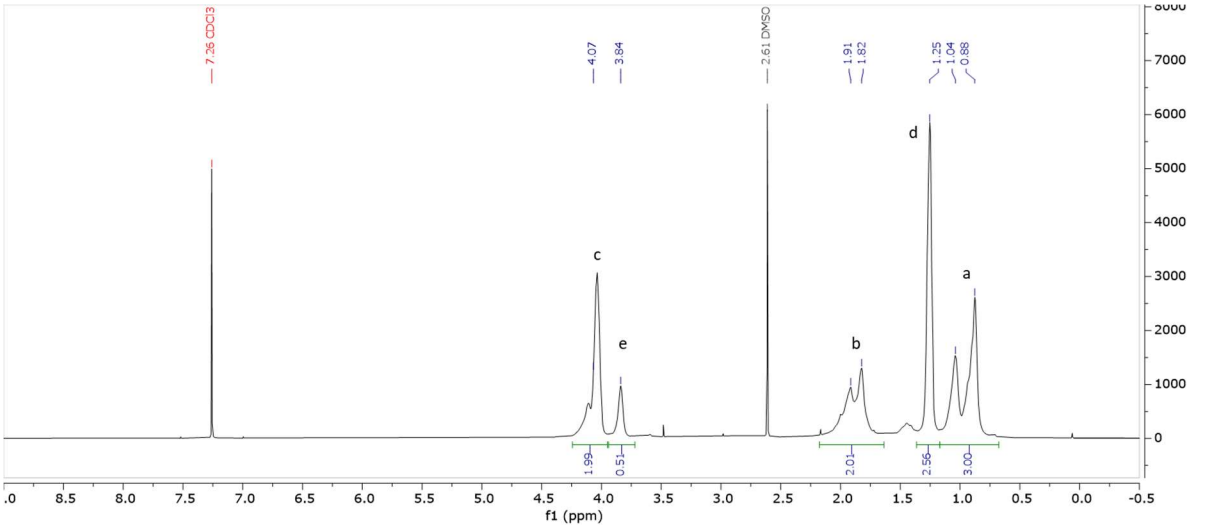

Figure 99: ^{1}H NMR spectrum of PEMA-HEMA-MAA 75-25-1.

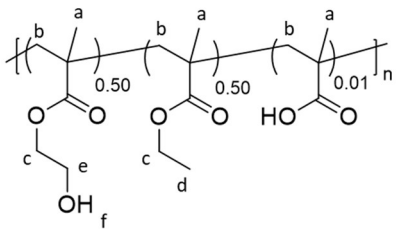

PEMA-HEMA-MAA 50-50-1: Monomers were dissolved in DMSO at a concentration of 2M. 14.85 mL of EMA (29.7 mmol, 50 eq), 7.35 mL of HEMA (29.7 mmol, 50 eq) and 0.3 mL of MAA (0.6 mmol, 1 eq) solutions were placed in a 50 mL round bottom flask. 2.52 mL of AIBN at 40 mg.mL^{-1} (0.6 mmol, 1 eq) were added and the mixture was flushed with argon during 5 min. It was then heated at 70 °C under inert atmosphere for 50 min and an aliquot was taken and analyzed using ^{1}H NMR spectroscopy. The ratio between the intensities of the O-CH_2- signals from the monomer and the polymer showed 58% of conversion. The mixture was then precipitated in 200 mL of cold MeOH/Water 6:4 mixture. The polymer was collected after centrifugation and redissolved in ACN before a second precipitation in identical medium. The obtained polymer was dried under vacuum to give 1.34 g of white solid (overall yield 18%). ^{1}H NMR (400 MHz, Acetone d_6) δ (ppm): 4.06 (m, 2H), 3.80 (m, 1.08H), 1.96-1.88 (m, 2H), 1.28 (m, 1.7H), 1.09-0.93 (m, 3H).

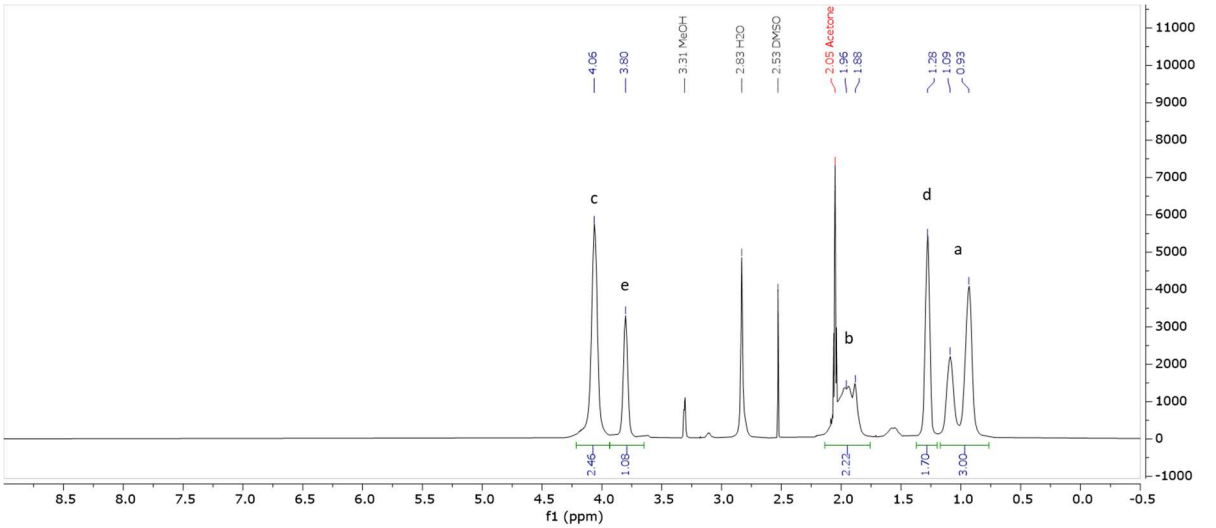

Figure 100: ^{1}H NMR spectrum of PEMA-HEMA-MAA 50-50-1.

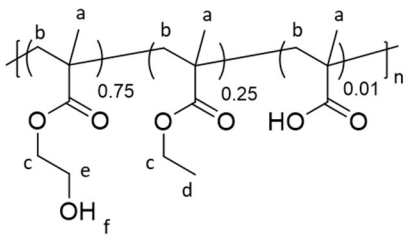

PEMA-HEMA-MAA 25-75-1: Monomers were dissolved in DMSO at a concentration of 2M. 7.5 mL of EMA (15 mmol, 25 eq), 22.5 mL of HEMA (45 mmol, 75 eq) and 0.6 mL of MAA (1.2 mmol, 1 eq) solutions were placed in a 50 mL round bottom flask. 1.2 mL of AIBN at 40 mg.mL^{-1} (0.3 mmol, 0.5 eq) were added and the mixture was flushed with argon during 5 min. It was then heated at 70 °C under inert atmosphere for 30 min and an aliquot was taken and analyzed using ^{1}H NMR spectroscopy. The ratio between the intensities of the O-CH_2-signals from the monomer and the polymer showed 37% of conversion. The mixture was then precipitated in 200 mL of cold MeOH/Water 3:7 mixture. The polymer was collected after centrifugation and redissolved in ACN/MeOH 7-3 mixture before a second precipitation in identical medium. The polymer was containing high amount of water even after drying so it was redissolved in an acetone/isopropanol mix and solvent were evaporated again, resulting in a reduced amount of water. The obtained polymer was dried under vacuum to give 1.9 g of white solid (overall yield 25%). ^{1}H NMR (400 MHz, DMSO d_6) δ (ppm): 4.81 (m, 0.8H), 3.97-3.91 (m, 2H), 3.59 (s, 1.64H), 1.79 (m, 2H), 1.19 (m, 0.97H), 0.95-0.78 (m, 3H).

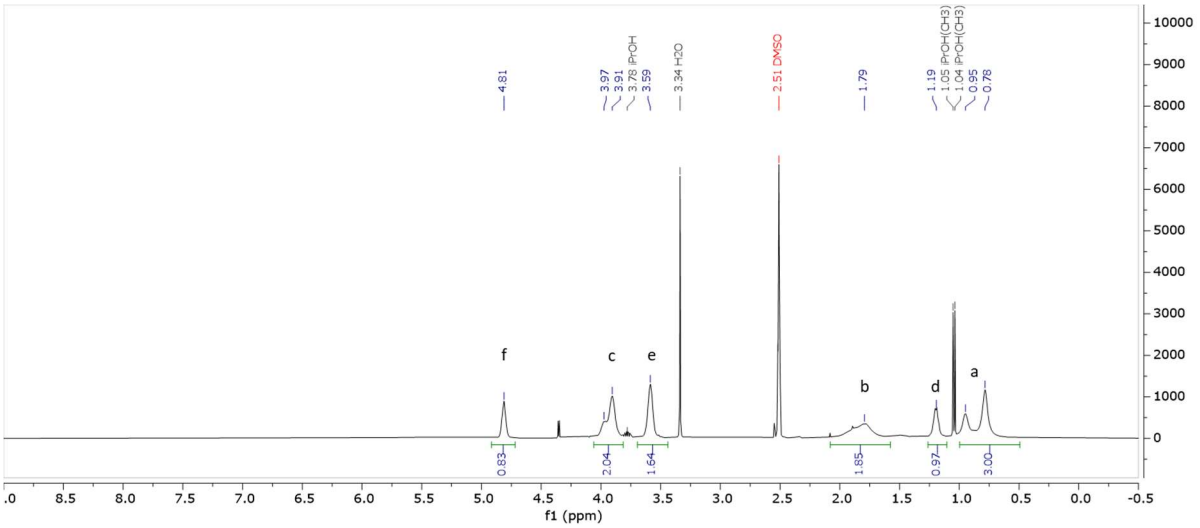

Figure 101: ^{1}H NMR spectrum of PEMA-HEMA-MAA 25-75-1.

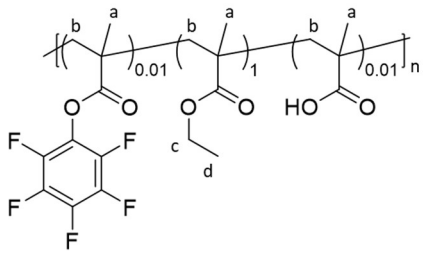

PEMA-MAA-PF5 100-1-1: Monomers were dissolved in DMSO at a concentration of 2M. 33.2 mL of EMA (66.5 mmol, 100 eq), 0.325 mL of PF5 (0.7 mmol, 1 eq) and 0.325 mL of MAA (0.7 mmol, 1 eq) solutions were placed in a 50 mL round bottom flask. 2.7 mL of AIBN at 40 mg.mL^{-1} (0.7 mmol, 1 eq) were added and the mixture was flushed with argon during 5 min. It was then heated at 70 °C under inert atmosphere for 35 min and an aliquot was taken and analyzed using ^{1}H NMR spectroscopy. The ratio between the intensities of the O-CH$_2$- signals from the monomer and the polymer showed 25% of conversion. The mixture was then precipitated in 150 mL of cold MeOH. The polymer was collected after centrifugation and redissolved in ACN before a second precipitation in 100 mL of MeOH/Water 7:3 mixture. The obtained polymer was dried under vacuum to give 1.39 g of white solid (overall yield 18%). NMR was performed with TFE as standard. ^{1}H NMR (400 MHz, Acetone d$_6$) δ (ppm): 4.07 (m, 2H), 3.99 (TFE, q, 2H), 1.97-1.88 (m, 2H), 1.28 (m, 3H), 1.07-0.91 (m, 3H). ^{19}F NMR (400 MHz, Acetone d$_6$) δ (ppm): -78 (TFE, s, 3F), -152 (m, 0.15F), -154 (m, 0.14F), -160 (m, 0.13F), -165 (m, 0.27F).

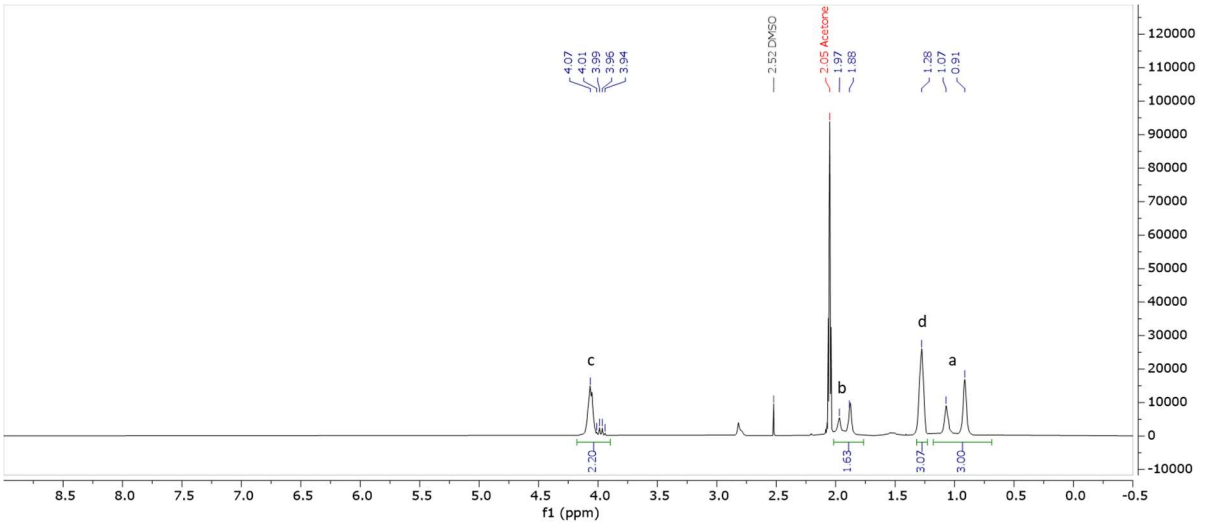

Figure 102: [1]H NMR spectrum of PEMA-MAA-PF5 100-1-1.

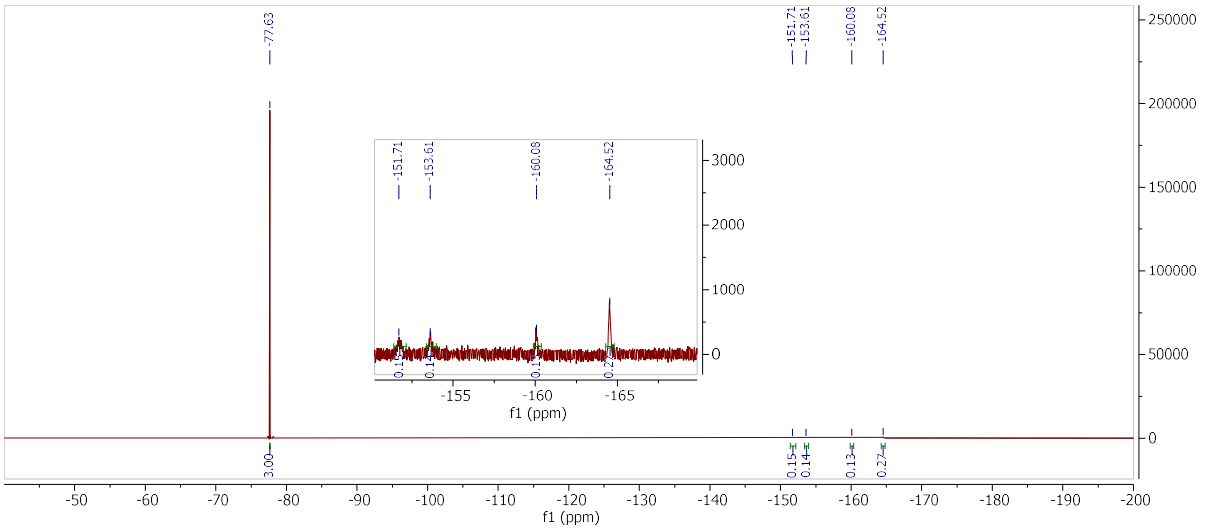

Figure 103: [19]F NMR spectrum of PEMA-MAA-PF5 100-1-1.

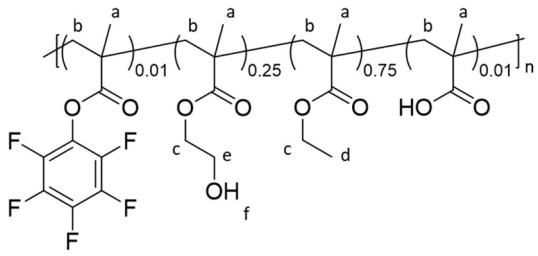

PEMA-HEMA-MAA-PF5 75-25-1-1: Monomers were dissolved in DMSO at a concentration of 2M. 15 mL of EMA (30 mmol, 75 eq), 5 mL of HEMA (10 mmol, 25 eq), 0.2 mL of PF5 (0.4 mmol, 1 eq) and 0.2 mL of MAA (0.4 mmol, 1 eq) solutions were placed in a 50 mL round bottom flask. 0.84 mL of AIBN at 40 mg.mL^{-1} (0.7 mmol, 0.5 eq) were added and the mixture was flushed with argon during 5 min. It was then heated at 70 °C under inert atmosphere for 30 min and an aliquot was taken and analyzed using ^{1}H NMR spectroscopy. The ratio between the intensities of the O-CH$_2$-signals from the monomer and the polymer showed 36% of conversion. The mixture was then precipitated in 80 mL of MeOH/Water 8:2 mixture. The polymer was collected after

centrifugation and redissolved in ACN before a second precipitation in identical medium. The obtained polymer was dried under vacuum to give 667 mg of white solid (overall yield 14%). NMR was performed with TFE as standard. ^{1}H NMR (400 MHz, Acetone d_6) δ (ppm): 4.06 (m, 2H), 3.98 (TFE, q, 2H), 3.79 (m, 0.55H), 1.97-1.88 (m, 2H), 1.27 (m, 2.44H), 1.07-0.92 (m, 3H). ^{19}F NMR (400 MHz, Acetone d_6) δ (ppm): -78 (TFE, t, 3F), -152 (m, 0.41F), -154 (m, 0.43F), -160 (m, 0.40F), -165 (m, 0.82F).

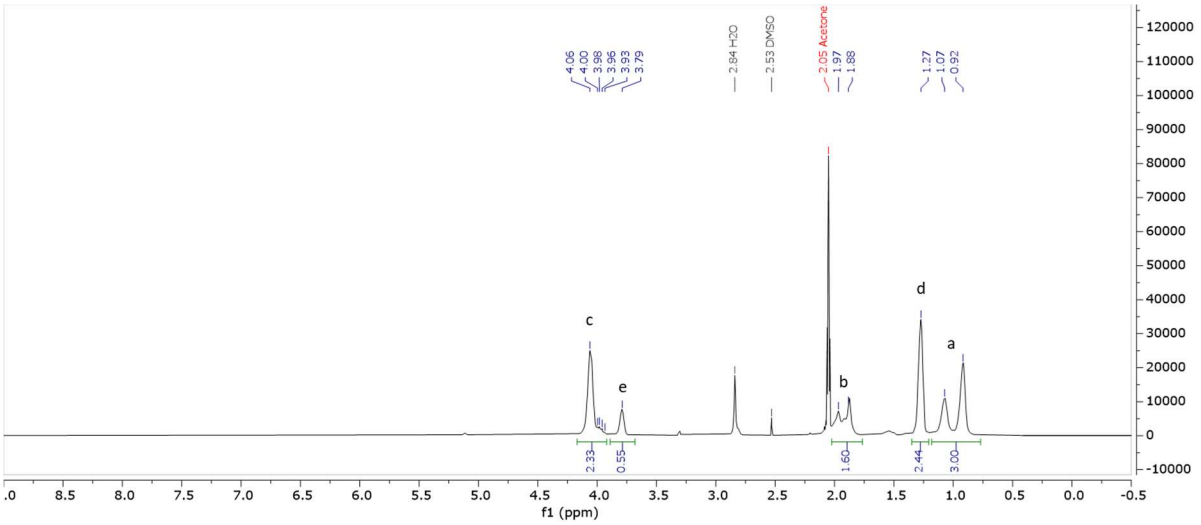

Figure 104: ^{1}H NMR spectrum of PEMA-HEMA-MAA-PF5 75-25-1-1.

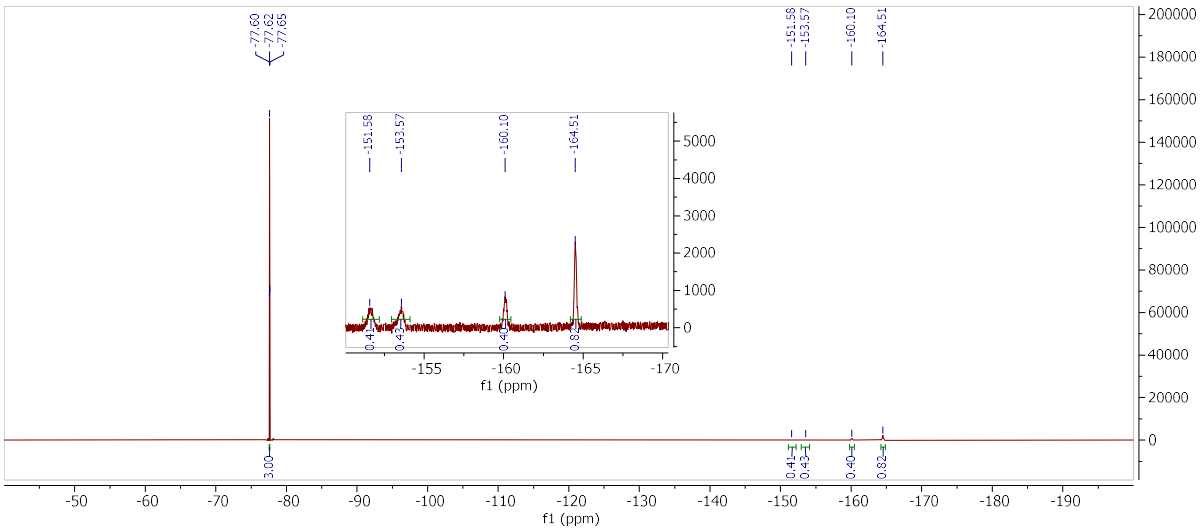

Figure 105: ^{19}F NMR spectrum of PEMA-HEMA-MAA-PF5 75-25-1-1.

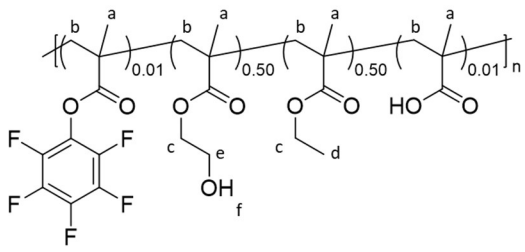

PEMA-HEMA-MAA-PF5 50-50-1-1: Monomers were dissolved in DMSO at a concentration of 2M. 10 mL of EMA (20 mmol, 50 eq), 10 mL of HEMA (20 mmol, 20 eq), 0.2 mL of PF5 (0.4 mmol, 1 eq) and 0.2 mL of MAA (0.4 mmol, 1 eq) solutions were placed in a 50 mL round bottom flask. 0.84 mL of AIBN at 40 mg.mL^{-1} (0.7 mmol, 0.5 eq) were added and the mixture was flushed with argon during 5 min. It was then heated at 70 °C under inert atmosphere for 30 min and an aliquot was taken and analyzed using ^{1}H NMR spectroscopy. The ratio between the intensities of the O-CH_2- signals from the monomer and the polymer showed 26% of conversion. The mixture was then precipitated in 80 mL of MeOH/Water 5:5 mixture. The polymer was collected after centrifugation and redissolved in ACN before a second precipitation in identical medium. The obtained polymer was dried under vacuum to give 737 mg of white solid (overall yield 15%). NMR was performed with TFE as standard. ^{1}H NMR (400 MHz, Acetone d_6) δ (ppm): 4.06 (m, 2H), 3.98 (TFE, q, 2H), 3.80 (m, 1.05H), 1.97-1.90 (m, 2H), 1.27 (m, 1.67H), 1.09-0.93 (m, 3H). ^{19}F NMR (400 MHz, Acetone d_6) δ (ppm): -78 (TFE, t, 3F), -151 (m, 0.27F), -153 (m, 0.29F), -160 (m, 0.24F), -164 (m, 0.48F).

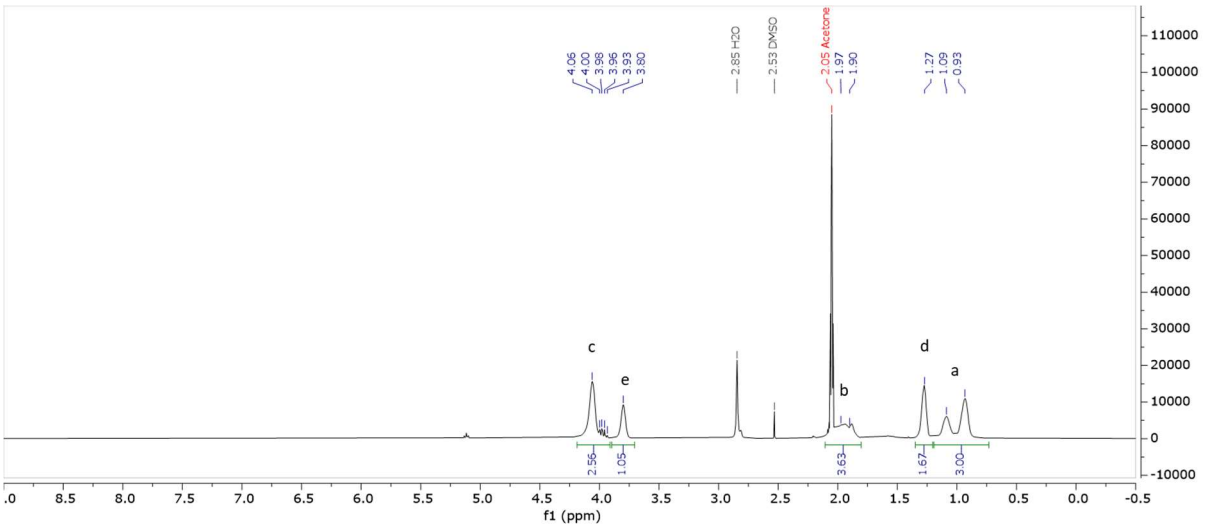

Figure 106: ^{1}H NMR spectrum of PEMA-HEMA-MAA-PF5 75-25-1-1.

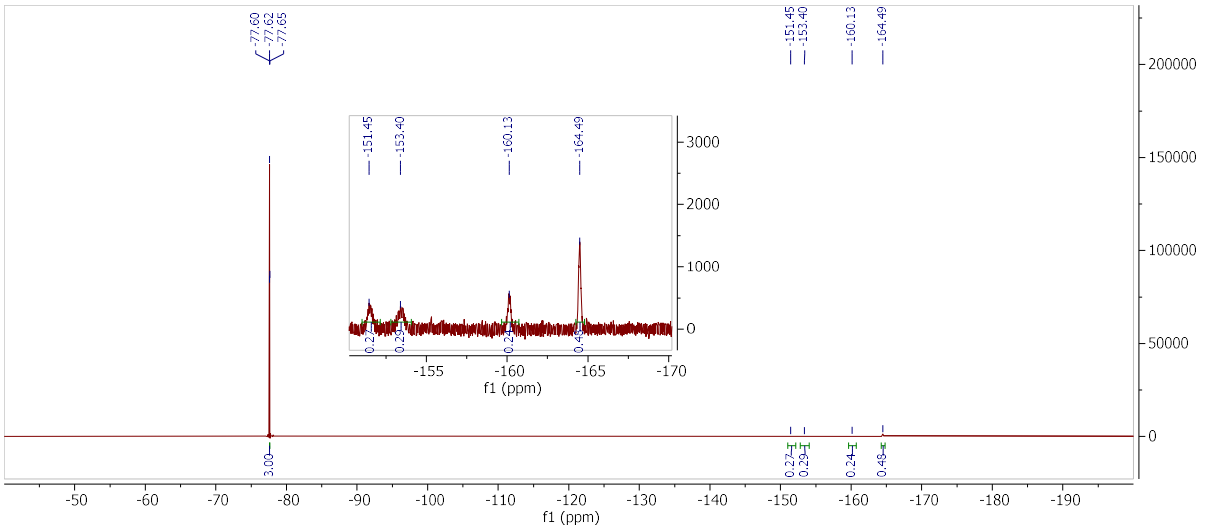

Figure 107: ^{19}F NMR spectrum of PEMA-HEMA-MAA-PF5 75-25-1-1.

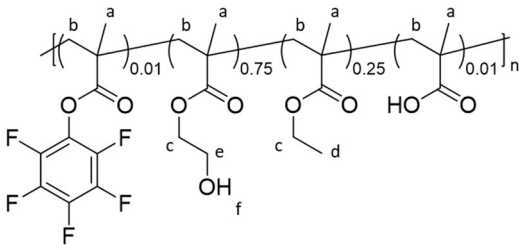

PEMA-HEMA-MAA-PF5 25-75-1-1: Monomers were dissolved in DMSO at a concentration of 2M. 7.3 mL of EMA (14.6 mmol, 25 eq), 22.1 mL of HEMA (44.2 mmol, 75 eq), 0.3 mL of PF5 (0.6 mmol, 1 eq) and 0.3 mL of MAA (0.6 mmol, 1 eq) solutions were placed in a 50 mL round bottom flask. 2.5 mL of AIBN at 40 mg.mL^{-1} (0.6 mmol, 1 eq) were added and the mixture was flushed with argon during 5 min. It was then heated at 70 °C under inert atmosphere for 35 min and an aliquot was taken and analyzed using ^{1}H NMR spectroscopy. The ratio between the intensities of the O-CH$_2$- signals from the monomer and the polymer showed 38.5% of conversion. The mixture was then precipitated in 200 mL of MeOH/Water 6:4 mixture. The polymer was collected after centrifugation and redissolved in ACN before a second precipitation in identical medium. The obtained polymer was dried under vacuum to give 886 mg of white solid (overall yield 12%). NMR was performed with TFE as standard. ^{1}H NMR (400 MHz, Acetone d$_6$) δ (ppm): 4.07 (m, 2H), 3.98 (TFE, q, 2H), 3.82 (m, 1.50H), 1.97 (m, 2H), 1.28 (m, 1.05H), 1.11-0.96 (m, 3H). ^{19}F NMR (400 MHz, Acetone d$_6$) δ (ppm): -78 (TFE, t, 3F), -151 (m, 0.2F), -153 (m, 0.21F), -160 (m, 0.2F), -164 (m, 0.4F).

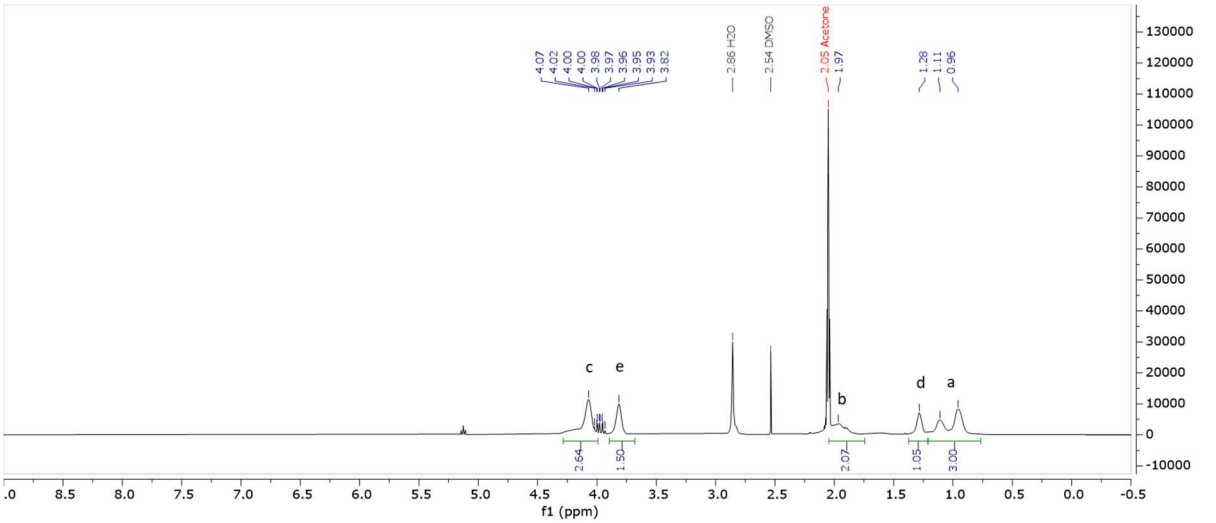

Figure 108: [1]H NMR spectrum of PEMA-HEMA-MAA-PF5 25-75-1-1.

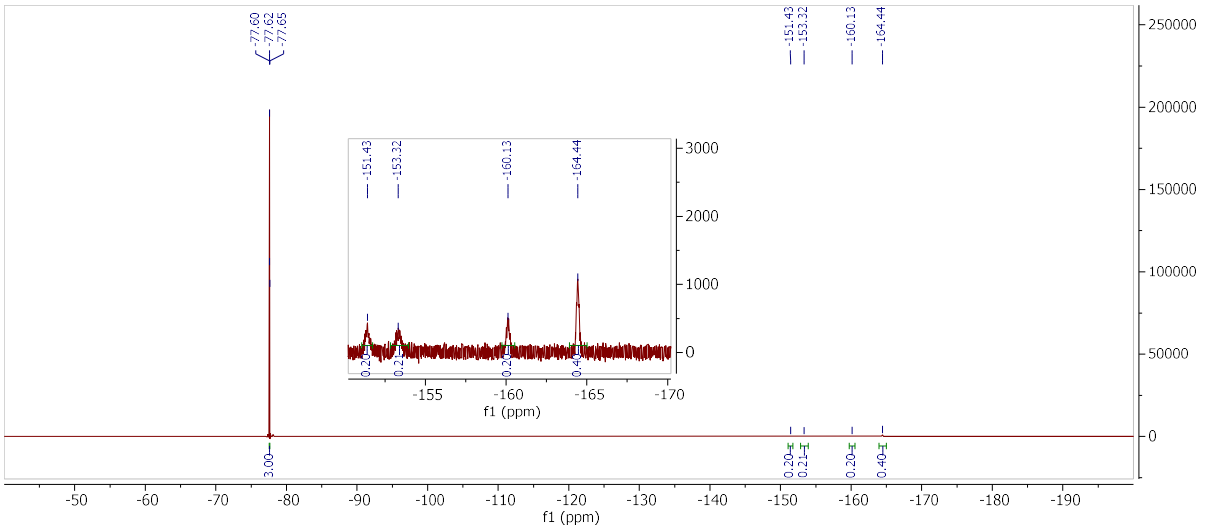

Figure 109: [19]F NMR spectrum of PEMA-HEMA-MAA-PF5 25-75-1-1.

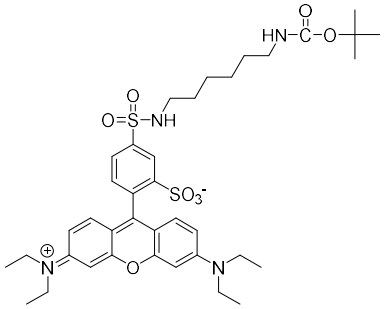

Lissamine N-boc-hexanediamine : 300 mg of Lissamine Rhodamine B sulfonyl Chloride (0.520 mmol, 1 eq) were dissolved in 6 mL of dry DCM and the mixture was cooled down at 0°C. 170 mg of N-Boc-1,6-hexanediamine (0.78 mmol, 1.5 eq) and 217 µL of triethylamine (1.56 mmol, 3 eq) in solution in 1mL of DCM were slowly added. The mixture was stirred 45 min at 0°C then at room temperature for 2h. The crude was purified by flash chromatography with a gradient from DCM/MeOH 95:5 to DCM/MeOH 90:10 over 90 min. [1]H NMR (400 MHz, MeOD) δ 8.64 (d, J = 1.8 Hz, 1H, ArH), 8.10 (dd, J = 7.9, 1.9 Hz, 1H, ArH), 7.51 (d, J = 8.0 Hz, 1H, ArH), 7.11 (d, J = 9.5 Hz, 2H, ArH), 7.01 (dd, J = 9.5, 2.5 Hz, 2H, ArH), 6.94 (d, J = 2.4 Hz, 2H, ArH), 3.68 (q, J = 7.2 Hz, 8H, CH_2 Rhodamine), 1.42 (s, 4H,

CH_2 alkyl), 1.42 (m, 17 H, CH_2 alkyl + CH_3 Boc), 1.30 (t, J = 7.1 Hz, 12 H, CH_3 Rhodamine). HRMS (ESI+) calculated for $C_{38}H_{53}N_4O_8S_2$ [M+H$^+$] 757.3305, found 757.3329.

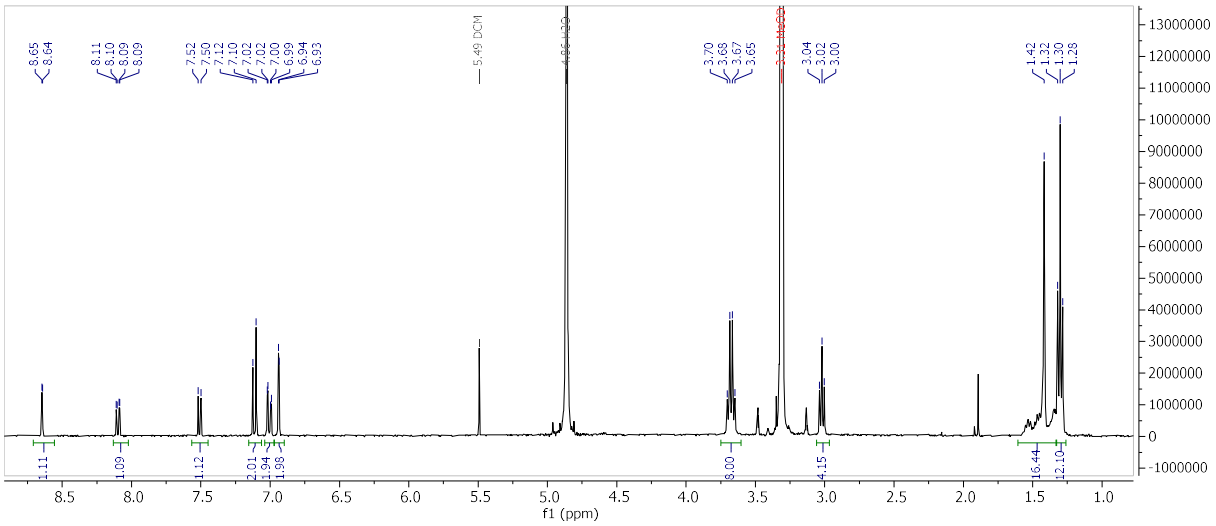

Figure 110: ^{1}H NMR spectrum of Lissamine N-boc-hexanediamine.

Polymer functionalization:

General procedure: Lissamine N-boc-hexanediamine was deprotected just before coupling with polymers. It was dissolved in 2 mL of DCM prior addition of 2 mL of TFA. The reaction was stirred at room temperature until TLC showed complete conversion. Functionalizable polymers were dissolved in DMF with the amine-bearing dye (3 eq) and triethylamine (30 eq). Reactions were set at 55°C for 48h prior addition of ethylamine (40 eq), then it was let for an additional 24h. The polymer was precipitated in a MeOH/Water mixture and purified with size-exclusion chromatography. The functionalization of **PEMA-HEMA-MAA-PF5 50-50-1-1** is given as an example:

2.3 mg of bodipy (0.006 mmol, 3eq) were dissolved in 600 µL of DMF, 42 µL of TEA (0.03 mmol, 30 eq) were added and this solution was put in a Schlenk tube with 25 mg of polymer previously weighted. The mixture was heated under inert atmosphere at 55°C for 48h. Then 40 µL of ethylamine (0.08 mmol, 40 eq) were added and reaction was let for additional 24h. The polymer was precipitated in 10 mL of H2O/MeOH mixture 8:2 and purified with steric exclusion chromatography. 17.4 mg of polymer were collected.

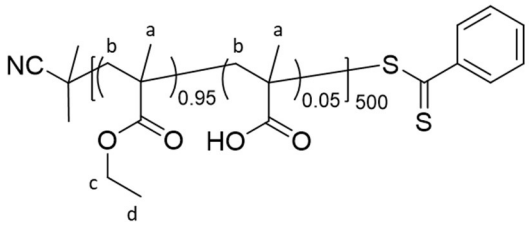

P[EMA 5%]$_{500}$ (RAFT): Reactant solutions were prepared in DMF. 1.58 mL of EMA 6M solution (9.5 mmol, 0.95 eq), 0.25 mL of MAA 2M solution (0.5 mmol, 0.5 eq), 44.2 µL of 2-Cyano-2-propyl benzodithioate 100 mg.mL^{-1} solution (0.02 mmol, 1/500 eq) and 54.6 µL of AIBN 10 mg.mL^{-1} solution (0.0033 mmol, 1/3000 eq) were put in a Schlenk tube under inert atm before undergoing three freeze-pump-thaw cycles. Reaction was set at 80°C under stirring overnight. An aliquot was taken and analyzed using ^{1}H NMR spectroscopy. The ratio between the intensities of the O-CH_2- signals from the monomer and the polymer showed 88% of conversion. 3 mL of DMF were added to the mixture prior precipitation in 40 mL of MeOH/Water 9:1 mixture. The polymer was collected after centrifugation and redissolved in ACN before a second precipitation in identical medium. The obtained polymer was dried under vacuum to give 598 mg of white solid (overall yield 53%). ^{1}H NMR (400 MHz, $CDCl_3$) δ (ppm): 4.03 (m, 2H), 1.92-1.82 (m, 2H), 1.25 (m, 3H), 1.03-0.87 (m, 3H). Molecular weight determined by SEC: M_n = 49000 g/mol, PDI = 1.05

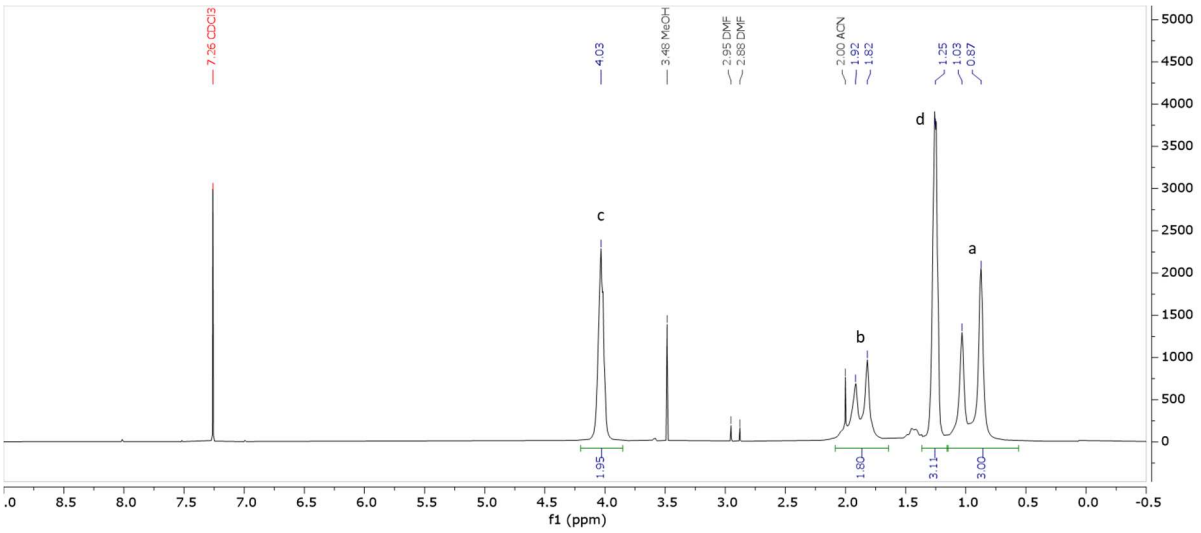

Figure 111: ^{1}H NMR spectrum of P[EMA 5%]$_{500}$.

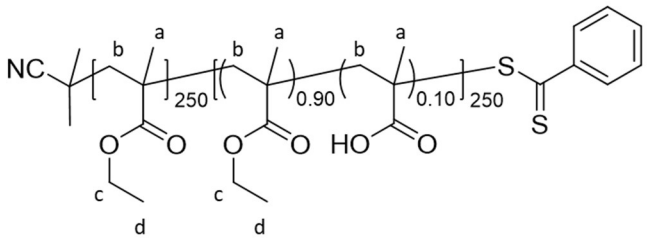

P[EMA]$_{250}$-b-[EMA 10%]$_{250}$: In a first step, the macro-RAFT agent **P[EMA]$_{250}$** was synthetized: Reactant solutions were prepared in DMF. 1.66 mL of EMA 6M solution (10 mmol, 1 eq), 88.4 µL of

2-Cyano-2-propyl benzodithioate 100 mg.mL^{-1} solution (0.04 mmol, 1/250 eq) and 54.6 µL of AIBN 10 mg.mL^{-1} solution (0.0033 mmol, 1/3000 eq) were put in a Schlenk tube under inert atm before undergoing three freeze-pump-thaw cycles. Reaction was set at 80°C under stirring overnight. An aliquot was taken and analyzed using ^{1}H NMR spectroscopy. The ratio between the intensities of the O-CH_2- signals from the monomer and the polymer showed 84% of conversion. 3 mL of DMF were added to the mixture prior precipitation in 40 mL of MeOH/Water 9:1 mixture. The polymer was collected after centrifugation and redissolved in ACN before a second precipitation in identical medium. The obtained polymer was dried under vacuum to give 423 mg of white solid (overall yield 37%).

Then, 100 mg of **P[EMA]$_{250}$** (0.0035 mmol, 1eq), 394 µL of EMA 2M (0.788 mmol, 225 eq), 43.8 µL of MAA 2M (0.0875 mmol, 25 eq) and 29 µL of AIBN 10 mg.mL^{-1} solution (0.00175 mmol, 0.5 eq) were put in a Schlenk tube under inert atm before undergoing three freeze-pump-thaw cycles. Reaction was set at 80°C under stirring overnight. An aliquot was taken and analyzed using ^{1}H NMR spectroscopy. The ratio between the intensities of the O-CH_2- signals from the monomer and the polymer showed 95% of conversion. 1 mL of DMF was added to the mixture prior precipitation in 10 mL of MeOH/Water 6:4 mix. The obtained polymer was dried under vacuum to give 51 mg of white solid (overall yield 25%). ^{1}H NMR (400 MHz, $CDCl_3$) δ (ppm): 4.03 (m, 2H), 1.92-1.82 (m, 2H), 1.25 (m, 3H), 1.03-0.88 (m, 3H). Molecular weight determined by SEC: M_n = 27000 g/mol, PDI = 1.12

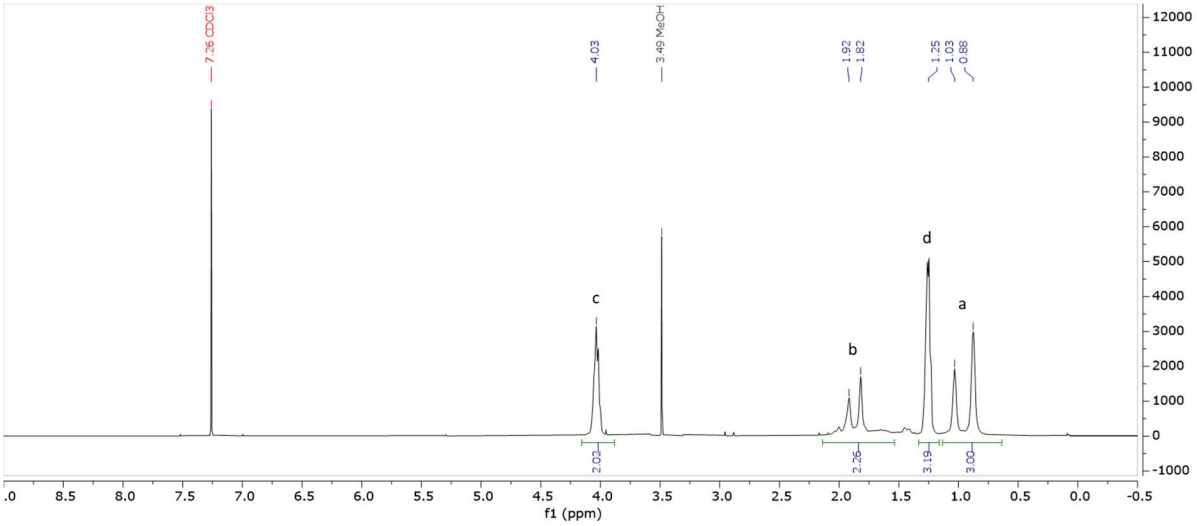

Figure 112: ^{1}H NMR spectrum of P[EMA]$_{250}$-b-[EMA 10%]$_{250}$.

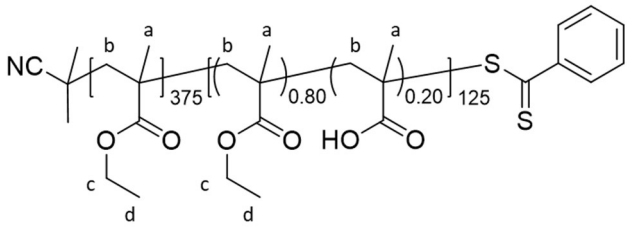

P[EMA]$_{375}$-b-[EMA 20%]$_{125}$: In a first step, the macro-RAFT agent **P[EMA]$_{375}$** was synthetized: Reactant solutions were prepared in DMF. 1.66 mL of EMA 6M solution (10 mmol, 1 eq), 58.9 µL of 2-Cyano-2-propyl benzodithioate 100 mg.mL^{-1} solution (0.0266 mmol, 1/375 eq) and 54.6 µL of AIBN 10 mg.mL^{-1} solution (0.0033 mmol, 1/3000 eq) were put in a Schlenk tube under inert atm before undergoing three freeze-pump-thaw cycles. Reaction was set at 80°C under stirring overnight. An aliquot was taken and analyzed using ^{1}H NMR spectroscopy. The ratio between the intensities of the O-CH$_2$- signals from the monomer and the polymer showed 87% of conversion. 3 mL of DMF were added to the mixture prior precipitation in 40 mL of MeOH/Water 9:1 mixture. The polymer was collected after centrifugation and redissolved in ACN before a second precipitation in identical medium. The obtained polymer was dried under vacuum to give 683 mg of white solid (overall yield 60%).

Then, 100 mg of **P[EMA]$_{375}$** (0.0023 mmol, 1eq), 117 µL of EMA 2M (0.234 mmol, 100 eq), 29.3 µL of MAA 2M (0.0585 mmol, 25 eq) and 19.2 µL of AIBN 10 mg.mL^{-1} solution (0.00117 mmol, 0.5 eq) were put in a Schlenk tube under inert atm before undergoing three freeze-pump-thaw cycles. Reaction was set at 80°C under stirring overnight. An aliquot was taken and analyzed using ^{1}H NMR spectroscopy. The ratio between the intensities of the O-CH$_2$- signals from the monomer and the polymer showed 85% of conversion. 1 mL of DMF was added to the mixture prior precipitation in 10 mL of MeOH/Water 5:5 mix. The obtained polymer was dried under vacuum to give 31 mg of white solid (overall yield 23%). ^{1}H NMR (400 MHz, $CDCl_3$) δ (ppm): 4.04 (m, 2H), 1.92-1.82 (m, 2H), 1.25 (m, 3H), 1.03-0.87 (m, 3H). Molecular weight determined by SEC: M_n = 34000 g/mol, PDI = 1.10

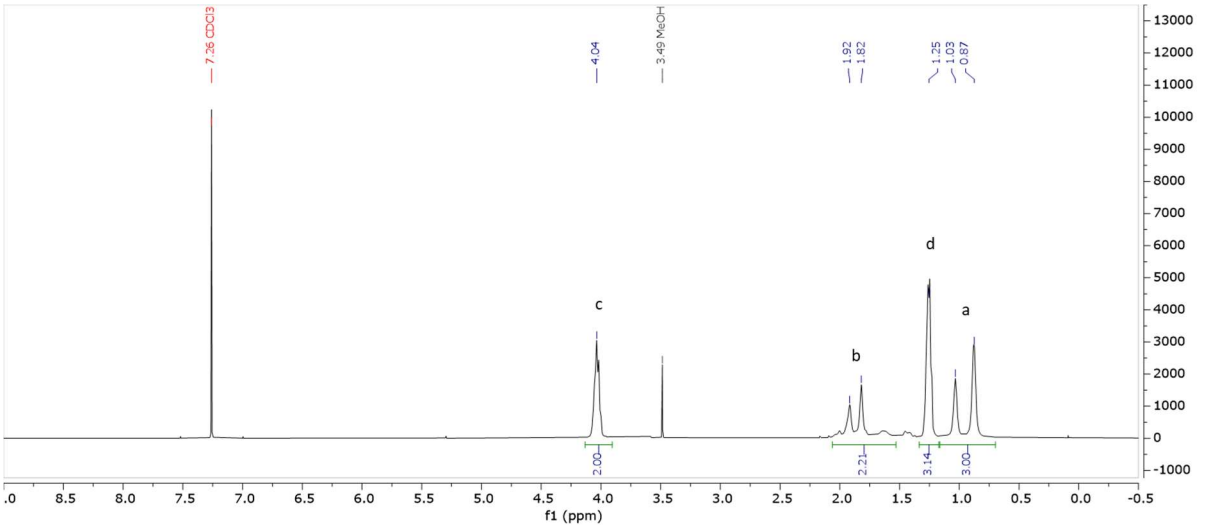

Figure 113: ^{1}H NMR spectrum of P[EMA]$_{375}$-b-[EMA 20%]$_{125}$.

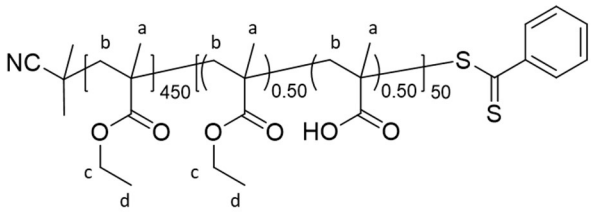

P[EMA]$_{450}$-b-[EMA 50%]$_{50}$: In a first step, the macro-RAFT agent **P[EMA]$_{450}$** was synthetized: Reactant solutions were prepared in DMF. 1.66 mL of EMA 6M solution (10 mmol, 1 eq), 49.1 µL of 2-Cyano-2-propyl benzodithioate 100 mg.mL^{-1} solution (0.0222 mmol, 1/450 eq) and 54.6 µL of AIBN 10 mg.mL^{-1} solution (0.0033 mmol, 1/3000 eq) were put in a Schlenk tube under inert atm before undergoing three freeze-pump-thaw cycles. Reaction was set at 80°C under stirring overnight. An aliquot was taken and analyzed using ^{1}H NMR spectroscopy. The ratio between the intensities of the O-CH$_2$- signals from the monomer and the polymer showed 82% of conversion. 3 mL of DMF were added to the mixture prior precipitation in 40 mL of MeOH/Water 9:1 mixture. The polymer was collected after centrifugation and redissolved in ACN before a second precipitation in identical medium. The obtained polymer was dried under vacuum to give 634 mg of white solid (overall yield 56%).

Then, 50 mg of **P[EMA]$_{450}$** (0.00195 mmol, 1eq), 24.4 µL of EMA 2M (0.049 mmol, 25 eq), 24.4 µL of MAA 2M (0.049 mmol, 25 eq) and 16 µL of AIBN 10 mg.mL^{-1} solution (0.975 µmol, 0.5 eq) were put in a Schlenk tube under inert atm before undergoing three freeze-pump-thaw cycles. Reaction was set at 80°C under stirring overnight. An aliquot was taken and analyzed using ^{1}H NMR spectroscopy. The ratio between the intensities of the O-CH$_2$- signals from the monomer and the polymer showed 66% of conversion. 1 mL of DMF was added to the mixture prior precipitation in 10 mL of MeOH/Water 5:5 mixture.

The obtained polymer was dried under vacuum to give 46 mg of white solid (overall yield 41%). ^{1}H NMR (400 MHz, $CDCl_3$) δ (ppm): 4.04 (m, 2H), 1.92-1.82 (m, 2H), 1.25 (m, 3H), 1.03-0.88 (m, 3H). Molecular weight determined by SEC: M_n = 28000 g/mol, PDI = 1.43

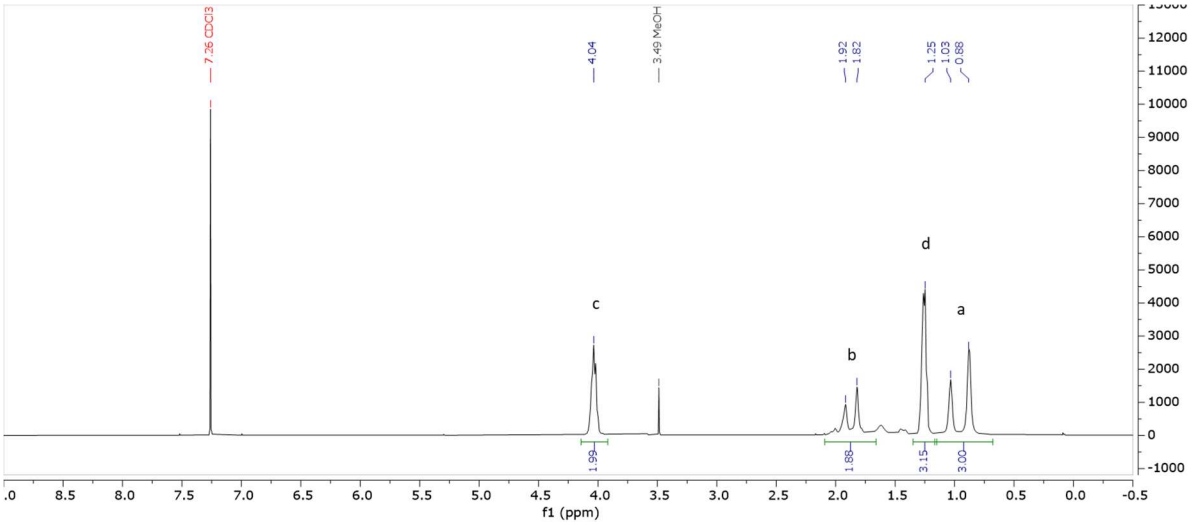

Figure 114: ^{1}H NMR spectrum of P[EMA]$_{450}$-b-[EMA 50%]$_{50}$.

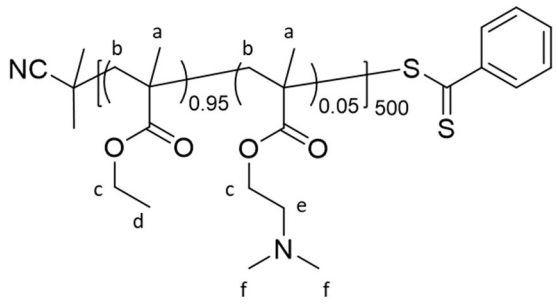

P[EMA-NMe$_2$ 5%]$_{500}$ (RAFT): Reactant solutions were prepared in DMF. 1.97 mL of EMA 2M solution (3.94 mmol, 475 eq), 104 µL of NMe_2 2M solution (0.21 mmol, 25 eq), 16 µL of TFA (0.21 mmol, 25 eq), 1.83 mg of 2-Cyano-2-propyl benzodithioate (8.3 µmol, 1 eq) and 0.14 mg of AIBN (0.83 µmol, 0.1 eq) were put in a Schlenk tube under inert atm before undergoing three freeze-pump-thaw cycles. Reaction was set at 80°C under stirring overnight. An aliquot was taken and analyzed using ^{1}H NMR spectroscopy. The ratio between the intensities of the O-CH_2- signals from the monomer and the polymer showed 81% of conversion. The mixture was precipitated in 10 mL of MeOH/$NaCl_{aq}$ 1M 7:3 mixture. The polymer was collected after centrifugation and redissolved in ACN before a second precipitation in identical medium. The obtained polymer was dried under vacuum to give 210 mg of yellowish solid (overall yield 44%).^{1}H NMR (400 MHz, $CDCl_3$) δ (ppm): 4.04 (m, 2H), 2.57 (m, 0.13H), 2.28 (m, 0.37H), 1.92-1.82 (m, 2H), 1.26 (m, 3H), 1.04-0.88 (m, 3H).

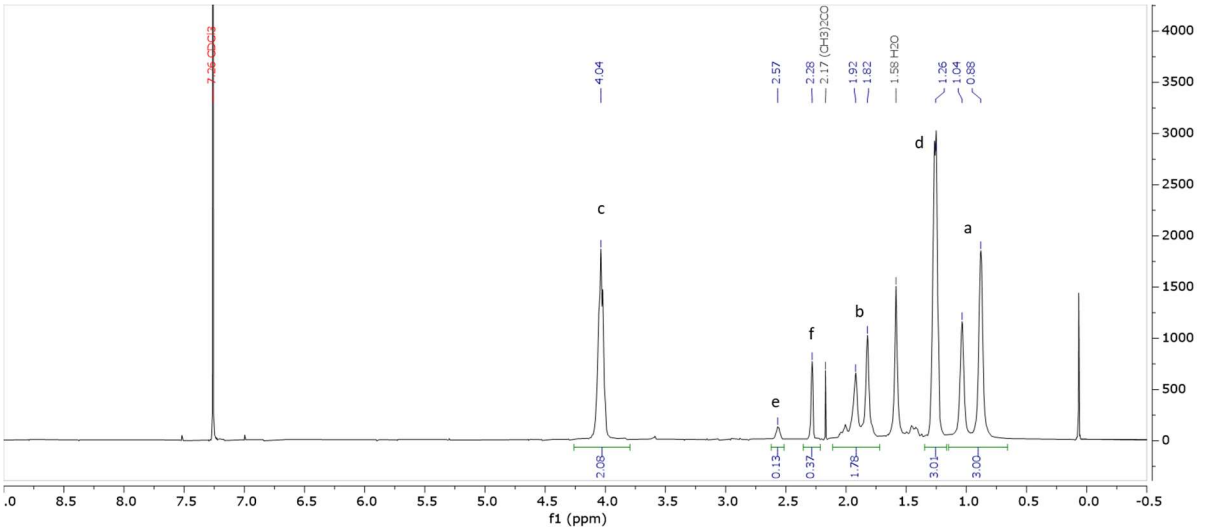

Figure 115: ^{1}H NMR spectrum of P[EMA-NMe$_2$ 5%]$_{500}$ (RAFT).

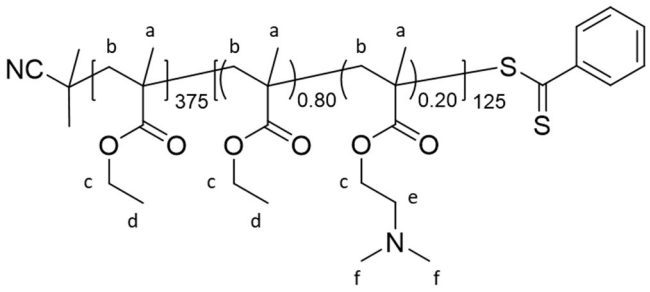

P[EMA]$_{375}$-b-[NMe$_2$ 20%]$_{125}$: In a first step, the macro-RAFT agent **P[EMA-NMe$_2$ 20%]$_{125}$** was synthetized: Reactant solutions were prepared in DMF. 1.34 mL of EMA 2M solution (2.63 mmol, 118 eq), 324 µL of NMe$_2$ 2M solution (0.65 mmol, 29 eq) 49 µL of TFA (0.65 mmol, 29 eq), 4.93 mg of CTA (22.3 µmol, 1 eq) and 0.37 mg of AIBN (2.23 µmol, 0.1 eq) were put in a Schlenk tube under inert atm before undergoing three freeze-pump-thaw cycles. Reaction was set at 80°C under stirring overnight. An aliquot was taken and analyzed using ^{1}H NMR spectroscopy. The ratio between the intensities of the O-CH$_2$- signals from the monomer and the polymer showed 77% of conversion. The mixture was precipitated in 10 mL of MeOH/NaCl$_{aq}$ 1M 7:3 mixture. The polymer was collected after centrifugation and redissolved in ACN before a second precipitation in identical medium. The obtained polymer was dried under vacuum to give 201 mg of yellowish solid (overall yield 49%).

Then, 50 mg of **P[EMA-NMe$_2$ 20%]$_{125}$** (3.6 µmol, 1 eq), 797 µL of EMA 2M solution (1.6 mmol, 441 eq) and 0.06 mg of AIBN (0.36 µmol, 0.1 eq) were put in a Schlenk tube under inert atm before undergoing three freeze-pump-thaw cycles. Reaction was set at 80°C under stirring overnight. An aliquot was taken and analyzed using ^{1}H NMR spectroscopy. The ratio between the intensities of the O-CH$_2$- signals from the monomer and the polymer showed 94% of conversion. The mixture was precipitated in 10 mL of

MeOH/$NaCl_{aq}$ 1M 8:2 mixture. The polymer was collected after centrifugation and redissolved in ACN before a second precipitation in identical medium. The obtained polymer was dried under vacuum to give 120 mg of yellowish solid (overall yield 54%). ^{1}H NMR (400 MHz, CDCl3): δ (ppm) 4.04 (m, 2H), 2.58 (m, 0.05H), 2.29 (m, 0.12H), 1.92-1.82 (m, 2H), 1.26 (m, 3H), 1.04-0.88 (m, 3H).

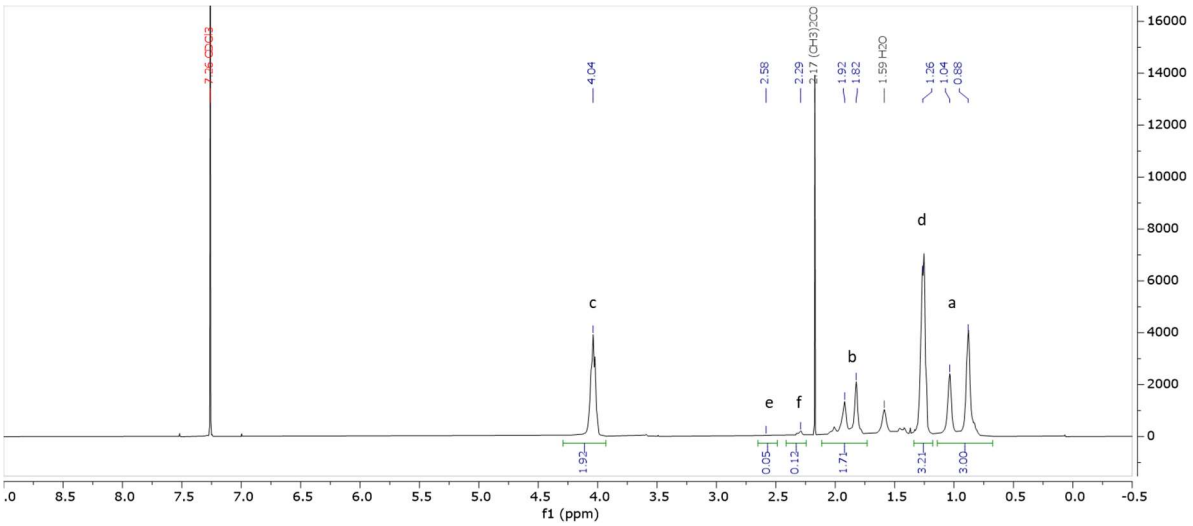

Figure 116: ^{1}H NMR spectrum of P[EMA]$_{375}$-b-[NMe_2 20%]$_{125}$.

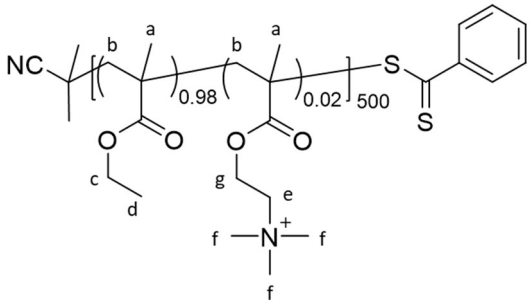

P[EMA-NMe_3^+ 2%]$_{500}$ (RAFT): Reactant solutions were prepared in DMF. 980µL of EMA 2M solution (1.96 mmol, 0.98 eq), 20 µL of 2-Trimethylammonioethyl methacrylate chloride (NMe_3^+) 2M solution (0.04 mmol, 0.02 eq), 8.84 µL of 2-Cyano-2-propyl benzodithioate 100 mg.mL^{-1} solution (0.004 mmol, 1/500 eq) and 8.66 µL of AIBN 10 mg.mL^{-1} solution (0.0033 mmol, 1/3750 eq) were put in a Schlenk tube under inert atm before undergoing three freeze-pump-thaw cycles. Reaction was set at 80°C under stirring overnight. An aliquot was taken and analyzed using ^{1}H NMR spectroscopy. The ratio between the intensities of the O-CH_2- signals from the monomer and the polymer showed 93% of conversion. The mixture was precipitated in 10 mL of MeOH/KCl_{aq} 1M 5:5 mixture. The polymer was collected after centrifugation and redissolved in ACN before a second precipitation in identical medium. The obtained polymer was rinsed with water to remove excess of salts and dried under vacuum to give 48 mg of white solid (overall yield 21%).^{1}H NMR (400 MHz, $CDCl_3$) δ (ppm): 4.04 (m, 2H), 3.57 (m, 0.29H), 1.92-1.82 (m, 2H), 1.26 (m, 3H), 1.03-0.88 (m, 3H).

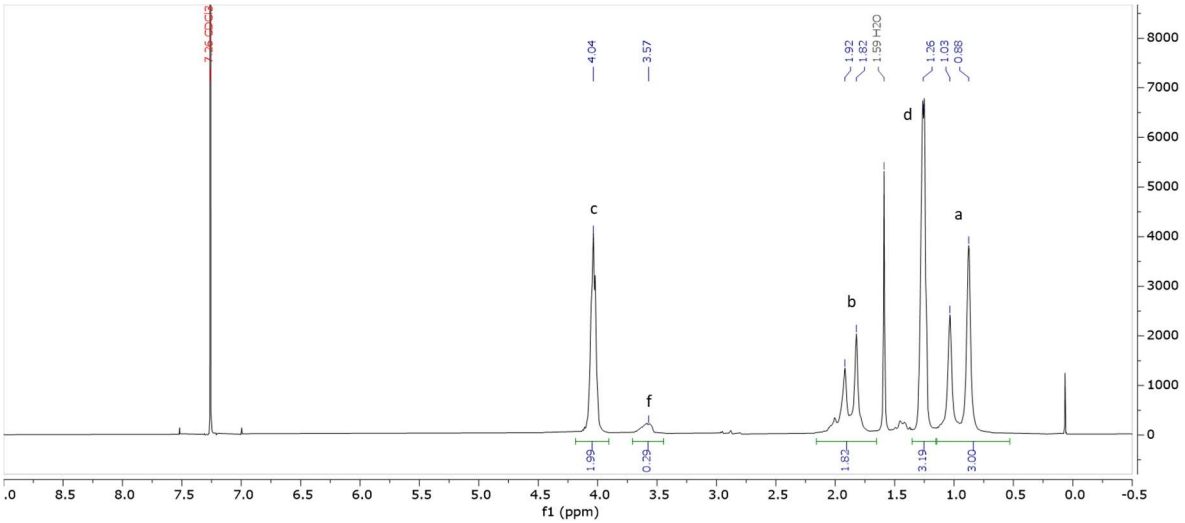

Figure 117: ^{1}H NMR spectrum of P[EMA-NMe$_3$ 2%]$_{500}$ (RAFT).

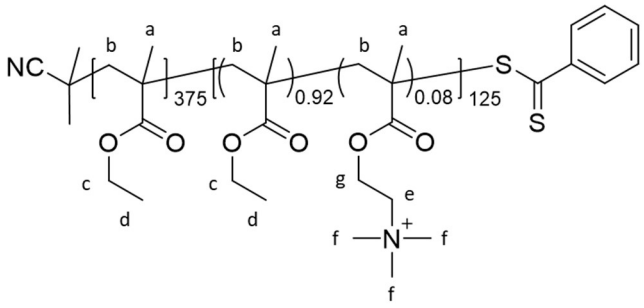

P[EMA]$_{375}$-b-[NMe$_3^+$ 8%]$_{125}$: In a first step, the macro-RAFT agent **P[EMA-NMe$_3^+$ 8%]$_{125}$** was synthetized: Reactant solutions were prepared in DMF. 2.19 mL of EMA 2M solution (4.38 mmol, 135 eq), 390 µL of NMe$_3^+$ 1M solution (0.39 mmol, 12 eq), 7.18 mg of CTA (32 µmol, 1 eq) and 0.53 mg of AIBN (3.2 µmol, 0.1 eq) were put in a Schlenk tube under inert atm before undergoing three freeze-pump-thaw cycles. Reaction was set at 80°C under stirring overnight. An aliquot was taken and analyzed using ^{1}H NMR spectroscopy. The ratio between the intensities of the O-CH$_2$- signals from the monomer and the polymer showed 96% of conversion. The mixture was precipitated in cold 10 mL of MeOH/NaCl$_{aq}$ 1M 2:8 mixture. The polymer was collected after centrifugation and redissolved in ACN before a second precipitation in identical medium. The obtained polymer was dried under vacuum to give 323 mg of white solid (overall yield 56%).

Then, 50 mg of **P[EMA-NMe$_3^+$ 8%]$_{125}$** (2.94 µmol, 1 eq), 735 µL of EMA 2M solution (1.3 mmol, 441 eq) and 0.048 mg of AIBN (0.29 µmol, 0.1 eq) were put in a Schlenk tube under inert atm before undergoing three freeze-pump-thaw cycles. Reaction was set at 80°C under stirring overnight. An aliquot was taken and analyzed using ^{1}H NMR spectroscopy. The ratio between the intensities of the O-CH$_2$- signals from the monomer and the polymer showed 97% of conversion. The mixture was precipitated in 10 mL of MeOH/NaCl$_{aq}$ 1M 8:2 mixture. The polymer was collected after centrifugation and

redissolved in ACN before a second precipitation in identical medium. The obtained polymer was dried under vacuum to give 100 mg of white solid (overall yield 50%). ^{1}H NMR (400 MHz, CDCl3): δ (ppm) 4.04 (m, 2H), 3.59 (m, 0.08H), 1.92-1.82 (m, 2H), 1.26 (m, 3H), 1.04-0.88 (m, 3H).

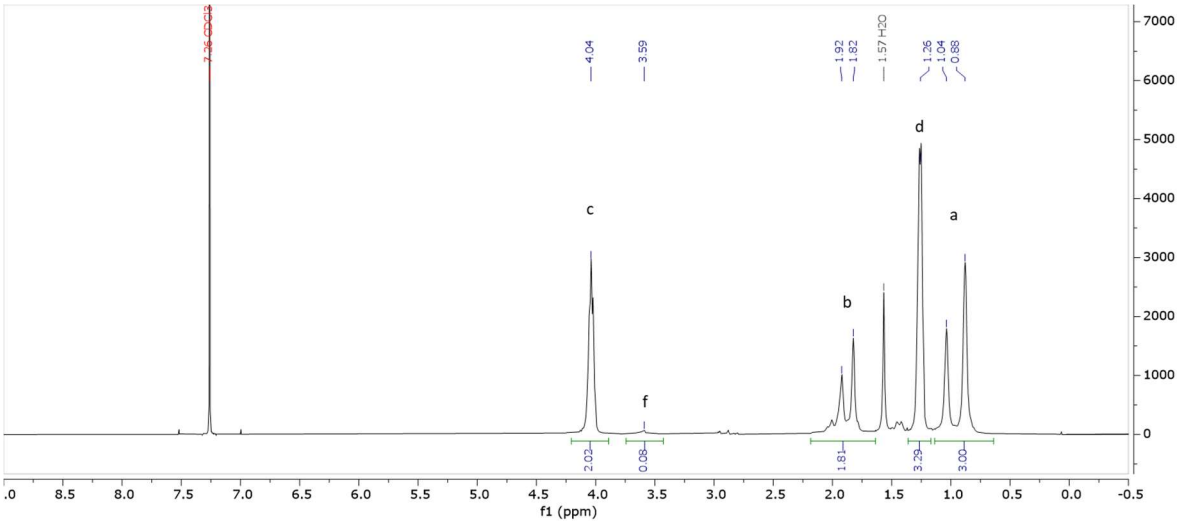

Figure 118: ^{1}H NMR spectrum of P[EMA]$_{375}$-b-[NMe$_3^+$ 8%]$_{125}$.

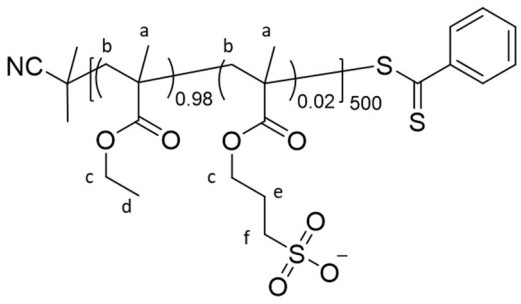

P[EMA-SO$_3$ 2%]$_{500}$ (RAFT): Reactant solutions were prepared in DMF. 2940 µL of EMA 2M solution (5.88 mmol, 0.98 eq), 29.4 mg of 3-Sulfopropyl methacrylate potassium salt (SO_3) (0.12 mmol, 0.02 eq), 26.5 µL of 2-Cyano-2-propyl benzodithioate 100 mg.mL^{-1} solution (0.012 mmol, 1/500 eq) and 26 µL of AIBN 10 mg.mL^{-1} solution (0.0016 mmol, 1/3750 eq) were put in a Schlenk tube under inert atm before undergoing three freeze-pump-thaw cycles. Reaction was set at 80°C under stirring during 43h. An aliquot was taken and analyzed using ^{1}H NMR spectroscopy. The ratio between the intensities of the O-CH_2-signals from the monomer and the polymer showed 75% of conversion. The mixture was precipitated in 10 mL of MeOH/KCl_{aq} 0.2M 5:5 mixture. The polymer was collected after centrifugation and redissolved in ACN before a second precipitation in identical medium. The obtained polymer lyophilized overnight to give 100 mg of white solid (overall yield 15%).^{1}H NMR (400 MHz, $CDCl_3$) δ (ppm): 4.04 (m, 2H), 1.92-1.82 (m, 2H), 1.25 (m, 3H), 1.04-0.88 (m, 3H).

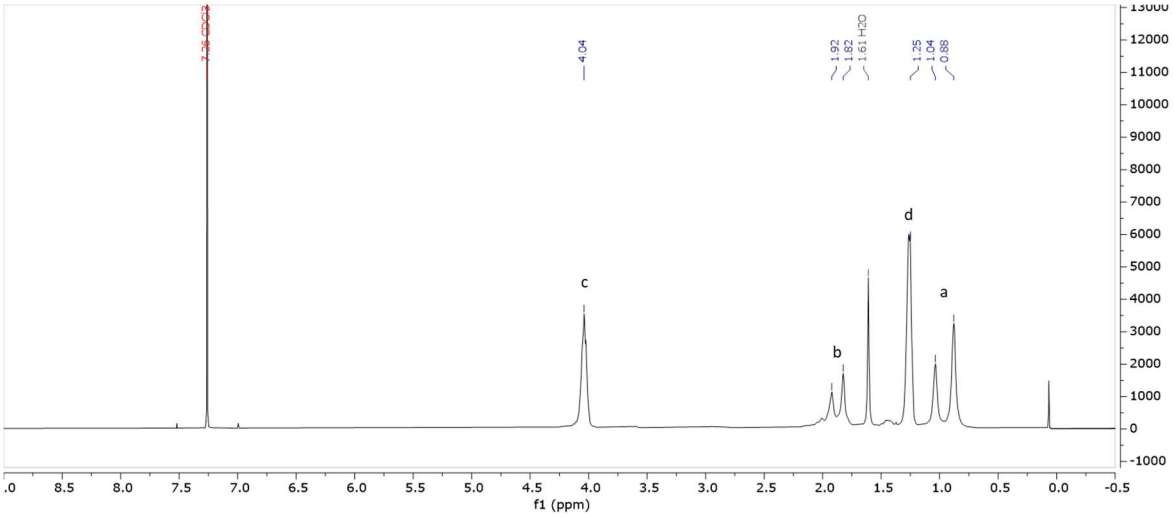

Figure 119: ^{1}H NMR spectrum of P[EMA-SO$_3$ 2%]$_{500}$ (RAFT).

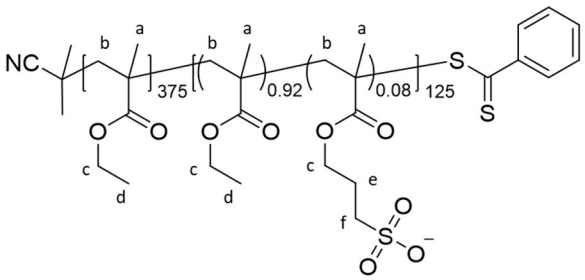

P[EMA]$_{375}$-b-[SO$_3^-$ 8%]$_{125}$: In a first step, the macro-RAFT agent **P[EMA-SO$_3^-$ 8%]$_{125}$** was synthetized: Reactant solutions were prepared in DMF. 2.19 mL of EMA 2M solution (4.38 mmol, 135 eq), 390 µL of SO$_3^-$ 1M solution (0.39 mmol, 12 eq), 7.18 mg of CTA (32 µmol, 1 eq) and 0.53 mg of AIBN (3.2 µmol, 0.1 eq) were put in a Schlenk tube under inert atm before undergoing three freeze-pump-thaw cycles. Reaction was set at 80°C under stirring overnight. An aliquot was taken and analyzed using ^{1}H NMR spectroscopy. The ratio between the intensities of the O-CH$_2$- signals from the monomer and the polymer showed 82% of conversion. The mixture was precipitated in cold 10 mL of MeOH/NaCl$_{aq}$ 1M 2:8 mixture. The polymer was collected after centrifugation and redissolved in ACN before a second precipitation in identical medium. The obtained polymer was dried under vacuum to give 306 mg of white solid (overall yield 51%).

Then, 50 mg of **P[EMA-SO$_3^-$ 8%]$_{125}$** (3.33 µmol, 1 eq), 735 µL of EMA 2M solution (1.47 mmol, 441 eq) and 0.054 mg of AIBN (0.33 µmol, 0.1 eq) were put in a Schlenk tube under inert atm before undergoing three freeze-pump-thaw cycles. Reaction was set at 80°C under stirring overnight. An aliquot was taken and analyzed using ^{1}H NMR spectroscopy. The ratio between the intensities of the O-CH$_2$- signals from the monomer and the polymer showed 97% of conversion. The mixture was precipitated in 10 mL of MeOH/NaCl$_{aq}$ 1M 8:2 mixture. The polymer was collected after centrifugation and redissolved in ACN before a second precipitation in identical medium. The obtained

polymer was dried under vacuum to give 111 mg of white solid (overall yield 52%). ^{1}H NMR (400 MHz, CDCl3): δ (ppm) 4.04 (m, 2H), 1.92-1.82 (m, 2H), 1.25 (m, 3H), 1.04-0.88 (m, 3H).

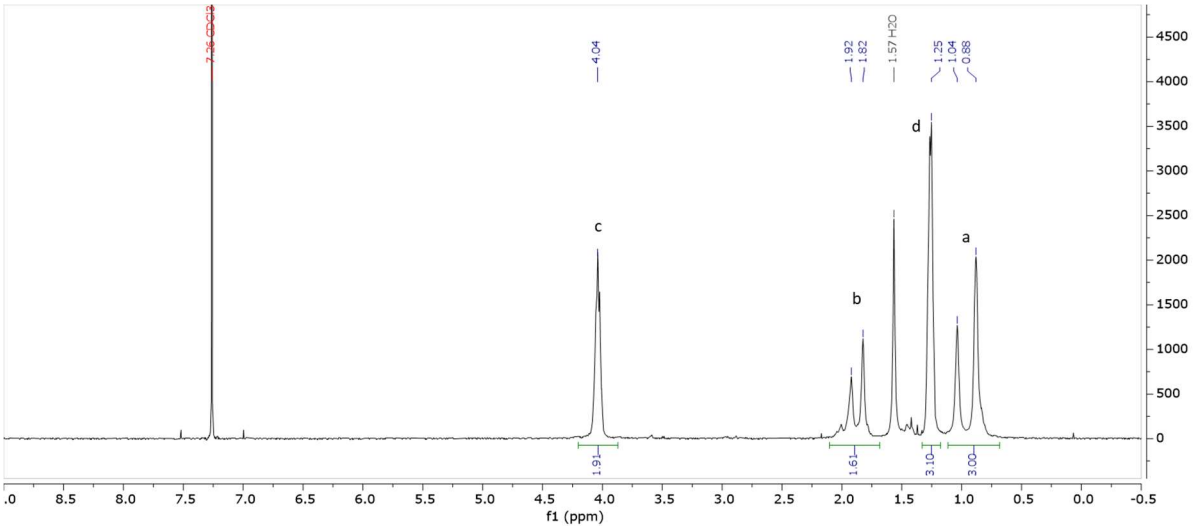

Figure 120: ^{1}H NMR spectrum of P[EMA]$_{375}$-b-[SO_3^- 8%]$_{125}$.

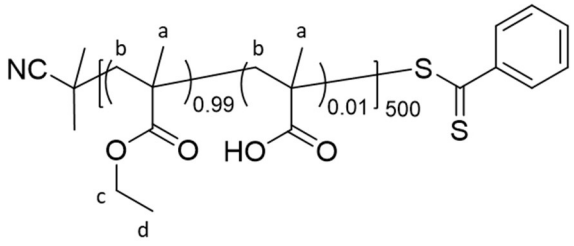

P[EMA 1%]$_{500}$ (RAFT): Reactant solutions were prepared in DMF. 3 mL of EMA 3M solution (9 mmol, 0.99 eq), 30 µL of MAA 3M solution (0.09 mmol, 0.01 eq), 100.5 µL of 2-Cyano-2-propyl benzodithioate 40 mg.mL^{-1} solution (0.0182 mmol, 1/500 eq) and 49 µL of AIBN 10 mg.mL^{-1} solution (0.003 mmol, 1/3000 eq) were put in a Schlenk tube under inert atm before undergoing three freeze-pump-thaw cycles. Reaction was set at 80°C under stirring overnight. An aliquot was taken and analyzed using ^{1}H NMR spectroscopy. The ratio between the intensities of the O-CH_2- signals from the monomer and the polymer showed 86% of conversion. The mixture was precipitated in 25 mL of cold 0°C MeOH. The polymer was collected after centrifugation and redissolved in ACN before a second precipitation in identical medium. The obtained polymer was dried under vacuum to give 329 mg of white solid (overall yield 32%). ^{1}H NMR (400 MHz, $CDCl_3$) δ (ppm): 4.03 (m, 2H), 1.92-1.82 (m, 2H), 1.25 (m, 3H), 1.03-0.87 (m, 3H). Molecular weight determined by SEC: M_n = 30000 g/mol, PDI = 1.28

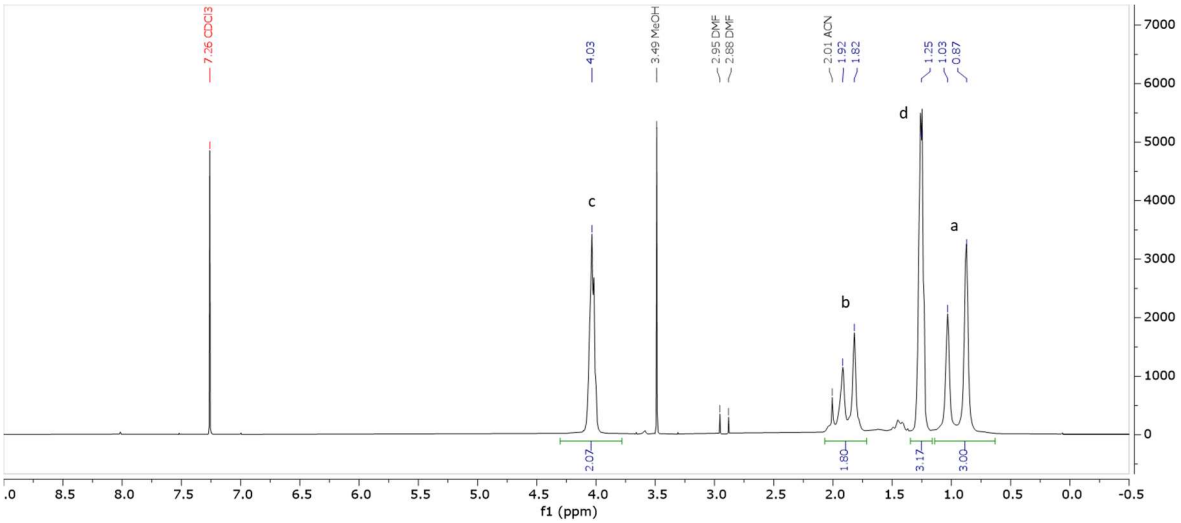

Figure 121: ^{1}H NMR spectrum of P[EMA 1%]$_{500}$ (RAFT).

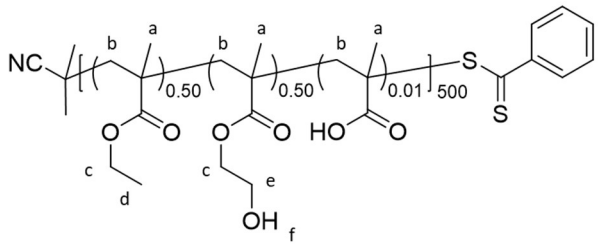

P[EMA-HEMA 1%]$_{500}$ (RAFT): Reactant solutions were prepared in DMF. 500 µL of EMA 2M solution (1 mmol, 0.50 eq), 500 µL of HEMA 2M solution (1 mmol, 0.50 eq), 10 µL of MAA 2M solution (0.02 mmol, 0.01 eq), 8.8 µL of 2-Cyano-2-propyl benzodithioate 100 mg.mL^{-1} solution (0.004 mmol, 1/500 eq) and 11 µL of AIBN 10 mg.mL^{-1} solution (0.66 µmol, 1/3000 eq) were put in a Schlenk tube under inert atm before undergoing three freeze-pump-thaw cycles. Reaction was set at 80°C under stirring overnight. An aliquot was taken and analyzed using ^{1}H NMR spectroscopy. The ratio between the intensities of the O-CH_2- signals from the monomer and the polymer showed 78% of conversion. The mixture was precipitated in 10 mL of MeOH/Water 5:5 mixture. The polymer was collected after centrifugation and redissolved in ACN before a second precipitation in identical medium. The obtained polymer was dried under vacuum to give 73 mg of white solid (overall yield 30%). ^{1}H NMR (400 MHz, Acetone d_6) δ (ppm): 4.06 (m, 2H), 3.81 (m, 1.37H), 1.96 (m, 2H), 1.28 (m, 1.33H), 1.10-0.94 (m, 3H). Molecular weight determined by SEC: M_n = 29000 g/mol, PDI = 1.54

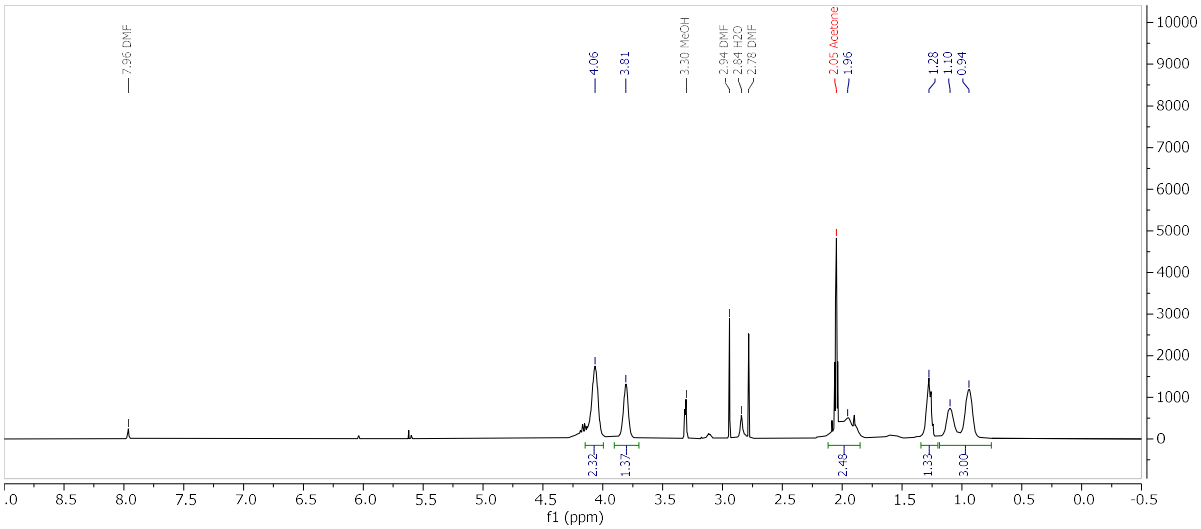

Figure 122: ^{1}H NMR spectrum of P[EMA-HEMA 1%]$_{500}$ (RAFT).

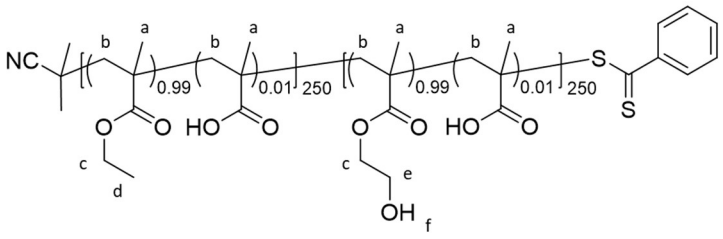

P[EMA 1%]$_{250}$-b-[HEMA 1%]$_{250}$: In a first step, the macro-RAFT agent **P[EMA 1%]$_{250}$** was synthetized: Reactant solutions were prepared in DMF. 1 mL of EMA 2M solution (2 mmol, 0.99 eq), 10 µL of MAA 2M solution (0.02 mmol, 0.01 eq) 17.6 µL of 2-Cyano-2-propyl benzodithioate 100 mg.mL^{-1} solution (0.008 mmol, 1/250 eq) and 22 µL of AIBN 10 mg.mL^{-1} solution (0.0033 mmol, 1/1500 eq) were put in a Schlenk tube under inert atm before undergoing three freeze-pump-thaw cycles. Reaction was set at 80°C under stirring overnight. An aliquot was taken and analyzed using ^{1}H NMR spectroscopy. The ratio between the intensities of the O-CH_2- signals from the monomer and the polymer showed 71% of conversion. The mixture was precipitated in 10 mL of MeOH/Water 9:1 mixture. The polymer was collected after centrifugation and redissolved in ACN before a second precipitation in identical medium. The obtained polymer was dried under vacuum to give 47 mg of white solid (overall yield 21%).

Then, 28 mg of **P[EMA 1%]$_{250}$** (0.982 µmol, 1eq), 123 µL of HEMA 2M (0.246 mmol, 250 eq), 24.5 µL of MAA 0.1M (2.45 µmol, 2.5 eq) and 8 µL of AIBN 10 mg.mL^{-1} solution (0.491 µmol, 0.5 eq) were put in a Schlenk tube under inert atm before undergoing three freeze-pump-thaw cycles. Reaction was set at 80°C under stirring overnight. An aliquot was taken and analyzed using ^{1}H NMR spectroscopy. The ratio between the intensities of the O-CH_2- signals from the monomer and the polymer showed 94% of conversion. The

mixture was precipitated in 10 mL of water The obtained polymer was dried under vacuum to give 40 mg of white solid (overall yield 65%). ^{1}H NMR (400 MHz, Acetone d_6 + MeOD d_4) δ (ppm): 4.04 (m, 2H), 3.78 (m, 0.7H), 1.95-1.86 (m, 2H), 1.26 (m, 2.34H), 1.05-0.89 (m, 3H). Molecular weight determined by SEC: M_n = 19000 g/mol, PDI = 1.92

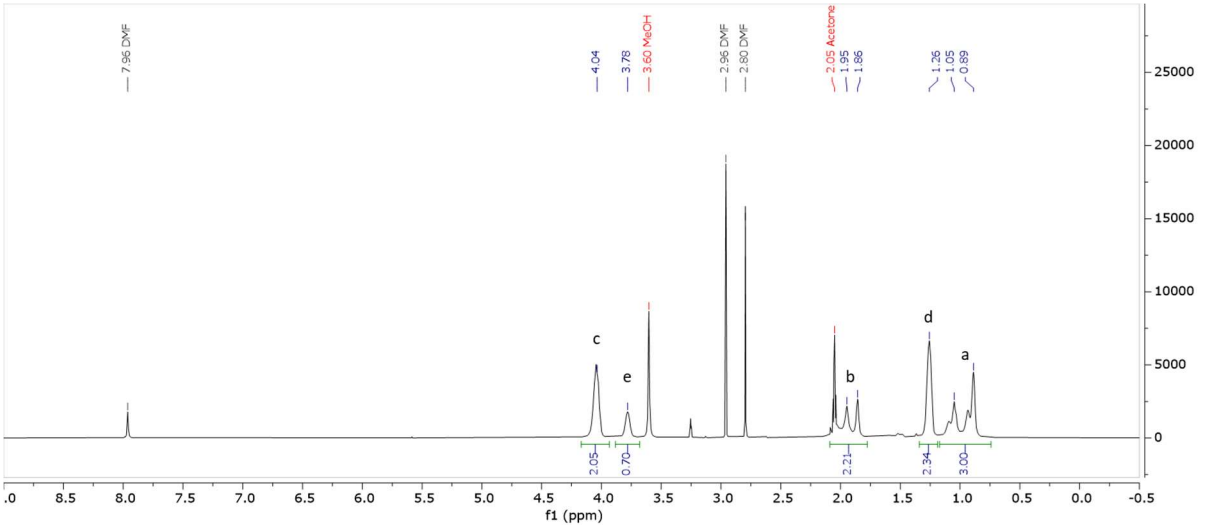

Figure 123: ^{1}H NMR spectrum of P[EMA 1%]$_{250}$-b-[HEMA 1%]$_{250}$.

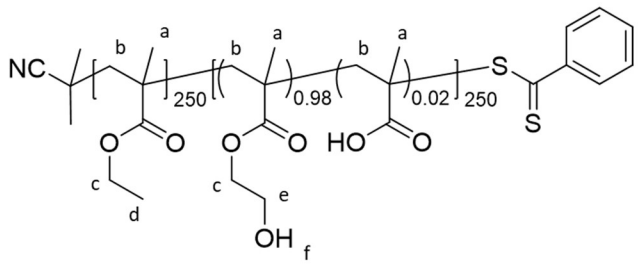

P[EMA]$_{250}$-b-[HEMA 2%]$_{250}$: Reactant solutions were prepared in DMF. 80 mg of **P[EMA]$_{250}$** (2.81 µmol, 1eq), 351 µL of HEMA 2M (0.703 mmol, 250 eq), 140 µL of MAA 0.1M (14 µmol, 5 eq) and 22.8 µL of AIBN 10 mg.mL^{-1} solution (1.4 µmol, 0.5 eq) were put in a Schlenk tube under inert atm before undergoing three freeze-pump-thaw cycles. Reaction was set at 80°C under stirring overnight. An aliquot was taken and analyzed using ^{1}H NMR spectroscopy. The ratio between the intensities of the O-CH_2- signals from the monomer and the polymer showed 94% of conversion. The mixture was precipitated in 10 mL of water. The obtained polymer was dried under vacuum to give 106 mg of white solid (overall yield 62%). ^{1}H NMR (400 MHz, DMSO d_6) δ (ppm): 4.81 (m, 1H), 3.90 (m, 2H), 3.58 (m, 1.81H), 1.79 (m, 2H), 1.21 (m, 0.78H), 0.94-0.78 (m, 3H).

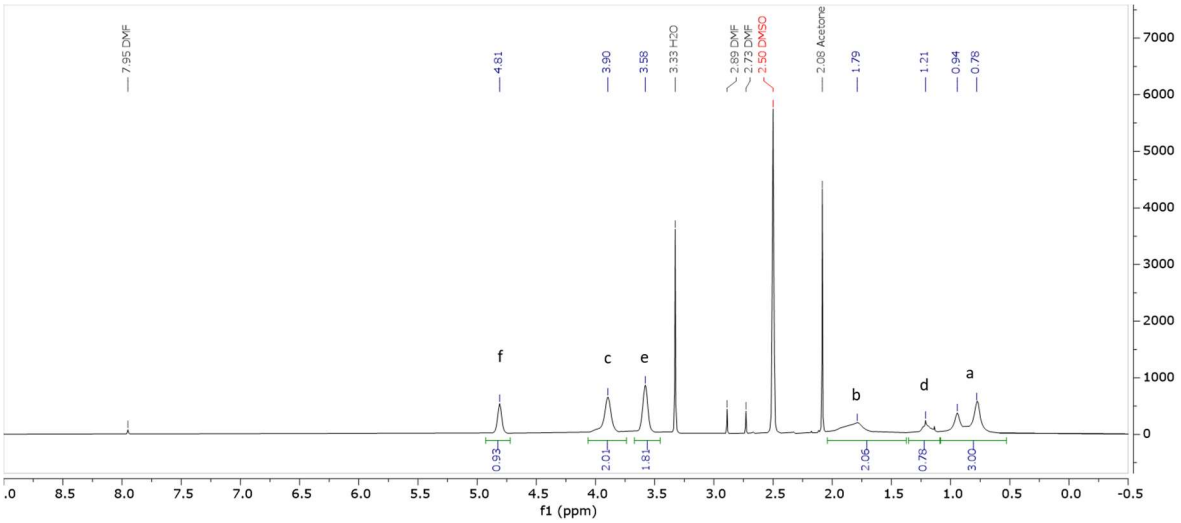

Figure 124: ^{1}H NMR spectrum of P[EMA]$_{250}$-b-[HEMA 2%]$_{250}$.

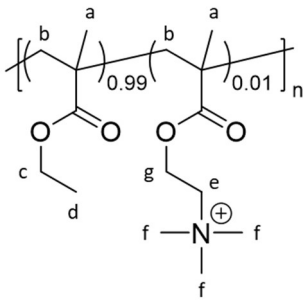

PEMA-NMe$_3^+$ 99-1: Monomers were dissolved in DMSO at a concentration of 2M. 40 mL of EMA (80 mmol, 99 eq) and 0.4 mL of NMe$_3^+$ (0.8 mmol, 1 eq) solutions were placed in a 100 mL round bottom flask. 1.68 mL of AIBN at 40 mg.mL^{-1} (0.41 mmol, 0.5 eq) were added and the mixture was flushed with argon during 5 min. It was then heated at 70 °C under inert atmosphere for 45 min and an aliquot was taken and analyzed using ^{1}H NMR spectroscopy. The ratio between the intensities of the O-CH$_2$- signals from the monomer and the polymer showed 27% of conversion. The mixture was then precipitated in 200 mL of MeOH/Water 9:1 mixture. The polymer was collected after centrifugation and redissolved in ACN before a second precipitation in 100 mL of MeOH/Water 4:6 mixture. The obtained polymer was dried under vacuum to give 632 mg of white solid (overall yield 7%). ^{1}H NMR (400 MHz, CDCl$_3$) δ (ppm): 4.03 (m, 2H), 3.54 (m, 0.07H), 1.91-1.82 (m, 2H), 1.25 (m, 3H), 1.03-0.88 (m, 3H).

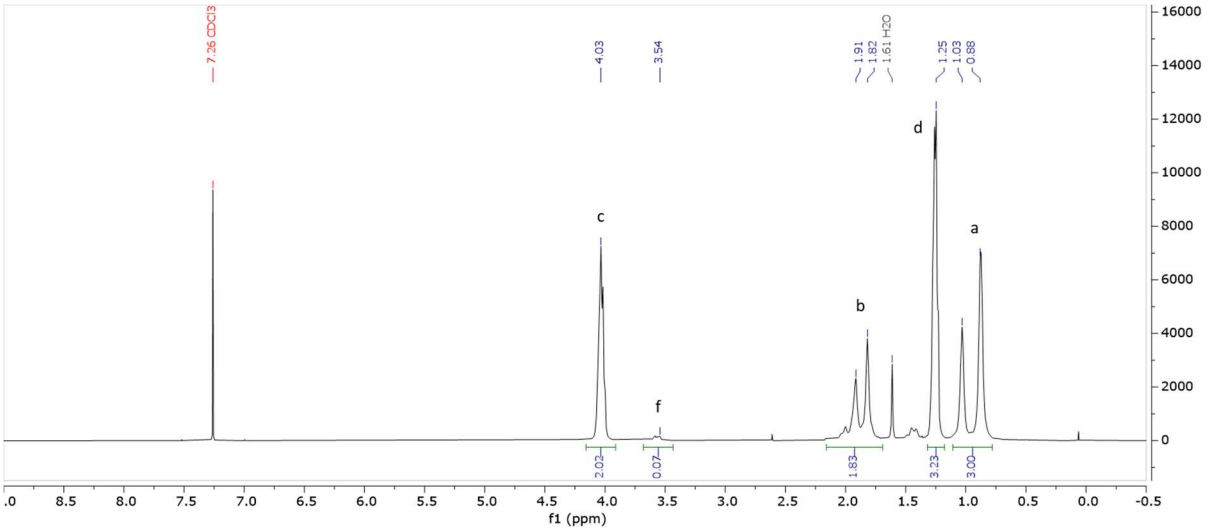

Figure 125: ^{1}H NMR spectrum of PEMA-NMe$_3^+$ 99-1.

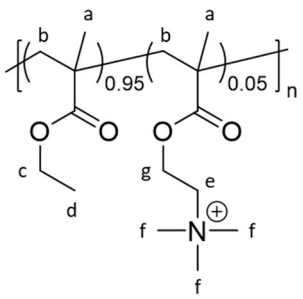

PEMA-NMe$_3^+$ 95-5: Monomers were dissolved in DMSO at a concentration of 2M. 38 mL of EMA (76 mmol, 95 eq) and 2 mL of NMe$_3^+$ (4 mmol, 5 eq) solutions were placed in a 100 mL round bottom flask. 1.68 mL of AIBN at 40 mg.mL^{-1} (0.41 mmol, 0.5 eq) were added and the mixture was flushed with argon during 5 min. It was then heated at 70 °C under inert atmosphere for 45 min and an aliquot was taken and analyzed using ^{1}H NMR spectroscopy. The ratio between the intensities of the O-CH$_2$- signals from the monomer and the polymer showed 30% of conversion. The mixture was then precipitated in 200 mL of MeOH/Water 7:3 mixture. The polymer was collected after centrifugation and redissolved in ACN before a second precipitation in 100 mL of NaCl$_{aq}$ 0.2M. The obtained polymer was rinsed with water to remove excess of salts and dried under vacuum to give 363 mg of white solid (overall yield 4%). ^{1}H NMR (400 MHz, Acetone d$_6$) δ (ppm): 4.60 (m, 0.05H), 4.25 (m, 0.05H), 4.07 (m, 2H), 3.58 (m, 0.30H), 1.97-1.88 (m, 2H), 1.28 (m, 3H), 1.07-0.91 (m, 3H).

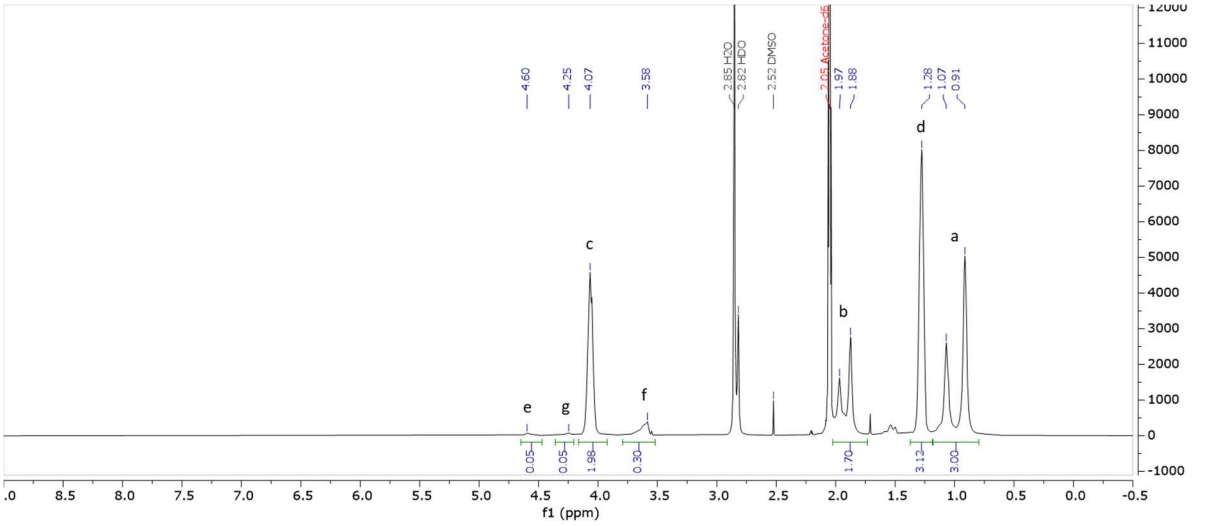

Figure 126: ^{1}H NMR spectrum of PEMA-NMe$_3^+$ 95-5.

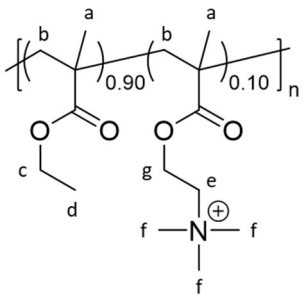

PEMA-NMe$_3^+$ 90-10: Monomers were dissolved in DMSO at a concentration of 2M. 72 mL of EMA (144 mmol, 90 eq) and 8 mL of NMe$_3^+$ (16 mmol, 10 eq) solutions were placed in a 100 mL round bottom flask. 3.36 mL of AIBN at 40 mg.mL^{-1} (0.82 mmol, 0.5 eq) were added and the mixture was flushed with argon during 5 min. It was then heated at 70 °C under inert atmosphere for 45 min and an aliquot was taken and analyzed using ^{1}H NMR spectroscopy. The ratio between the intensities of the O-CH$_2$- signals from the monomer and the polymer showed 31% of conversion. The mixture was then precipitated in 200 mL of MeOH/Water 3:7 mixture. The polymer was collected after centrifugation and redissolved in ACN before a second precipitation in 100 mL of NaCl$_{aq}$ 0.2M. The obtained polymer was rinsed with water to remove excess of salts and dried under vacuum to give 363 mg of white solid (overall yield 1%). ^{1}H NMR (400 MHz, Acetone d$_6$) δ (ppm): 4.60 (m, 0.11H), 4.28 (m, 0.10H), 4.07 (m, 2H), 3.62 (m, 0.64H), 1.97-1.88 (m, 2H), 1.28 (m, 3H), 1.07-0.91 (m, 3H).

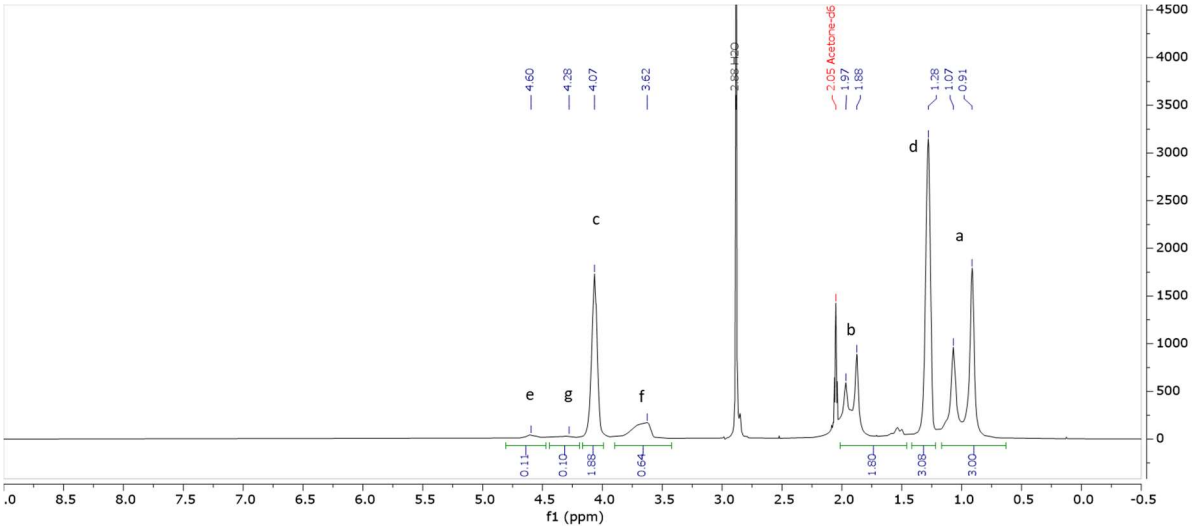

Figure 127: ^{1}H NMR spectrum of PEMA-NMe$_3^+$ 90-10.

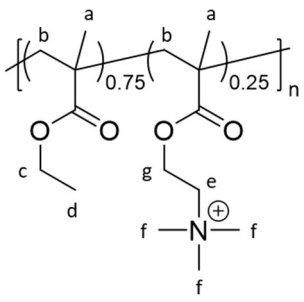

PEMA-NMe$_3^+$ 75-25: Monomers were dissolved in DMSO at a concentration of 2M. 30 mL of EMA (60 mmol, 75 eq) and 10 mL of NMe$_3^+$ (20 mmol, 25 eq) solutions were placed in a 100 mL round bottom flask. 1.68 mL of AIBN at 40 mg.mL^{-1} (0.41 mmol, 0.5 eq) were added and the mixture was flushed with argon during 5 min. It was then heated at 70 °C under inert atmosphere for 40 min and an aliquot was taken and analyzed using ^{1}H NMR spectroscopy. The ratio between the intensities of the O-CH$_2$- signals from the monomer and the polymer showed 36% of conversion. The mixture was then precipitated in 200 mL cold NaCl$_{aq}$ 0.2M. The polymer was collected after centrifugation and redissolved in ACN before a second precipitation in 100 mL of the same medium. The obtained polymer was rinsed with water to remove excess of salts and dried under vacuum to give 476 mg of white solid (overall yield 4%). ^{1}H NMR (400 MHz, DMSO d$_6$) δ (ppm): 4.38 (m, 0.46H), 4.00 (m, 1.82H), 3.74 (m, 0.42H), 3.24 (m, 2.02H, integration determinated after deconvolution of H$_2$O signal), 1.77 (m, 2H), 1.22 (m, 2.71H), 0.95-0.80 (m, 3H).

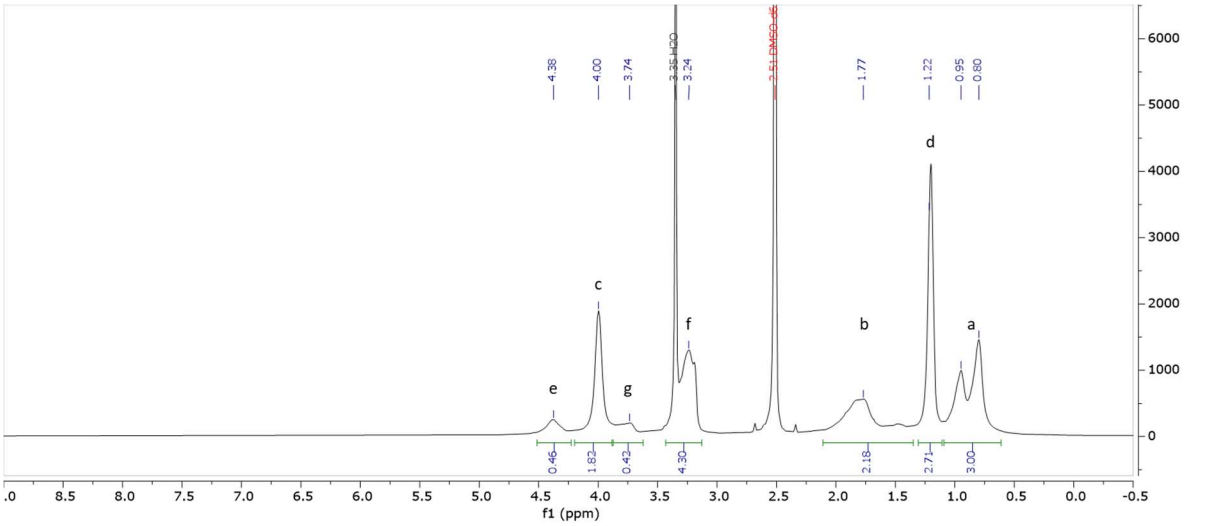

Figure 128: ^{1}H NMR spectrum of PEMA-NMe$_3$ 75-25.

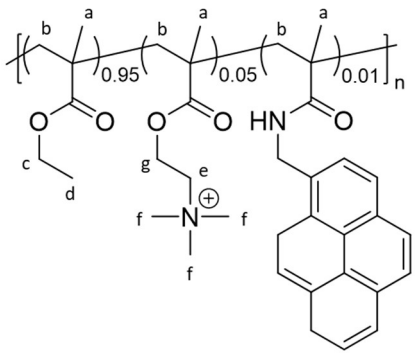

PEMA-NMe$_3^+$ 95-5 Pyrene functionalized: In a first step the functionalizable polymer **PEMA-NMe$_3^+$-PF5 95-5-1** was synthetized. Monomers were dissolved in DMSO at a concentration of 2M. 19 mL of EMA (38 mmol, 95 eq), 1 mL of NMe$_3$ (2 mmol, 5 eq) and 0.2 mL of PF5 (0.04 mmol, 1 eq) solutions were placed in a 50 mL round bottom flask. 0.84 mL of AIBN at 40 mg.mL^{-1} (0.2 mmol, 0.5 eq) were added and the mixture was flushed with argon during 5 min. It was then heated at 70 °C under inert atmosphere for 40 min and an aliquot was taken and analyzed using ^{1}H NMR spectroscopy. The ratio between the intensities of the O-CH$_2$- signals from the monomer and the polymer showed 30% of conversion. The mixture was then precipitated in 100 mL of MeOH/Water 6:4 mixture. The polymer was collected after centrifugation and redissolved in ACN before a second precipitation in 40 mL of NaCl$_{aq}$ 1M. The obtained polymer was rinsed with water to remove excess of salts and dried under vacuum to give 942 mg of white solid (overall yield 19%).

46.5 mg of 1-Pyrenemethylamine hydrochloride (0.16 mmol, 8eq) were dissolved in 2mM of DMF in a Schlenk tube. 114 mg of **PEMA-NMe$_3^+$-PF5 95-5-1** (0.02 mmol, 1eq) were added followed by 110 µL of TEA (0.8 mmol, 40 eq). The reaction was put under inert atmosphere and heated at 55°C during 48h. Then 400 µL of ethylamine 2M in THF (0.8 mmol, 40 eq) were added and reaction was let for additional 24h. The mixture was then precipitated in 10 mL of MeOH/Water 2:8 mixture. The polymer was collected after

centrifugation and redissolved in ACN before purification with size-exclusion chromatography. The obtained polymer was dried under vacuum to give 26 mg of white solid (overall yield 23%). ^{1}H NMR (400 MHz, $CDCl_3$) δ (ppm): 8.31-8.04 (m, 0.11H, ArH), 4.41 (m, 0.12H), 4.03 (m, 2H), 3.56 (m, 0.34H), 1.91-1.81 (m, 2H), 1.25 (m, 3H), 1.03-0.87 (m, 3H).

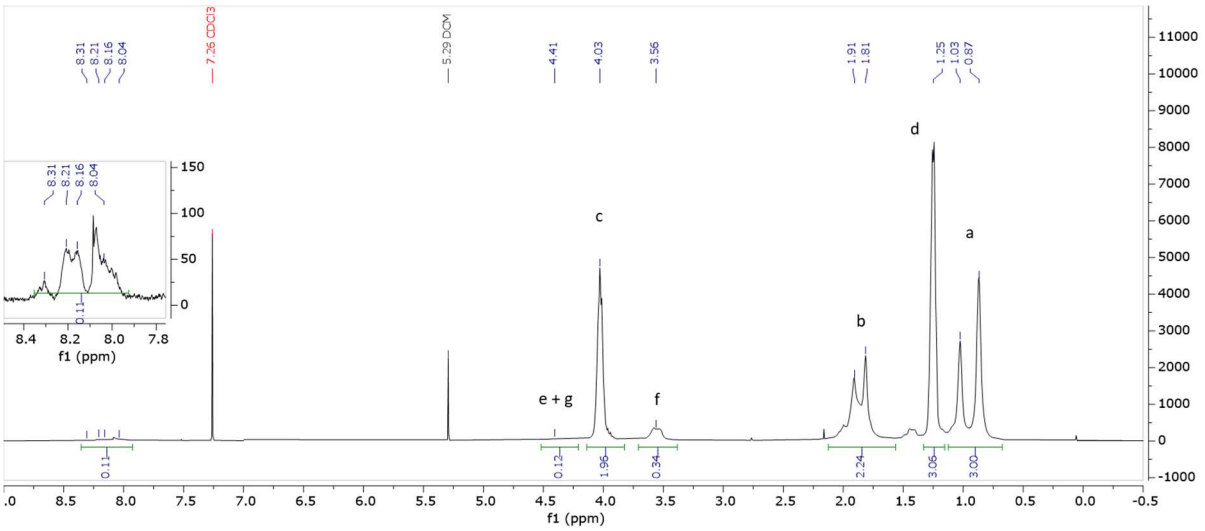

Figure 129: ^{1}H NMR spectrum of PEMA-NMe$_3$ 95-5 Pyrene functionalized.

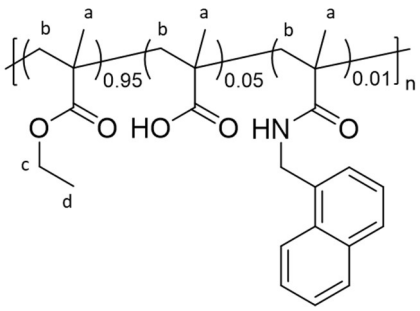

PEMA-COOH 95-5 Naphtalene functionalized: In a first step the functionalizable polymer **PEMA-COOH - PF5 95-5-1** was synthetized. Monomers were dissolved in DMSO at a concentration of 2M. 34.5 mL of EMA (69 mmol, 95 eq), 1.725 mL of MAA (3.45 mmol, 5 eq) and 0.345 mL of PF5 (0.69 mmol, 1 eq) solutions were placed in a 50 mL round bottom flask. 1.52 mL of AIBN at 40 mg.mL^{-1} (0.37 mmol, 0.5 eq) were added and the mixture was flushed with argon during 5 min. It was then heated at 70 °C under inert atmosphere for 35 min and an aliquot was taken and analyzed using ^{1}H NMR spectroscopy. The ratio between the intensities of the O-CH_2- signals from the monomer and the polymer showed 28% of conversion. The mixture was then precipitated in 100 mL of MeOH/Water 9:1 mixture. The polymer was collected after centrifugation and redissolved in ACN before a second precipitation in 100 mL of the same medium. The obtained polymer was dried under vacuum to give 1.68 g of white solid (overall yield 20%).

62 µL of 1-Naphtylmethylamine (0.4 mmol, 20eq) were dissolved in 2mM of DMF in a Schlenk tube. 114 mg of **PEMA-COOH-PF5 95-5-1** (0.02 mmol, 1eq) were added followed by 110 µL of TEA (0.8 mmol, 40 eq). The reaction was put under inert atmosphere and heated at 55°C during 48h. Then 400 µL of ethylamine 2M in THF (0.8 mmol, 40 eq) were added and reaction was let for additional 24h. The mixture was then precipitated in 10 mL of MeOH/Water 2:8 mixture. The polymer was collected after centrifugation and redissolved in ACN before purification with size-exclusion chromatography. The obtained polymer was dried under vacuum to give 43 mg of white solid (overall yield 38%). ^{1}H NMR (400 MHz, $CDCl_3$) δ (ppm): 8.02-7.46 (m, 0.11H, ArH), 4.03 (m, 2H), 1.92-1.82 (m, 2H), 1.26 (m, 3H), 1.03-0.87 (m, 3H).

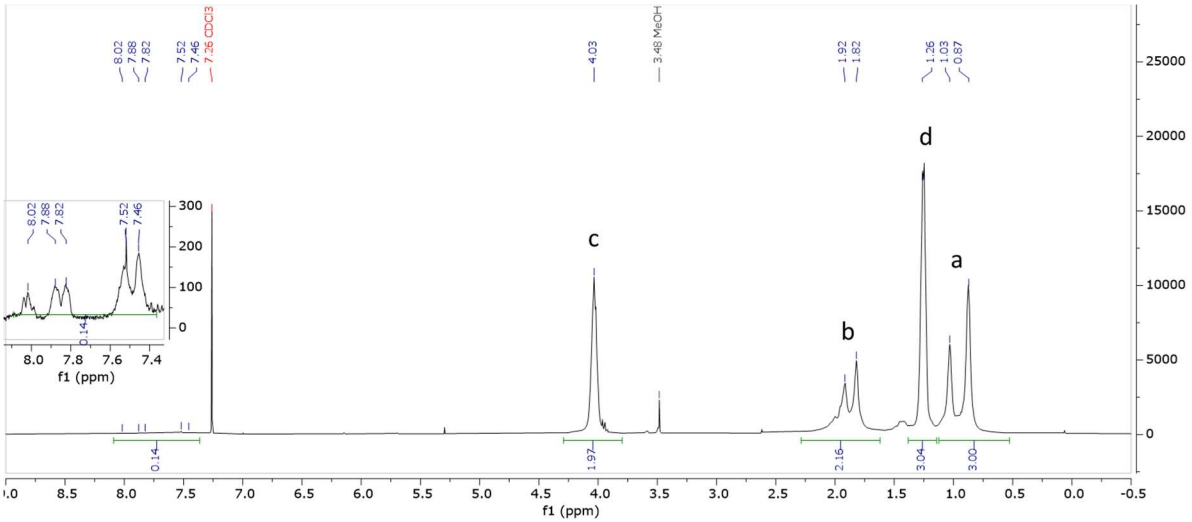

Figure 130: ^{1}H NMR spectrum of PEMA-COOH 95-5 Naphtalene functionalized.

Antoine COMBES

Influence de la structure des polymères sur la formation de nanoparticules fonctionnelles par nanoprécipitation

Résumé

Les nanoparticules polymériques sont largement utilisées pour des applications biomédicales en tant que vecteurs de médicaments ou d'agents de contraste. Une des méthodes les plus couramment employée pour leur fabrication est la nanoprécipitation. Ce processus comporte de nombreux paramètres ayant une influence sur les propriétés des particules obtenues. Or ces propriétés vont à leur tour déterminer le comportement des particules en milieu biologique, il est donc crucial de pouvoir les moduler avec précision, ce qui passe par une bonne connaissance de leur processus de formation. Dans ce contexte, nous avons souhaité étudier l'influence de la chimie et de l'architecture des polymères sur la formation des particules obtenues par nanoprécipitation. Dans un premier temps, nous avons évalué l'impact de la chimie des polymères sur la cinétique de formation des particules, puis nous avons observé l'influence de l'architecture des polymères. Enfin, nous avons exploité le contrôle cinétique offert par la nanoprécipitation sur l'assemblage des chaines de polymères pour formuler des particules portant des charges positives et négatives sur leurs surfaces. Ces particules de petite taille (< 25nm) présentent un potentiel Zeta dépendant du pH et une bonne stabilité en milieu salin.

Mots clé : Nanoprécipitation, nanoparticules polymériques, cinétique, architecture, fluorescence, FRET.

Abstract

Polymeric nanoparticles are widely used as drug or contrast agent nanocarriers in biomedical applications. Nanoprecipitation is commonly used for their production. This process involves many parameters influencing nanoparticle properties. However, the latter have a tremendous impact on the fate of the particles in biological media. Therefore, it is crucial to be able to tune them precisely, which implies to have a good knowledge of their formation process. In this context, we studied the influence of polymer chemistry and architecture on the formation of particles obtained by nanoprecipitation. Firstly, we measured the effects of polymer chemistry on the kinetics of nanoparticle formation, and then we studied the influence of polymer architecture. Finally, we used the kinetic control of nanoprecipitation on polymer assembly to create particles bearing oppositely charged groups on their surface. These particles have a small size (<25 nm), a pH dependent ζ-potential and an excellent stability in saline solutions.

Keys words: Nanoprecipitation, polymeric nanoparticles, kinetics, architecture, fluorescence, FRET.